# SUSTAINABLE SLOPE STABILIZATION USING RECYCLED PLASTIC PIN IN TEXAS

By

MOHAMMAD SADIK KHAN

Presented to the Faculty of the Graduate School of

The University of Texas at Arlington in Partial Fulfillment

of the Requirements

for the Degree of

DOCTOR OF PHILOSOPHY

THE UNIVERSITY OF TEXAS AT ARLINGTON

DECEMBER 2013

Copyright © by Mohammad Sadik Khan 2013

All Rights Reserved

Acknowledgements

First, I would like to express my deepest gratitude to my supervisor Dr. Sahadat Hossain, for his valuable time, guidance, encouragement, help and unconditional support throughout my graduate studies. Without his constant guidance and support, this dissertation would not have been completed.

I would like to give my special thanks to Dr. Laureano R. Hoyos, Dr. Stefan A. Romanoschi, Dr. Xinbao Yu and Dr. Ashfaq Adnan for their precious time, valuable suggestions and participation as my committee member.

I would like to thank Texas Department of Transportation (TxDOT) for funding this research, especially Dr. Nicasio Lozano for his support during all stages of this research.

Special thanks extended to Golam Kibria, Sonia Samir, Mahsa Hedayati and Dipak Tiwari for their active cooperation and assistance in all stages of work. I would also like to thank my dearest friends Shahed Redwan Manzur, Istiaque Hasan, Jubair Hossain and Ziaur Rahman for their worthy friendship and the good times.

I wish to acknowledge the cooperation, patience, sacrifice and unconditional support from my wife Nusrat Kabir throughout my graduate studies. I would like to thank my sister Sifat Khanm and brother Sadat Khan for giving me support.

Finally, and most of all, I would like to dedicate this dissertation to my parents for all their love, encouragement, and great support. It is the best thing in my life to be a part of their family.

October 30, 2013

Abstract

SUSTAINABLE SLOPE STABILIZATION USING RECYCLED PLASTIC PIN IN TEXAS

Mohammad Sadik Khan, PhD

The University of Texas at Arlington, 2013

Supervising Professor: MD. Sahadat Hossain

Shallow slope failures are predominant in the North Texas area and pose significant maintenance problems for the Texas Department of Transportation (TxDOT). As a cost effective alternative, the Recycled Plastic Pin (RPP) can be utilized to stabilize the shallow slope failure. RPP are fabricated from recycled plastics and waste materials (i.e. polymers, sawdust, and fly ash). It is a lightweight material and less susceptible to chemical and biological degradation than alternative reinforcing element. RPPs are driven into the slope face, which provide additional resistance along the slip surface and increase the factor of safety. The current study summarized the remediation of shallow slope failure using RPP. Two highway slopes, one located over US 287 near the St. Paul overpass in Midlothian and one over Loop 12 near the UP RP rail overpass in Dallas, Texas were stabilized using RPP. Three 50 ft. sections were selected and reinforced using RPP after a crack, caused by slope movement, was observed over the shoulder in the US 287 slope. Two 50 ft. control sections were placed between the reinforced sections to compare the performances of the slope. A 50 ft. section over top slope and a 100 ft. section at the bottom slope of Loop 12 were reinforced with RPP as a temporary solution. The field performance of the slope was monitored using instrumented RPPs, inclinometers and surveying instruments. The performance monitoring results of US 287 slope indicated that the unreinforced control sections had significant settlement at the crest of the slope, as much as 15 inches. In addition, a total of 3 inch increments in settlement had taken place during the year. In contrast, almost no increment in

settlement was observed at the reinforced section in US 287 slopes. Moreover, the total settlements in the reinforced sections were 2 inch to 4 inch which was less compared to the unreinforced sections. The horizontal displacement of the US 287 slope had taken place after 1 year of construction which ranged up to 1.5 inch. After 1 year, the horizontal displacement became less than 0.1 inch at the Reinforced Section 1. The performance monitoring results of the Loop 12 slope presented that the top of the retaining wall is still moving after the installation of RPP. However, RPP installed adjacent to the footing provided lateral resistance and restricted the sliding of the wall. The maximum resistance was observed with closer RPP spacing. The cost analysis for the US 287 slope indicated that the cost for slope stabilization using RPP can be 50% lower compared to the cost of conventional slope stabilization approaches. The performance of the US 287 slope was further evaluated in numerical study and a parametric study was conducted to evaluate the effect of length and spacing of RPP which indicated that the deformation of reinforced slope increase with wider RPP spacing. Finally, a performance-based design method was developed to design the slope stabilization for surficial failure. The design method considers three limiting criteria which consider restricting failure of soil, limit horizontal displacement of RPP and limit maximum flexure in RPP. Based on the design method, the calculated factors of safeties were in good agreement with the safety analysis results in numerical study.

Table of Contents

Acknowledgements ..... iii

Abstract ..... iv

List of Illustrations ..... xii

List of Tables ..... xxii

Chapter 1 Introduction ..... 1

1.1 Background ..... 1

1.2 Problem Statement ..... 3

1.3 Research Objectives ..... 4

1.4 Thesis Organizations ..... 4

Chapter 2 Literature Review ..... 7

2.1 Slope Failure ..... 7

2.2 Shallow Slope Failure ..... 9

2.3. Fully Soften Clay of High Plastic Clay Soil ..... 11

2.4 Method of Repair of Shallow Slope Failure ..... 18

2.4.1 Rebuild Slope ..... 19

2.4.2 Pipe Pile and Wood lagging ..... 19

2.4.3 Geogrid Repair ..... 20

2.4.4 Soil Cement Repair ..... 21

2.4.5 Repair Using Launched Soil Nails ..... 22

2.4.6 Earth Anchors ..... 22

2.4.7 Geofoam ..... 23

2.4.8 Wick Drains ..... 25

2.4.9 Anchored Geosynthetic Systems (AGS) ..... 26
2.4.10 Retaining Wall ..... 28
2.4.11 Reinforced Soil Slopes ..... 31
2.4.12 Pin Piles (Micropiles) ..... 31
2.4.13 Slender Piles ..... 32
2.4.14 Plate Piles ..... 35
2.4.15 Recycled Plastic Pin ..... 36
2.5 Recycled Plastic Pin ..... 37
2.5.1 Manufacturing Process of RPP ..... 37
2.5.2 Engineering Properties of RPP ..... 38
2.5.3 Long Term Engineering Properties of RPP ..... 45
2.5.4 Creep of RPP ..... 50
2.5.5 Design Consideration for Structural Application ..... 56
2.6 Slope Stabilization using Recycled Plastic Pin ..... 58
2.6.1 Stability of Reinforced Slopes ..... 58
2.6.2 Design Method of RPP Reinforced Slope ..... 60
2.6.3 Installation Method ..... 64
2.6.4 Field Performance ..... 67
2.7 Limitation of Previous Study ..... 80
Chapter 3 Site Investigation ..... 82
3.1 Background ..... 82
3.2 Site Investigation of US 287 Slope ..... 82
3.2.1 Project Background ..... 82
3.2.2 Investigation of Slope Failure ..... 84
3.2.3 Analyses of Site Investigation Results ..... 88

3.2.4 Slope Stability Analyses at US 287 Slope ..... 89
3.3 Site Investigation of Loop 12 Slope ..... 91
3.3.1 Project Background ..... 91
3.3.2 Investigation of Slope Failure ..... 93
3.3.3 Analyses of Site Investigation Results ..... 97
3.3.4 Stability Analysis Using Plaxis ..... 98
Chapter 4 Slope Stabilization Using Recycled Plastic Pin ..... 100
4.1 Mechanism of Slope Stabilization ..... 100
4.2 Material Selection ..... 101
4.3 Experimental Study ..... 102
4.4 Design of Slope Stabilization Scheme: US 287 ..... 103
4.5 Installation of RPP: US 287 Slope ..... 106
4.6 Design of Slope Stabilization Scheme: Loop 12 ..... 109
4.7 Installation of RPP: Loop 12 Slope ..... 112
Chapter 5 Instrumentation and Performance Monitoring ..... 115
5.1 Instrumentation in US 287 Slope ..... 115
5.1.1 Rain Gauge ..... 115
5.1.2 Instrumentation of RPP ..... 115
5.1.3 Inclinometers ..... 117
5.1.4 Topographic Survey ..... 119
5.1.5 Moisture Sensor and Matric Suction Monitoring ..... 120
5.2 Performance Monitoring Results: US 287 Slope ..... 123
5.2.1 Instrumented RPP ..... 123
5.2.2 Topographic Survey ..... 129

5.2.3 Inclinometer ..... 135
5.2.4 Inclinometer Displacement with the Moisture and Suction Variation ..... 139
5.3 Instrumentation in Loop 12 Slope ..... 150
5.3.1 Instrumented RPP ..... 150
5.3.2 Topographic Survey ..... 151
5.4 Field Performance of Loop 12 Slope ..... 152
5.4.1 Strain Gauge Results of the Loop 12 Slope ..... 152
5.4.2 Surveying Results of the Loop 12 Slope ..... 153
5.5 Cost Analysis ..... 156
Chapter 6 Numerical Study ..... 158
6.1 Introduction ..... 158
6.2 Model Calibration ..... 159
6.3 Performance Evaluation of Reinforced Section 1 ..... 161
6.4 Performance Evaluation of Reinforced Section 2 ..... 165
6.5 Parametric Study: Effect of Uniform Spacing and Depth of RPP ..... 168
6.6 Parametric Study Results ..... 169
6.6.1 Factor of Safety ..... 169
6.6.2 Deformation Analysis ..... 170
6.7 Parametric Study: Smaller RPP Spacing at Crest ..... 174
6.8 Results of FEM analysis with Closer RPP Spacing at Crest ..... 176
6.81 Variation of Factor of Safety ..... 176
6.8.2 Horizontal Displacement at Crest ..... 178
6.9 Summary ..... 184

Chapter 7 Development of Design Chart ..... 187

7.1 Introduction ..... 187

7.2 Limiting Criteria ..... 189

7.2.1 Limit Failure of Adjacent Soil of RPP ..... 189

7.2.2 Limit Resistance of RPP ..... 191

7.3 Determination of Limit Soil Pressure ..... 194

7.3.1 Calculation of Limit Soil Pressure ..... 194

7.3.2 Calculation of Limit Soil Resistance ..... 196

7.4 Limit Horizontal Displacement and Maximum Flexure of RPP ..... 200

7.5 Finalizing Design Chart ..... 206

7.6 Calculation of Factor of Safety ..... 207

7.6.1 Approach 1: Conventional Method of Slices ..... 207

7.6.2 Approach 2: Infinite Slope ..... 211

7.7 Validation ..... 214

7.7.1 Unreinforced Slope ..... 215

7.7.2 Reinforced Slope ..... 218

7.8 Limitation of the Design Method ..... 221

Chapter 8 Conclusions and Recommendations ..... 222

8.1 Summary and Conclusion ..... 222

8.2 Recommendation for Future Studies ..... 225

Appendix A Borehole Log: US 287 Slope ..... 227

Appendix B Design Charts ..... 231

Appendix C Sample Calculations ..... 290

References ..... 305

Biographical Information ..... 311

List of Illustrations

Figure 2.1 Types of Clay movement (redrawn after Abramson et al., 2002) ..... 8
Figure 2.2 Typical surficial slope failures (redrawn after Day, R. W. 1989) ..... 10
Figure 2.3 Comparisons of peak, residual and fully softened shear strength (redrawn after Skempton, 1970) ..... 12
Figure 2.4 Shear strength envelopes in terms of effective stress a. Beaumont clay, b. Paris clay (Kayyal and Wright, 1991) ..... 14
Figure 2.5 Stress strain curve of Eagle Ford Shale a. as compacted, b. normally consolidated, c. specimen subjected to cyclic drying and wetting (Zornberg et al., 2007) ..... 16
Figure 2.6 Modified Mohr Failure envelop of Eagle Ford Shale a. as compacted, b. normally consolidated, c. specimen subjected to cyclic drying and wetting (Zornberg et al., 2007) ..... 17
Figure 2.7 Schematic of Pipe pile and wood lagging repair (Day, R. W. 1996) ..... 20
Figure 2.8 Repair of Surficial slope failure by Geogrid (Day, R. W. 1996) ..... 21
Figure 2.9 Soil cement repair of shallow slope failure (Day, R. W. 1996) ..... 21
Figure 2.10 Schematic of Repair of soil nails in slope stabilization (replotted after Titi and Helwany, 2007) ..... 22
Figure 2.11 Earth Anchors in slope stabilization (Titi and Helwany, 2007) ..... 23
Figure 2.12 Typical section of treatment. ..... 24
Figure 2.13 Schematic of AGS (redrawn after Vitton et al., 1998) ..... 27
Figure 2.14 Cross section of a low wall with vegetation planted on the slope for stabilization (USDA, 1992). ..... 29
Figure 2.15 Schematic of Shallow MSE wall (redrawn after Berg et al., 2009) ..... 31
Figure 2.16 Load Test Set up ..... 33

Figure 2.17 Load vs Shear Displacement from Lateral Load test ..... 34
Figure 2.18 Schematic of Plate Pile for Slope Stabilization (Short and Collins, 2006) ..... 36
Figure 2.19 Comparison of compressive strength (Lampo and Nosker, 1997) ..... 41
Figure 2.20 Comparison of Compressive modulus (Lampo and Nosker, 1997) ..... 42
Figure 2.21 Tensile strength of HDPE (Malcolm, M. G. (1995)) ..... 44
Figure 2.22. Compression modulus measurements for both cross-sectional and in-plane dimensions for plastic lumber collected from the West Meadow pier over a 24 months period (Breslin et al., 1998). ..... 48
Figure 2.23 Bending modulus measurements for both cross-sectional and in-plane directions for plastic lumber collected from the west Meadow pier over a 24 month period. ..... 49
Figure 2.24 Creep curve for recycled plastic beam at room temperature ..... 51
Figure 2.25 RPP testing set up for Creep a. Compression creep, b. Flexure Creep (redrawn after Chen et al., 2007) ..... 53
Figure 2.26 Typical deflections under constant axial stress versus time of RPP (redrawn after Chen et al., 2007) ..... 54
Figure 2.27 Method to estimate flexural creep at field (redrawn after Chen et al., 2007). ..... 56
Figure 2.28 Static equilibrium of individual slice in the method of slices (Loehr and Bowders, 2007) ..... 59
Figure 2.29 Reinforcement force on an individual slice in the method of slice ..... 59
Figure 2.30 Schematic and limit resistance curve for failure mode 1 (Loehr and Bowders, 2007) ..... 61

Figure 2.31 Schematic and limit resistance curve for failure mode 2 (Loehr and Bowders, 2007) ..... 62
Figure 2.32 Schematic and limit resistance curve for failure mode 3a ..... 62
Figure 2.33 Schematic and Limit resistance curve for failure mode 3b ..... 63
Figure 2.34 Combined Limit Resistance Curve (Loehr and Bowders, 2007) ..... 63
Figure 2.35 Location of the Slide areas in I-70 site (Parra et al., 2003) ..... 68
Figure 2.36 Layout of RPP at the slide area of I-70 site (Parra et al., 2003) ..... 69
Figure 2.37 Inclinometer data from I-2 at I-70 Site (Parra et al., 2003) ..... 71
Figure 2.38 Bending moment diagram from Instrumented RPP at I-70 site (Parra et al., 2003) ..... 72
Figure 2.39 Layout of RPP and location of instrumentation in I-435 Wornall Road site (Parra et al., 2003) ..... 73
Figure 2.40 Cumulative Displacement plot of Inclinometer I-2 at I-435 site (Parra et al., 2003) ..... 74
Figure 2.41 Bending moment diagram from Instrumented RPP at I-435 site (Parra et al., 2003) ..... 75
Figure 2.42 Summary of field measurement at I-435 site (Loehr et al., 2007) ..... 77
Figure 2.43 locations of RPP at US 36-Stewartsville site (Loehr et al., 2007) ..... 78
Figure 2.44 Bending Moment and Deformation of isolated member placed within the control slide area at US36 site (Loehr et al., 2007) ..... 79
Figure 2.45 Cumulative Horizontal Displacement of Inclinometer at US 36 slope, a. Section 1, b. Section 2, c. Section 3 and d. Section 4 ..... 81
Figure 3.1 Location of the US 287 Slope. ..... 83
Figure 3.2 Cracks along the Shoulder over US 287 Slope. ..... 83
Figure 3.3 Layout of bore holes and resistivity imaging lines ..... 84

Figure 3.4 Laboratory test results a. Moisture Distribution along the bore holes, b. Plasticity Chart along the bore holes. ..... 85
Figure 3.5 Resistivity Imaging Field Set-up of (a) RI-1, and (b) RI-2 ..... 86
Figure 3.6 Resistivity Imaging at the US 287 Slope a. Resistivity profile for RI-1, b. Resistivity profiles for RI-2, c. Variation of Resistivity along the boreholes. ..... 87
Figure 3.7 Schematic of Possible Surficial Slope Failure ..... 89
Figure 3.8 Slope Stability Analysis using Plaxis 2D a. Soil Model, b. Critical Slip Surface for Factor of Safety = 1.05 ..... 90
Figure 3.9 Location of Loop 12 slope ..... 92
Figure 3.10 Site Visit Picture of Loop 12 ..... 93
Figure 3.11 Layout of the Bore Holes ..... 94
Figure 3.12 Moisture Content of Collected Soil Samples at Loop 12 Slope ..... 94
Figure 3.13 Resistivity Imaging Layout at Loop 12 Slope ..... 95
Figure 3.14 Resistivity Imaging Field Set-up at Loop 12 Slope a. Resistivity Line 1 and b. Resistivity Line 2 ..... 96
Figure 3.15 Resistivity Imaging Results at Loop 12 Slope, a. Resistivity Line-1, b. Resistivity Line-2 ..... 96
Figure 3.16 Mechanism of Slope failure at Loop 12 Slope ..... 98
Figure 3.17 Slope Stability Analysis a. Soil Model with Saturated Zone, b. Slip Surface with FS = 1.01 ..... 99
Figure 4.1 Schematic of Resistances from RPP as Slope Reinforcement. ..... 100
Figure 4.2 Stress-Strain Response of RPP at Different Loading Rates ..... 102
Figure 4.3 Proposed RPP Layout at US 287 Slope. ..... 104
Figure 4.4 Section Details of Slope Stabilization on US 287 Slope, a. Reinforced Section 1, b. Reinforced Section 2, c. Reinforced Section 3 ..... 105

Figure 4.5 Slope Stability Analyses using RPP a. Reinforced Section 1 with FS 1.43, b. Reinforced Section 2 with FS 1.48 c. Reinforced Section 3 with FS 1.54 ..... 106
Figure 4.6 Installation Photo of RPP at Reinforced Section 1 and Reinforced Section 2. ..... 107
Figure 4.7 Installation of RPP at the Crest of Reinforced Section 3 ..... 107
Figure 4.8 Layout of the Reinforced Loop 12 Slope a. Plan, b. Section A-A, c. Section B-B ..... 111
Figure 4.9 Slope Stability Analysis at Loop 12 Slope, a. at Section A-A (F.S = 1.219), b. at Section B-B (F.S = 1.189) ..... 112
Figure 4.10 RPP installations at Loop 12 Slope ..... 114
Figure 5.1 Schematic Diagram of Instrumented Plastic Pin ..... 116
Figure 5.2 Installation of Strain Gauges of RPP ..... 117
Figure 5.3 Layout of Instrumented RPP ..... 117
Figure 5.4 Layout of Inclinometers at US 287 Slope ..... 118
Figure 5.5 Site Photos during Inclinometer Installation ..... 118
Figure 5.6 Layout of Survey Line at US 287 Slope ..... 119
Figure 5.7 Instrumentation Layout ..... 120
Figure 5.8 a. EC-5 soil moisture sensors, b. MPS-1 Water Potential Probe ..... 122
Figure 5.9 Data collection a. Instrumentation locations, b. Em-50 Data logger ..... 123
Figure 5.10 Comparison of Strain between IM3, IM5 and IM8 ..... 125
Figure 5.11 Comparison of Strain between IM4, IM6 and IM9 ..... 126
Figure 5.12 Comparison of Strain between IM2’ and IM5’ ..... 127
Figure 5.13 Comparison of Strain at Different Depths along IM5 ..... 128
Figure 5.14 Total Settlements along the Crest of US 287 Slope ..... 130
Figure 5.15 Incremental Settlements in US 287 Slope ..... 130

Figure 5.16 Survey Results along Line A-A, a. Incremental Horizontal Displacement, b. Incremental Settlement ..... 132
Figure 5.17 Survey Results along Line D-D, a. Incremental Horizontal Displacement, b. Incremental Settlement ..... 133
Figure 5.18 Survey Results along Line G-G, a. Incremental Horizontal Displacement, b. Incremental Settlement ..... 134
Figure 5.19 Variation of Horizontal Displacement along Inclinometer 1 at Reinforced Section 1. ..... 136
Figure 5.20 Variation of Horizontal Displacement along Inclinometer 3 at Reinforced Section 2. ..... 137
Figure 5.21 Comparison of Horizontal Displacement between Inclinometer 1 and Inclinometer 3 a. At 2.5 ft., b. At 10.5 ft. ..... 138
Figure 5.22 Variation of Horizontal Displacement along Inclinometer 1 at Reinforced Section 1, a. Rainfall, b. Moisture Content, c. Matric Suction and d. Hor. displacement ..... 142
Figure 5.23 Variation of Horizontal Displacement along Inclinometer 1 at Reinforced Section 1, a. Rainfall, b. Moisture Content, c. Matric Suction and d. Hor. displacement ..... 143
Figure 5.24 Variation of Horizontal Displacement along Inclinometer 3 at Reinforced Section 2, a. Rainfall, b. Moisture Content, c. Matric Suction and d. Hor. displacement ..... 144
Figure 5.25 Variation of Horizontal Displacement along Inclinometer 3 at Reinforced Section 2, a. Rainfall, b. Moisture Content, c. Matric Suction and d. Hor. displacement ..... 145
Figure 5.26 Variation of horizontal displacement with daily highest temperature ..... 146

Figure 5.27 Schematic of loss of support condition for RPP during the dry period, a. Formation of desiccation crack during summer, b. Passive Resistance reduced due to loss of support, c. Desiccation crack disappear during wet period and RPP regain passive resistance. ..... 147
Figure 5.28 Comparison of Horizontal Movement for base line October 23, 2012, a. Inclinometer 1 at Reinforced Section 1, b. Inclinometer 3 at Reinforced Section 2 ..... 148
Figure 5.29 Site Photo on June 2012 a. new crack initiation from mid-width of Reinforced Section 1 toward control section, b. 12 inch settlement over control section, c. new crack over the shoulder of control section, d. new crack due to control section ends at Reinforced Section 2, e. 9 inch settlement over control section 2, f. probable crack line over roadway near control section 2. ..... 149
Figure 5.30 Layout of the Instrumented RPPs at Loop 12 Slope ..... 150
Figure 5.31 Layout of the Survey Line over Loop 12 Slope ..... 151
Figure 5.32 Variation of Strain with Rainfall a. IM-1 over Top Slope ..... 152
Figure 5.33 Incremental Horizontal Displacement of Retaining wall ..... 154
Figure 5.34 Incremental Horizontal Displacement of 1st Line of RPP at Bottom Slope ..... 154
Figure 5.35 Front View of the Crack of Retaining Wall at Loop 12 Slope on a. March 14, 2012, b. August 5, 2012, c. March 19, 13, d. August 2, 13 ..... 155
Figure 5.36 Comparison of Horizontal Displacement between Line C-C and Line D-D ..... 155
Figure 5.37 Comparison of construction cost data for various systems (Data from Sabatini et al., 1997,cited in Lazarte et al., 2003) ..... 157

Figure 6.1 Back Analysis a. Soil model of Control section, b. Settlement at control section 14.6 in ..... 160
Figure 6.2 Deformation analysis at Reinfroced Secton 1, a. Horizontal Displacement at Crest = 3.2 inch, b. Settlement at the crest of the slope 2.3 inch ..... 162
Figure 6.3 Horizontal displacement of 1st 7 row of RPP at Reinforced Section 1..... 163
Figure 6.4 Moment along the length of RPP a. Bending moment, b. Percentage of moment transfer ..... 164
Figure 6.5 Deformation analysis at Reinfroced Secton 2, a. Horizontal Displacement at Crest = 3.25 inch, b. Settlement at the crest of the slope 2.62 inch..... 166
Figure 6.6 Horizontal displacement of 1st 7 row of RPP at Reinforced Section 2..... 166
Figure 6.7 Moment along the length of RPP a. Bending moment, b. Percentage of moment transfer ..... 167
Figure 6.8 Variation of FS with RPP Length and Spacing ..... 170
Figure 6.9 Horizontal Displacement Profile of RPP with Different Spacing a. RPP Length 12 ft, b. RPP Lengh 10 ft, c. RPP Length 8 ft. ..... 172
Figure 6.10 Maximum Horizontal Displacement of RPP at Crest of Slope..... 173
Figure 6.11 RPP Spacing at Top and Bottom Sections of Slope. a. 0.6 m c/c RPP Spacing at Top Section, b. 0.9 m c/c RPP Spacing at Top Section, c. 1.2 m c/c RPP Spacing at Top Section ..... 175
Figure 6.12 Effect of RPP Length and Spacing on Factor of Safety a. RPP Spacing 2 ft. c/c at Top Section b. RPP Spacing 3 ft. c/c at Top Section and c. RPP Spacing 4 ft. c/c at Top Section..... 177
Figure 6.13 Horizontal Displacement Profile for RPP Spacing 2 ft c/c at Top Section ..... 179

Figure 6.14 Horizontal Displacement Profile for RPP Spacing 3 ft c/c at Top Section ..... 180
Figure 6.15 Horizontal Displacement Profile for RPP Spacing 4 ft c/c at Top Section ..... 181
Figure 6.16 Effect of RPP Length and Spacing on Maximum Horizontal Displacement at a. RPP Spacing 2 ft. c/c at Top Section b. RPP Spacing 3 ft. c/c at Top Section and c. RPP Spacing 4 ft. c/c at Top Section ..... 183
Figure 7.1 Static Equilibrium of Individual Slice in the Method of Slices a. Unreinforced Slope, b. Reinforced slope. (Loehr and Bowders, 2007) ..... 188
Figure 7.2 Combined Limit Resistance Curve (Loehr and Bowders, 2007). ..... 188
Figure 7.3 Schematic Diagram of Calculation of Limit Resistance Force: a. Limit Soil Pressure and b. Equivalent Lateral Resistance Force (Loehr and Bowders, 2007) ..... 191
Figure 7.4 Schematic of load over RPP as slope reinforcement ..... 192
Figure 7.5 Flexural Creep at Field Condition (Chen et al., 2007) ..... 193
Figure 7.6 Assumed Region of Plastic Deformation for Theory Proposed by Ito and Matsui (1975) ..... 194
Figure 7.7 Limit Soil Pressure with Depth of RPP ..... 196
Figure 7.8 Schematic Diagram of Failure Mode-1 (Loehr and Bowders, 2007) ..... 197
Figure 7.9 Limit Soil Resistance based on Failure Mode-1 ..... 197
Figure 7.10 Schematic Diagram of Failure Mode-2 (Loehr and Bowders, 2007) ..... 198
Figure 7.11 Limit Soil Resistance based on Failure Mode-2 ..... 199
Figure 7.12 Composite limit resistance curve of Failure Modes 1 and 2 ..... 200
Figure 7.13 Flow Chart for development of design charts ..... 202

Figure 7.14 Soil Model for determination of horizontal displacment with applied load, a. Slope Ratio 2H:1V, b. Slope Ratio 3H:1V, c. Slope Ratio 4H:1V ..... 204
Figure 7.15 Determination of Response of RPP due to Applied Load, a. Maximum Horizontal Displacement, b. Maximum Bending Moment ..... 205
Figure 7.16 Limit Resistance Curve for RPP for c = 200 psf and $\phi = 10^{\circ}$, a. Load vs Horizontal Displacement for Slope 3H:1V, b. Load vs Maximum Flexure for Slope 3H:1V ..... 206
Figure 7.17 Schematic of ordinary method of slice ..... 209
Figure 7.18 Schematic of Reinforced Slope using Ordinary Method of Slice ..... 209
Figure 7.19 Schematic of Infinite Slope approach, a. Unreinforced Slope, b. Reinforced Slope ..... 213
Figure 7.20 Failure Surface of Unreinforced Slope using FEM Analysis, a. Slope 1, b. Slope 2 and c. Slope 3. ..... 216
Figure 7.21 Failure Surface of Unreinforced Slope using Modified Bishop Method, a. Slope 1, b. Slope 2 and c. Slope 3. ..... 217
Figure 7.22 Failure Surface of Unreinforced Slope using Modified Bishop Method, a. Slope 1, b. Slope 2 and c. Slope 3. ..... 219

List of Tables

Table 2.1 Summary of Shear Strength Parameters from drained direct shear tests on specimens subjected to wetting and drying cycles (Rogers and Wright, 1986) ..... 13

Table 2.2 Uniaxial compression test results (Bowders et al., 2003) ..... 39

Table 2.3 Four point bending test results (Bowders et al., 2003) ..... 39

Table 2.4 Average values of specific gravity, modulus, specific modulus, yield stress, ultimate stress and specific strength for each samples type (Lampo and Nosker, 1997) ..... 41

Table 2.5 Engineering properties of plastic lumber properties (Breslin et. al, 1998) ..... 43

Table 2.6 Comparison of flexural properties of typical RPP materials with and without hygrothermal cycling (Krshnaswamy and Francini, 2000) ..... 45

Table 2.7 Three-point bending test results of the RPP samples after weathering (The exposed side was tested in tension) (Lynch et al., 2001) ..... 46

Table 2.8 3-point bending test results of the RPP samples after weathering (The unexposed side was tested in tension) (Lynch et al., 2001) ..... 47

Table 2.9 Summary results of typical compressive creep test (Chen et al., 2007) ..... 54

Table 2.10 Summary of Flexural Creep test result (Chen et al., 2007) ..... 55

Table 2.11 Summery of failure mode to establish the limit resistance curve (Loehr and Bowders, 2007) ..... 60

Table 3.1 Soil Parameters ..... 91

Table 3.2 Soil Strength Parameters for Loop 12 Slope ..... 98

Table 4.1 Average RPP Driving Time at US 287 Slope ..... 109

Table 4.2 Average RPP driving time at Loop 12 Slope ..... 113

Table 5.1 Instrumentation Detail (According to Hossain, J. (2012)) ..... 121
Table 5.2 Summary of cost of slope stabilization using recycled plastic pin in US 287 slope ..... 156
Table 6.1 Parameters from FE analysis ..... 160
Table 6.2 Numerical Model Matrix for Parametric Study ..... 168
Table 6.3 Numerical Modeling Matrix ..... 175
Table 7.1 Summary of Soil Failure Mode for Establishing Limit Lateral Resistance of RPP ..... 190
Table 7.2 Parameters for Estimating Limit Soil Pressure ..... 195
Table 7.3 Consideration for the Development of Design Chart ..... 201
Table 7.4 Soil Parameters ..... 201
Table 7.5 Parameters from FE analysis ..... 205
Table 7.6 Soil Properties and Geometry for Validation of Design Method ..... 215
Table 7.7 Factor of Safety of Unreinforced Slope using Different Methods ..... 218
Table 7.8 Limit Resistance of RPP ..... 219
Table 7.9 Factor of Safety of Unreinforced and Reinforced Slope for Allowed Horizontal Displacement 1 inch ..... 220
Table 7.10 Factor of Safety of Unreinforced and Reinforced Slope for Allowed Horizontal Displacement 2 inch ..... 220

# Chapter 1

# Introduction

## 1.1 Background

The slope failure and landslide cause significant hazards to public and private sectors. According to Turner and Schuseter, (2006), the total cost for maintenance and repair of major U.S. highways exceed $100 million annually. The US highways are only 20% of the total road network which also require maintenance due to landslides. Moreover, there are indirect costs and loss of revenue associated with landslides, such as the use and access to facilities which sometime exceeds the direct cost (Turner and Schuster, 1996). Another significant, but generally neglected, loss of landslides is the costs associated with routine maintenance and repair of "surficial" slope failures (Loehr and Bowders, 2007). The depths and plan dimensions of surficial failure vary with soil type and slope geometry and are generally characterized by sliding depths of less than 10 ft. However, the 3 ft to 6 ft depth become very common (Loehr and Bowders, 2007). Tumer and Schuster, (1996) conservatively estimated the cost to repair of shallow slides which was equal or even greater than the costs associated with repair of major landslides. In addition, shallow failure often cause significant hazards to infrastructure such as guard rail, shoulder, portion of roadways, and if not properly maintained, it requires more extensive and expensive repairs (Loehr et al., 2007).

Moderate to steep slopes and embankments underlain by expansive clayey soils are known to be susceptible to shallow land slide during intense and prolonged rainfall events. Typically, failure occurs due to an increase in pore water pressure and reduction of soil strength due to progressive wetting of soil near-surface soil. This condition is further exacerbated by moisture variations due to seasonal climatic changes which results cyclic shrink and swell of the upper soils. The shrinkage cracks act as a conduit

for surface water infiltration from rainfall (McCormick and Short, 2006). Due to the wetting drying cycle, sloughing and shallow slope failures are predominant in the North Texas area and posses a significant maintenance problem to the Texas Department of Transportation (TxDOT).

The conventional slope stabilization technique includes installation of drilled shaft, replacement of slope using retaining wall, installation of soil nail and reinforcing the slope using geogrids. However, the conventional techniques are might be expensive in some instances for the repair of shallow slope failure. A recent innovation in stabilization of shallow slope failure includes the installation of recycled plastic pin (Parra et al., 2004), Plate pile stabilization (Mccormick and Short, 2006) and reinforcing slope using small diameter piles (Thompson and White, 2006) showed great potential in terms of cost and effectiveness.

Recycled Plastic Pin (RPP) had been utilized in the state of Missouri and Iowa as cost effective solution for the stabilization of shallow slope failure (Loehr and Bowders, 2007). RPPs are predominantly a polymeric material, fabricated from recycled plastics and other waste materials (Chen et al., 2007, Bowders et al., 2003). RPP is composed of High Density Polyethylene, HDPE (55% – 70%), Low Density Polyethylene, LDPE (5% - 10%), Polystyrene, PS (2% – 10%), Polypropylene, PP (2% -7%), Polyethylene-terepththalate, PET (1%-5%), and varying amounts of additives i.e. sawdust, fly ash (0%-5%) (Chen et al., 2007, McLaren, M. G., 1995; Lampo and Nosker, 1997).

RPPs are installed in the slope to intercept potential sliding surfaces which provided additional resistance to maintain the long term stability of the slope. It is a light weight material and is less susceptible to chemical and biological attack, resistant to moisture, required almost no maintenance, thus making it an attractive alternative compared to other structural materials (Krishnaswamy and Francini, 2005). Use of plastic

pin reduces the waste volume entering the landfill and provides additional market for recycled plastic (Loehr et al. 2000).

## 1.2 Problem Statement

Previous study was conducted over past few years to stabilize shallow slope failure using RPP and offered great potential as an effective alternative technique. In addition, a limit state design technique is available in the literature that considers the resistance from the RPP to resist the shallow slope failure. However, the design technique was limited where geotechnical engineers need to develop the limit design chart before performing the design. In addition, the design procedure lacks any information about the deformation of the RPP as well as the stabilized slope.

It is imperative to develop an effective design protocols to design the slope stabilization using RPP that will connect different important parameters such as the length and spacing of RPP, the height and angle of slope, and the soil parameters. Moreover, the creep of the RPP is an important consideration for structural use and should be included for the design consideration.

The slope stability analysis by elasto-plastic finite element (FE) is robust and simple method. The graphical presentation of the FE program allows better understanding of the failure mechanism (Griffiths and Lane, 1999). The shear strength reduction finite element method had been successfully used to evaluate the stability of slopes reinforced with piles and anchors (Wei and Cheng, 2009; Yang et al., 2011, Cai and Ugai, 2003). This technique was utilized to evaluate the stability of slopes reinforced with piles or anchors under a general frame, where soil-structure interactions are considered using zero thickness elasto plastic interface element. However, no pervious study was conducted using the FEM method using the RPP. On the other hand, the FEM

analysis can be effectively utilized to observe the influence different length and spacing of RPP on the factor of safety and deformation of the stabilized slope.

## 1.3 Research Objectives

The overall objective of the current study was to establish a sustainable slope stabilization technique and establishment of an optimum design method for shallow slope failure using Recycled Plastic Pin. The specific objective of the study included:

- Site Investigation and selection of full scale study area.
- Material selection and Experimental study on Recycled Plastic Pin
- Development of preliminary slope stabilization scheme using RPP based on FEM analysis.
- Field Installation of RPP.
- Instrumentation of the RPP stabilized slope to evaluate the performance.
- Performance monitoring of the study area.
- Optimization and calibration of preliminary FEM analysis with field performance results.
- Numerical Study on RPP length and spacing on factor of safety and deformation of slope.
- Development of a design standard for slope stabilization using RPP.

## 1.4 Thesis Organizations

The thesis is divided into eight chapters that can be summarized as follows:

Chapter 1 provides an introduction, presents the problem statement and objective of the study.

Chapter 2 presents different techniques of slope stabilization to stabilize shallow failure. The chapter also included a review of the manufacturing method, physical properties, strength and modulus of recycled plastic pin for structural application as well

as for slope stabilization. Finally, few case studies and performance monitoring results of highway slope stabilization using RPP is enclosed in the chapter.

Chapter 3 describes the details of site investigation of two highway slopes that are located over highway US 287 and highway Loop 12. The chapter described the details of site investigation program that included the soil test boring, laboratory testing and geophysical investigation using resistivity imaging. The strength parameters of the slope at failure condition were back calculated using FEM analysis and presented in Chapter 3.

Chapter 4 presents the mechanisms of slope stabilization using recycled plastic pin. The chapter presents an experimental study to determine physical properties of recycled plastic pin with different loading rate for slope stabilization. Based on the strength properties of RPP, the slope stabilization scheme using RPP was developed for both slopes. Finally, the installation process of RPP for slope stabilization is enclosed.

Chapter 5 depicts the instrumentation and performance evaluation of the reinforced slope. The chapter described the methods utilized to monitor the performance of the stabilized slope. The reinforced and unreinforced slope was monitored periodically and the results of the performance of the slope are also reported in the chapter.

Chapter 6 demonstrated a numerical study on the performance of the stabilized slope. A parametric study on the effect of the length and spacing of RPP of the reinforced slope is utilized and a comparison between the field study and the numerical analysis is presented.

Chapter 7 described the development of a design method for slope stabilization using RPP. The design method consider three limiting criteria which included the failure of soil adjacent to RPP as well as the horizontal displacement and creep stress of RPP.

Finally the chapter introduced the design steps and presented a comparison of factor of safety with the finite element method.

Chapter 8 summarizes the main conclusions from the current research and provides recommendation for future work.

# Chapter 2

# Literature Review

## 2.1 Slope Failure

Slope failures are common occurrences in soils. Usually, failures occur after prolonged rainfall events which lead to the reduction of soil strength (Titi and Helwany, 2007). Sometimes, slope failures take place after showing warning signs; however, they can also fail without any warning. Slopes are generally characterized as stable when the shear strength of the soil provides enough resisting force against the gravitational forces that are trying to move the soil mass down slope. Therefore, the stability of slope is governed by the balance between the driving and resisting forces. Changes in these forces may lead to the loss of slope stability and subsequent slope failure. An increase in driving (gravitational) forces can be triggered by changes in slope geometry, seepage pressure, or added surcharge from traffic loads on highway embankments (Titi and Helwany, 2007). On the other hand, reduction in resisting forces can take place due to increased pore water pressure as water perches on impermeable underlying soil layers.

Slopes fail when the soil mass between the slope surface and slip surface moves toward down slope. According to Titi and Helwany, (2007), the soil movement and depth of slip surface depends on the type of soil, soil stratification, slope geometry, and presence of water. Abramson et al. (2002) described typical slides that can occur in clay soils, such as (1) translational, (2) plane or wedge surface, (3) circular, (4) noncircular, and (5) a combination of these types. The different slope failure types are illustrated in Figure 2.1.

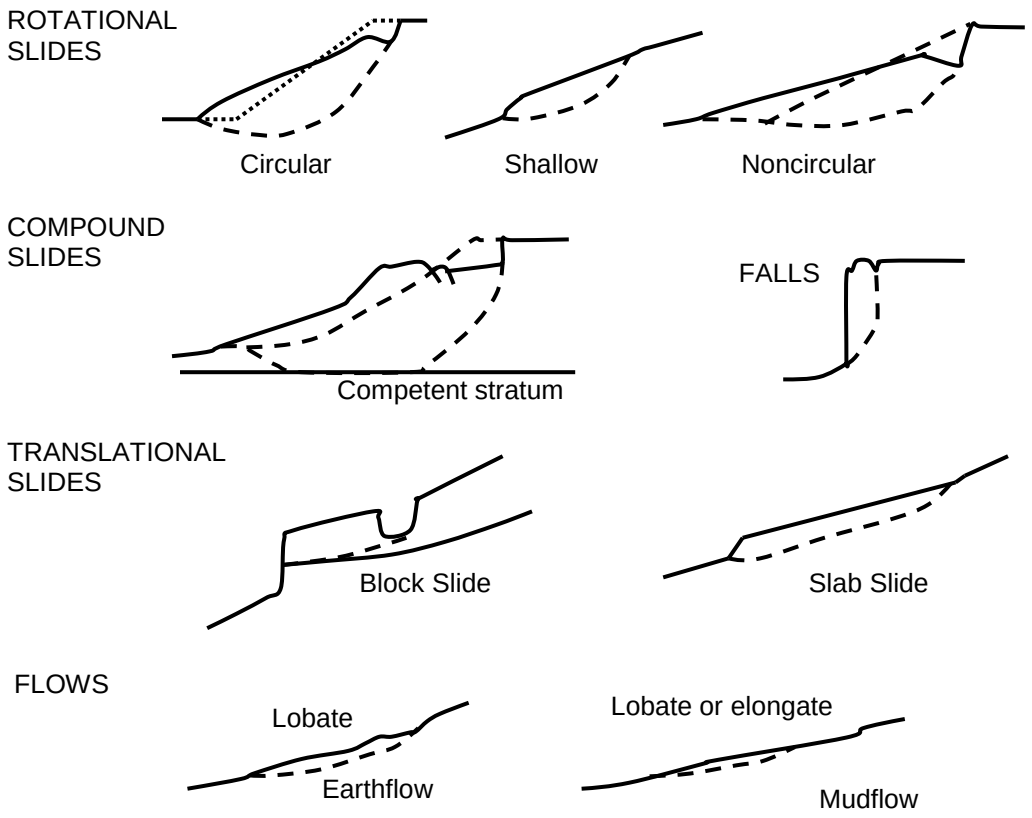


Figure 2.1 Types of Clay movement (redrawn after Abramson et al., 2002)

Design of stable slope require a rational selection and use of a factor of safety that accounts for the various uncertainties associated with the determination of soil strength, distribution of pore pressures, and soil stratification. It is suggested to consider a high factor of safety of slope when the level of soil investigation is of low quality and the experience of the engineer is limited (Abramson et al., 2002).

The factor of safety of slope is calculated by comparing the available shear strength along a potential slipping plane with the equilibrium shear stress that is needed to maintain a just-stable slope. The factor of safety is assumed to be constant along the slip surface and can be defined in terms of stresses (total and effective), forces, and moments, selecting a factor of safety for a typical slope design depends on many factors,

including the level and accuracy of soil data, the experience of the design engineer and the contractor, level of construction monitoring and consequence of slope failure (risk level) (Titi and Helweny, 2007). For a typical slope design, the required factor of safety ranges between 1.25 and 1.50 (Abramson et al., 2002).

## 2.2 Shallow Slope Failure

Surficial failures of slopes are quite common throughout the United States. Shallow slope failure refers to surficial slope instabilities along highway cut and fill slopes and embankments. These instabilities commonly occur in fine-grained soils, especially after prolonged rainfalls. The surficial failure by definition is shallow with the failure surface usually at a depth of 4 ft or less (Day, R. W., 1989). In many cases, the failure surface is parallel to the slope face as illustrated in Figure 2.2.

Shallow slope failures generally do not constitute a hazard on human life or cause major damage. However, it can constitute a hazard to infrastructure by causing damage to guardrails, shoulders, road surface, drainage facilities, utility poles, or the slope landscaping (Titi and Helwany, 2007). In some cases, shallow slope failures can have impact on regular traffic flow if debris flows onto highway pavements. Moreover, shallow slope failures can have an economic impact on the highway agencies at the local/district level. In general, the repairs of shallow slope failures are conducted at the district and local levels and often performed by maintenance crews as routine maintenance work. In many cases, such repairs may provide a temporary fix of slope failures as the slope failure generally reoccurs after a rainfall season (Titi and Helwany, 2007).

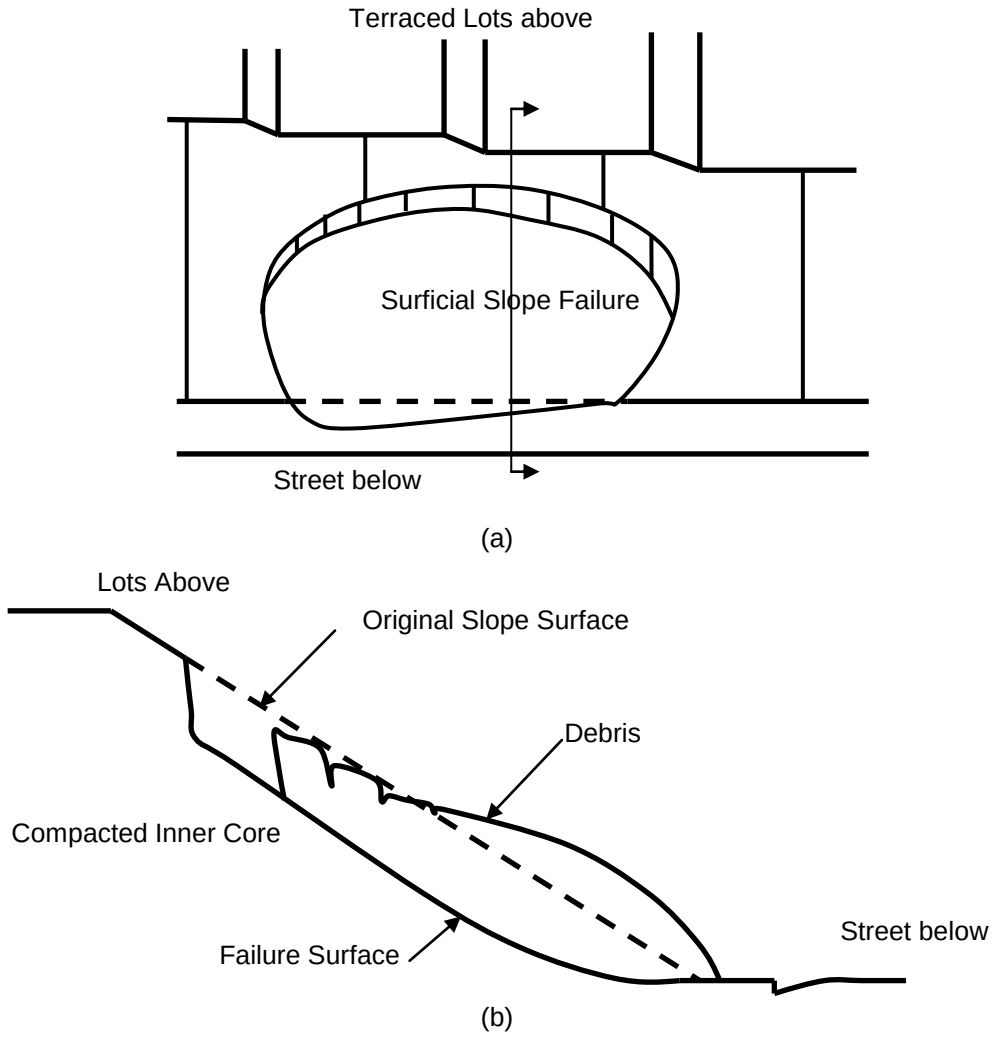


Figure 2.2 Typical surficial slope failures (redrawn after Day, R. W. 1989)

In general, the shallow slope failures vary in depth and extent of the failed area. The depth and extend of shallow slope failures largely depends on slope geometry, soil type, degree of saturation of soil, seepage and climatic condition (Titi and Helwany, 2007). According to Abramson et al., (2002), many shallow slope failures occur when the rainfall intensity is larger than the soil infiltration rate and the rainfall lasts long enough to saturate the slope up to a certain depth, which leads to the buildup of pore water pressure at that depth.

Shallow slope failures often are parallel to the slope surface and usually are considered as infinite slope failures. Various depths were reported in the literature based on case histories, but all studies indicated a shallow nature of surficial failures. Evans, D. A. (1972), cited in Titi and Helwany, (2007), defined the failure surface depth of shallow slope to be equal to or less than 4 ft. According to Loehr et al. (2000), the depth of shallow slope failure as less than 10 ft, however, in general it varies in between 3 ft to 6 ft. According to Titi and Helwany, 2007, the recommended shallow failure depth ranges from approximately 2 to 4 ft.

### 2.3. Fully Soften Clay of High Plastic Clay Soil

Moderate to steep slope constructed on high plasticity clay is susceptible to the softening behavior at the top soil due to wet-dry cycle. The fully softened shear strength corresponds to the shear strength of high plastic clay seems to develop over time due to the wetting and drying cycle (Wright, S. G., 2005). Skempton (1977) first proposed the concept of fully softened strength for natural and excavated slopes in the London Clays. Skempton (1977) reported that over time the strength of slopes in the highly plastic London Clay lost strength, eventually reaching what Skempton termed as “fully-softened” strength which lies between peak and residual strength as presented in Figure 2.3. Skempton (1977) indicated that the fully-softened strength is comparable to the shear strength of the soil in a normally consolidated state.

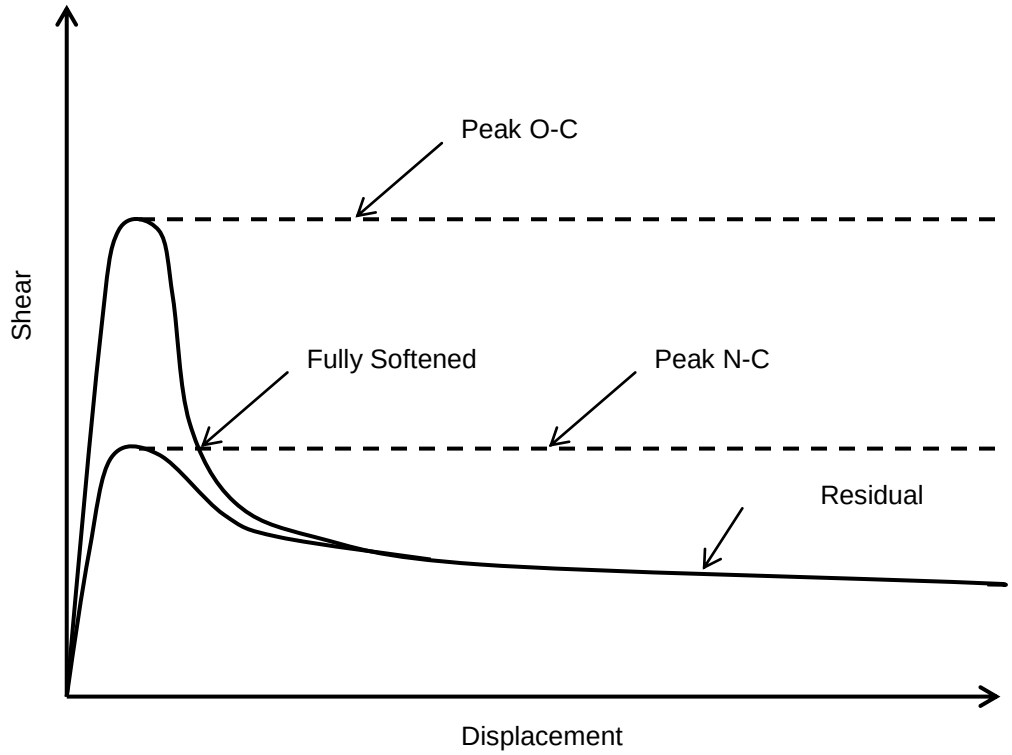


Figure 2.3 Comparisons of peak, residual and fully softened shear strength (redrawn after Skempton, 1970)

Rogers and Wright (1986) conducted a study to investigate the failure of slope constructed over highly plastic clay soil in Texas. The author reported that the high plasticity of the clays involved the shrink-swell characteristics which make it probable to the repeated wetting and drying in the field which might be one sources of the softening. Accordingly, Rogers and Wright (1986) performed direct shear tests on specimens that were subjected to repeated cycles of wetting and drying. These tests were all performed on the clay from the Scott Street and I. H. 610 site in Houston, Texas identified as the red clay. Four series of drained direct shear tests were performed on specimens subjected to 1, 3, 9 and 30 cycles of wetting and drying. Shear strength parameters obtained from the study are summarized below in Table 2.1.

Table 2.1 Summary of Shear Strength Parameters from drained direct shear tests on specimens subjected to wetting and drying cycles (Rogers and Wright, 1986)

| Number of Wet-Dry Cycles | Cohesion, c (psf) | Friction Angle, Φ |
|---|---|---|
| 1 | 29 | 23˚ |
| 3 | 77 | 26˚ |
| 9 | 33 | 25˚ |
| 30 | 0 | 27˚ |

Rogers and Wright (1986) reported that cyclic wetting and drying of the soil produces a significant shear strength loss, particularly in terms of effective cohesion intercept, c'. The direct shear test also indicated that the loss in cohesion occurs within a relatively few numbers of cycles of wetting and drying. In fact, most of the loss in strength occurred on the first cycles. However, Rogers and Wright suggested that the wetting and drying that specimen were subjected to in laboratory was much severe compared to that expected to occur during any wetting and drying cycles in the field. Even so, the effects of wetting and drying in laboratory and field are believed to be similar.

Kayyal and Wright (1991) developed a new procedure for triaxial specimens subjected to repeated cycles of wetting and drying. The procedure allowed the specimens to have greater access to moisture and exposure for drying. In addition, the procedure allowed substantial lateral expansion and volume change to occur in the soil during drying. Two soils were tested during the study are Red clay or Beaumont clay from Houston, Texas and Highly plastic clay soil from Paris, Texas.

Kayyal and Wright (1991) conducted several series of consolidated undrained compression tests with pore pressure measurement. Tests were performed on

specimens subjected to repeated wetting and drying on specimens as well as on freshly compacted samples. Based on the study, the shear strength envelops for specimens of Beaumont clay and Paris clay tested in the as-compacted and after wetting and drying is presented in Figure 2.4. The results presented that both envelops were distinctly nonlinear. In addition, the strength envelope for the specimens subjected to wetting and drying cycles lied significantly below the envelope for the specimens tested in the as-compacted condition at lower values of normal stress. Moreover, the intercept of the strength envelope for specimens subjected to wetting and drying is small and could be considered negligible.

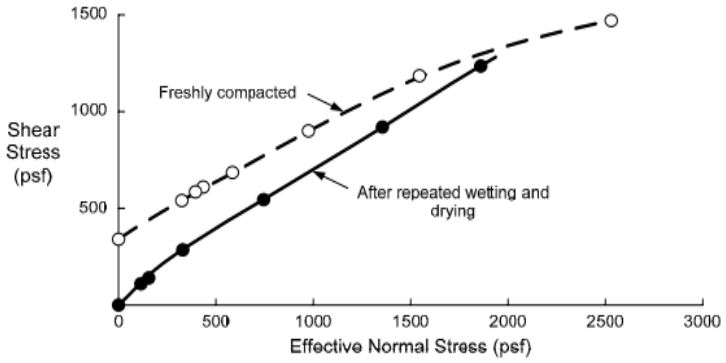


(a)

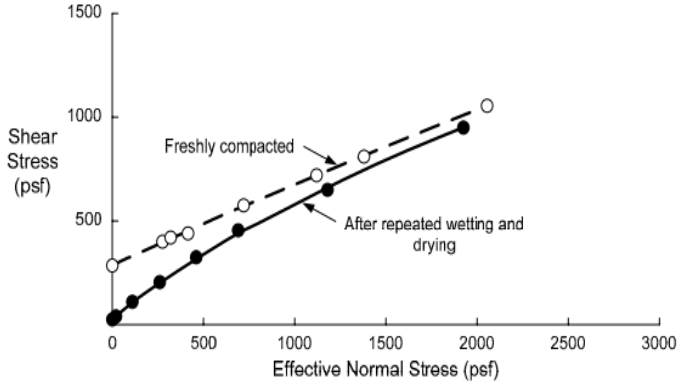


(b)

Figure 2.4 Shear strength envelopes in terms of effective stress a. Beaumont clay, b. Paris clay (Kayyal and Wright, 1991)

Zornberg et al. (2007) also reported the shear strength of Eagle Ford clay from triaxial compression test with pore pressure measurement that had experienced seasonal wetting and drying in the field. In addition, the study presented the comparison between the sample tested in as compacted samples, normally consolidated slurry and specimens subjected to wetting and drying cycles. The specimens were subjected to a total of 20 wetting and drying cycles. Based on the study, the stress strain response as well as the modified Mohr Column failure envelop of Eagle Ford shale with 3 different conditions are presented in Figure 2.5 and Figure 2.6, respectively.

Zornberg et al. (2007) reported that a higher effective consolidation pressure, more softening occurred for as compacted samples once the peak strength was reached. On the other hand, the observed modified Mohr Failure envelope was almost linear. The stress strain curves showed a decrease in stress after the peak principal stress difference was reached on normally consolidated samples from slurry. A scatter in the data for the normally consolidated samples was observed, however, the modified Mohr Column failure envelope was curved at low effective stresses. The study also reported that a zero value in cohesion intercept is generally expected for normally consolidated clay unless the soil is cemented.

The stress-strain curves for specimens subjected to cyclic wetting and drying were not appeared to be as brittle-like as for the as-compacted specimens. In addition, the stress paths for the specimens subjected to cyclic wetting and drying appear very similar to the specimens normally consolidated from slurry. The modified Mohr failure envelope also showed curvature, and it appeared that cohesion is negligible for specimen subjected to wet-dry cycles.

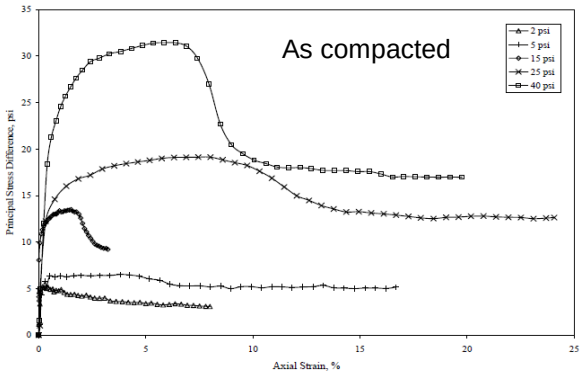


(a)

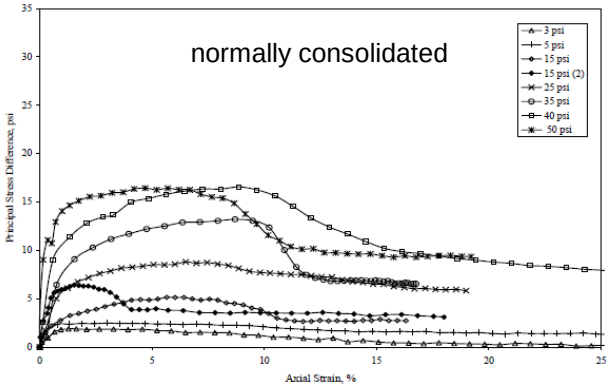


(b)

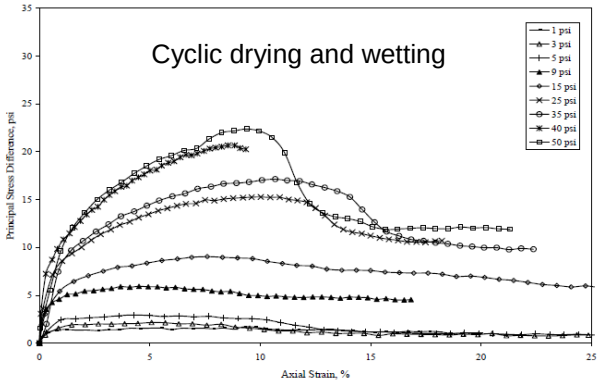


(c)

Figure 2.5 Stress strain curve of Eagle Ford Shale a. as compacted, b. normally consolidated, c. specimen subjected to cyclic drying and wetting (Zornberg et al., 2007)

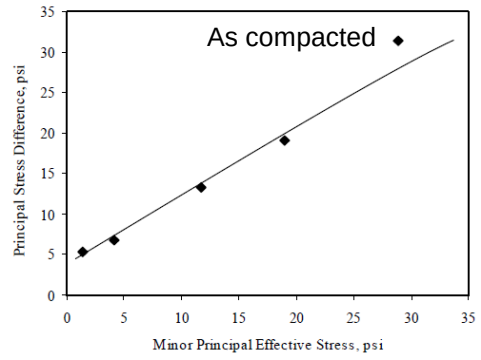


(a)

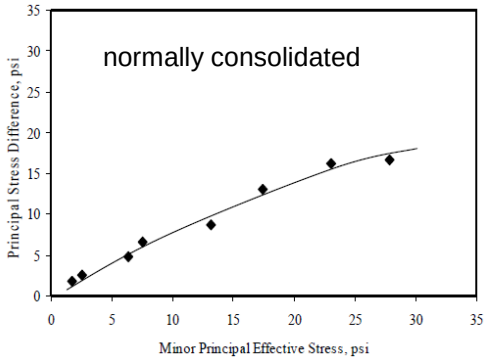


(b)

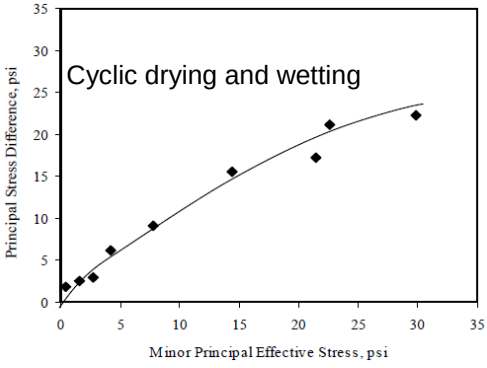


(c)

Figure 2.6 Modified Mohr Failure envelop of Eagle Ford Shale a. as compacted, b. normally consolidated, c. specimen subjected to cyclic drying and wetting (Zornberg et al., 2007)

Wright S. G. (2005) reviewed different research projects on slope and embankments constructed on highly plastic clay soil in Texas. Wright reported that the compacted high plastic fills are generally very strong immediately after construction. In general, at the end of construction the factors of safety probably exceeds 2, though, the soils tend to soften and weaken over time. As a result, the factor of safety decreases to values that approach 1, i.e., failure. The softening is probably enhanced by the repeated expansion and shrinkage which take place due to seasonal wetting and drying of the soil, respectively. The fully-softened strength of the soil is best characterized by a curved Mohr failure envelope. In addition, the failure envelope for fully-softened conditions lies below the failure envelope for the soil immediately after compaction. As the slope failure is a common occurrence due to the extreme weather condition in Texas, it is important to utilize a slope stabilization method which should be cost effective as well as require less maintenance after installation. Different slope stabilization methods are currently available into the literature which is utilized in different states in USA. A brief summary of different slope stabilization methods are presented in the subsequent sections.

## 2.4 Method of Repair of Shallow Slope Failure

Different repair methods are used to stabilize surficial slope failures. Selection of an appropriate repair technique depends on the importance of the project (consequence of failure), budget availability, site access, slope steepness, the availability of construction equipment and experienced contractors. The most commonly used method to repair surficial failures is to rebuild the failed area by pushing the failed soil mass back and re-compact it.

Mechanical stabilization techniques utilize rock, gabion baskets, concrete, geosynthetics, and steel pins to reinforce slopes. These techniques can provide stability to both cut and fill slopes (Fay et al., 2012). Mechanical stabilization techniques include

retaining walls, mechanically stabilized earth, geosynthetically reinforced soil, and other in-situ reinforcement techniques. For anchoring shallow soils, use of in-situ earth reinforcements and recycled plastic pins has been reported in slope stabilization (Pearlman et al. 1992; Loehr et al. 2000).

Earthwork techniques involve the physical movement of soil, rock, and/or vegetation for the purpose of erosion control and slope stabilization. It involves reshaping the surface slope by methods such as creating terraces or benches, flattening over-steepened slopes, soil roughening, or land forming. In addition, earthwork techniques can be used to control surface runoff and erosion and sedimentation during and after construction. (Fay et al., 2012). The different techniques available in the literature as well as few case studies to stabilize surficial slope failure are presented below.

*2.4.1 Rebuild Slope*

Rebuild the slope considers of rebuilding the failed zone through compaction. This method consists of air-drying the failed soil, pushing it back to the failure area, and re- compacting it. Rebuilding the slope is considered one of the most economical methods of repair and is performed as routine maintenance work on failed slopes. However, this method is not very effective, particularly in clays as it does not significantly increase the shear strength of the re-compacted soil, especially when the soil becomes wet again (Titi and Helwany, 2007)

*2.4.2 Pipe Pile and Wood Lagging*

This repair method considers installation of Pipe Pile and wood logging system in the failed zone which provides resistance along the failed soil mass. During the process, the failed debris of the site are disposed in a different places followed by cutting benches into the natural ground below the slip surface. Galvanized steel pipe piles are then installed (driven or placed in pre-drilled holes) and filled with concrete. Wood lagging

(pressure treated) is placed behind the piles and a drainage system is then built behind the wood. A selected fill is compacted in layers and the face of the slope is protected with erosion control fabric and landscaping (Day, R. W., 1996). The schematic of pipe pile and wood lagging is presented in Figure 2.7.

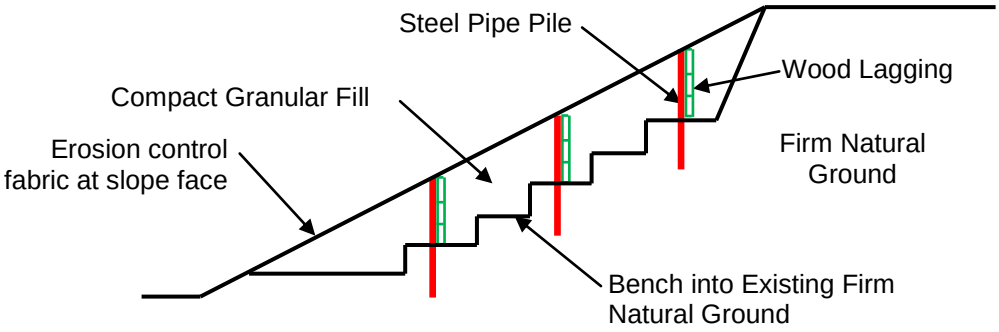


Figure 2.7 Schematic of Pipe pile and wood lagging repair (Day, R. W. 1996)

One of the disadvantages of this method is that lateral soil pressure against the wood lagging is transferred directly to the pipe piles, which are small in diameter and have low flexural capacity and low resistance to lateral loads. Pile failure in bending is a common occurrence in this repair method (Titi and Helwany, 2007).

*2.4.3 Geogrid Repair*

Geogrids are fabricated from high density polyethylene resins. It has open structure which allows interlocking with granular materials used to rebuild slope failures. According to Day, R. W., (1996), repair of surficial slope failures using geogrid materials consists of complete removal of the failed soil mass. Benches are then excavated in the undisturbed soil below the slip surface. Vertical and horizontal drains are installed to collect water from the slope and dispose it off-site. Finally, the slope is built by constructing layers of geogrid and compacted granular material. The schematic of Geogrid repair is presented in Figure 2.8.

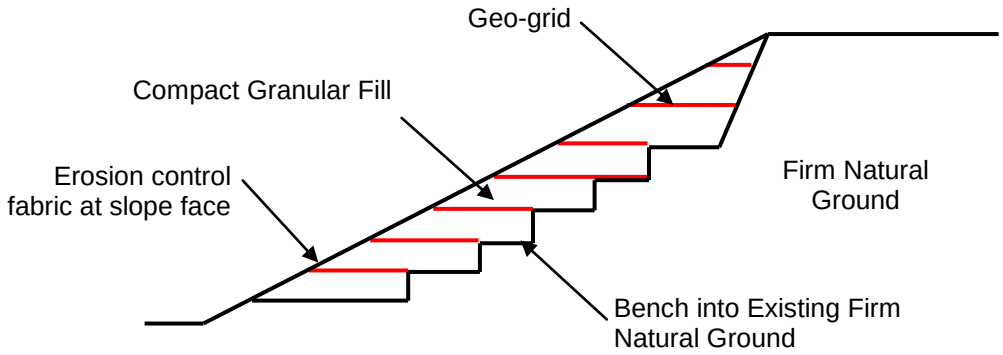


Figure 2.8 Repair of Surficial slope failure by Geogrid (Day, R. W. 1996)

*2.4.4 Soil Cement Repair*

The soil cement repair for shallow slope failure is conducted by excavation and removal of the failed zone similar to the geogrid repair. Benches are then excavated in the undisturbed soil below the slip surface and drains are installed to collect water from the slope and dispose it off-site. Granular fill material usually is mixed with cement (~6%) and the mix is compacted to at least 90% of modified Proctor maximum unit weight (Day, R. W., 1997). The soil-cement mix will develop high shear strength and lead to slope with higher factor of safety. The schematic of the soil cement repair is presented in Figure 2.9.

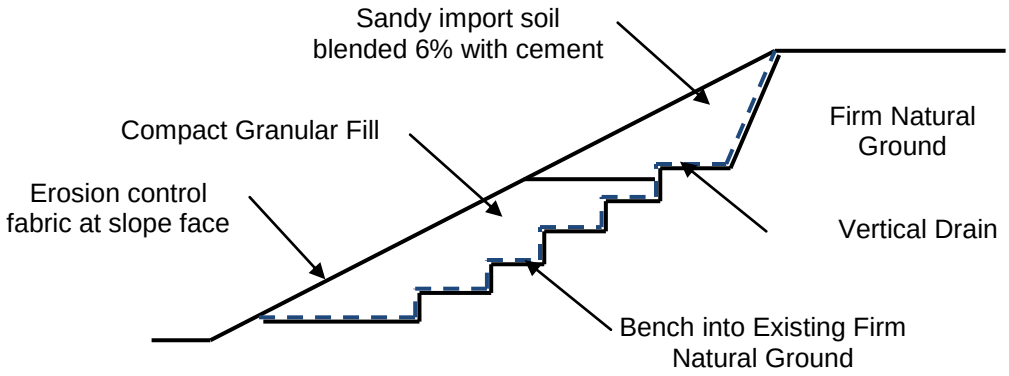


Figure 2.9 Soil cement repair of shallow slope failure (Day, R. W. 1996)

*2.4.5 Repair Using Launched Soil Nails*

Soil nails are inserted into the slope face at a high speed utilizing high pressure compressed air. During the technique, the soil nails are installed in staggered pattern throughout the failed zone which provide resistance along the slipping plane and increase the factor of safety as presented in Figure 2.10. Typical soil nails can be solid or hollow steel bars, however, galvanized soil nails also can be used in highly abrasive environments as they provide resistance to corrosion. Typical hollow non-galvanized steel bars have an outer diameter of 1.5 in. (0.12 in wall thickness) and length of 20 ft., The suggested minimum yield strength of the steel bars is 36 ksi (Titi and Helwany, 2007). After installing launched soil nails, the slope surface can be treated with erosion mat, steel mesh, and shotcrete.

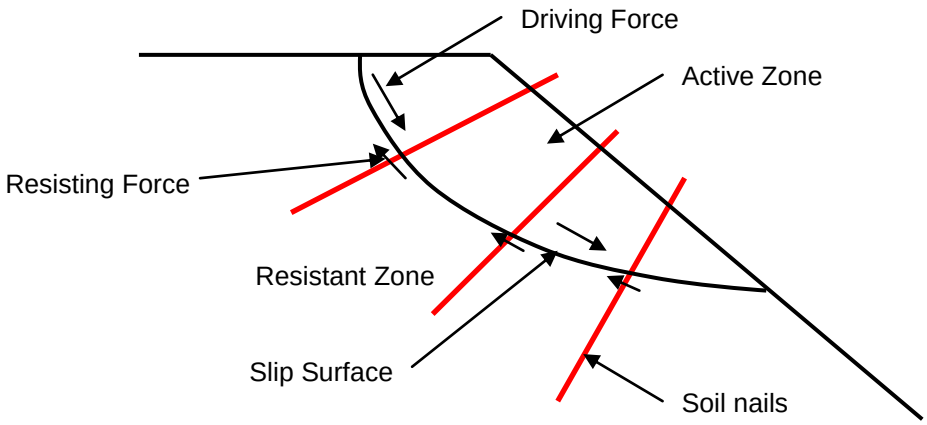


Figure 2.10 Schematic of Repair of soil nails in slope stabilization (replotted after Titi and Helwany, 2007)

*2.4.6 Earth Anchors*

Earth anchors have been used in many geotechnical applications including stabilizing surficial slope failures. Earth anchoring systems consist of a mechanical earth anchor, wire rope/rod and end plate with accessories. Repair of surficial slope failures

with earth anchoring systems starts with regarding the failed slope. The earth anchors are installed by pushing the anchor into ground below the failure surface and wire tendon of the anchor is pulled to move the anchors to its full working position. The wire tendon is locked against the end plastic cap (end-plate) and the system is tightened. A schematic of earth anchors for stabilizing shallow slope failure is presented in Figure 2.11.

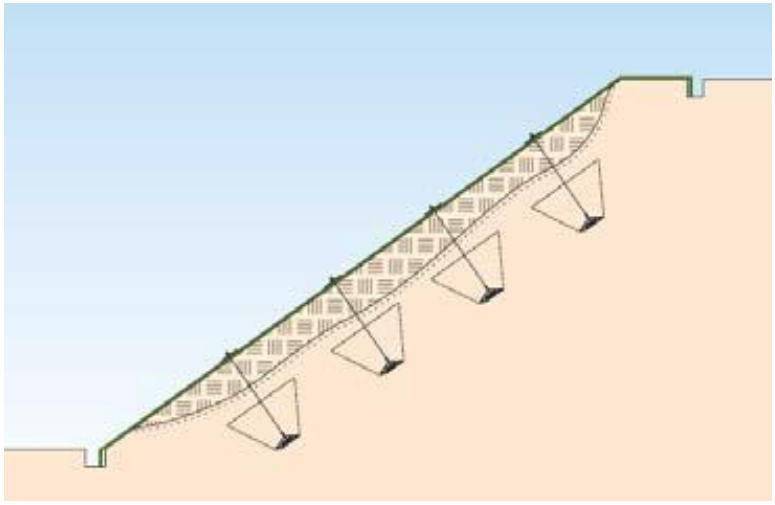

Figure 2.11 Earth Anchors in slope stabilization (Titi and Helwany, 2007)

*2.4.7 Geofoam*

Geofoam is generic term of rigid cellular polystyrene, is highly used in geotechnical applications and has provided solutions worldwide to many difficult sub soils. The most common type of geofoam are expanded polystyrene (EPS) and extruded polystyrene (XPS). EPS is formed with low-density cellular plastic solids that have been expanded as lightweight, chemically stable, environmentally safe blocks. It generally behaves like elastoplastic strain hardening material. The unit weights of the material ranged from 0.7 to 1.8 pcf and have compression strength ranged between 13 psi to 18 psi.

Jukofsky et al., (2000) performed a case study of a problematic highway slope over route 23A at New York State which was stabilized using EPS type Geofoam. At the beginning of the study, the author performed various stabilizing treatments including a berm, lowering the grade, realignment away from the failure area, lightweight aggregate, and stone columns; however, the alternatives were observed as impractical, environmentally sensitive, cost-prohibitive or all three. Based on slope stability analysis using Bishop Method, it was observed that by replacing the top 9 ft of soil, the factor of safety of the slope increased to 1.25. The designed stabilization scheme is presented in Figure 2.12. The stabilized slope was monitored using inclinometer, extensometers, piezometers and thermistors to determine the seepage pressure, change of temperature, lateral displacement and subsurface slope movement.

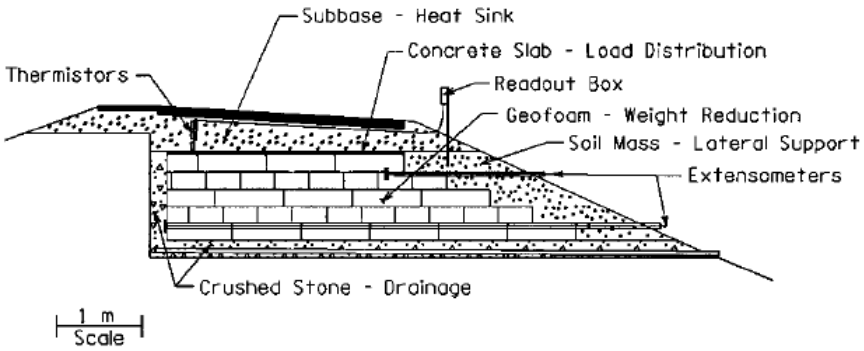


Figure 2.12 Typical section of treatment.

The field observation presented that there was no change is water table and pore pressure through piezometer results. The inclinometer result presented a 4.3 inch movement during installation due to vibration; however, no post construction lateral movement had taken place. In addition, the extensometer presented negligible movement between the geofoam after construction.

Based on the temperature reading from different thermistors installed at different location, the author observed that the ground temperatures near the bottom of the subbase layer remain nearly constant with time and not responding much to change in air temperature and no differential icing had taken place. On the other hand, the typical pavement surface had significant change in temperature with differential icing problems.

Finally, the author concluded that use of geofoam to reduce the driving force of a slope provided effective results in stabilizing the slope at the New York State Route 23A site. In addition, no movement was observed since the treatment was completed, the differential icing problem was addressed and no such phenomenon occurred over the roadway.

*2.4.8 Wick Drains*

Santi, et al. (2001) evaluated horizontal geosynthetic wick drains with a new installation method to determine an effective option to stabilize landslides by reducing amount of water that it contains. Horizontal wick drains are inexpensive; resist clogging and may be deformed without rupture thereby offers several advantages over conventional horizontal drains. A study was conducted by the Santi, et al. (2002) where 100 drains were installed at eight sites in Missouri, Colorado and Indiana using bulldozers, backhoes and standard wick drain driving cranes. The study indicated that drains have been driven 100 ft through soil with standard penetration test values as high as 28. In addition, both experience and research indicate that drains should be installed in clusters that fan outward, aiming for average spacing of 25 ft apart for typical clayey soils.

Santi, et al. (2001) first installed and tested the effectiveness of horizontal wick drains during 1998 in an instrumented embankment in Rolla, Missouri. The embankment which had the slope ratio 1:1 was instrumented with 6 piezometers, 16 nested soil

moisture gauges and 20 survey markers. One half of the slope was stabilized using six wick drains, whether, other half of the slope was kept as control section. The influence of the wick drain was tested by artificial simulation of 100 year, 24 hour rainfall using sprinkler. The result indicated that the wick drain removed substantial amount of water from the slope, thereby lowering the ground water level by 1 ft resulted significant less movement in the stabilized zone. Following to the test sites, the author stabilized several locations with varying geology using various driving equipment. No evidence of clogging by dirt or algae was observed after installation and the stabilization scheme was performing better.

Based on the experience, Santi et al. (2001) suggested that the drains should not extend more than 10 ft to 18 ft beyond the existing or potential failure surface. In addition, the drains should be installed horizontally, in clusters that fan outward within 25 ft spacing. During installation, the smear zone was created that reduce the flow of water. The smear zone could be reduced by pushing pipe that containing the drain, instead of using pounding or vibration method. However, the wick drains have few limitations. For the successful use of wick drains to be driven, the recommended SPT value is 20 or less. The maximum drain length is expected to be 100 ft for harder soils and 150 to 200 ft for soft soils. In addition, there could be a significant number of dry drains on a project.

*2.4.9 Anchored Geosynthetic Systems (AGS)*

Vitton et al. (1998) conducted a study using a comparatively new slope stabilization technique, known as Anchored geosynthetics system (AGS) to evaluate and provide cost effective and more efficient alternatives for landslide remediation. The basic function of an AGS is to provide active stabilization of the slope by tensioning a geosynthetics over a slope with ground anchors. As the soil beneath the geosynthetics deforms, membrane stresses develop in the tensioned geosynthetics and impart a

compressive load over the slope that increase the factor of safety of slope. Anchorage of the geosynthetics is achieved with small-diameter, ribbed steel rebars which are driven into the soil with hand-held vibro-percussion hammer in a grid pattern through the geo-synthetic at right angle to the top surface of slope. The geosynthetics then is fastened to the anchor and the anchor is driven the remaining distance, thereby tensioning the geosynthetics and creating a curved geosynthetics-soil interface thereby impart a compressive stress over the soil. The schematic of the AGS is presented in Figure 2.13.

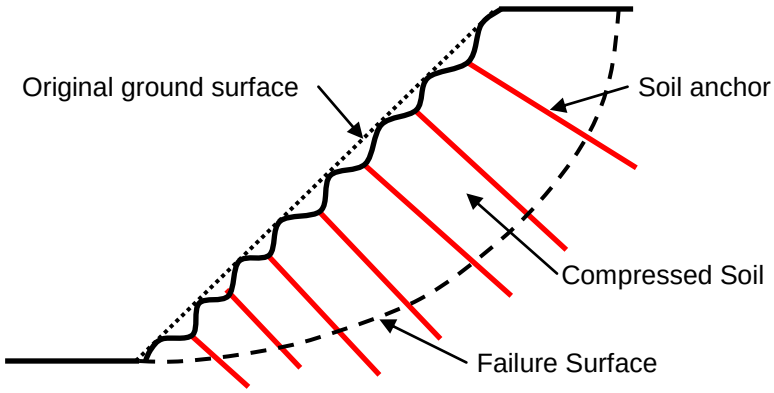


Figure 2.13 Schematic of AGS (redrawn after Vitton et al., 1998)

To evaluate the effectiveness and implications, Vitton et al., 1998 conducted a field study to investigate the performance of the scheme after successful drive test of the anchor in to the soil using hand held tools. The author remediated an abandoned-mine landslide in eastern Kentucky using AGS. The field installation of the work began during March 1994 and took approximately 2.5 weeks working hour with four installation personnel to complete the work. However, the weather and soil condition extended the installation period to 4 months. A high-strength geotextile was utilized during the study. As the geotextile was susceptible to stress relaxation and UV radiation stability, only 60 % of the strength was utilized to limit the strength loss. The AGS was monitored with load cell, soil pressure cells, rain gauge, and temperature sensors. The load cell result

presented an increase over the load cell reading which sustained only 20 days after installation period. The study presented that the loss of load was a combination of soil consolidation immediately below the anchor geotextile connection and due to stress relaxation in the geotextile. Consequently, even if sufficient deformation developed, constant re-tensioning of the geotextile would be required.

Based on the study and field monitoring results, Vitton et al., (1998) concluded that the AGS could not function as an active remediation system; instead, it was appeared to function well as a passive remediation system. However, the monitoring period was very limited to confirm that the system would function well into the future. The study presented that AGS may provide an effective system for certain types of slope prone to creep, however, further research was suggested.

*2.4.10 Retaining Wall*

Retaining structures are used to retain materials at a steep angle and are very useful when space (or right-of way) is limited. According to USDA (1992), low retaining structures at the toe of a slope make it possible to grade the slope back to a more stable angle and can be successfully revegetated without loss of land at the crest. Such structures can also protect the toe against scour and prevent undermining of the cut slope (Gray and Sotir 1996). The advantage of using short structures at the top of a fill slope is that it can provide a more stable road bench or extra width to accommodate a road shoulder. Retaining structures can be built external to the slope (such as a concrete or masonry retaining wall), or utilize reinforced soil (such as a burrito wall or deep patch) (Fay et al, 2012).

It should be noted that using retaining walls in slope stabilization can also apply to large failures such as deep seated failures; however, it can be utilized to stabilize shallow instabilities which are presented in the subsequent sections.

2.4.10.1 Low Masonry or Concrete Walls

Masonry or poured concrete retaining walls are rigid structures that do not tolerate differential settlement or movement and are appropriate only at sites where little additional movement is expected. Generally, gravity walls can be constructed with plain concrete, stone masonry, or concrete with reinforcing bar. Masonry walls that incorporate mortar and stone are easier to construct and stronger than dry stone masonry walls; however, they do not drain as well (Fay et al, 2012). Cantilever walls use reinforced concrete and have a stem connected to a base slab.

A schematic of a low cantilever retaining wall used to flatten a slope and establish vegetation is illustrated in Figure 2.14. Retaining walls with free-draining compacted backfill can be designed and constructed more efficiently compared to cohesive backfill soils. In this case, a drainage system should be installed behind the wall to facilitate the flow of water in order to resist the formation of perched water zone behind the wall (Fay et al., 2012).

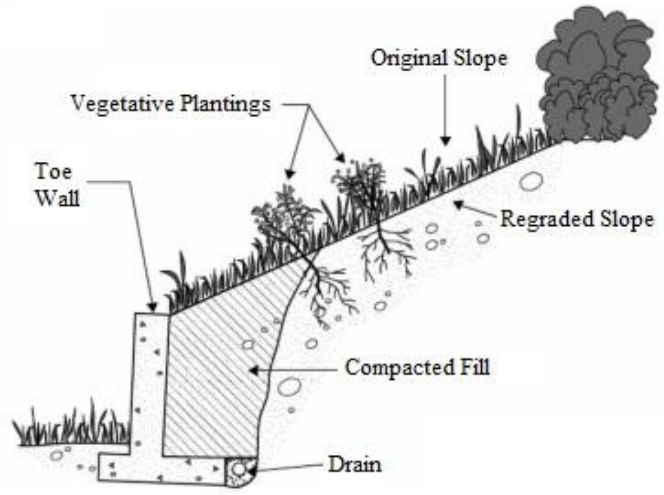


Figure 2.14 Cross section of a low wall with vegetation planted on the slope for stabilization (USDA, 1992).

#### 2.4.10.2 Gabion Walls

Gabion baskets are made of heavy wire mesh and assembled on site, set in place, then filled with rocks. Once the rocks have been placed inside the gabion basket, horizontal and vertical wire support ties are used to achieve the reported strength. Gabion walls are composed of stacked gabion baskets and are considered unbound structures. Their strength comes from the mechanical interlock between the stones or rocks (Fay et al., 2012). Gabion walls can be used at the toe of a cut slope or the top of a fill slope. The walls can be vertical or stepped and are adaptable to a wide range of slope geometries. Gabion walls can accommodate settlement without rupture and provide free drainage through the wall (Kandaris, P. M., 2007).

#### 2.4.10.3 Shallow Mechanically Stabilized Earth Walls

MSE walls are constructed with reinforced soil as presented in Figure 2.15. The reinforcement can be metal strips (galvanized or epoxy-coated steel), welded wire steel grids, or geogrids. MSE walls can be designed and built to accommodate complex geometries and to heights greater than 80 ft. It offer several advantages over gravity and cantilever concrete retaining walls such as: simpler and faster construction, less site preparation, lower cost, more tolerance for differential settlement, and reduced right-of-way acquisition (Elias et al. 2001).

The economic savings of MSE walls compared with traditional concrete retaining walls are significantly better at heights greater than 10 ft.; however, short MSE walls can also be constructed economically (Fay et al., 2012). For shallow MSE walls, the less expensive option is usually modular block facing, compared to precast concrete or metal sheet (Elias et al. 2001). It is suggested to use good quality backfill materials to facilitate drainage especially for high walls; however, the short walls can be constructed using poor quality soils (Fay et al. 2012)

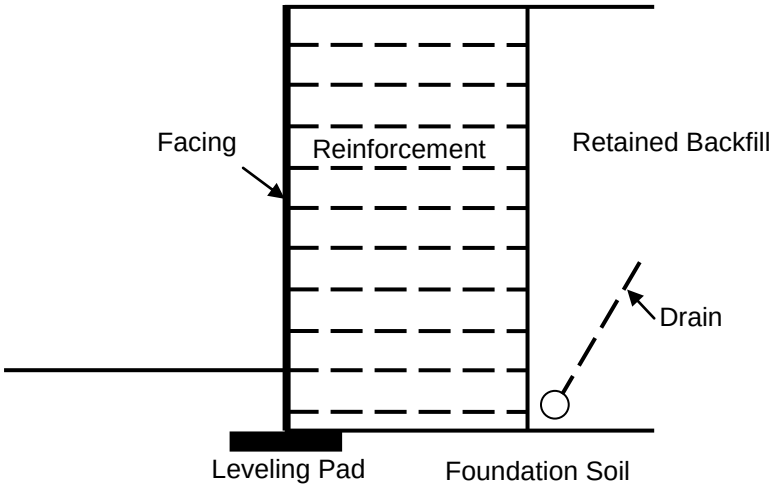


Figure 2.15 Schematic of Shallow MSE wall (redrawn after Berg et al., 2009)

*2.4.11 Reinforced Soil Slopes*

Reinforced soil slopes (RSS) can generally be steeper than conventional unreinforced slopes as geosynthetics provide tensile reinforcement that allows slopes to be stable at steeper inclinations. According to Elias et al., (2001), the design methods for RSSs are conservative so that they are more stable compared to flatter slopes designed to the same safety factor. RSSs offer several advantages over MSE wall. The backfill soil requirements for RSS are usually less restrictive, the structure is more tolerant of differential settlement and no facing element is required which make it less expensive compared to MSE wall. Moreover, vegetation can be incorporated into the face of the slope for erosion protection.

*2.4.12 Pin Piles (Micropiles)*

Pin piles (also known as micropiles) are more commonly used for foundations than slope stabilization (Taquinio and Pearlman 1999). The micro pile have great potential to be used in slope stabilization, however, they had been used in very limited applications (Fay et al., 2012).

*2.4.13 Slender Piles*

The flexible and rigid piles are used in slope stabilization application recently. The free field soil movements associated with the slope stability induce lateral load distributions along structural elements which vary with the p-y response, pile stiffness and section capacity of piles. In this case, each pile element offers passive resistance to lateral soil movement by transferring the loads to stable foundation. Basically, there are two approaches available in the literature known as the pressure based and displacement based method. The stabilizing piles are designed as passive piles in pressure based method, where ultimate soil pressures are estimated and applied to the piles directly or as an equivalent loading condition. In contrast, the assumptions of pressure based method are often not satisfied for free headed slender pile elements for cases of larger pile deformation or plastic flow. As an alternative, the pile soil reaction and passive pile response can be evaluated as a function of relative displacement between the soil and piles. However, the evaluation of the relative displacement between the soil and pile is complicated as the pile displacement depends on the soil displacement near the pile; and therefore, the analysis of the displacement response consider the soil pile interaction.

White et al., (2008) has conducted a large scale lateral load test to obtain pile behavior data for evaluating finite difference method proposed by Reese and Wang (2000) for its applicability to slender piles. During the study, the author conducted lateral loading test using short concrete pile (7 ft) with 2 different diameters (4.5 and 7 inch) on 3 different soil conditions (Loess, Glacial till and weathered shale) in the state of Iowa. The schematic of the lateral load test is presented in Figure 2.16.

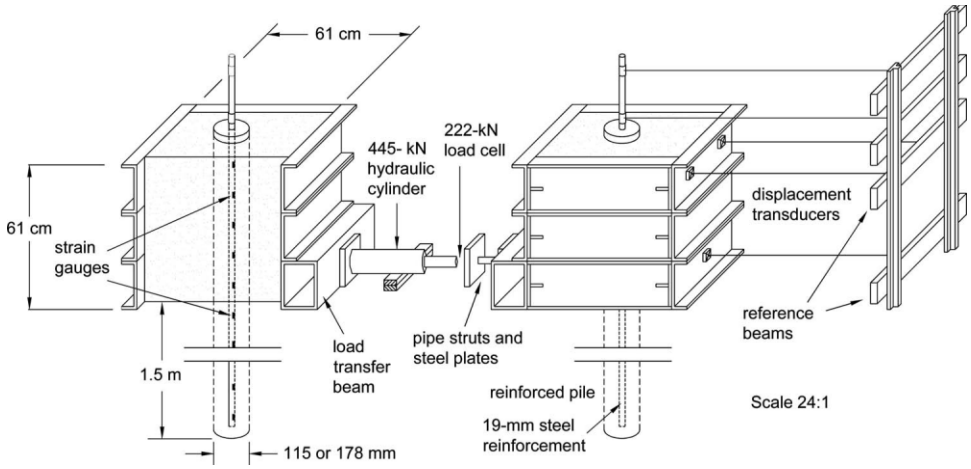


Figure 2.16 Load Test Set up

During the lateral load test, the author also performed a full scale direct shear test with no reinforcement to evaluate the effect of placing the reinforcement that provides resistance along the displacement plane. Based on the study, the response due to lateral loading considering both the reinforced and unreinforced condition is presented in Figure 2.17.

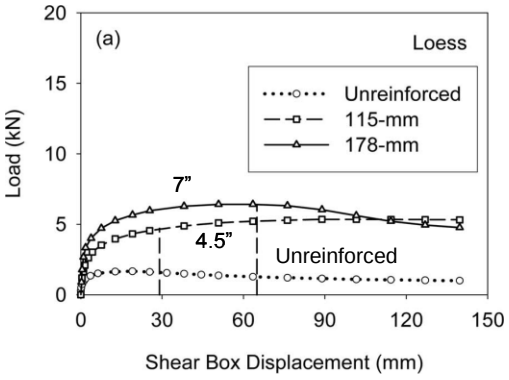


(a)

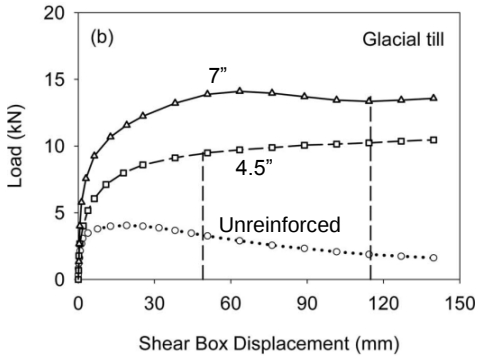


(b)

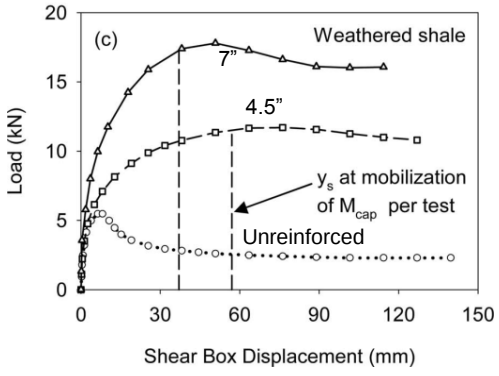


(c)

Figure 2.17 Load vs Shear Displacement from Lateral Load test

Based on the study, White et al., (2008) concluded that the installation of slender piles in unstable soil can offer considerable resistance to lateral soil movement, with improvement factor from loads range between 2.1 to 3.9 including the pile moment

capacities were eventually mobilized for all piles and the flexible or long pile failure mode was achieved. In addition, the depth of maximum moment ranged between 2.7 to 5.4 pile diameters below the bottom of shear box.

White et al., (2008) also investigated the behavioral stage of the slender pile element based on relative soil pile displacement at the soil surface i.e. 1.mobilization of soil shear stresses and elastic bending of pile; 2. Mobilization of pile concrete compressive strength; and 3. pile failure due to pile moment capacity mobilization. The moment curvature analysis result presented that the behavior of slender piles are mainly controlled by structural pile behavior.

*2.4.14 Plate Piles*

Short and Collins (2006) conducted a study using plate piles to stabilize shallow slope failure in state of California. The plate piles increase the resistance to sliding through reducing the shear stress and are installed vertically into the slope similar to pile-slope system. In a typical application, the plate piles are 6 ft to 6.5 ft long, 2.5 in by 2.5 in steel angle iron sections with a 2 ft by 1 ft wide, rectangular steel plate welded to one end (Mccormick and Short, 2006). The plate piles are driven into an existing landslide or potentially unstable slope which have 2-3 ft of soil or degraded clay fill over stiffer bedrock, as presented in Figure 2.18. As a result, the plate reduces the driving forces of the upper slope mass by transferring the load to the stiffer subsurface strata.

Short and Collins (2006) presented that the critical component in determining initial pile spacing was the angle iron resistance. In a experimental test section, the Plate piles were installed on a staggered grid pattern at 4 ft c/c. Depending on the stiffness of the underlying materials, plate pile can be installed either by direct push method by an excavator bucket or driven by either a hoe-ram or “head-shaker” compactor at rates of 20 to 25 blows per hour.

This shallow slope stabilization using Plate piles is the latest innovation and presented lot of potential as an alternative approach. The field implementation and controlled slope experiments conducted by Short and Collins (2006) presented that the plate pile technique can increase the factor of safety against slide up to 20% or greater and can reduce the cost of slope stabilization up to 6 to 10 times compared to the cost of conventional slope repairs. However, one of the major demerits of the technique included the failure depth that ranged only 3 ft.

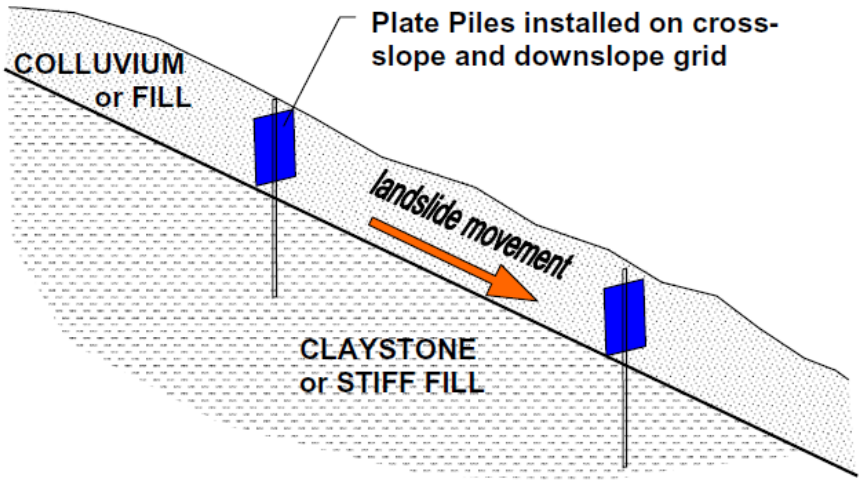


Figure 2.18 Schematic of Plate Pile for Slope Stabilization (Short and Collins, 2006)

*2.4.15 Recycled Plastic Pin*

Recycled Plastic Pins (RPP) had been utilized in other states (Missouri, Iowa) as a cost effective solution for slope stabilization compared to conventional techniques (Loehr and Bowders, 2007). Typically, RPPs are fabricated from recycled plastics and waste materials such as polymars, sawdust and fly ash (Chen et al., 2007). It is a lightweight material and less susceptible to chemical and biological degradation compared to other structural materials. RPPs are installed in the failed area to provide resistance along the slipping plane to increase factor of safety. RPP has great potential to

be a popular and cost effective alternative for stabilization of shallow slope failure. However, more study should be conducted in this aspect.

## 2.5 Recycled Plastic Pin

The recycled plastic pin, which is commercially known as, recycled plastic lumber are manufactured using post consumer waste plastic, has been proposed as an acceptable material for use in the construction of docks, piers and bulkheads. Plastic lumber is also marketed as one of the environmentally preferable materials. Based on environmental and life cycle cost analysis (LCCA) standpoint, the recycled plastic pin (RPP) is under serious consideration as structural materials for marine and waterfront application. The RPP require no maintenance, is resistant to moisture, corrosion, rot and insects. It is made of recycled, post-consumer materials and helps reduce the problem associated with disposal of plastics. Typically, 50% or more of the feedstock used for plastic lumber composed of polyolefin in terms of high density polyethylene (HDPE), low density polyethylene (LDPE) and polypropylene (PP). The polyolefin acts as an adhesive and combine high melt plastics and additives such as fiberglass, wood fibers within a rigid structure.

### *2.5.1 Manufacturing Process of RPP*

The manufacture of plastic lumber begins with the collection of raw materials. After collection, the plastic is cleaned and pulverized. The resulting confetti arrives at the production site where it is melted in an extrusion machine. Malcolm, G. M., (1995) presented two methods of manufacturing the recycled plastic lumber, such as the Injection molding process and the continuous extrusion process. In an injection molding process, the molten plastic is injected into a mold that defines the shape and length of the product. The mold is then cooled uniformly and the product is removed from the mold.

The process is relatively simple and inexpensive. However, the production volume is limited (Malcolm, G. M., 1995).

The continuous extrusion process allows producing varying length of the recycled plastic lumber. During this process, the molten plastic is continuously extruded through series of dies which shape the materials during its cooling. However, it is challenging for the manufacturer to provide uniform controlled cooling of the sample to prevent warpage and caving of the lumber.

It should be noted that continuous extrusion process requires considerable investment compared to injected molding process. However, the continuous extrusion process requires less labor and can produce miles of product quickly and suitable for mass production.

Another manufacturing process of the recycled plastics that is widely used is the compression molding process (Lampo and Nosker, 1997). This process mixes batches consisting of 50-70% of thermoplastics with other materials by melting. An automatically adjusted scraper then removes the melted material from the plasticator and presses it through a heated extruder die into premeasured, roll-shaped loaves. The loaves are then conveyed to a press-charging device that fills a sequence of compression molds alternately. The products are cooled in the molds to a temperature of 40 °C and ejected into a conveyor which carried it to a storage area.

*2.5.2 Engineering Properties of RPP*

Bowders et al., (2003) conducted a study on the different engineering properties of RPP. The motivation of the study was to evaluate the engineering properties of wide varieties of production standard and to develop specification for the slope stabilization. As a part of the study Uni-axial compression tests and four point flexure test were performed. The samples were collected from three manufacturers. The experimental

results for the uni-axial compression and four point bending test are presented in Table 2.2 and Table 2.3, respectively.

Table 2.2 Uniaxial compression test results (Bowders et al., 2003)

| Specimen Batch | No. of Specimen tested | Nom. Strain Rate (%/min) | Uniaxial Compressive Strength (ksi) | | Young's Modulus, E1% (ksi) | | Young's Modulus E5% (ksi) | |
|---|---|---|---|---|---|---|---|---|
| | | | Avg. | Std. Dev. | Avg. | Std. Dev. | Avg. | Std. Dev. |
| A1 | 10 | - | 2.76 | 0.13 | 133.7 | 7.7 | 56.6 | 3.9 |
| A2 | 7 | 0.005 | 2.90 | 0.12 | 186.4 | 10.0 | 54.8 | 2.2 |
| A3 | 6 | 0.006 | 2.90 | 0.13 | 176.9 | 15.7 | 52.6 | 3.9 |
| A4 | 3 | 0.004 | 2.90 | 0.13 | 199.7 | 23.9 | 52.6 | 3.6 |
| A5 | 4 | 0.006 | 1.74 | 0.15 | 93.5 | 23.1 | 32.6 | 2.5 |
| A6 | 4 | 0.006 | 1.89 | 0.13 | 114.0 | 15.4 | 34.5 | 4.9 |
| B7 | 2 | 0.007 | 2.03 | 0.07 | 78.5 | 5.2 | 38.9 | 0.4 |
| B8 | 2 | 0.006 | 2.32 | 0.06 | 93.3 | 0.1 | 44.7 | 0.1 |
| C9 | 3 | 0.0085 | 2.47 | 0.16 | 77.3 | 12.2 | 56.1 | 5.8 |

Table 2.3 Four point bending test results (Bowders et al., 2003)

| Specimen Batch | No of Specimens Tested | Nom. Def. Rate (in/min) | Flexural Strength (ksi) | Secant Flexural Modulus $E_{1\%}$ (ksi) | Secant Flexural Modulus $E_{5\%}$ (ksi) |
|---|---|---|---|---|---|
| A1 | 13 | - | 1.6 | 113.0 | 96.0 |
| A4 | 3 | 0.168 | 2.6 | 201.3 | - |
| A5 | 3 | 0.226 | 1.6 | 103.1 | 73.1 |
| A6 | 4 | 0.143 | 1.5 | 92.0 | 64.3 |
| B7 | 1 | 0.159 | 1.3 | 78.9 | 61.6 |
| B8 | 1 | 0.223 | - | 118.4 | - |
| C9 | 2 | 0.126 | 1.7 | 100.2 | 80.2 |

Lampo and Nosker, (1997) conducted a comparative experimental study on the compressive strength of Recycled Plastic Lumber. During the study, a total of 10 plastic

samples were obtained from eight manufacturers. The composition of the product varied greatly, such as: some were mixed plastics, some were pure resigns and others contained fillers such as wood pulp or fiberglass. Lampo and Nosker (1997) performed the experimental study according to ASTM 695-85 with the sample height nearly 12 inch. To calculate the mechanical properties, the study included an effective cross sectional area which was calculated based on a specific gravity measurement. It should be noted that the compressive strength test was performed at 0.1 in/min rate. Based on the experimental results, the modulus, ultimate strength at 10% strain and yield strength at 2% offset were calculated from the load-displacement data. The specific modulus and specific strength are the modulus divided by specific gravity and the ultimate strength divided by specific gravity, respectively. These "specific" properties display the mechanical properties of the materials normalized with respect to density during the study. It was expected that the normalization should minimize the effects of voids when comparing the material properties and the effects from different methods of extrusion during the manufacturing process that varied among manufacturers. Based on the study, the compressive strength results are presented in Table 2.4. In addition, the comparisons of compressive strength between different samples are presented in Figure 2.19 and Figure 2.20.

Table 2.4 Average values of specific gravity, modulus, specific modulus, yield stress, ultimate stress and specific strength for each samples type (Lampo and Nosker, 1997)

| Sample | Specific Gravity | Modulus (ksi) | Specific Modulus (ksi) | Yield Stress (ksi) | Ultimate Strength (ksi) |
|---|---|---|---|---|---|
| 51A | 0.2789 | 38.00 | 121.83 | 0.71 | 0.78 |
| 1B | 0.7012 | 61.93 | 88.33 | 1.38 | 1.89 |
| 2D (BR) | 0.8630 | 85.28 | 98.92 | 1.67 | 2.32 |
| 2D (G) | 0.8098 | 116.03 | 143.30 | 2.10 | 2.86 |
| 1E | 0.862 | 80.79 | 93.84 | 1.77 | 2.42 |
| 1F | 0.7888 | 108.20 | 137.06 | 2.19 | 2.81 |
| 1J(B) | 0.7534 | 93.26 | 123.86 | 1.90 | 2.36 |
| 1J(W) | 0.9087 | 110.08 | 121.25 | 2.16 | 2.83 |
| 23L | 0.7856 | 191.45 | 243.66 | 1.71 | 1.93 |
| 1M | 0.5652 | 57.87 | 102.25 | 0.96 | 1.23 |
| 1S | 0.9090 | 80.50 | 88.47 | 1.67 | 2.05 |
| 1T | 0.8804 | 117.92 | 133.58 | 2.25 | 3.12 |
| 9U | 0.774 | 86.73 | 111.53 | 1.83 | 2.41 |

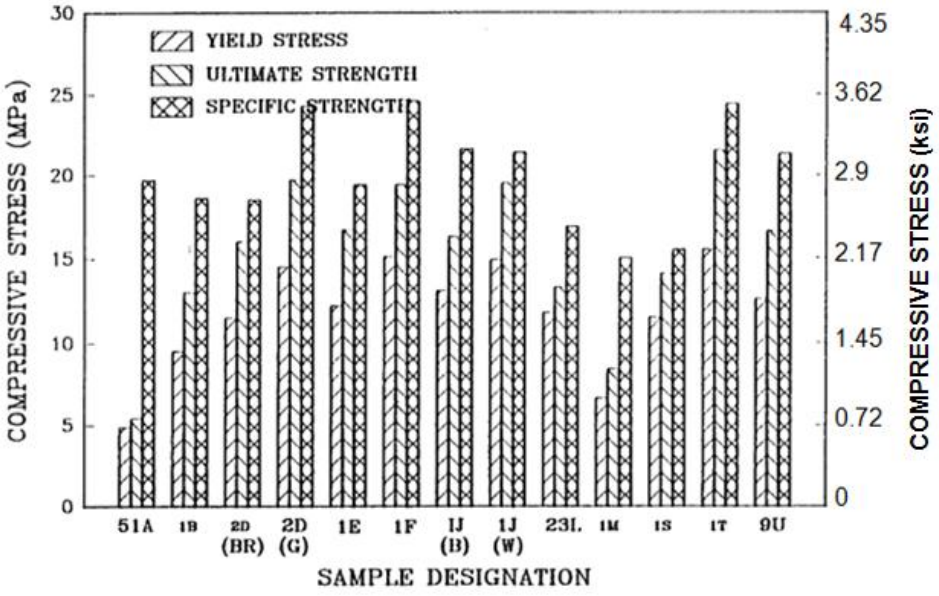


Figure 2.19 Comparison of compressive strength (Lampo and Nosker, 1997)

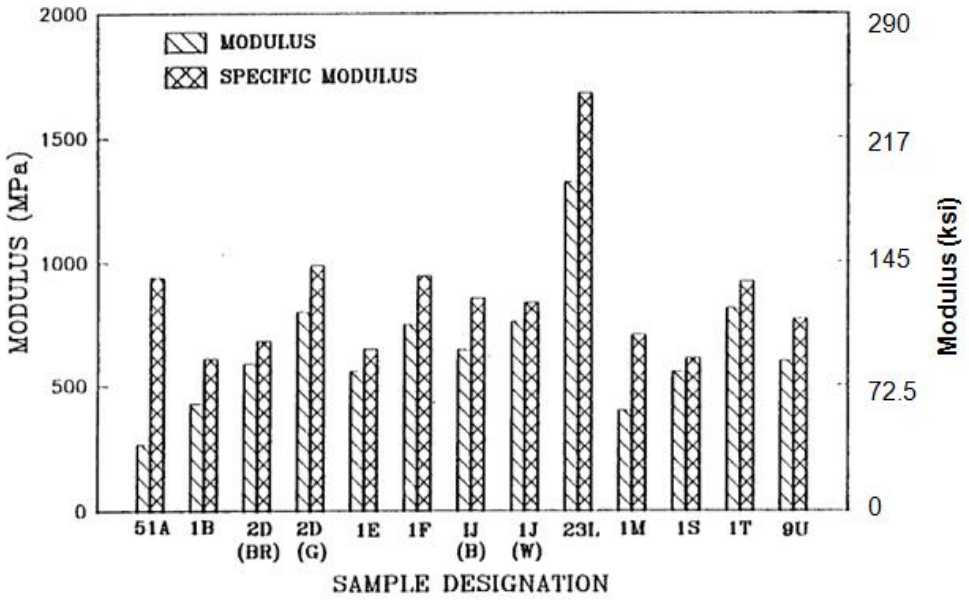


Figure 2.20 Comparison of Compressive modulus (Lampo and Nosker, 1997)

Based on the experimental study, Lampo and Nosker (1997) summarized that the values for RPP lumber ranged between 1.74 ksi to 3.5 ksi for compression and 1.25 ksi to 3.5 ksi in tension. However, the RPP reach it ultimate strength at different strain level compared to softwood.

Breslin et al. (1998) also conducted comparison between different test results observed from the literature as presented in Table 2.5. The study presented that different additives have been incorporated into plastic lumbers (glass fibers, wood fibers, polystyrene) and had shown to increase the stiffness of the lumber.

Table 2.5 Engineering properties of plastic lumber properties (Breslin et. al, 1998)

| Product | Composition | Compressive Strength (psi) | Modulus of Elasticity (psi) | Tensile Strength (psi) | Source |
|---|---|---|---|---|---|
| TRIMAX | HDPE / Glass Fiber | 1740 | 450 000 | 1250 | TRIMAX Literature SUNY at Stony Brook |
| TRIMAX | HDPE / Glass Fiber | | | 1189 | www.lumberlast.com |
| Lumber Last | Commingled Recycled Plastic | 3755 (ultimate) (D198) | 140 000 (D790) | 1453 (ultimate) (D198) | www.ecpl.com |
| | Post-consumer milk jugs | 3205 (D695) | 93 000 – 102 500 (D790) | 2550 (D638) | Zarillo and Lockert (1993) |
| Earth Care recycle maid | 80% HDPE / 20% LDPE | 89 814 | | | Zarillo and Lockert (1993) |
| Hammer's Plastic | HDPE/LDPE (20PSGF) | 527 000 | | | |
| | HDPE / LDPE (40PS20GF) | 653 000 (D790) | 1793 (D638) | | |
| Superwood Selma, Alabama | 33% HDPE / 33% PP | 3468 (D695) | 146 171 (D790) | 1793 (D638) | |
| California Recycling Company | 100% Commingled | 81 717 | | | Beck, R. (1993) |
| | 10% PP / 50% HDPE | 79 319 | | | |
| RPL-A | HDPE / Glass Fiber | 92 636 (D790) 2000 | | | Smith and Kyanka (1994) |
| RPL-B | 49% HDPE / 51% Wood Fiber | | | | Smith and Kyanka (1994) |
| Rutgers University | 100% Curb tailings | 3049 | 89 500 | | Renfee et al. (1989) |
| | 60% Milk bottles, 15% Detergent bottles, 15% | | | | Renfee et al. (1989) |

Table 2.5 - *Continued*

| Product | Composition | Compressive Strength (psi) | Modulus of Elasticity (psi) | Tensile Strength (psi) | Source |
|---|---|---|---|---|---|
| | Curb tailings, 10% LDPE 50% Milk bottles, 50% Densified PS | 4120 (D695) | 164 000 (D790) | | Renfee et al. (1989) |
| Earth Care Products | HDPE | | 173 439 (D790) | | www.ecpl.com |
| BTW Recycled Plastic Lumber | Post-Consumer | 1840-2801 | 162 000 | | BTW/Hammers Brochure |

Plastic is a temperature dependent material. At low temperature, the plastic is strong and brittle. With the increase in temperature, the plastic become weaker and become more ductile. Malcolm, M. G. (1995) presented the effect of temperature change on the tensile strength of HDPE materials as presented in Figure 2.21.

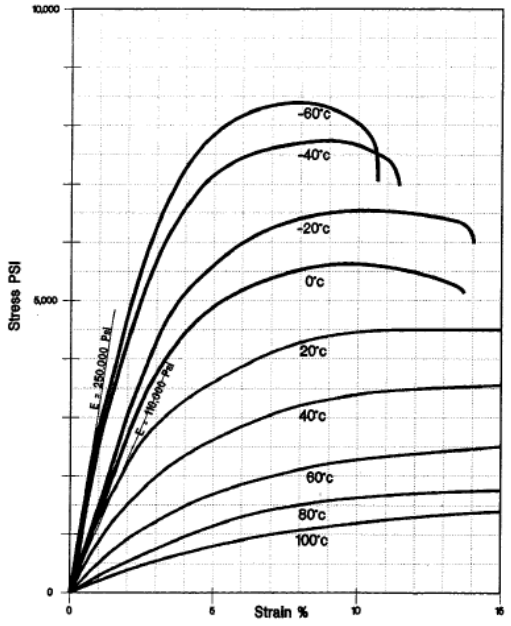


Figure 2.21 Tensile strength of HDPE (Malcolm, M. G. (1995))

*2.5.3 Long Term Engineering Properties of RPP*

Breslin et al. (1998) conducted a study on the long term engineering properties of plastic lumber manufactured using post-consumer plastic. During the study, the plastic lumber samples were removed from the deck over a two year period and returned to the laboratory for testing. At the initial process, the author investigated the initial engineering properties of recycled plastics lumber which was manufactured using a continuous extrusion process. The plastic lumbers were collected at regular interval for 2 years of monitoring period. It should be noted that the lumber did not face severe traffic; however, it was subjected to two summer cycles where the highest temperatures and UV intensities had taken place. The author did not observed any noticeable change such as warping, cracking and discoloration in the plastic lumber.

Krishnaswamy and Francini (2000) performed a study on the effect of outdoor weathering and environmental effects including the degradation due to UV radiation, thermal expansion and combined effects of moisture and temperature on the mechanical behavior of RPP. The author did not observe significant variation of the flexural modulus and strength of RPP according to ASTM D6109 before and after the hydrothermal cycling, as presented in Table 2.6.

Table 2.6 Comparison of flexural properties of typical RPP materials with and without hygrothermal cycling (Krishnaswamy and Francini, 2000)

| | Secant Modulus (ksi) | Stress at 3% strain (ksi) |
|---|---|---|
| Before cycling | 97.8 ± 6.4 | 1.9 ± 0.12 |
| After cycling | 113.6 ± 14.4 | 2.4 ± 0.4 |

Lynch et al. (2001) had investigated the effect of the weathering on the mechanical behavior of recycled HDPE based plastic lumber. During the study, flexural properties of weathered deck boards were obtained by performing flexural tests in three

points loading, for comparison to original flexural properties according to ASTM D796. The study investigated both the exposed and unexposed side of the deck board in tension. The original flexural properties of the RPP deck boards determined before the weathering action had flexural modulus of 171 ksi and a flexural strength of 2.5 ksi. The three-point bending test results of the weathered sample are presented in Table 2.7 and Table 2.8.

Table 2.7 presented the flexural properties of RPP when the exposed side was tested in tension. On the other hand, Table 2.8 presented the flexural properties when the unexposed side was tested in tension. Comparing the test results of as presented in Table 2.7 and Table 2.8 with the original mechanical properties, it was observed that both the modulus and strength increased after the outdoor exposure. The modulus increased by 28 % from the original when the exposed side was tested in tension and increased by 25 % when the unexposed side was tested in tension. In addition, the strength at three percent strain increased by 4 % from the original value, for both the exposed and unexposed side tested in tension.

Table 2.7 Three-point bending test results of the RPP samples after weathering (The exposed side was tested in tension) (Lynch et al., 2001)

| Sample | Modulus (ksi) | Strength at 3% strain (ksi) | Ultimate strength (ksi) |
|---|---|---|---|
| 1A | 240.47 | 2.77 | 3.43 |
| 2A | 213.79 | 2.48 | 3.12 |
| 3A | 200.88 | 2.44 | 2.86 |
| 4A | 214.22 | 2.55 | 3.32 |
| 5A | 227.42 | 2.73 | 3.31 |
| AVERAGE | 219.30 | 2.59 | 3.21 |

Table 2.8 3-point bending test results of the RPP samples after weathering (The unexposed side was tested in tension) (Lynch et al., 2001)

| Sample | Modulus (ksi) | Strength at 3% strain (ksi) | Ultimate strength (ksi) |
|---|---|---|---|
| 1B | 217.56 | 2.77 | 3.49 |
| 2B | 204.50 | 2.47 | 3.05 |
| 3B | 190.29 | 2.45 | 3.05 |
| 4B | 219.30 | 2.43 | 3.11 |
| 5B | 234.67 | 2.76 | 3.25 |
| AVERAGE | 213.21 | 2.58 | 3.19 |

Breslin et al. (1998) investigated the compression modulus of the sample periodically, both in cross sectional and in-plane axes, as presented in Figure 2.22. The study indicated that the measured in-plane compression modulus (192 MPa) was 6 to 8 times higher compared to the cross sectional compression modulus (24 MPa). In addition, no significant change in both of the compression modulus was observed with time till 19 months; however, the 24 month modulus was significant higher in both of the plane compared to the initial value. The significant change in 24 months period might have taken place due to the variability in the material properties of the lumber profiles.

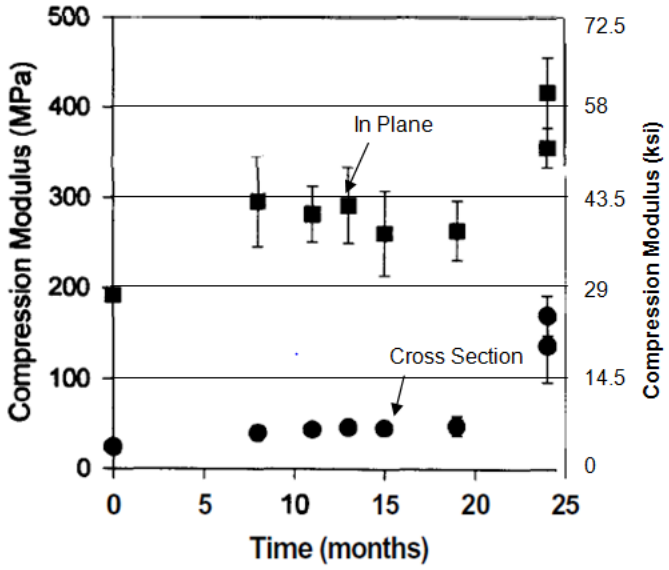


Figure 2.22 Compression modulus measurements for both cross-sectional and in-plane dimensions for plastic lumber collected from the West Meadow pier over a 24 months period (Breslin et al., 1998).

Breslin et al. (1998) also presented a study on the modulus of elasticity based on different compositions of plastic lumber. The study included the modulus of elasticity on in plane direction as well as in cross sectional direction. Based on the study, the variations of modulus of elasticity of plastic lumbers from different manufacturers are summarized in Figure 2.23.

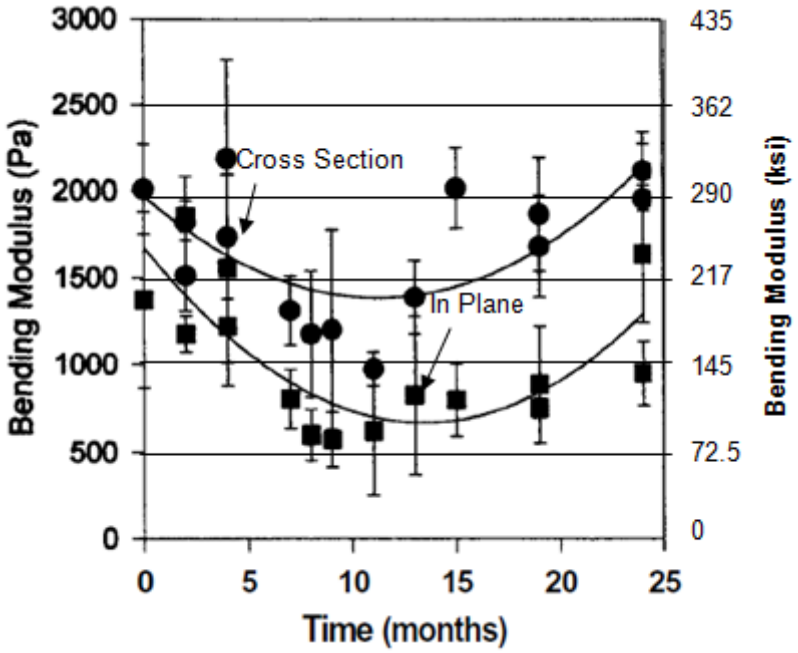


Figure 2.23 Bending modulus measurements for both cross-sectional and in-plane directions for plastic lumber collected from the west Meadow pier over a 24 month period.

Breslin et al. (1998) observed that the poorest engineering properties resulted in for the lumber manufactured using mixture of post-consumer waste plastics. The use of single polymer, such as HDPE with glass fiber additives resulted in significantly better engineering properties. In addition, the use of glass and wood fiber additives significantly improves the modulus of elasticity for plastic lumber. The modulus of elasticity for plastic lumber manufactured without fiber additives ranged from 79-173 ksi. With the addition of wood or plastic fibers, the modulus of elasticity ranged from 146-653 ksi which was 2-4 times higher compared to the fiber without fiber additives.

Breslin et al. (1998) observed high initial bending modulus in the cross sectional direction (0.27 psi) compared to the in-plane direction (0.2 psi). The author also observed changes in the bending modulus over time for the samples collected from the pier as

presented in Figure 2.23. The author noticed significant decrease in the bending modulus measured in the in-plane direction (0.108 psi) compared to an initial value of 0.198 psi. The similar drop in bending modulus was also observed for the bending modulus in the cross sectional direction. However, significant increases both in plane and cross sectional bending moduli were measured for the lumber profiles tested at 24 months. The changes measured in the cross sectional bending modulus may be a reflection of the heterogeneity of the material rather than a change in the initial lumber properties due to weathering.

*2.5.4 Creep of RPP*

The Recycled Plastic lumber is a nearly isotropic material with considerable strength, durability and workability. It can be reinforced strengthen and formed as composite materials. It is as strong as wood, however, the modulus of elasticity of unreinforced plastic lumber is generally 1/10 to 1/3 that of Southern Yellow Pin Lumber (Malcolm, M. G., 1995). In addition, it is visco-elastic materials susceptible to creep and increased deflection with time under a static sustained load.

Malcolm, M. G., 1995 conducted a study on the creep behavior of a 1.5x3.5 in recycled plastic lumber sample subjected to a sustained mid span bending stress of 516.7 psi that produced the creep curve as presented in Figure 2.24. It is important for the plastic lumber to be maintained in the low stress level for the sustained load.

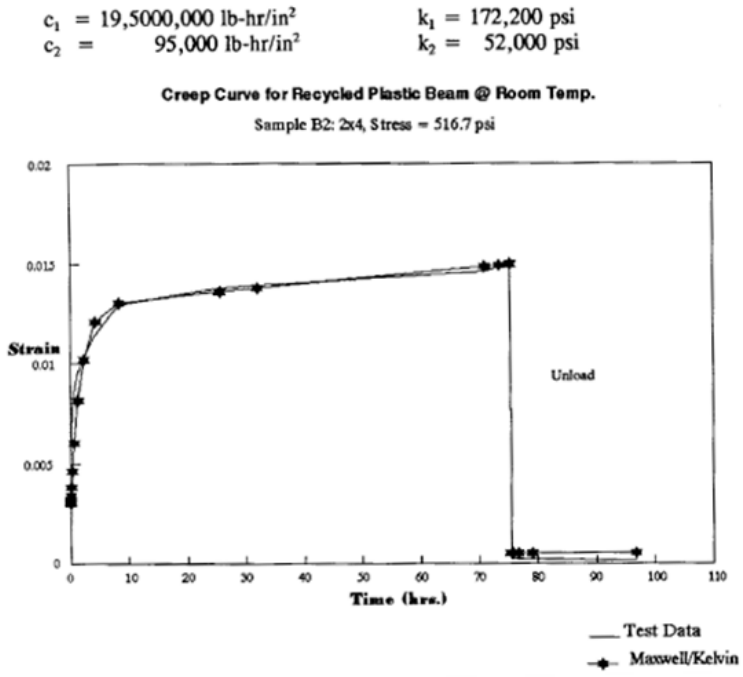


Figure 2.24 Creep curve for recycled plastic beam at room temperature

Van Ness et al. (1998) conducted a study on the long term creep behavior of commercially available plastic lumber. Creep of the recycle plastic lumber presents the time dependence of the mechanical properties of plastic lumber. To investigate the long term creep behavior, the study included four groups of plastic lumbers, manufactured by four different companies. It should be noted that the composition of four plastic groups varied significantly such as: some contained blends of polyolefin, one contained glass fibers but all of the samples were constituted principally of recycled polyethylene. Based on the experimental study, Van Ness et al. (1998) observed that the recycled plastic lumber that contained oriented glass fiber was the most creep resistant over time.

Gopu and Seals (1999) performed a study on the effect of composition, member size, service temperature, service stress level, duration and orientation of loading on the mechanical properties of recycled plastic lumbers. The study indicated that the non-

homogeneity of the plastic lumber is evident and influenced the orientation of loading with respect to member axes. In addition, the author proposed to adjust the flexural strength and stiffness values to account for the effect of creep and temperature. Moreover, the author emphasized the use of glass fiber to improve the stiffness of the Recycled Plastic Lumber.

Lampo and Nosker (1997) presented that the serious concern using the RPP for any load bearing application is creep. Due to the visco-elastic properties of plastics, a piece of plastic lumber will begin to sag over time under a static load. The time dependent effect increases with elevated temperature. In general, Civil engineers study this time-dependent phenomenon and develop load-duration factors for design use. This effect is crucial to take into account in developing design guidelines for plastic lumber.

2.5.4.1 Creep of RPP in Slope Stabilization

Chen et al., (2007) had performed a study on the creep behavior of RPP. Due to variety of manufacturing process and constituent, the engineering properties of commercially available materials vary substantially. The polymeric materials are durable in terms of environmental degradation; however, they can exhibit higher creep rates compared to other structural materials such as timber, concrete or steel.

Chen et al., 2007 tested 3.5 inch by 3.5 inch rectangular specimen from 3 different manufacturers to evaluate the creep behavior. During the study, a total of 8 samples were tested. Tests were performed on specimens from three manufacturers. The compressive creep tests were performed on specimens cut from full size RPP, with nominal dimensions of 3.5 inch squares by 7 inch in length. The compressive load was applied using a spring with a 3 kip/ft spring constant. All specimens were tested at room temperature of 21˚c. On the other hand, the flexural creep responses were performed on scaled RPP of 2x2x24 in. The test set up for both compressive and flexural creep is

presented in Figure 2.25. The flexural creep test was performed at different temperature (21, 35, 56, 68, and 80°C). The study considered Arrhenious method to estimate the long term creep behavior.

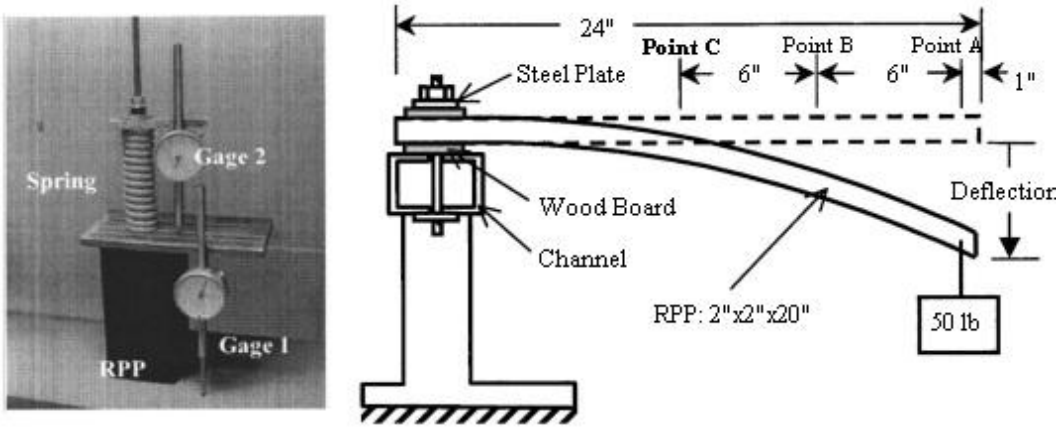


Figure 2.25 RPP testing set up for Creep a. Compression creep, b. Flexure Creep (redrawn after Chen et al., 2007)

A typical plot of deflection vs. time for the compression creep and the compression creep results are presented in Figure 2.26 and Table 2.9, respectively. Figure 2.26 indicated that the primary creep was completed within one day after the load applied for all specimens. Secondary creep occurred after primary creep and continued for a year at a steady rate.

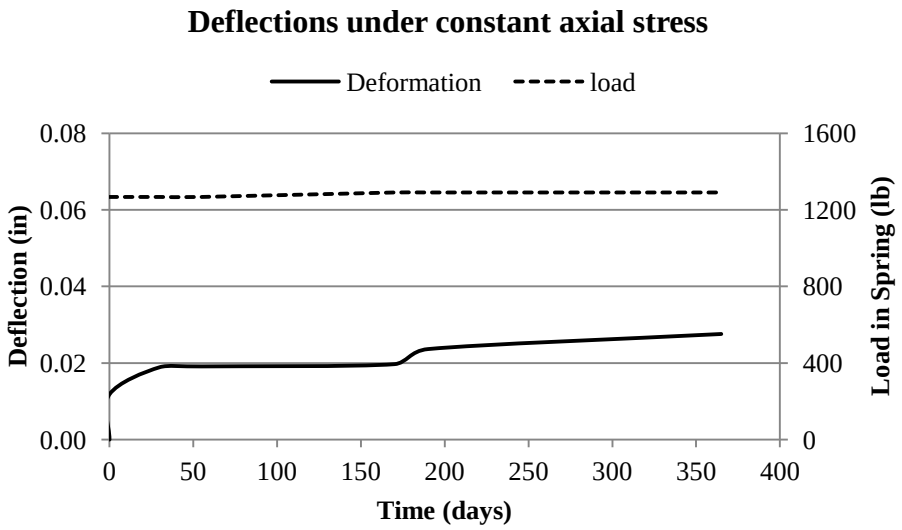


Figure 2.26 Typical deflections under constant axial stress versus time of RPP (redrawn after Chen et al., 2007)

Table 2.9 Summary results of typical compressive creep test (Chen et al., 2007)

| Manufacturing | Number of Specimens | Creep Stress (psi) | Ratio of Creep stress to compressive strength | Maximum Creep Strain (%) |
|---|---|---|---|---|
| A3 | 2 | 105 | 3.7 | 0.1 |
| A6 | 2 | 100 | 6.3 | 0.1 |
| B7 | 1 | 110 | 5.3 | 0.4 |
| C9 | 1 | 120 | 5.1 | 0.4 |

The flexural creep test results are presented in Table 2.10. As the temperature increased, the time to reach failure decreased for the same load condition. Results showed that the loading levels, along with temperature, affected the creep behavior of the recycled plastic specimens. In addition, it was presented that the higher the load levels or

the closer to the ultimate strength of the material, the faster the creep rate and shorter time to reach failure. Based on the study, the author presented a method to investigate the design life of RPP, based on percentage load mobilization as presented in Figure 2.27. The higher the mobilized loads, the design life of RPP become susceptible to creep failure. The author suggested to perform effective design procedure to reduce the load mobilization which could be obtained through increasing the number of RPP thereby, reducing the spacing, changing the constituents or changing the section of RPP to increase moment of inertia.

Table 2.10 Summary of Flexural Creep test result (Chen et al., 2007)

| Loading Conditions | Temperature (˚C) | Number of Specimens tested | Average time to reach failure (days) | Comments |
|---|---|---|---|---|
| 44 N at 5 points | 21 | 2 | 1.185[a] | Not failed |
| | 56 | 2 | 195 | failed |
| | 68 | 2 | 3.5 | failed |
| | 80 | 2 | 0.8 | failed |
| 93 N single load | 21 | 2 | 1.185[a] | Not failed |
| | 56 | 2 | 574 | failed |
| | 68 | 2 | 17.5 | failed |
| | 80 | 2 | 8.5 | failed |
| 156 N single load | 21 | 2 | 1.185[a] | Not failed |
| | 56 | 2 | 71.5 | failed |
| | 68 | 2 | 0.6 | failed |
| | 80 | 2 | 0.8 | failed |
| 222 N single load | 21 | 2 | 1.185[a] | Not failed |
| | 35 | 4 | 200 | failed |
| | 56 | 2 | 3.1 | failed |
| | 68 | 2 | 0.4 | failed |
| | 80 | 2 | 0.8 | failed |

[a] Last day of testing: specimen not ruptured

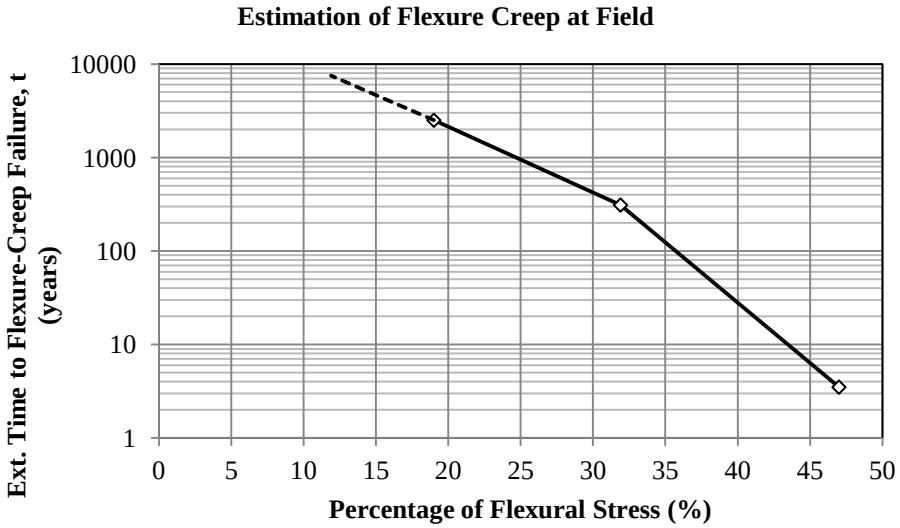


Figure 2.27 Method to estimate flexural creep at field (redrawn after Chen et al., 2007).

*2.5.5 Design Consideration for Structural Application*

Malcolm M. G. (1995) and Mclaren and Pensiero (1999) presented a simplified approach to design the recycled plastic as a structural material that is predominantly applicable to HDPE materials.

The design method included the load duration factor (LDF) similar to timber design to accommodate the effect of creep over the design period. The design method proposed the LDF ranged between 1.0 and 7.0, based on the time of application. On the other hand, the method included a temperature factor Ct, based on the effect of temperature over the tensile strength. The value of Ct ranged between 0.87 for 60 C (140 F) and 1.8 for 0 C (32 F) with Ct = 1 at 50 C (122 F). According to Malcolm, M. G. (1995), the allowable design stress Fa for Recycled Plastic Lumber is,

$$F_a = F_a * LDF * F' \qquad (2.1)$$

It should be noted that allowable stress is applicable for the structural member subjected to Dead and Live loads. However, it cannot explain the behavior of the RPP that could be installed in Slope and subjected to sustained lateral loads.

Lampo and Nosker (1997) addressed three main limitations of the designers planning for the structural application of RPP which are the lower modulus of RPP, creep and its co-efficient of thermal expansion. The author suggested accounting the first two issues by specifying a stiffened product or change in the design of support and spans. The thermal expansion can be taken care of by providing additional space for the expansion and contraction which is not a major issue for the RPP in slope stabilization application.

Nosker and Renfree (2000) presented the evaluation of the recycled plastic lumber and its applications on different civil engineering applications. For the successful utilization of the recycled plastic lumbers, the major concern for the structural application is the elastic modulus and the time dependent mechanical behavior (creep). To improve the mechanical properties and stiffness of the recycled plastics, the composites were produced. This initiative was first undertaken during 1990's where around 20-30% fiberglass were mixed in continuous extrusion process to produce stiffer product. The product had been successfully utilized for sheet piling, as structural plastic lumbers and for marine pilling.

Researches from Rutgers University developed a polymer-polymer composite with high stiffness and high strength during 1988-89 (Nosker et al., 1989) and later found that short glass fibers were capable of being oriented in a curbside tailing matrix, require about 10%-12% fiber glass to obtain high strength and stiffness value (Nosker et al., 1999).

Another innovation in the recycled plastic lumber had been conducted utilizing continuous glass fiber reinforcement with thermosetting plastics (in the shape of rebar) molded with HDPE (Lampo et al, 1998). The fiberglass members act as rebar supporting the less rigid thermoplastic material. The fiberglass rods are placed strategically and symmetrically about central axis. This technology has been used to produce marine piles which also performed well as fender pile.

## 2.6 Slope Stabilization Using Recycled Plastic Pin

### *2.6.1 Stability of Reinforced Slopes*

The general approach in limit equilibrium method to evaluate the stability of reinforced and unreinforced slope considers a potential sliding surface and then calculates the factor of safety for the sliding surface. The factor of safety of slope is considered as

$$F = \frac{\int s}{\int \tau} \qquad (2.2)$$

Where, F is the factor of safety, s is the shear strength from soil at the sliding surface and τ is the mobilized shear stress to maintain equilibrium. Using Mohr Coulomb failures envelop, the slope stability analysis has been conducted using the method of slice approach where the sliding body is divided into a number of vertical slices and equilibrium of the individual slices is consider to determine the normal and shear stress on the sliding surface and the factor of safety with assumed sliding surface is determined. The process is repeated for other potential surfaces until the lowest factor of safety is obtained. The sliding bodies with the slices are presented in Figure 2.28. On the other hand, installing RPP into the slope provide direct resistance along the slipping plane and therefore, increase the factor of safety. The analysis method considers the similar procedure of method of slide except a force due to the reinforcing member is added to

the other forces on the slide that are intersected by reinforcing members as presented in Figure 2.29.

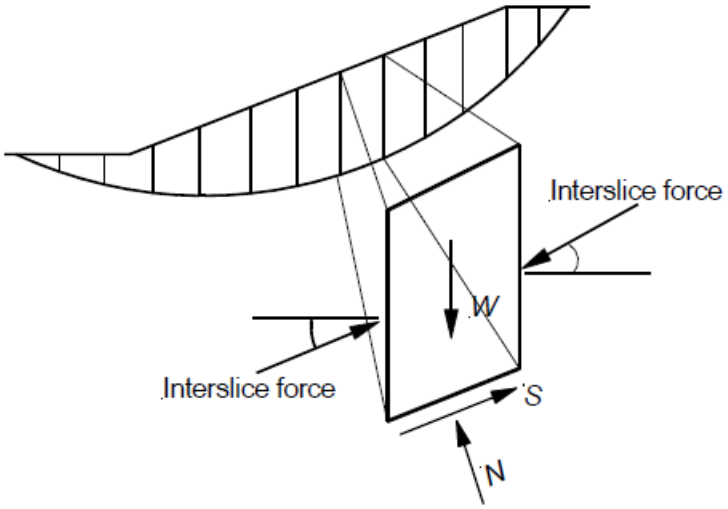


Figure 2.28 Static equilibrium of individual slice in the method of slices (Loehr and Bowders, 2007)

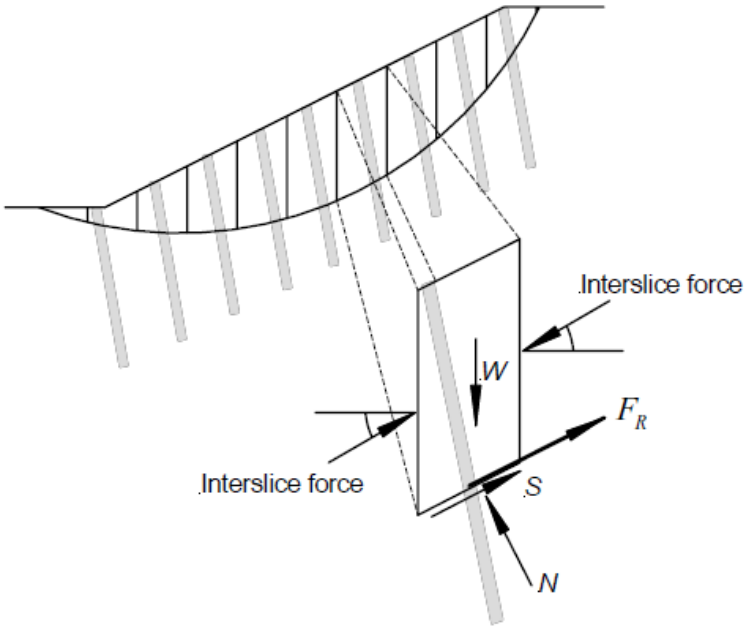


Figure 2.29 Reinforcement force on an individual slice in the method of slice

*2.6.2 Design Method of RPP Reinforced Slope*

Loehr and Bowders, 2007, presented a limit equilibrium method to investigate the factor of safety of a reinforced slope. The reinforcement force provides a direct resistance along the slip surface thereby increase the factor of safety. Loehr and Bowders (2007) mentioned the reinforcement force as the limit resistance which varies along the depth of RPP. The limit resistance varies with depth along the depth of RPP. To develop the limit resistance curve along RPP, the author considered two soil failure mechanisms and 2 structural failure modes to establish the limit resistance curve. The failure modes are summarized in Table 2.11.

Table 2.11 Summery of failure mode to establish the limit resistance curve (Loehr and Bowders, 2007)

| Failure Mode | Description |
|---|---|
| Mode 1 | Failure of soil above sliding surface around and between reinforcing members |
| Mode 2 | Failure of soil below sliding surface due to insufficient anchorage length |
| Mode 3 | Structural failure of member in bending |
| Mode 4 | Structural failure of member in shear |

In Failure Mode 1, the soil above the sliding surface is considered to fail by flowing between or around the reinforcing members. The reinforcing member is assumed sufficiently anchored into stable foundation soil below the sliding surface. A schematic of this idea with the limit resistance curve as a function of position along the RPP for Failure Mode 1 is shown in Figure 2.30.

Loehr and Bowders, (2007), undertook a similar process to calculate the resistance for Failure Mode 2, where, the soil below the sliding surface adjacent to the reinforcing member was assumed to fail while the member is sufficiently anchored in the

moving soil above the sliding surface. The schematic of the failure mode 2 as well as limit resistance along the depth of RPP is presented in Figure 2.31. The Failure Mode 3 was considered into two subcategories: failure due to excessive moments from the applied soil pressure above sliding surface (Failure Mode 3a) and failure due to excessive moments from the soil pressure below the sliding surface (Failure Mode 3b). The schematics and limit resistance curve for failure mode 3a and failure mode 3b are presented in Figure 2.32 and Figure 2.33, respectively.

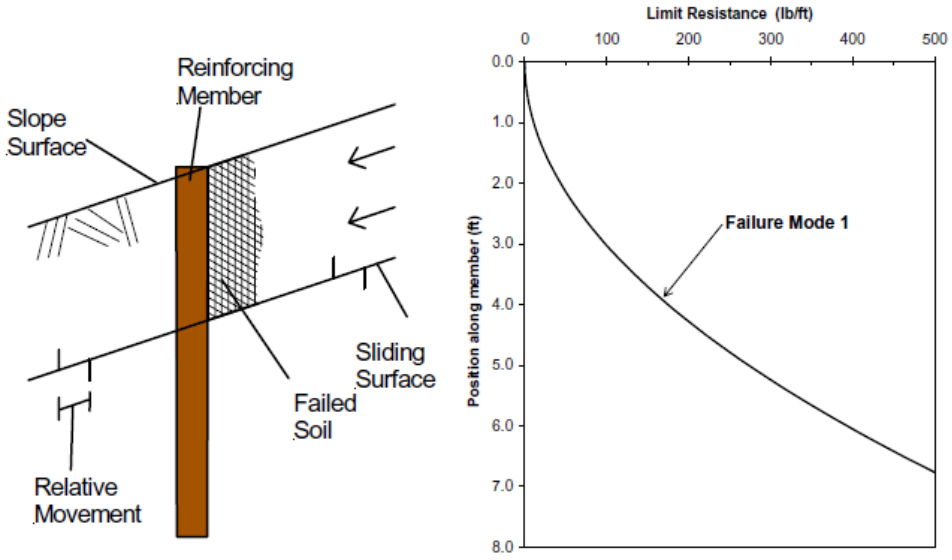


Figure 2.30 Schematic and limit resistance curve for failure mode 1 (Loehr and Bowders, 2007)

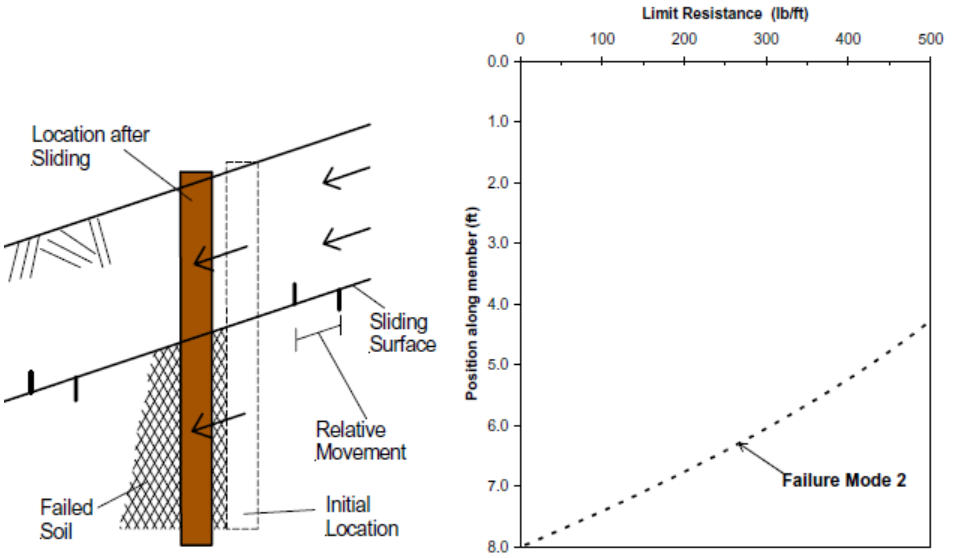


Figure 2.31 Schematic and limit resistance curve for failure mode 2 (Loehr and Bowders, 2007)

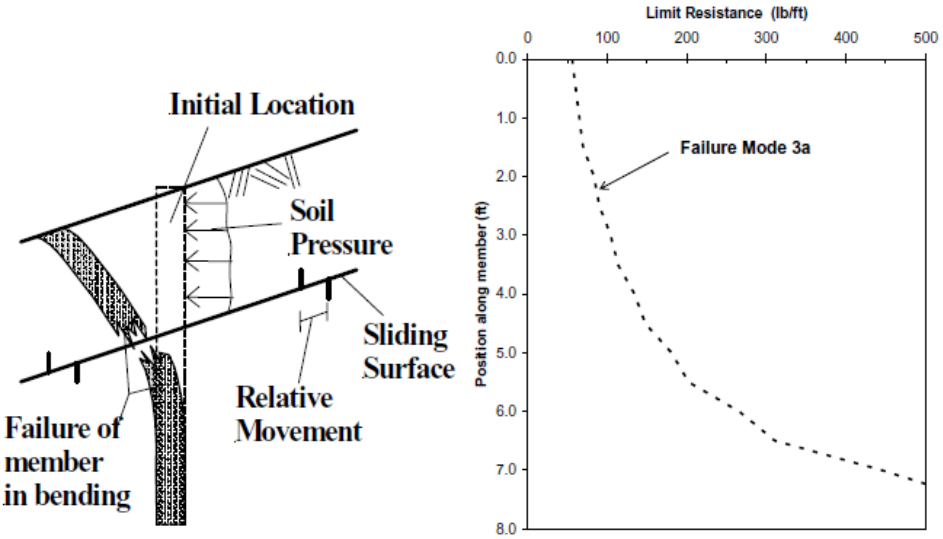


Figure 2.32 Schematic and limit resistance curve for failure mode 3a

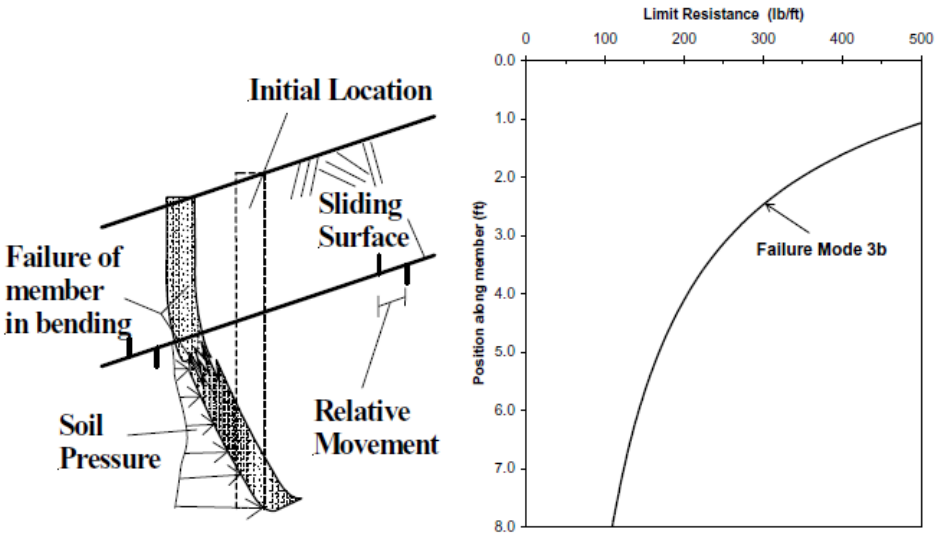


Figure 2.33 Schematic and Limit resistance curve for failure mode 3b

Based on all failure modes and considering a moment reduction factors to resist the structural failure, Loehr and Bowders (2007) proposed a combined limit resistance curve as presented in Figure 2.34.

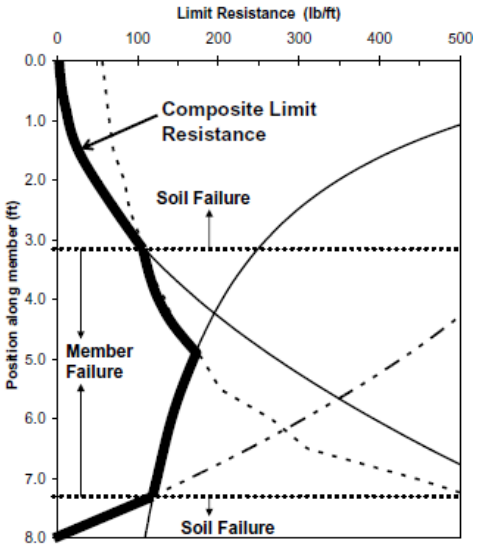


Figure 2.34 Combined Limit Resistance Curve (Loehr and Bowders, 2007)

Once the combined limit resistance curve is developed for a particular condition and slope, the factor of safety of the reinforced slope can be determined using the limit resistance slope stability analysis software including the resistance from the RPP.

The design approach considered by Loehr and Bowders (2007) was very straight forward; however, it considered few assumptions. The limit resistance force of RPP is computed by integrating the limit soil pressure over the length of the reinforcing member above the depth of sliding where it was assumed that the limit soil pressure is fully mobilized along the entire length of the member above the sliding surface. In addition, the limit resistance force is assumed to act perpendicular to the reinforcing member at the sliding surface. On the other hand, the stress strain analysis could be performed to determine the factor of safety of a slope. The major advantage of the stress strain method is that no previous assumption is required to determine the factor of safety. Thus, this method could be a viable alternative to perform slope stability analysis using RPP. However, no previous study was conducted including the issue.

*2.6.3 Installation Method*

Sommers et al., (2000) conducted a study on different construction methods for slope stabilization using recycled plastic pin (RPP). The objective of the study was to evaluate an alternative instrument to install RPP. The author considered several options to evaluate a equipment which must be simple, robust and operable with typical construction labor, readily available with minor changes to conventional equipment, installation rate should be cost effective and the installation should be conducted with minimum damage to RPP. The study was conducted in two phases. During the first phase, a series of small scale laboratory and field tests were conducted using both impact and pseudo vibratory driving method to install reduced scale RPP. On the other

hand, during phase 2, full scale 4 in x 4 in by 8 ft long RPP were driven in field trials using variations of pseudo vibratory installation method.

Sommers et al., (2000) has performed both impact and vibratory methods in the small scale laboratory experiment to evaluate the alternative installation method at minimal cost. Impact driving was evaluated using small drop weight driving mechanism to drive 1.5 inch by 1.5 inch RPP into a drum filled with soil. The method presented that the recycled materials were resilient to driving stresses; however, the driving rate was unacceptable. On the other hand, vibratory driving was evaluated using slightly modified 60 lb pavement breaker which presented that the penetration rates for the pseudo vibratory method performed far better compared to the drop hammer method.

Based on the small scale driving test, the authors selected the pseudo vibratory method for the full scale demonstration site near St. Joseph in Missouri, to install RPP. During the field demonstration test, the driving mechanism consisted of a modified Indeco MES 351 hydraulic breaker mounted on a rubbertired 835 Bobcat® skid loader to install a total of seven 4 inch by 4 inch RPP of 4 ft and 8 ft length. The Penetration rates observed during the field trials varied from 12 ft/min to 0.8 ft/min due to varying soil conditions at the locations of the test drives. However, the relative short wheelbase of the skid loader made it unstable and prone to rolling when working on slopes, particularly when operating the boom and hydraulic hammer at maximum height. In addition, the skid loader lacked sufficient head doom to drive full length of 8 ft RPP. Furthermore, the study was continued to install RPP over a 1:2.5 slope near eastbound entrance ramp to I70 which was located approximately 60 mile west of Columbia, Missouri. A total of four stabilization areas were selected over the slope to install 317 number of RPP. The initial installation equipment was consist of an Okada OKB 305 1695 N-m (1250 ft-lb.) energy class hydraulic hammer mounted on a Case 580 backhoe. However, the attempt using

the equipment was unsuccessful for several reasons. The rubber-tired backhoe was difficult to maneuver on the slope and caused excessive rutting while trying to reach the top of the slope. In addition, maintaining a fixed position during driving was also difficult with the backhoe that tend to slide toward down slope even with the outriggers placed thereby further damaging the slope and making driving RPPs with the correct alignment and placement extremely difficult.

The installation at the slope was further resumed using a Davey-Kent DK 100B crawler mounted drilling rig equipped with a mast capable of 50 deg tilt from vertical forward, 105 tilt backward and side to side tilt of 32 deg with vertical. The study presented that, the rig had numerous advantages compared to all previously used equipment to install RPP. First, the drilling mast provided the alignment of hammer and RPP during driving without requiring any movement of chassis. In addition, the crawler mounted rig was much easier to maneuver on the slope and reduced the set up time between pins. It should be noted that the rig was equipped with a Krupp HB28A hydraulic hammer drill attached to the mast providing a maximum of 295 ft-lbs of energy at a maximum frequency of 1800 blows/min. The hammer energy was further amplified by a push/pull of by the drill mast. The study documented that the penetration rates for pins driven perpendicular to the slope reached 10 ft/min and averaged 5.2 ft/ min. Penetration rates for pins driven vertically were only slightly lower reaching a maximum of 9.6 ft/min and averaging 4.1 ft/min. Installation of RPP using the equipment was significantly faster due to the stability of the equipment that reduced the set up time. Overall, based on the few attempts and using different equipments, the study suggested that the mast mounted system was much more accurate and effective method. In addition, the crawler mounted rig caused much less damage to the slope compared to rubber tired equipment.

*2.6.4 Field Performance*

Parra et al., (2003) had presented a field performance study of two slope sites stabilized with Recycled Plastic Pin (RPP). The sites had experienced recurring surficial slides that ranged in depth between 3 ft to 5 ft. All the sites were dominantly composed of clayey soils. The details of the installation and performance monitoring results are presented below.

2.6.4.1 Interstate-70 (I-70)–Emma Field Test Site

The I-70 Emma field test site is located on I70, approximately 65 mi west of Columbia, Missouri. The height of the slope is 22-ft with 2.5:1 (horizontal: vertical) side slopes that forms the eastbound entrance ramp to I-70 in Saline County. The slope is composed of mixed lean clays with scattered cobbles and construction rubble (concrete and asphalt). The slope had experienced recurring slides in four areas of the embankment over the past decade or more. The plan view of the slide areas of the slope denoted as S1, S2, S3, and S4 is presented in Figure 2.35. The study considered that, S1 and S2 should be stabilized with RPP whereas; the slide area S3 and S4 should serve as the control section. The soil samples from the slide area S1 and S2 were tested in the laboratory and further back analyzed to determine the failure condition. On the basis of these conditions, a 3 ft staggered grid covering the failed areas was selected for stabilization with factor of safety of 1.2.

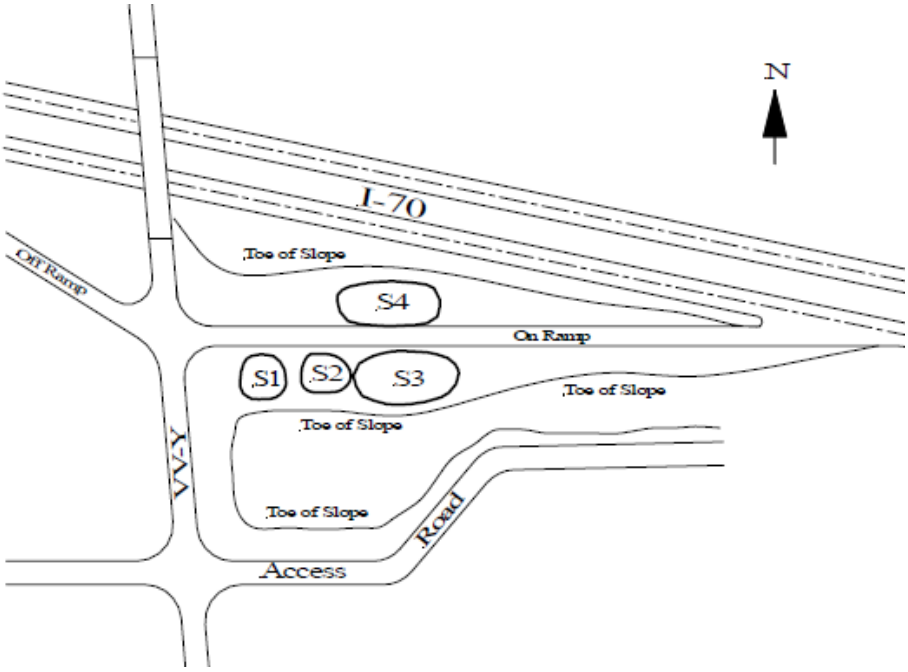


Figure 2.35 Location of the Slide areas in I-70 site (Parra et al., 2003)

The installation at Slides S1 and S2 was conducted during November and December 1999. In Slide S1, reinforcing members were installed approximately perpendicular to the slope face; besides, reinforcing members were installed with a vertical orientation in Slide S2. A total of 199 RPPs were installed into Slide S1 and 163 RPPs were installed into Slide S2. The layouts of the RPP at both of the sections are presented in Figure 2.36.

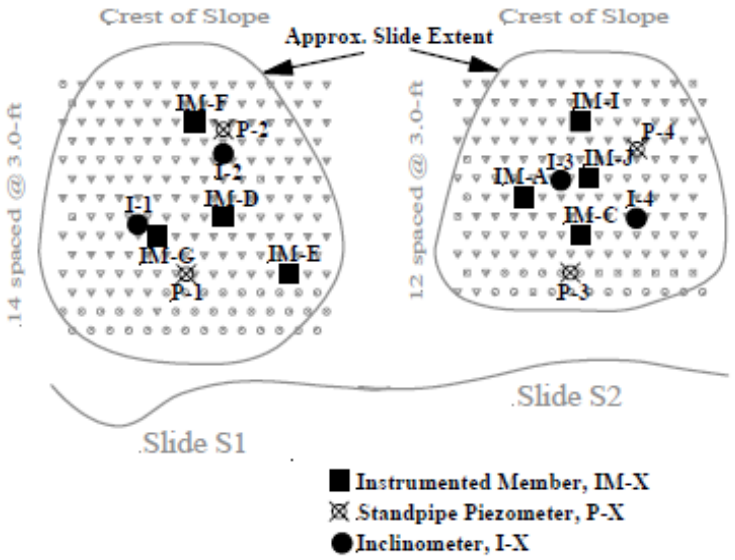


Figure 2.36 Layout of RPP at the slide area of I-70 site (Parra et al., 2003)

After installation, inclinometers and instrumented RPPs were installed to monitor the performance of the stabilized slides. Based on the field monitoring results from inclinometer, the cumulative displacement vs. depth and cumulative displacement vs. time for I-2 is presented in Figure 2.37. It was observed that movements were generally minimal for the first year following installation, after then, the movements increased to a maximum of approximately 0.8 inch over next 6 months. Movements since that time became minimal afterwards. Parra et al. (2003) presented that the observed movements corresponded closely with the rainfall data at the site. Both control slides (S3 and S4) failed in late spring of 2001 when small movements were observed in the stabilized areas. In addition, the continuously screened piezometers and tensiometers installed at the site indicated that increased pore water pressures were present during spring of 2001 of the control slide failures.

The maximum bending moments determined from the strain gauge on three instrumented RPPs are presented in Figure 2.38. The field monitoring results indicated that, member IM-C which was installed in slide S2 gradually increased between installation and April 2001 followed by a small but rapid increase in measured bending moment in May 2001 around the time of control section failure. Besides, Member IM-G in Slide S1 showed a relatively large initial increase in bending moment over the first 6 months after installation followed by essentially constant maximum bending moment with time before being damaged by mowing operations in May 2001. On the other hand, Member IM-H in the control slide showed behavior similar to that observed for IM-C except that the bending moments increased more dramatically in the months leading up to the failure. At the time of the failure, IM-H indicated bending moments of approximately 850 lb-ft, a value that is very near the average moment capacity of the reinforcing members of 900 lb-ft. Member IM-H failed in bending when the control slide failed.

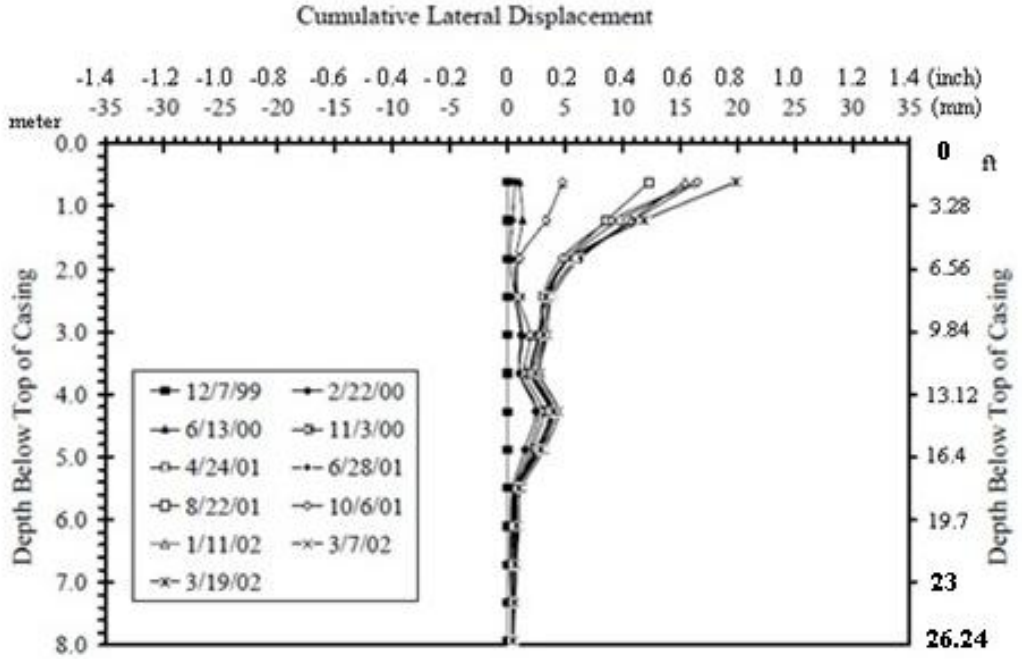


(a)

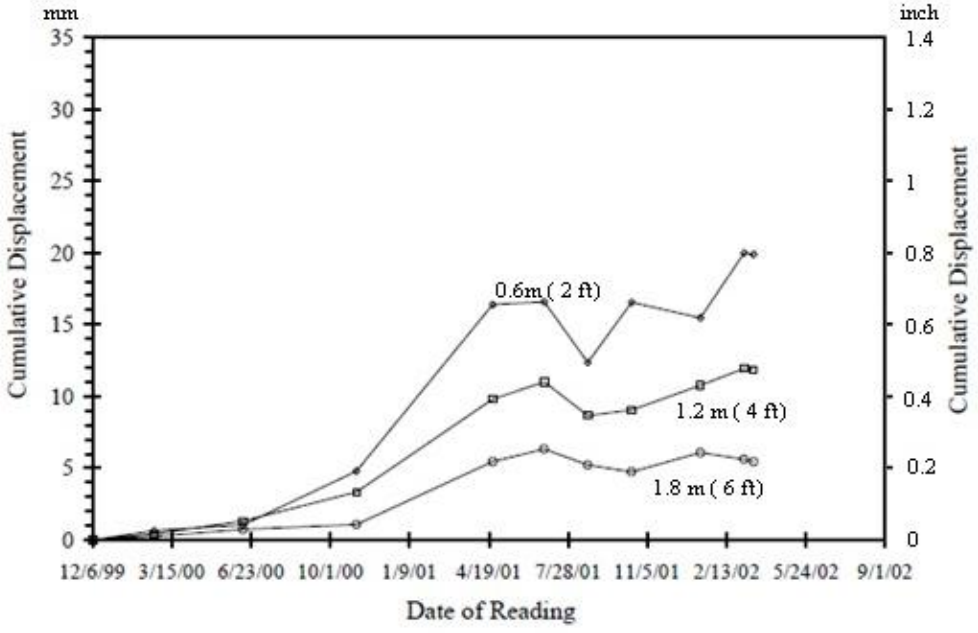


(b)

Figure 2.37 Inclinometer data from I-2 at I-70 Site (Parra et al., 2003)

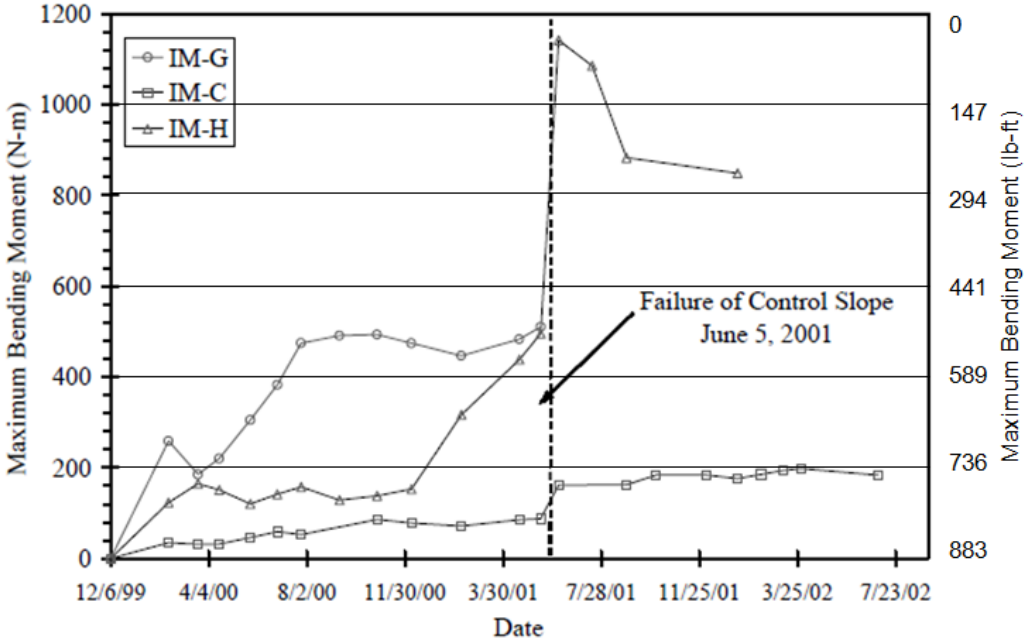


Figure 2.38 Bending moment diagram from Instrumented RPP at I-70 site (Parra et al., 2003)

2.6.4.2 Interstate-435 (I-435)–Wornall Road Field Test Site

The I-435–Wornall Road test site is located at the intersection of I- 435 and Wornall Road in southern Kansas City, Missouri. It was a zoned-fill embankment consisting of a 3-ft to 5-ft surficial layer of mixed lean to fat clay with soft to medium consistency overlying stiffer compacted clay shale. The slope was approximately 31.5 ft high with side slopes of 2.2:1 (horizontal:vertical) and had experienced at least two surficial slides along the interface between the upper clay and was selected for stabilization using RPP. The site was stabilized with 3 ft RPP in a staggered grid with factor of safety ranged between 1.15 and 1.5. The layout of slope stabilization scheme is presented in Figure 2.39. A total of 616 RPPs were installed in 10 working days in the site.

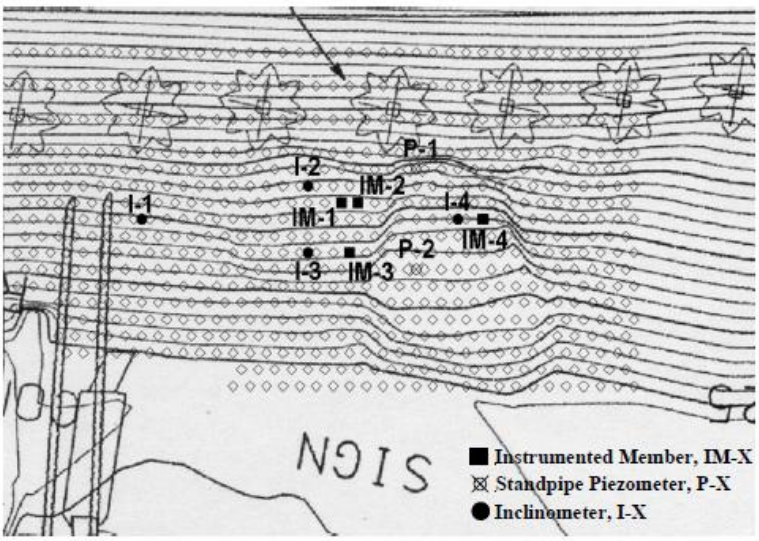


Figure 2.39 Layout of RPP and location of instrumentation in I-435 Wornall Road site (Parra et al., 2003)

Cumulative displacements for Inclinometer I-2 at the I-435–Wornall Road site are presented in Figure 2.40. In I-435 site, Para et al., (2003) observed that the displacements were negligible over a period of several months after installation, followed by increasing displacements during the spring season, after which the displacements essentially ceased. The maximum observed displacement was approximately 1.2 inch during the study. The observed movements were attributed to movements required to mobilize resistance in the reinforcing members.

Based on the study, the maximum moment mobilized in the instrumented RPP at the I-435 site is presented in Figure 2.41. Parra et al. (2003) observed that the maximum moment closely correlated with the movement in the slope. The maximum moments were generally very low during first 4 months following installation. The performance monitoring results indicated that maximum bending moments increased between April and July 2002 during a period of above-average rainfall in the area. The maximum observed moment for all members was approximately 428 lb-ft in instrumented Member

IM-3, near the center of the prior slide area. In addition, moments for the remaining instrumented members remained below 300 lb-ft.

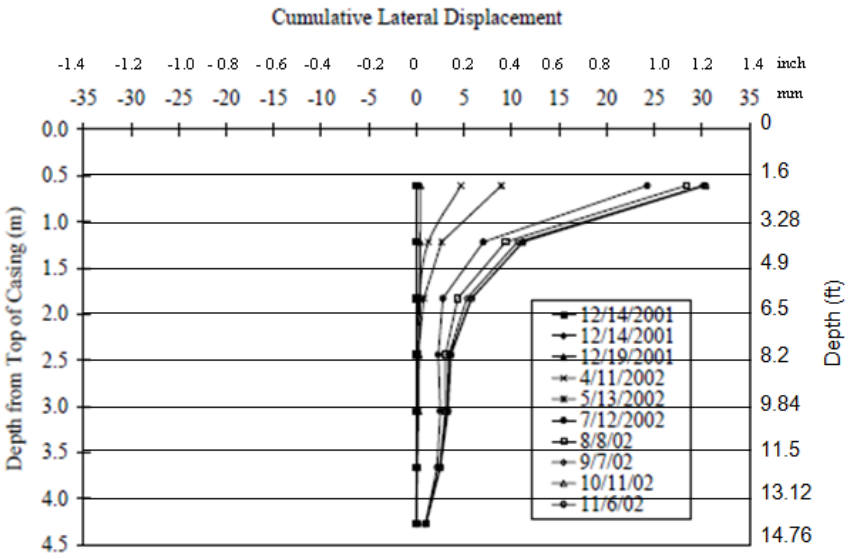


(a)

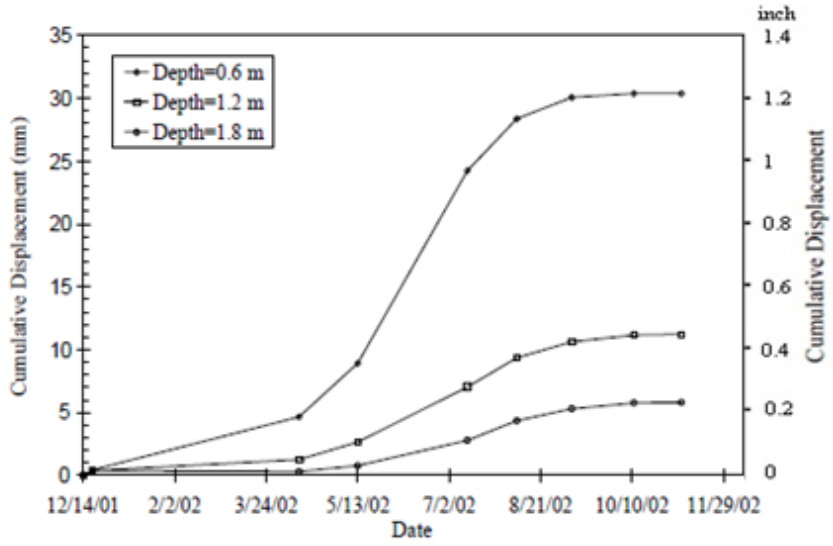


(b)

Figure 2.40 Cumulative Displacement plot of Inclinometer I-2 at I-435 site (Parra et al., 2003)

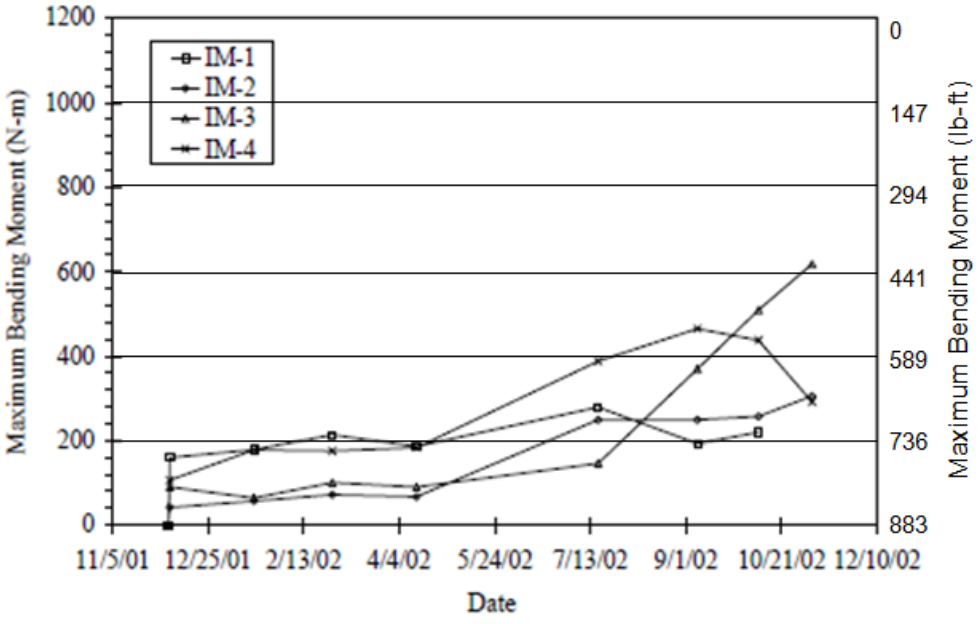


Figure 2.41 Bending moment diagram from Instrumented RPP at I-435 site (Parra et al., 2003)

Loehr et al., 2007 further evaluated the performance of I-435 site based on the monitoring data that ranged between December 2001 and January 2005. Based on the performance monitoring results the variation of precipitation, piezometric levels, cumulative lateral displacement, and mobilized bending moments is presented in Figure 2.42. Loehr et al., (2007) noticed significant deviations from normal trends include extremely heavy precipitation in May 2002 and precipitation drastically greater than normal in the spring and summer of 2004. In addition, a perched water level was observed at top 3 to 5 ft at the lean clay layer near the surface. The piezometric levels were observed at the highest level during the spring and early summer and lowest during winter.

Loehr et al., (2007) observed that the load transfer mechanism was consisted with the precipitation and piezometric levels. The field performance result presented

substantial increment in displacement during first period of above precipitation at the site. At the same time, the bending moments in the instrumented reinforcing members were also increased which was an indication of resistance of the reinforcing member that was mobilized to maintain the stability of the slope. The movement of the slope continued until sufficient resistance from RPP was mobilized to the slope to maintain stability. Afterwards, the author also noticed slight deformation; however, in general the lateral deformation had been minimal following the initial period of mobilization. In addition, the study noticed that the mobilized load was between 10% and 40% of the nominal capacity of RPP and had load capacity left to resist further deformation.

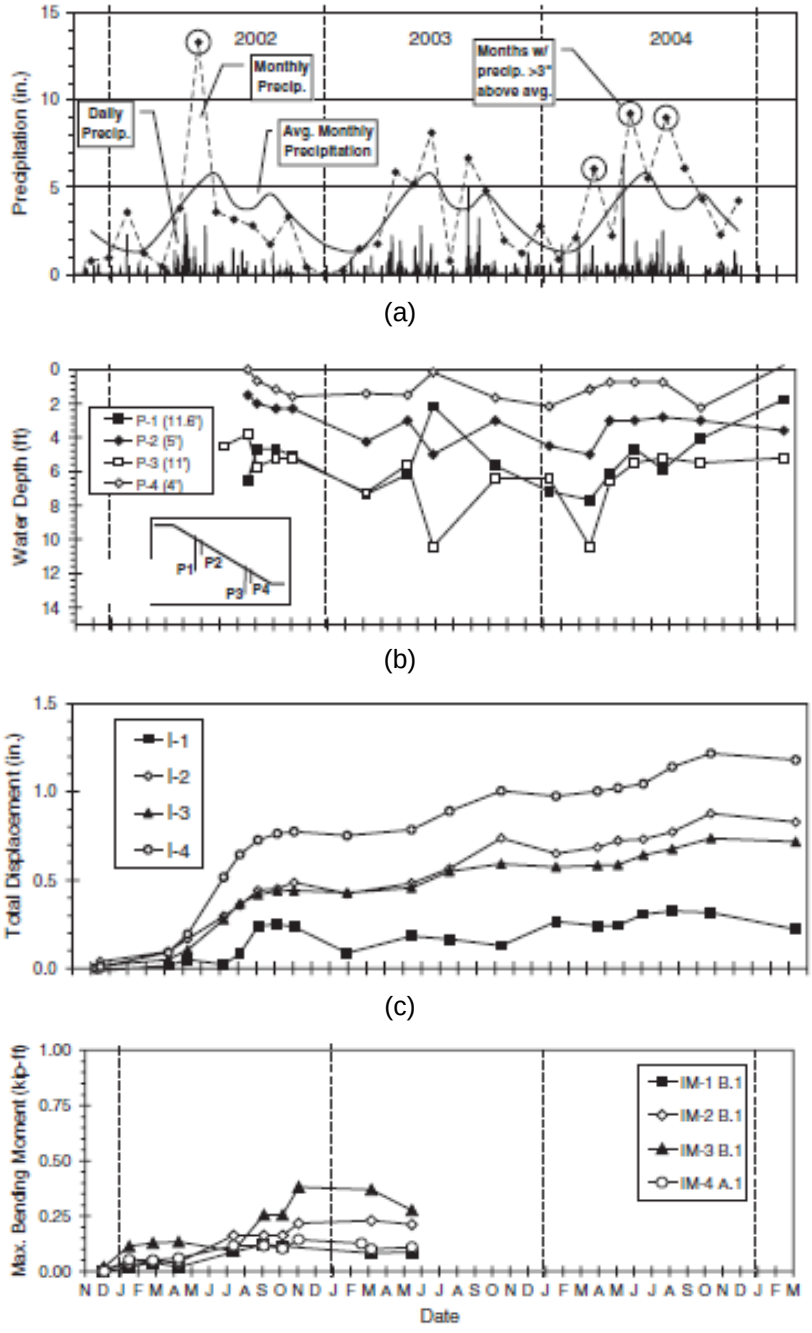


Figure 2.42 Summary of field measurement at I-435 site (Loehr et al., 2007)

2.6.4.3 US 36 Site

Loehr et al., 2007 presented another study of a slope which was stabilized with RPP. The slope was located over the US36-Stewartsville site lies in the median of US36 between the eastbound and westbound sections of the roadway. The extent of the slide was approximately 150-ft wide which was measured parallel to US36. The slope at the site is approximately 29-ft high with an inclination of 2.2:1 (horizontal: vertical). The layout of RPP at US 36 site is presented in Figure 2.43.

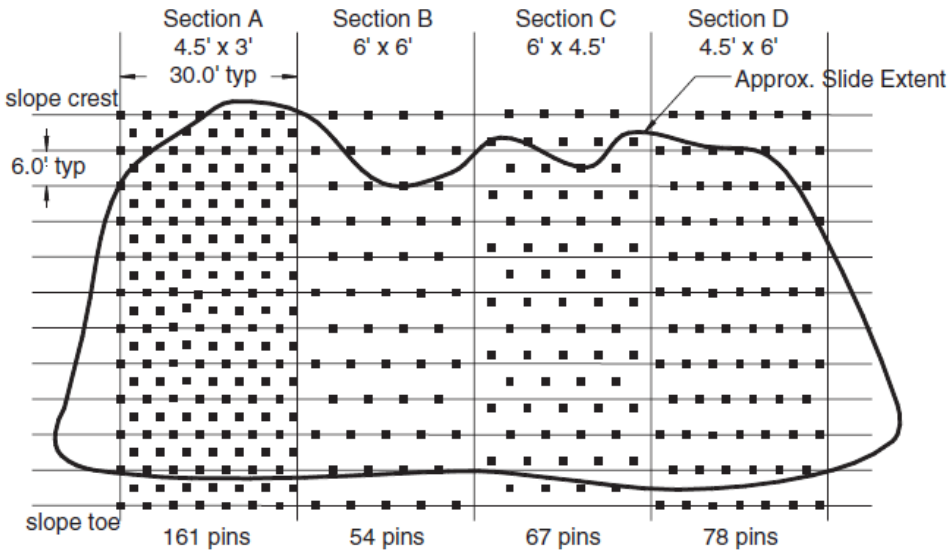


Figure 2.43 locations of RPP at US 36-Stewartsville site (Loehr et al., 2007)

Loehr et al., (2007) illustrated the relationship between lateral deformation and mobilization of load in reinforcing member for US 36 sites as presented in Figure 2.44. The author presented that the lateral deformation and mobilized bending moment observed for an isolated RPP placed within the control section for US36 site. These data indicated little mobilization of load in the reinforcement throughout 2002 and most of 2003 as a result of an extended dry period at the site. However, as precipitation increased both lateral deformations and mobilized bending moments increased in early 2004. In the

summer of 2004, deformations increased dramatically and failure of the control slide area was observed. During this event the maximum bending moment also increased substantially, eventually reaching the moment capacity of the member of approximately 950 lb-ft. Exhumation of the isolated member revealed that it had ruptured at a depth of approximately 5 ft, which is near the location of the maximum measured moments for readings before and following the failure event.

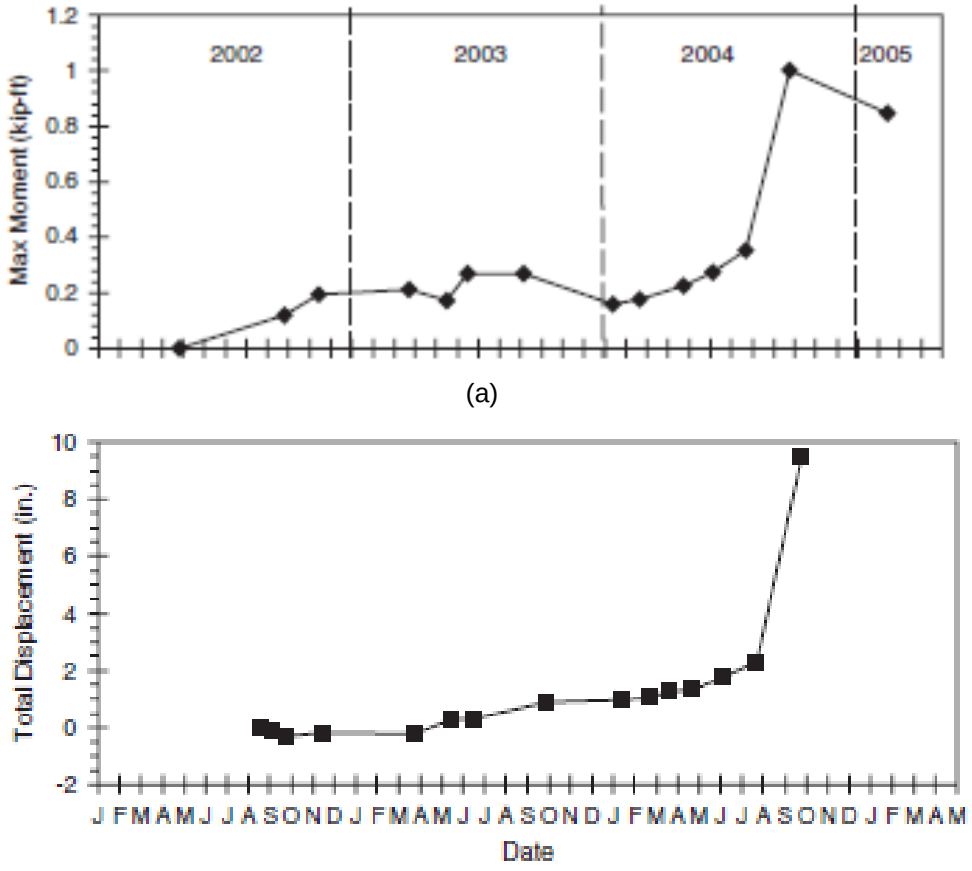


Figure 2.44 Bending Moment and Deformation of isolated member placed within the control slide area at US36 site (Loehr et al., 2007)

On the other hand, Loehr and Bowders, (2007) presented that at different location the observed cumulative displacement was less at different sections located on the stabilized zone. The variation of cumulative displacement at US 36 site is presented in Figure 2.45. The maximum cumulative displacement was observed 2 in which was very less compared to the displacement at the control slope.

Finally, Loehr et al., (2007) summarized that the technique of using RPP to stabilize surficial slope failures in excavated and embankment slopes has proved effective. Based on 6 years of monitoring period, the author observed that the failure to control sections established at several of the sites demonstrated that these sites have likely been subjected to conditions that were at least as bad as those that caused the original failures and that the installed reinforcement is in fact providing additional stabilization.

## 2.7 Limitation of Previous Study

The previous study indicated that RPP could be an effective alternative to stabilize shallow slope failure. However, the performance of stabilized slope using RPP in different in different geological and weather conditions has not been studied. In addition, the previous design method was limited and did not consider the effect of creep of RPP. Therefore, a study is important to verify the performance as well as establish a design protocol using RPP to stabilize shallow slope failure.

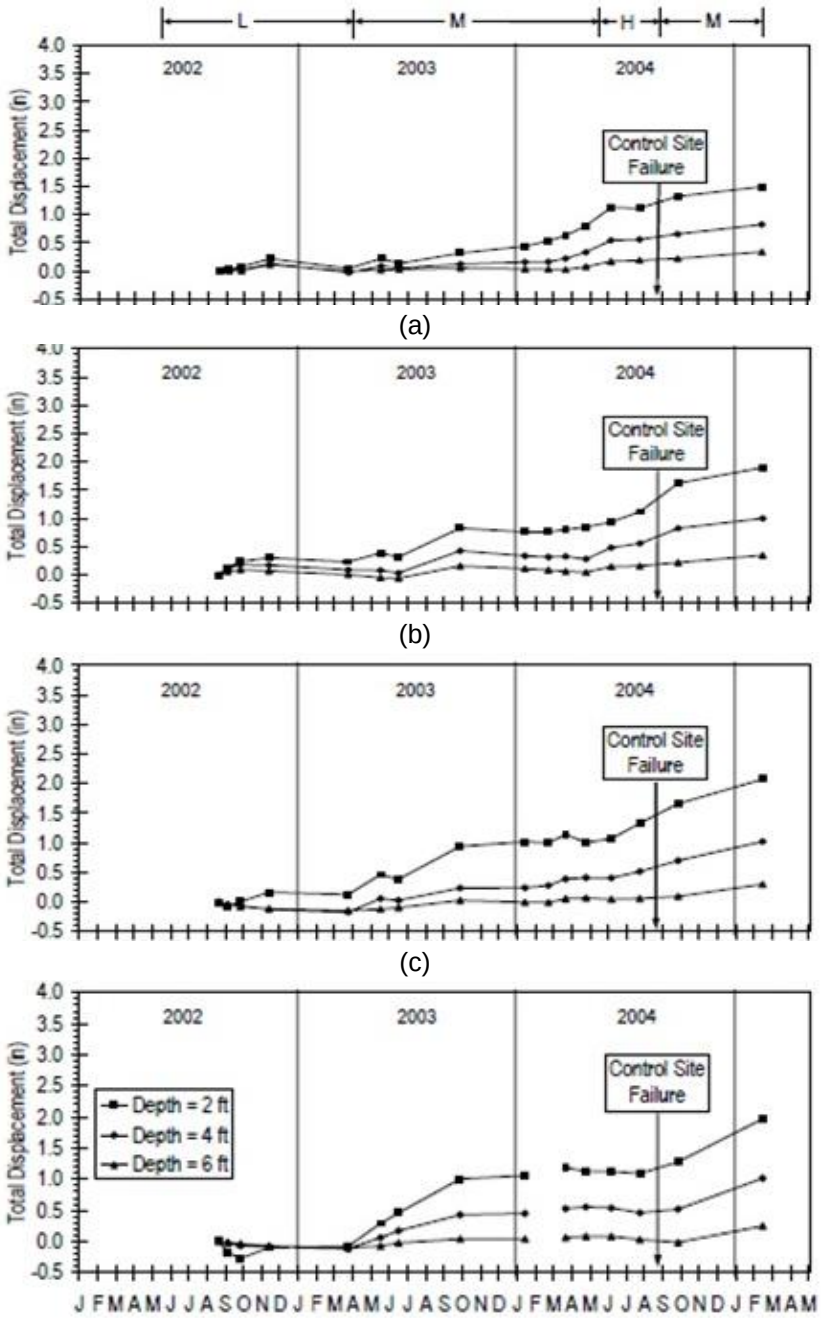


(a)

(b)

(c)

(d)

Figure 2.45 Cumulative Horizontal Displacement of Inclinometer at US 36 slope, a. Section 1, b. Section 2, c. Section 3 and d. Section 4

# Chapter 3

# Site Investigation

## 3.1 Background

The objective of the current study was to establish a sustainable slope stabilization method using Recycled Plastic Pin to stabilize shallow slope failure. Typically, the highway slope constructed using high plastic clay is susceptible to shrinkage and swelling behavior which result in shallow slope failure around the North Texas area. Therefore, two highway slopes were selected in the North Texas region during this current study. The first slope is located over highway US 287 in Midlothian, Texas. Besides, the second slope is located over Highway Loop 12 in Dallas, Texas. Surficial movement was observed in US 287 slopes whereas, crest settlement was observed in Loop 12 slope. A site investigation program was conducted to investigate the cause of the movement of the slopes. The details of the site investigation program are presented in this chapter.

## 3.2 Site Investigation of US 287 Slope

### *3.2.1 Project Background*

The slope is located over Highway US 287, near the St. Paul overpass in Midlothian, Texas. It was a fill slope, constructed during year 2003-2004. The location of the slope is presented in Figure 3.1. The maximum slope height is about 30 ft. to 35 ft., with slope geometry of 3 (H): 1(V). During September 2010, cracks were observed on the shoulder, near the crest of a highway slope, as presented in Figure 3.2.

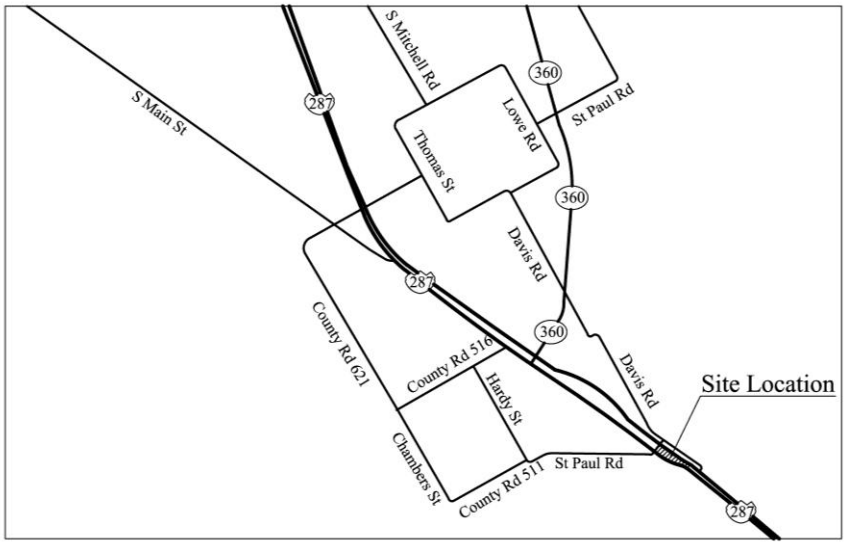


Figure 3.1 Location of the US 287 Slope.

Figure 3.2 Cracks along the Shoulder over US 287 Slope.

*3.2.2 Investigation of Slope Failure*

As a part of the investigation, a subsurface exploration program was conducted on October 2010. Two 2D RI tests were also conducted in the site. The layout of boreholes and the RI lines are presented in Figure 3.3.

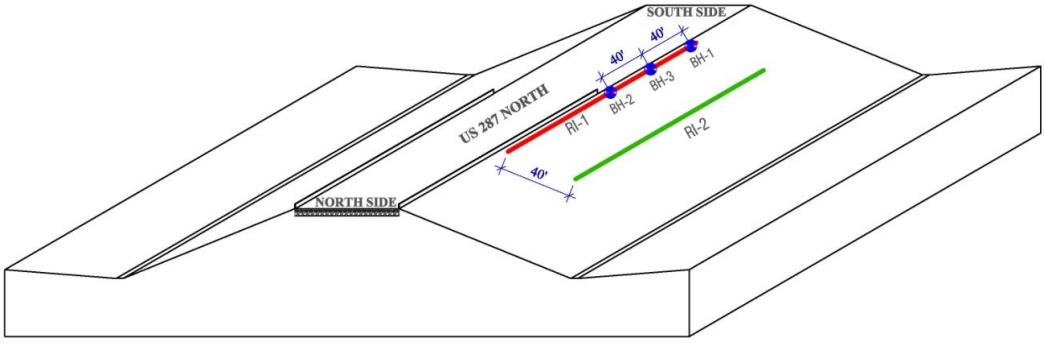


Figure 3.3 Layout of bore holes and resistivity imaging lines

3.2.2.1 Soil Boring and Laboratory Testing

A total of 3 soil test borings were performed near the crest of the slope. The depths of soil test boring ranged from 20 ft. - 25 ft. Both the disturbed and undisturbed soil samples were collected from different depths and tested to determine geotechnical properties of the subsoil. Based on the laboratory investigation results, all the collected soil samples were classified as high plastic clay (CH) soil according to the Unified Soil Classification System (USCS). The liquid limits and the plasticity indices of the samples ranged between 48-79 and 25-51, respectively. The moisture profiles on the depth and plasticity chart along the 3 bore holes are presented in Figure 3.4. In addition, the borehole logs are attached in Appendix A (Figure A1 to Figure A3). The moisture profile indicated an increase in moisture below 5 ft. that ranged up to 20 ft.

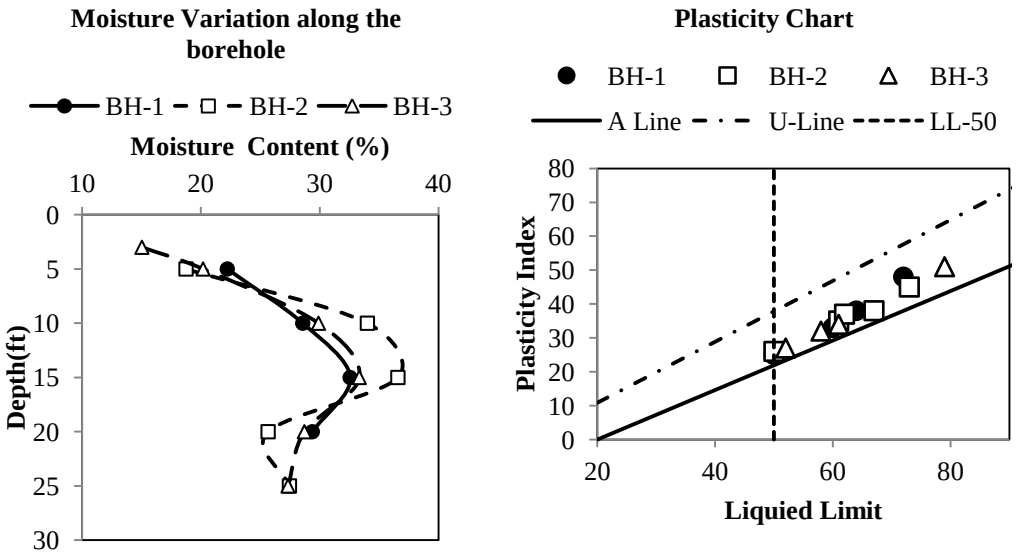


Figure 3.4 Laboratory test results a. Moisture Distribution along the bore holes, b. Plasticity Chart along the bore holes.

The project site is located in the Eagle Ford geological formation, which is composed of residual soils consisting of clay and weathered shale (shaly clay), underlain by un-weathered shale (USGS, 2013). The weathered shale contains gypsum in-fills and debris, jointed and fractured with iron pyrites. The un-weathered shale is typically gray to dark gray and commonly includes shell debris, silty fine sand particles, bentonite and pyrite. The Eagle ford formation consists of sedimentary rock that is in the process of degrading into a soil mass. This formation also contains smectite clay minerals and sulfates. It should be noted that the smectite clay minerals are highly expansive in nature.

3.2.2.2 Resistivity Imaging

With the advancement of new software for the interpretation of resistivity measurements, 2D resistivity imaging (RI) is extensively used in shallow geophysical investigations and geo-hazard studies (Hossain et al., 2010). During the current study,

the RI test was used to investigate the subsurface condition of US 287 slope. A total of two 2D RI lines, designated as RI-1 and RI-2, were conducted at the slope. RI -1 was conducted at the top of the slope near the crest, as presented in Figure 3.5. RI-2 was conducted at the middle of the slope, 40 ft. apart from RI-1.

(a) (b)

Figure 3.5 Resistivity Imaging Field Set-up of (a) RI-1, and (b) RI-2

The RI investigations were conducted using 8-channel Super Sting equipment, which is faster than the conventional single channel unit. A total of 56 electrodes were utilized during the resistivity imaging. The length of the investigated line was 275 ft., with electrode spacing of 5 ft. c/c. The 2D RI profiles along RI -1 and RI -2 are presented in Figure 3.6 (a) and Figure 3.6(b), respectively. In addition, the variations of resistivity along the boreholes are presented in Figure 3.6 (c).

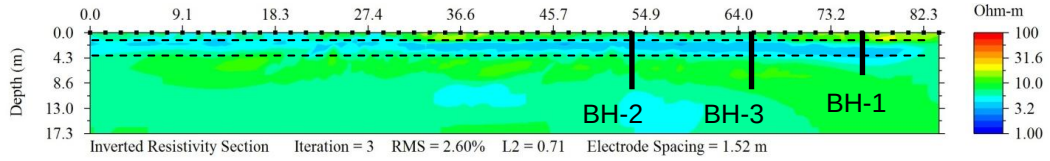


(a)

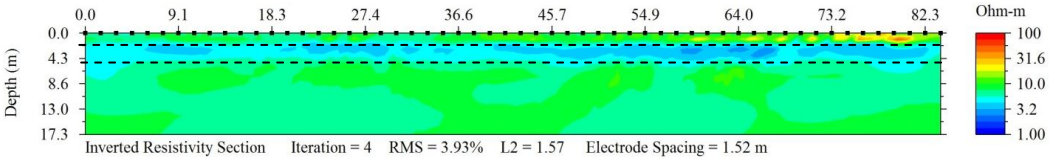


(b)

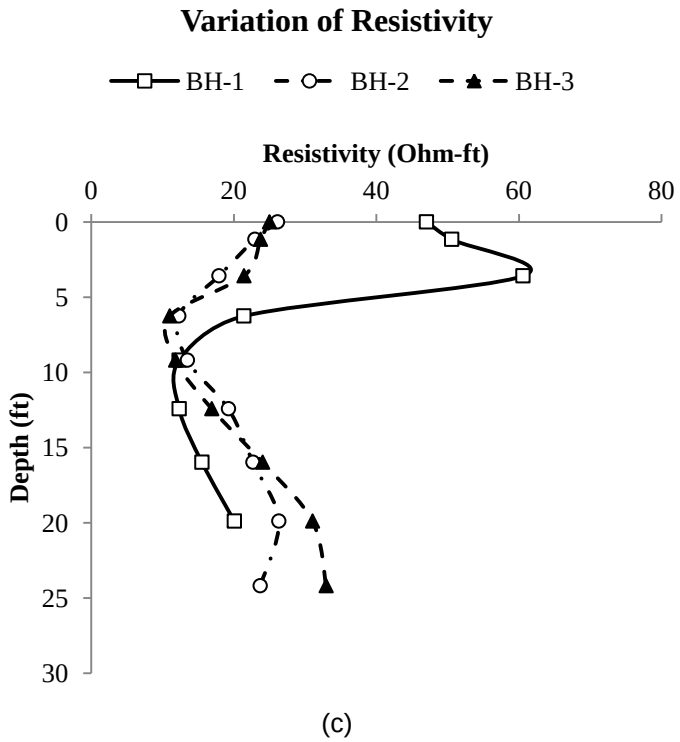


(c)

Figure 3.6 Resistivity Imaging at the US 287 Slope a. Resistivity profile for RI-1, b. Resistivity profiles for RI-2, c. Variation of Resistivity along the boreholes.

Based on the 2D RI profile, a low resistivity zone was observed near the top soil at both RI-1 (at crest) and RI-2 (middle of the slope). The resistivity of slope significantly decreased up to 16.4 ohm-ft. at depth from 5 ft. to 14 ft. It should be noted that the

significant low resistivity might have occurred due to the presence of high moisture in the soil.

*3.2.3 Analyses of Site Investigation Results*

The subsoil investigation results indicated that the US 287 slope was constructed using high plastic clay. In addition, the dominant mineral of the soil is montmorillonite. The high plastic clay, with the presence of montmorillonite, makes it highly susceptible to swelling and shrinking upon wetting and drying. It should be noted that fully softened strengths are eventually developed in high plastic clays in field condition after being exposed to environmental conditions (i.e. shrink and swell, wetting-drying etc) and provide the governing strength for first-time slides in both excavated and fill slopes (Saleh and Wright, 1997). The reduction in friction angle is not significantly due to cyclic wetting and drying of soil; however, the cohesion of the soil almost disappears in the fully softened state (Saleh and Wright, 1997). The near surface soil at the US 287 slope may have been softened due to shrinkage and swell behavior which led to the initiation of movement of slope and resulted the crack over the shoulder.

Based on the subsoil investigation and resistivity imaging, it was evident that a high moisture zone existed between 5 ft. and 14 ft. near the crest of the slope. The shoulder crack provided easy passage of rain water into the slope which eventually led to saturation of soil near the crest. As a result, the driving forces increased, which decreased the factor of safety. It should be noted that the US287 slope did not failed during the investigation. However, the slope might fail within the next few years, as the movement initiated at the crest which is an indication of initiation of failure. The initiated movement might follow any of the possible slip surfaces, as presented in Figure 3.7. A back analysis was performed, using the finite element method, to evaluate the critical shear strength at factor of safety equal to 1.

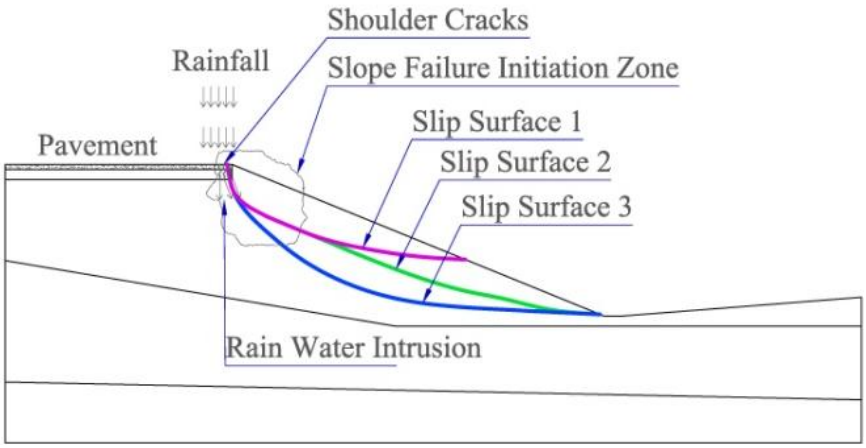


Figure 3.7 Schematic of Possible Surficial Slope Failure

*3.2.4 Slope Stability Analyses at US 287 Slope*

The slope stability analysis by the elasto-plastic finite element method (FEM) is accurate, robust and simple. In addition, the graphical presentation of the FEM program allows better understanding of the failure mechanism. During this study, the slope stability analyses were performed using the FEM program, PLAXIS. The elastic perfectly plastic Mohr-Coulomb soil model was utilized for stability analyses using 15 node triangular elements. The 15-node element provides a fourth order interpolation for displacements and numerical integration that involves twelve stress points. The 15-node triangle is a very accurate element and has produced high quality stress results for different problems. Standard fixities were applied as a boundary condition, where the two vertical boundaries were free to move vertically and were considered fixed in the horizontal direction. The bottom boundary was modeled as fixed boundary.

During the slope stability analyses, it was considered that the initiation of movement of the slope was going to take place with limiting FS equal to 1.0. To evaluate the soil parameters during the initiation of slope movement, back analyses were performed, using PLAXIS 2D. The shear strength reduction method (phi-C reduction

analysis) was utilized to determine the factor of safety (FS). The factor of safety of a soil slope is defined as the factor by which original shear strength parameters can be reduced in order to reach the slope to the point of failure in shear strength reduction method.

The soil profile for the model is presented in Figure 3.8 (a). The top 7 ft. of soil was considered as failure zone, with a fully softened strength. Other soil parameters for different soil layers were utilized from field investigation results. Several iterations were performed during numerical analyses to evaluate soil parameters at failure. The soil parameters observed at failure from numerical modeling are presented in Table 3.1. Based on the FE analysis, the factor of safety was found to be 1.05, as presented in Figure 3.8 (b).

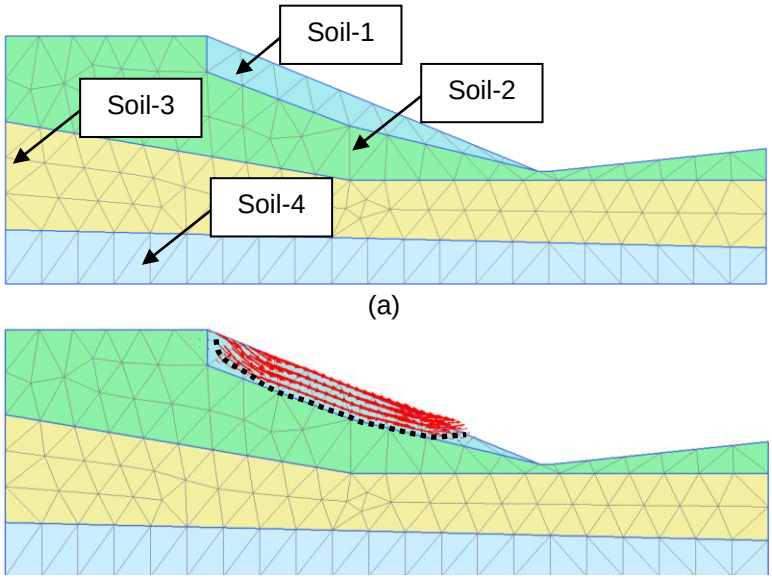


Figure 3.8 Slope Stability Analysis using Plaxis 2D a. Soil Model, b. Critical Slip Surface for Factor of Safety = 1.05

Table 3.1 Soil Parameters

| Soil Type | Friction Angle | Cohesion | Unit Weight | Elastic Modulus | Poisson Ratio |
|---|---|---|---|---|---|
| | φ | c | Ɣ | E | v |
| - | ◦ | psf | Pcf | psf | - |
| 1 | 10 | 100 | 125 | 100000 | 0.35 |
| 2 | 23 | 100 | 125 | 150000 | 0.3 |
| 3 | 15 | 250 | 130 | 200000 | 0.25 |
| 4 | 35 | 3000 | 140 | 250000 | 0.2 |

The FEM analysis indicated the typical failure pattern of shallow slope failure, which resembled the observed displacement trend at the US 287 slope. In addition, the slip surface, as presented in Figure 3.8 (b), was similar with the slip surface 1, as presented in Figure 3.7. To resist any further failure of the slope, it was essential to take remedial action.

## 3.3 Site Investigation of Loop 12 Slope

### *3.3.1 Project Background*

The site is located over Highway Loop 12, near the UP RP overpass in Dallas, Texas. The location of the site is presented in Figure 3.9. The slope at the Loop 12 site has a concrete retaining wall that divides the slope into top slope and bottom slope.

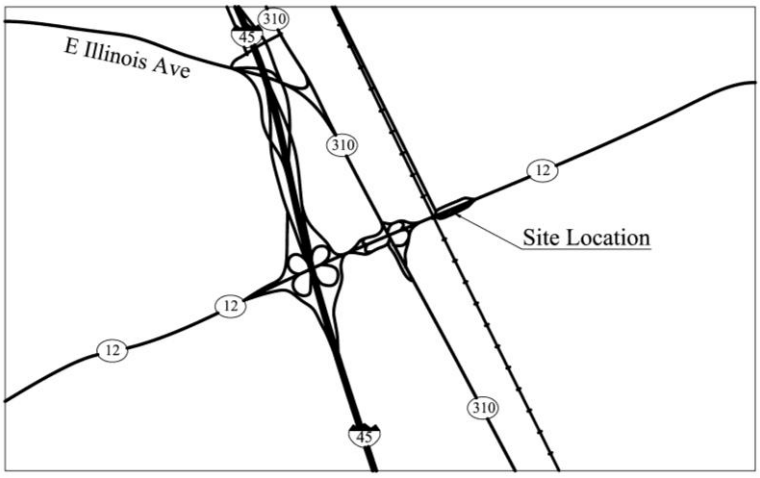


Figure 3.9 Location of Loop 12 slope

A site visit at Loop 12 was performed on August, 2011. Based on the preliminary site visit, it was observed that the crest of the slope, near the end of the bridge, was settled up to 12 inches. At the downstream of the settled portion of the slope, a crack in the concrete retaining wall was observed near the joint. It was also observed that the top of the retaining wall moved out along the bottom slope, near the joint. The site visit pictures are presented in Figure 3.10.

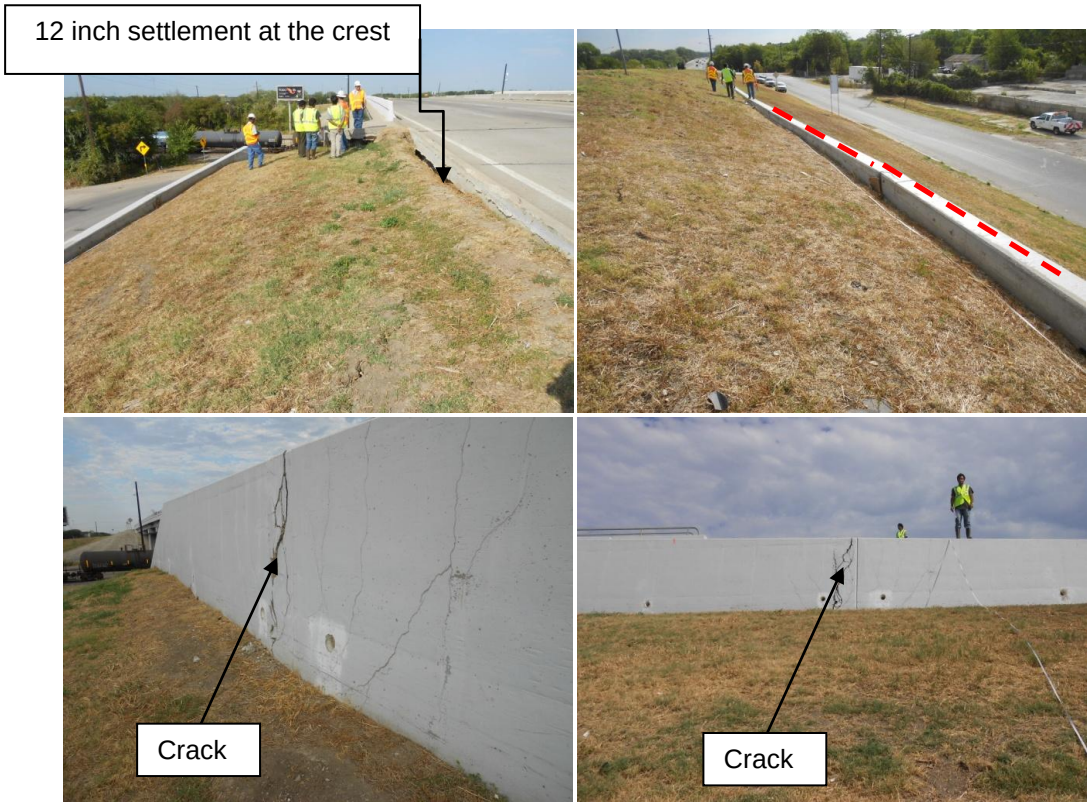


Figure 3.10 Site Visit Picture of Loop 12

*3.3.2 Investigation of Slope Failure*

The site investigation of the Loop 12 slope was performed on August 2011. The site investigation program included geophysical testing using resistivity imaging (RI) and soil test borings. The existing site investigation report that was conducted on the other site of the highway was also reviewed.

3.3.2.1 Soil Boring and Laboratory Testing

Two soil test borings, labeled BH-1 and BH-2, were conducted at the crest of the top slope. The locations of the soil test boring are illustrated on Figure 3.11. Both disturbed and undisturbed samples were collected from the boreholes.

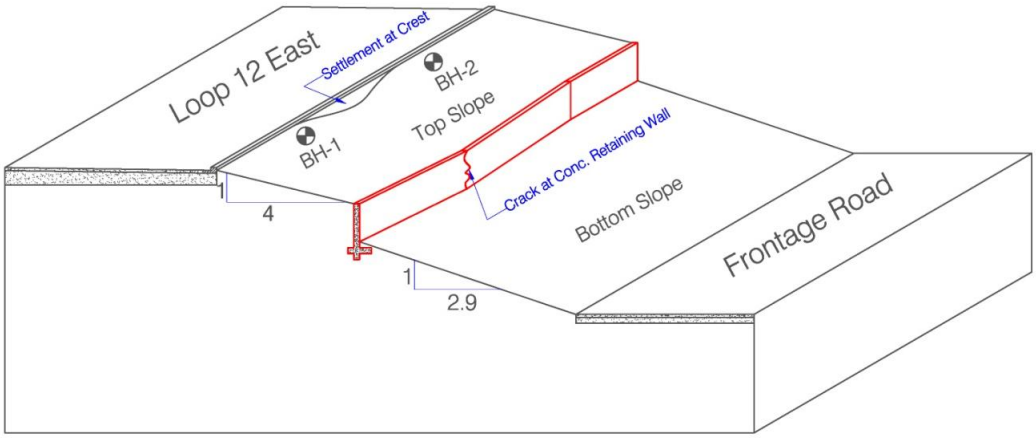


Figure 3.11 Layout of the Bore Holes

The soil test borings and laboratory test results indicated that the Loop 12 slope was constructed using medium-to-high plastic clay soil. In addition, a high moisture zone was observed between 10 ft. and 15 ft. from the laboratory investigation, as presented in Figure 3.12. The Unconfined Compression (UC) test showed the cohesive strength of the soil between 2400 psf (at 10 ft. depth) and 3040 psf (at 20 ft. depth).

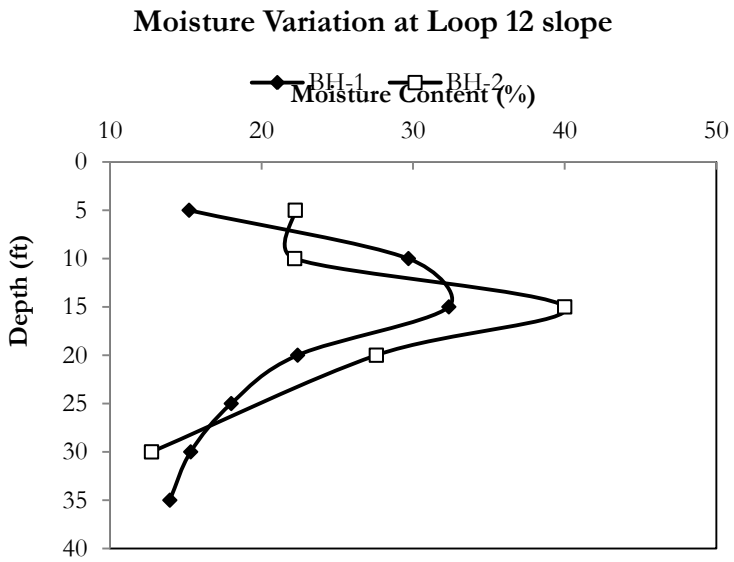


Figure 3.12 Moisture Content of Collected Soil Samples at Loop 12 Slope

3.3.2.2 Resistivity Imaging

Two lines of 2D resistivity imaging, designated as Resistivity Line-1 and Resistivity Line-2, were conducted at the top slope, near the failed area. The layout and field set-up of the resistivity imaging is presented in Figure 3.13 and Figure 3.14. The Resistivity Line-1 was located near the crest of the top slope. The Resistivity Line-2 was located close to the concrete retaining wall. Both of the lines were conducted using an 8 channel Super Sting resistivity meter. A total of 56 electrodes were utilized at 5 ft. c/c spacing. The length of the test line was 275 ft. It should be noted that dipole-dipole array was utilized during the resistivity imaging at Loop 12 slope.

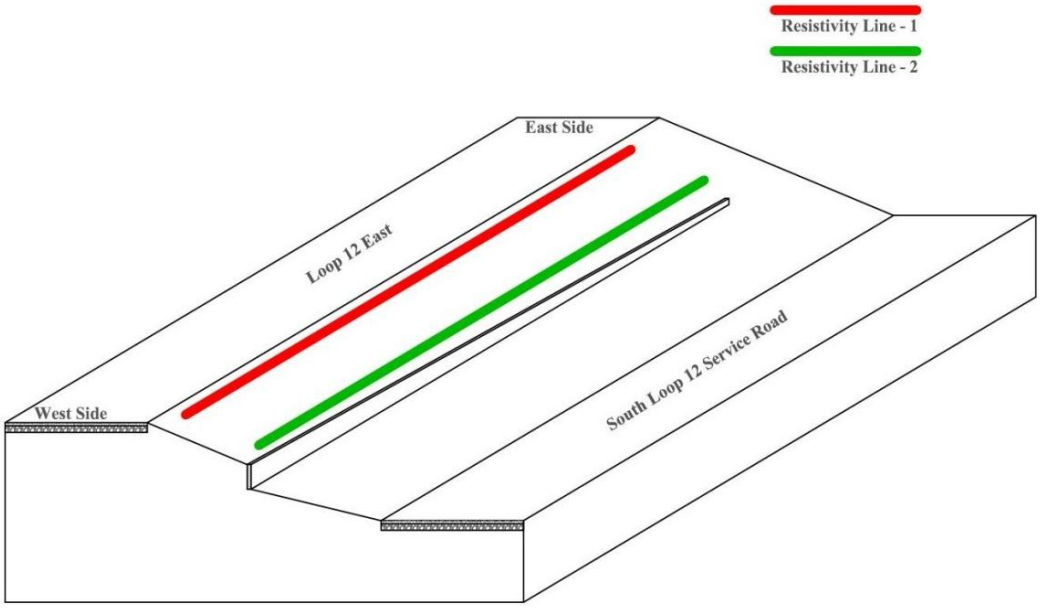


Figure 3.13 Resistivity Imaging Layout at Loop 12 Slope

(a) (b)

Figure 3.14 Resistivity Imaging Field Set-up at Loop 12 Slope a. Resistivity Line 1 and b. Resistivity Line 2

The 2D imaging results are presented in Figure 3.15. Based on the RI results, low resistivity areas were observed at a depth of 5 ft. to 10 ft. below the existing ground surface. It should be noted that the presence of low resistivity may take place due to the presence of high moisture content at the location.

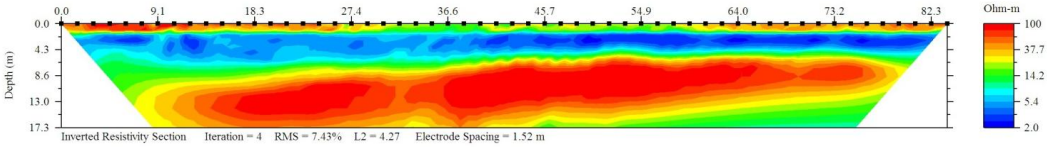


(a)

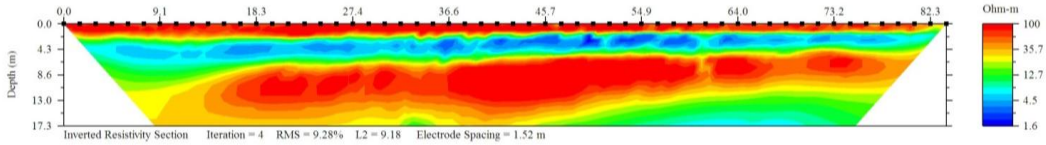


(b)

Figure 3.15 Resistivity Imaging Results at Loop 12 Slope, a. Resistivity Line-1, b. Resistivity Line-2

*3.3.3 Analyses of Site Investigation Results*

The soil boring results presented that the soil type is medium-to-high plastic clay soil. In addition a high moisture zone was observed, which ranged between 5 ft. and 15 ft. The resistivity imaging results also indicated a low resistivity zone near the top soil, which might take place due to the existence of high moisture. Therefore, the soil boring and resistivity imaging results were in good agreement.

The medium-to-high plastic clay soil is susceptible to shrinkage and swelling behavior during wet-dry cycles. Due to the wet-dry cycle, the strength of the soil might reduce to fully soften strength. In addition, the shrinkage cracks act as a potential conduit for the intrusion of rain water. It should be noted that the failure of the slope occurred after the rainfall events. During and after rainfall, the soil at the top slope became saturated due to moisture intrusion. The permeability of the high plastic clay is relatively low. Therefore, the percolated rain water may not have drained quickly, thereby creating a perched water condition. The perched water zone caused an increase in pore water pressure and decrease in shear strength. There is a possibility of increased lateral pressure on the concrete retaining wall with the presence of perched water zone. As a result, the retaining wall slid toward the bottom slopes. The movement of the wall resulted in a crack near the construction joint and settlement at the top slope. The possible failure mechanism of the slope is illustrated in Figure 3.16.

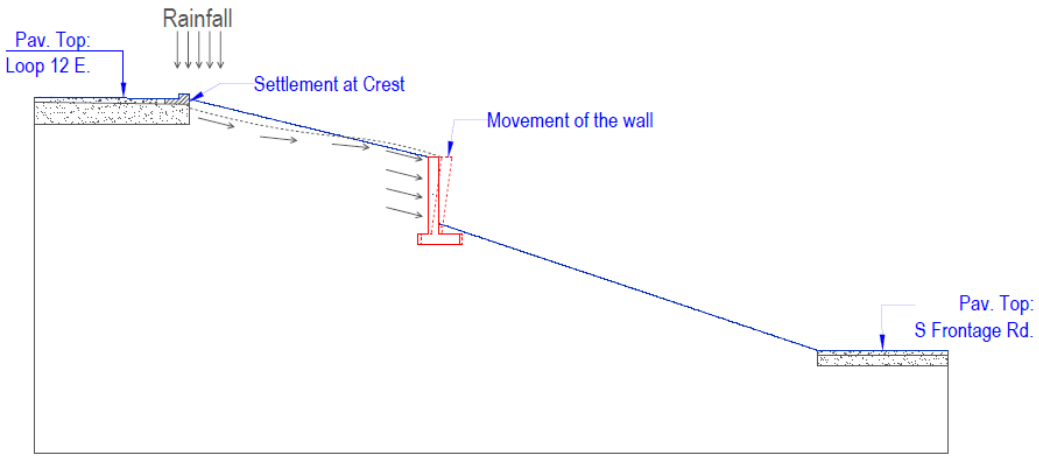


Figure 3.16 Mechanism of Slope failure at Loop 12 Slope

*3.3.4 Stability Analysis Using Plaxis*

Slope stability analyses were performed using the Finite Element program PLAXIS. The general Mohr-Coulomb soil model was used for the stability analyses. Three different soil layers were identified during the field investigation. Modeling was performed, using the fully softened shear strength of the soil for the top soil. In addition, a perched water condition was considered at the top slope. Soil strength beyond the failure zone was not reduced for the analysis. Soil parameters used for the analyses are presented in Table 3.2. Soil parameters were used from the existing soil report.

Table 3.2 Soil Strength Parameters for Loop 12 Slope

| Material | $\gamma_{unsat}$ (lb/ft$^3$) | γsat (lb/ft$^3$) | c (psf) | phi | E (lb/ft$^2$) | N |
|---|---|---|---|---|---|---|
| Top Soil (Soil 1) | 115 | 123 | 35 | 23 | 150000 | 0.35 |
| Embankment (Soil 2) | 115 | 123 | 100 | 25 | 200000 | 0.3 |
| Sand (Soil 3) | 120 | 125 | 0 | 30 | 250000 | 0.25 |

The factor of safety obtained from the analysis without RPP was found to be 1.01. The soil model and result for the stability analysis is presented in Figure 3.17. Plastic calculation was conducted for elasto-plastic deformation analysis, and a Phi C reduction analysis was conducted for the slope stability analysis of the slope.

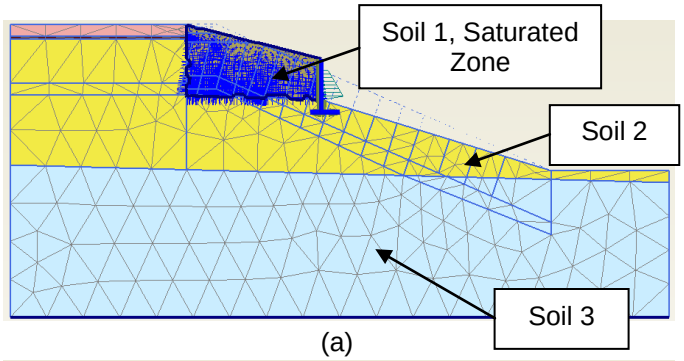


(a)

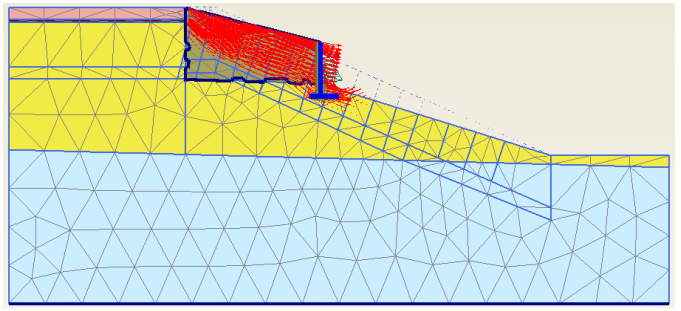

(b)

Figure 3.17 Slope Stability Analysis a. Soil Model with Saturated Zone, b. Slip Surface with FS = 1.01

Chapter 4

Slope Stabilization Using Recycled Plastic Pin

## 4.1 Mechanism of Slope Stabilization

RPP driven into the slope face may cross the slip surface that provides an additional resistance force along the slip plane to increase the factor of safety. In general, the definition of factor of safety is the ratio of resisting moment ($M_R$) to the driving moment ($M_D$), as presented in Eq. 4.1. RPP installed at the slope offers an additional resisting moment ($\Delta M_R$) that increases the factor of safety, as presented in Eq. 4.2. The schematic diagram of RPP as slope reinforcement is presented in Figure 4.1.

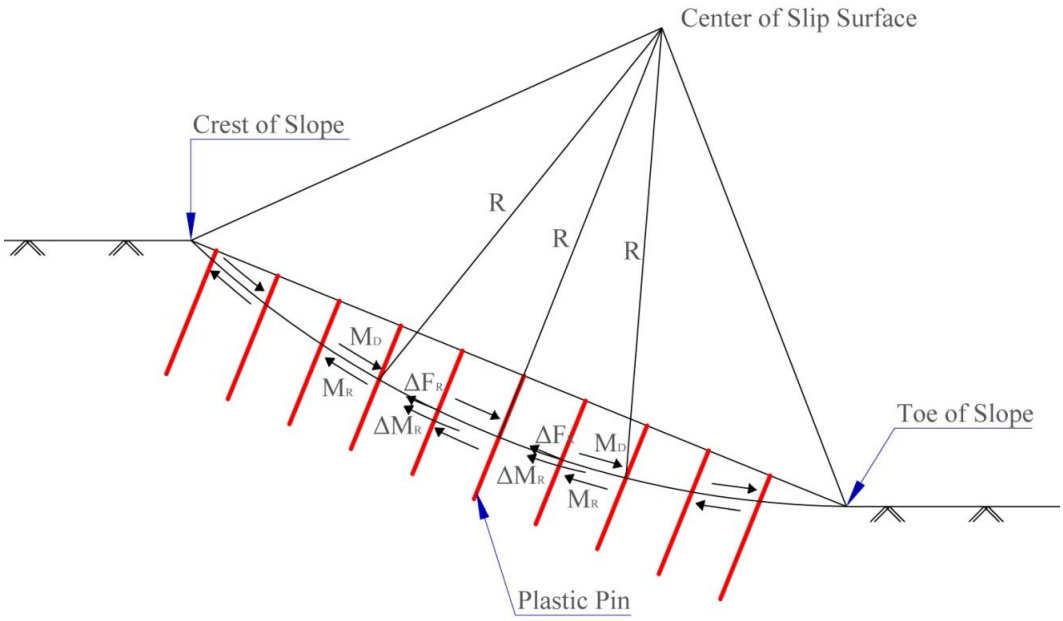


Figure 4.1 Schematic of Resistances from RPP as Slope Reinforcement.

$$FS=F_R/F_D \quad (4.1)$$

$$FS = (F_R+\Delta F_R)/F_D \quad (4.2)$$

Where, $F_R$ = Resisting Moment along Slip Surface

$F_D$ = Driving Moment along Slip Surface

$\Delta F_R$ = Additional Resisting Moment from Plastic Pin

## 4.2 Material Selection

A typical RPP is composed of High Density Polyethylene, HDPE (55% – 70%), Low Density Polyethylene, LDPE (5% -10%), Polystyrene, PS (2% – 10%), Polypropylene, PP (2% -7%), Polyethylene- terephthalate, PET (1%-5%), and varying amounts of additives i.e. sawdust, fly ash (0%-5%) (McLaren, M. G., 1995). Nosker and Renfree (2000) presented a study on the evaluation of the recycled plastic lumber and its applications on different civil engineering applications. For the successful utilization of the recycled plastic lumber, the major concern for the structural application is the elastic modulus and the time-dependent mechanical behavior (creep). To improve the mechanical properties and stiffness of the recycled plastics, glass and wood fibers were added to produce recycled plastic composites. The use of glass and wood fiber additives improves the modulus of elasticity for plastic lumber significantly (Breslin et al. 1998; Lampo and Nosker, 1997, Nosker and Renfree, 2000). According to Van Ness et al. (1998), the recycled plastic lumber that contained oriented glass fiber was most creep resistant over time.

RPP is commercially available in different lengths, sizes and shapes (i.e. rectangular, circular, square). Moreover, the composition of RPP also varied, as it is manufactured from the recycled plastics from different sources. Based on available options, 4 in. x 4 in. fiber-reinforced RPP was selected due to its improved elastic modulus and creep resistant behavior. The selected RPP samples were tested to determine the flexural strength for the remedial design of the US 287 slope and the Loop 12 slope.

## 4.3 Experimental Study

A total of 9 RPP samples were tested to evaluate the flexural strength, using 3 point bending test in accordance with ASTM D790. Loehr and Bowders, (2007) presented that the strength and stiffness of RPP is sensitive to loading rate. Bowders et al. (2003) conducted an experimental study of RPP for slope stabilization where the deformation rates were utilized 5 to 10 times lower than the suggested value in ASTM D6109. Since the loading rate in slope stabilization is much lower than the suggested loading rate in accordance to ASTM D790, the 3 point bending test was conducted at 3 different loading rates (0.5 kips/min, 2.7 kips/min and 4.9 kips/min) that ranged between the ASTM D790 and suggested loading rate for slope stabilization. A total of 3 samples were tested for each loading rate.

The stress strain response at different loading rates is presented in Figure 4.2. The flexural strength and elastic modulus of RPP ranged between 3.1 to 4.7 ksi and 190 to 200 ksi, respectively. The experimental results were further utilized for the design of slope remediation.

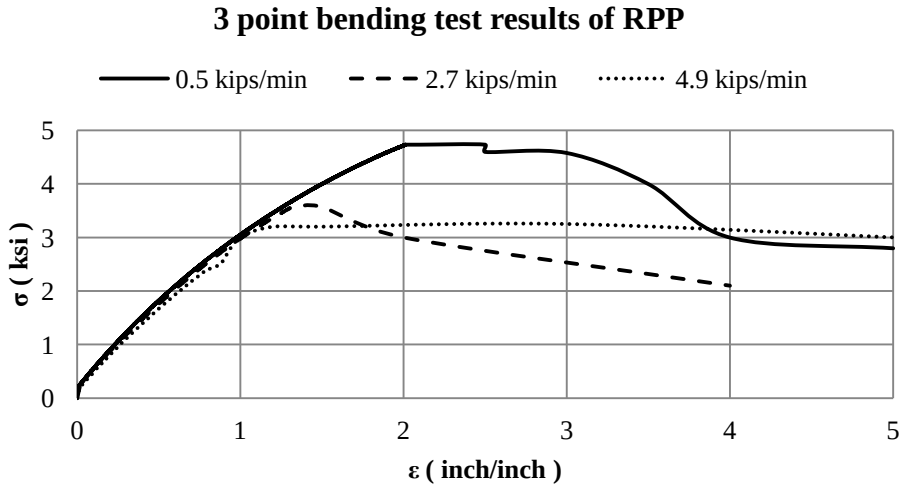


Figure 4.2 Stress-Strain Response of RPP at Different Loading Rates

## 4.4 Design of Slope Stabilization Scheme: US 287

Two sections over the US 287 slope, designated as Reinforced Section 1 and Reinforced Section 2, were considered for stabilization at the beginning of the study. In addition, an unreinforced control section was considered between the reinforced sections to evaluate the performance of the reinforced section. A new reinforced section, designated as Reinforced Section 3, and unreinforced section, identified as Control Section 2, were considered later of tater. The width of each section was 50 ft.

A combination of different lengths and spacing of RPP was considered for Reinforced Section 1. On the other hand, RPP at uniform spacing was considered for Reinforced Section 2 and Reinforced Section 3. During rainfall, water easily gets into the slope through the crack over the shoulder and saturated the soil near the crest. As a result, the pore water pressure at the saturated zone increases and decreases the shear strength. It was evident that the cracked zone was the initiation point of critical slip surface of the US 287 slope. Therefore, to resist the movement of the slope and provide additional support, RPP at closer spacing was provided at the crest of the slope. As a result, 10 ft. long RPP at 3 ft. c/c spacing was considered near the crest of the slope at Reinforced Section 1. It was expected that the resistance from the RPP at the middle of the slope was not critical. Therefore, 6 ft. c/c spacing of RPP was taken into account at the middle of the Reinforced Section 1. Near the toe, 5 ft. c/c spacing was proposed, with 8 ft. length of RPP.

Different lengths of RPP (10 ft. at the crest and 8 ft. near the toe) were considered at Reinforced Section 2; whereas, Reinforced Section 3 was considered with constant length of RPP (10 ft.) throughout the entire slope. During this current study, RPP spacing of 4 ft. c/c was utilized for both Reinforced Section 2 and Reinforced Section 3. However, the first 2 rows of RPP at the crest of Reinforced section 3 were considered

with 3 ft. c/c spacing. In addition, the first 2 rows should be installed below a 2 ft. depth from the existing slope surface. RPP was considered to be placed in a staggered grid over the reinforced sections. The proposed layout and cross section at each of the sections are presented in Figure 4.3 and Figure 4.4.

Based on the proposed distribution of RPP, the slope stability analyses were further conducted to evaluate the factor of safety of each reinforced section. The factor of safety was observed as 1.43, 1.48 and 1.54 for the Reinforced Section 1, Reinforced Section 2 and Reinforced Section 3 respectively. The critical slip surfaces for each of the reinforced sections are presented in Figure 4.5.

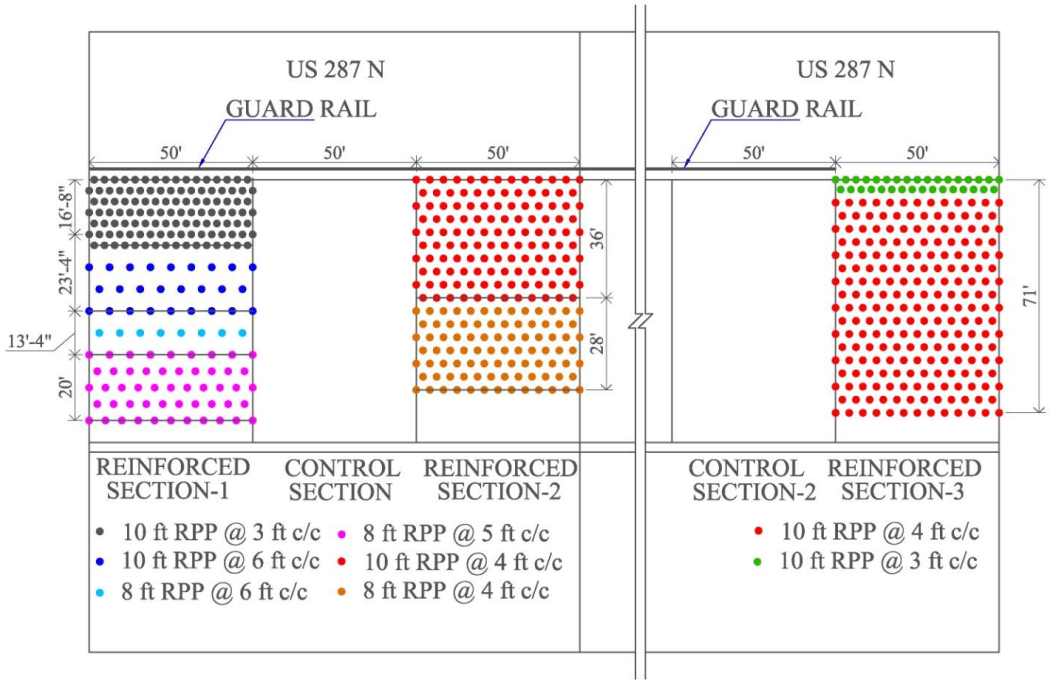


Figure 4.3 Proposed RPP Layout at US 287 Slope.

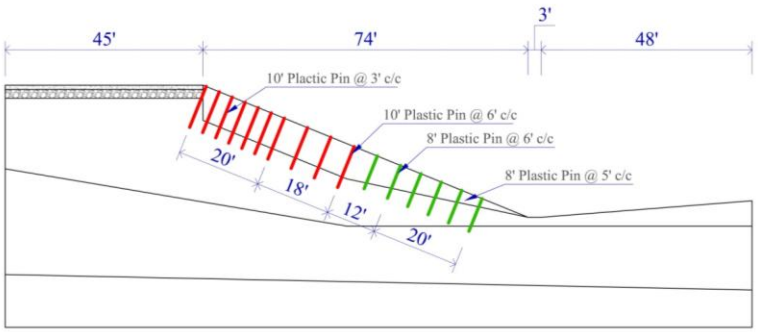


(a)

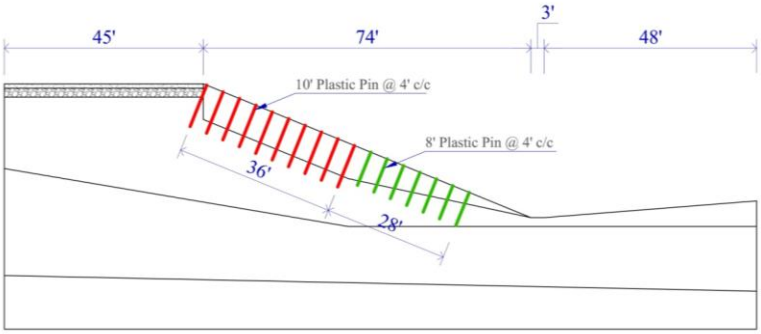


(b)

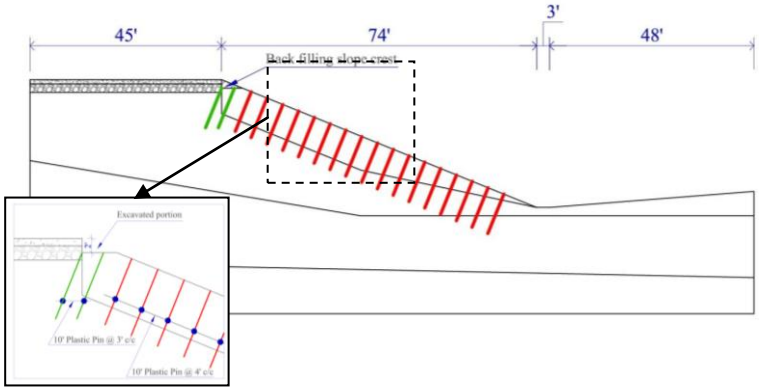


(c)

Figure 4.4 Section Details of Slope Stabilization on US 287 Slope, a. Reinforced Section 1, b. Reinforced Section 2, c. Reinforced Section 3

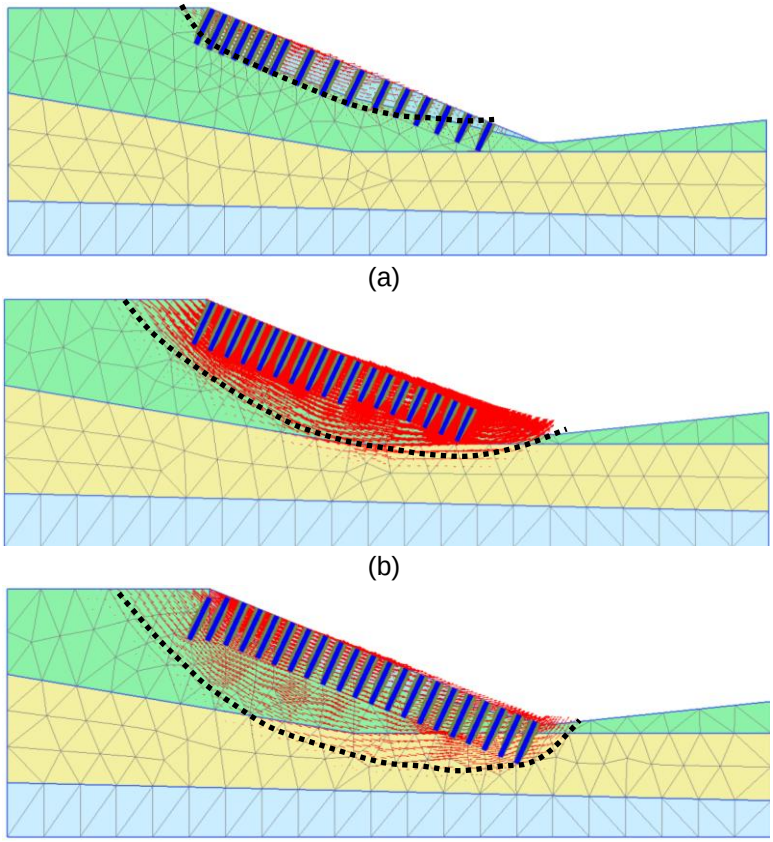


Figure 4.5 Slope Stability Analyses using RPP a. Reinforced Section 1 with FS 1.43, b. Reinforced Section 2 with FS 1.48 c. Reinforced Section 3 with FS 1.54

## 4.5 Installation of RPP: US 287 Slope

Sommers et al., (2000) performed a study on different construction techniques that could be used to install RPP in field scale. The study summarized that the mast-mounted pseudo vibratory hammer system worked well for field installation. The mast-mounted hammer system maintains the alignment of the hammer and restricts imposing additional lateral loads during the RPP driving process (Bowders et al., 2003). Therefore, a similar crawler-type drilling rig that had a mast-mounted vibrator hammer (model: Klemm 802 drill rig along with KD 1011 percussion head drifter) was utilized during the

current study to install the RPP. The crawler-type rig is suitable for the installation process over the slopes, as no additional anchorage is required to maintain the stability of the equipment, which reduces labor, cost and time of the installation process. The RPP installation photographs at the US 287 slope are presented in Figure 4.6 and Figure 4.7.

Figure 4.6 Installation Photo of RPP at Reinforced Section 1 and Reinforced Section 2.

Figure 4.7 Installation of RPP at the Crest of Reinforced Section 3

The RPP driving time was measured during the installation process. Based on the measured driving time, the average installation time, as well as the driving rate, is summarized in Table 4.1. It should be noted that the installation time per RPP is the summation of the time required to install and to maneuver the rig to the next location. At Reinforced Section 1, the driving rate was observed as 2.85 ft/min. at 3 ft. c/c spacing for 10 ft. long RPP. The driving rate reduced to 2 ft/min. along the middle of the slope, with increase in RPP spacing of 6 ft. c/c. The reduction in driving rate was observed due to the longer maneuver time to shift equipment between higher spacing of RPP. Conversely, the highest driving rate of 3 ft/min. was observed near the toe of the Reinforced Section 1. The soil near the toe of the Reinforced Section 1 was very soft during the installation process. As a result, the installation time to drive RPP into the slope was reduced drastically, resulting in the highest driving rate. The overall average driving rate for Reinforced Section 1 was observed as 2.72 ft/min.

The driving rate was observed as 3.6 ft./min. at the top of Reinforced Section 2, where the RPP spacing was 4 ft. c/c. The driving rate was higher than the Reinforced Section 1, as the installation team became more efficient with the installation process. The driving rate was 2.6 ft./min. near the toe of Reinforced Section 2. It was lower due to the existence of a stiff foundation layer at that location. The overall driving rate at Reinforced Section 2 was observed as 3.18 ft/min.

The installation in Reinforced Section 3 was conducted in the following year that had similar RPP spacing as Reinforced Section 2. However, a lower driving rate of 2.13 ft./min at Reinforce Section 3 was observed compared to the Reinforced Section 2. It should be noted that a new team installed the RPPs in Reinforced Section 3. Moreover, the RPP experienced a stiff foundation soil after a 7 ft. depth from the surface, which resulted in a higher installation time. The installation process was also delayed due to

some driving equipment mechanical problems. As a result, the driving rate was low at the Reinforced Section 3.

Based on the study, the average driving rate, considering all three reinforced sections, was 2.66 ft/min., which signified that a 10 ft. long RPP could be installed within 4 min. Therefore, on average, a total of 100 to 120 numbers of RPPs could be installed within a day.

Table 4.1 Average RPP Driving Time at US 287 Slope

| Location of RPP | Length of RPP (ft.) | RPP Spacing (ft.) | Average RPP Driving Time (min) | Average RPP Driving Rate (ft./min) |
|---|---|---|---|---|
| Reinforced Section 1 | 10 | 3 | 3.55 | 2.9 |
| | 10 | 6 | 4.76 | 2.1 |
| | 8 | 6 | 3.65 | 2.2 |
| | 8 | 5 | 2.63 | 3.1 |
| Reinforced Section 2 | 10 | 4 | 2.76 | 3.6 |
| | 8 | 4 | 3.08 | 2.6 |
| Reinforced Section 3 | 10 | 4 | 4.65 | 2.1 |

## 4.6 Design of Slope Stabilization Scheme: Loop 12

The slope stabilization scheme for Loop 12 was designed as a temporary solution (for 1-2 years). As a part of the temporary solution, a 50 ft. failed section over the top slope and 100 ft. section of the bottom slope was selected for the remedial measure. The remedial action of the top slope included 4 rows of 10 ft. RPP placed at 3 ft. c/c staggered grid. Considering the ease of construction, the first row of the RPP should be installed perpendicular to the slope surface. On the other hand, the rest 3 rows of RPP at the top slope should be installed vertically. A 100 ft. section was selected for the stabilization of the bottom slope with 4 rows of RPP. Spacing of the RPP at the bottom slope was selected to be 4 ft. c/c at staggered grid. However, near the cracked area of

the wall, a 24 ft. section was selected to stabilize the slope with 2 ft. c/c spacing to provide higher resistance. The first rows of RPP at the bottom slope were installed along the edge of the retaining wall footing to resist the sliding of the wall. The layout and section of the stabilization scheme are presented in Figure 4.8.

Based on the proposed distribution of RPP, the slope stability analyses were further conducted to evaluate the factor of safety of the Loop 12 slope for temporary solution. The factor of safety was observed as 1.22 and 1.19 for Section A-A and Section B-B, respectively. The critical slip surfaces for each of the sections are presented in Figure 4.9. It should be noted that the back calculated slope model was utilized and RPP was modeled as lateral supporting member (plate element in Plaxis 2D) during this analysis.

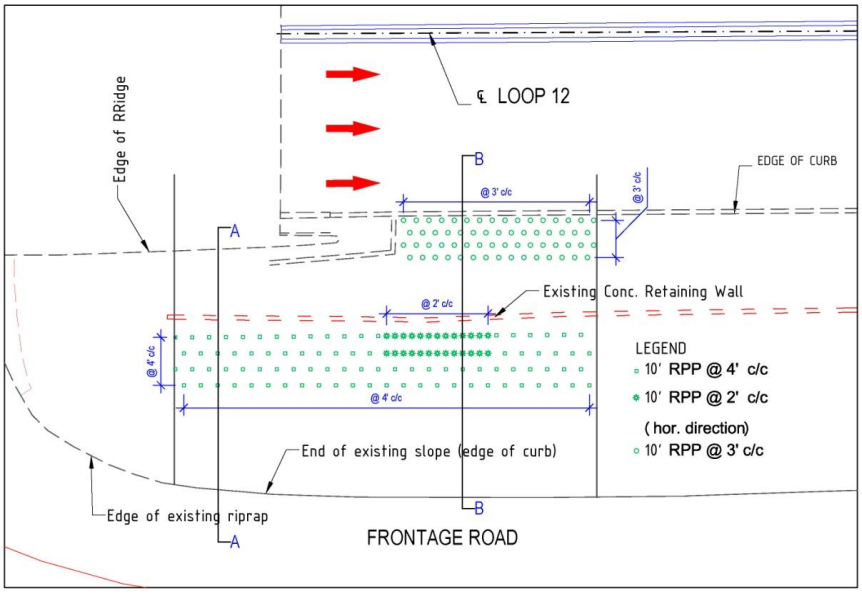


(a)

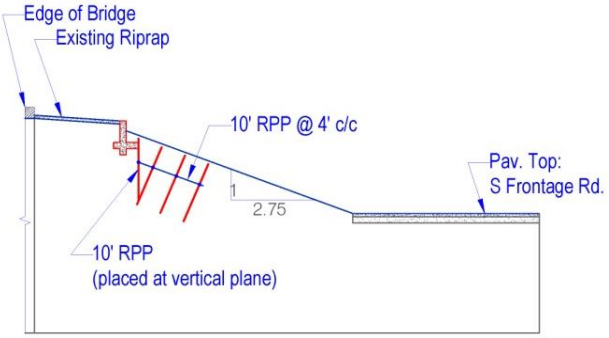


(b)

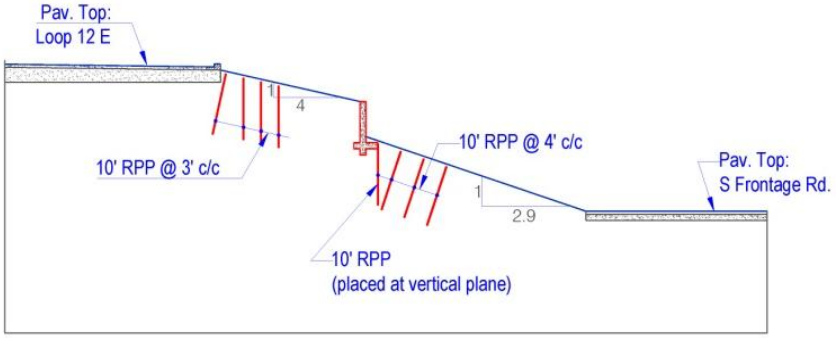


(c)

Figure 4.8 Layout of the Reinforced Loop 12 Slope a. Plan, b. Section A-A, c. Section B-B

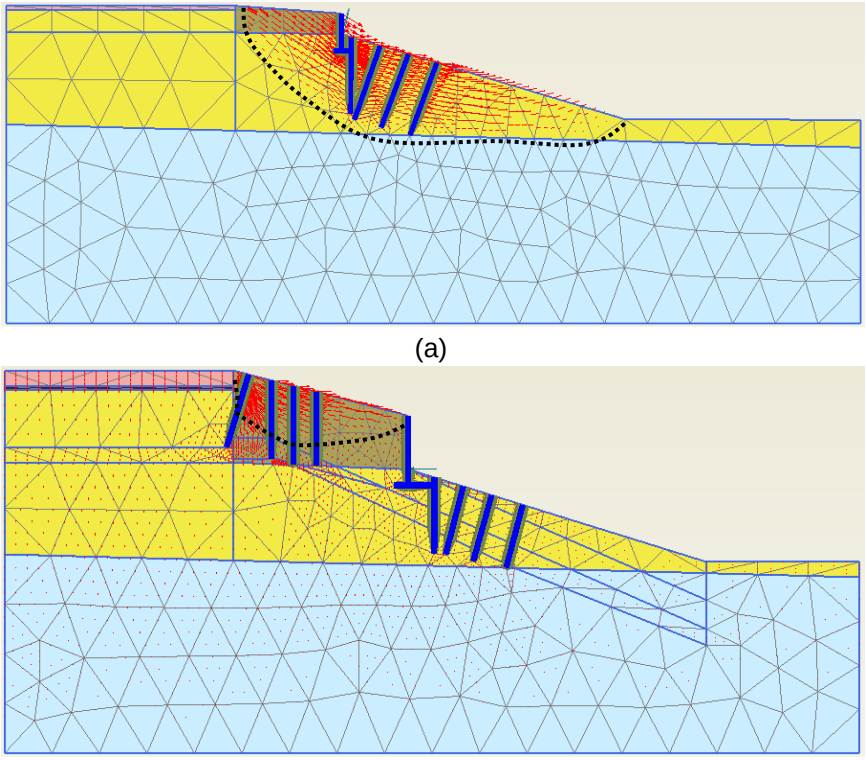

(a)

(b)

Figure 4.9 Slope Stability Analysis at Loop 12 Slope, a. at Section A-A (F.S = 1.219), b. at Section B-B (F.S = 1.189)

## 4.7 Installation of RPP: Loop 12 Slope

The site investigation program indicated that the failure occurred at the top of the slope. It was evident that the installation of RPP at the top might reduce the factor of safety of the slope due to the additional load created by the drilling rig. Therefore, the installation of RPP was started from the bottom slope. To resist the sliding of the retaining wall, the first row of RPP at the bottom slope was installed in a vertical plane, along the edge of the retaining wall foundation. Therefore, it was crucial to mark the edge of the foundation before pin installation. Hand auger boring was performed in the bottom slope near the edge of the foundation, and the location of the pin was clearly marked and flagged.

The field installation in the Loop 12 slope started on February 17, 2012. However, due to rainfall and mechanical problems of the equipment, only 17 pins were installed in the bottom slope of the Loop 12 up to February 23, 2012. The installation resumed on February 24, 2012, and the installation work at the bottom slope was finished on February 28, 2012. The observed installation rate for 2 ft. c/c spacing of RPP on the first row of the bottom slope was 1.7 ft./min. The average installation rate was 1.17 ft./min. for the 4 ft. c/c spacing. The installation rate was significantly lower than the installation rate at the US 287 slope as the installation work was hampered by repeated adverse weather conditions, as well as the mechanical failure of the installation equipment. The installation of RPP at the top slope started on February 28, 2012 and finished on the same day. Therefore, the observed installation rate was higher (2.15 ft/min.) for the top slope than the bottom slope. The summary of the installation rate of RPP and field installation photos at the Loop 12 slope are presented in Table 4.2 and Figure 4.10 respectively.

Table 4.2 Average RPP driving time at Loop 12 Slope

| Location of RPP | Length of RPP (ft.) | RPP Spacing (ft.) | Average RPP Driving Time (min.) | Average RPP Driving Rate (ft./min.) |
|---|---|---|---|---|
| Top Slope | 10 | 3 | 4.67 | 2.15 |
| Bottom Slope | 10 | 2 | 5.87 | 1.7 |
| | 10 | 4 | 8.56 | 1.17 |

Figure 4.10 RPP installations at Loop 12 Slope

# Chapter 5

# Instrumentation and Performance Monitoring

## 5.1 Instrumentation in US 287 Slope

To evaluate the performance of the reinforced slope, a rain gauge, instrumented RPP and inclinometers were installed after completion of field installation at Reinforced Section 1 and Reinforced Section 2. In addition, a topographic survey was conducted on a monthly basis after installation of RPP at the Reinforced Section 3. The details of the performance monitoring scheme is presented below.

### *5.1.1 Rain Gauge*

A high resolution rain gauge was installed to monitor the daily rainfall at the slope. The rain gauge has a double spoon tipping bucket-type sensor that is capable of measuring rainfall amount up to 0.08 inch. The rain gauge is connected with a data logger placed at the field to record the amount of hourly rainfall. The total daily rainfall amount is the summation of all the recorded data in a day.

### *5.1.2 Instrumentation of RPP*

RPPs used in slope stabilization were instrumented with strain gauges. The objective of instrumentation was to determine the developed strain in RPPs at different sections. The strain gauges have the advantage of being inexpensive and commercially available. However, the strain gauges have a disadvantage is that they are not generally well suited for long term monitoring, particularly in a buried environment (Loehr and Bowders, 2007). During the current study, 350-ohm electrical resistance gauges, with a gauge length of both 0.5 inch and 0.25 inch, were utilized to instrument the RPP. The strain gauges are fabricated with annealed constantan foil, along with tough, high-elongation polyimide backing strain gauges which are capable of measuring strain up to 20%. The gauges were placed on the RPP in a recessed area, which was 0.25 inch

deep, to prevent the gauges from being ripped off during installation. Gauges were attached using a special adhesive that was selected to be compatible with RPP and cures almost instantly to produce an essentially creep-free, fatigue-resistant bond, with elongation capability of 5% or more. The gauges were then sealed with waterproof sealant, and the recessed areas were filled using silicone caulk. The schematic and photograph of installed strain gauges are presented in Figure 5.1 and Figure 5.2.

A total of 9 RPPs, designated as IM-1 to IM-9, were instrumented with strain gauges and installed in Reinforced Section 1, Control Section and Reinforced Section 2. Four of them were placed in Reinforced section 1, two in the Control section and three in Reinforced section 2. A total of 6 instrumented RPPs, designated as IM-1 to IM-6, were utilized for Reinforced Section 3 and Control Section 2. Four instrumented RPPs, IM-1' to IM-4', were installed in Reinforced Section 3. The Control Section 2 was instrumented with IM-5' and IM-6'. The locations of the instrumented RPPs are presented in Figure 5.3. The instrumented RPPs were driven in the site during the field installation.

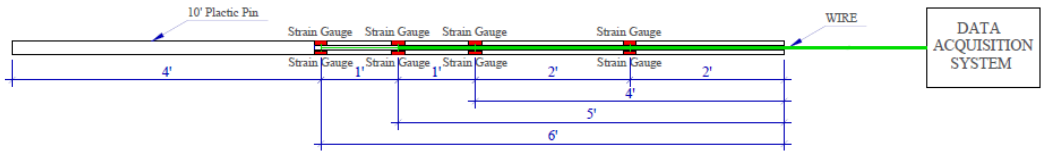


Figure 5.1 Schematic Diagram of Instrumented Plastic Pin

Figure 5.2 Installation of Strain Gauges of RPP

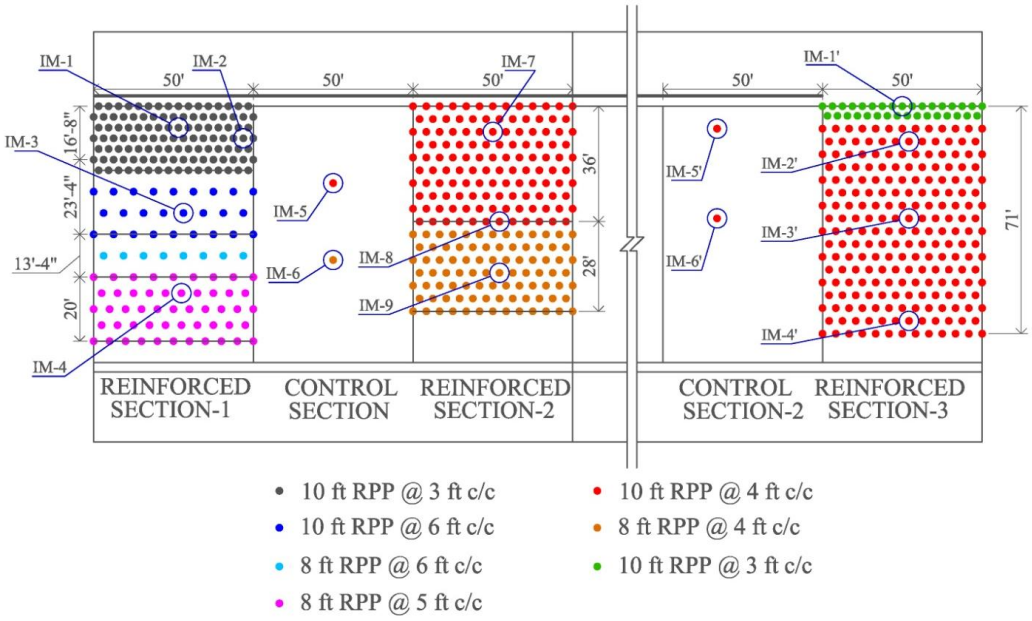


Figure 5.3 Layout of Instrumented RPP

*5.1.3 Inclinometers*

A total of 3 inclinometers, designated as Inclinnometer-1, Inclinometer 2 and Inclinometer 3, were installed at Reinforced Section-1, Control Section and Reinforced

Section-2 to monitor the horizontal movement of the slope. The depth of each inclinometer casing was 30 ft., and they were installed perpendicular to the slope surface, 20 ft. below the crest. The layouts and installation photos of the inclinometers are presented in Figure 5.4 and Figure 5.5.

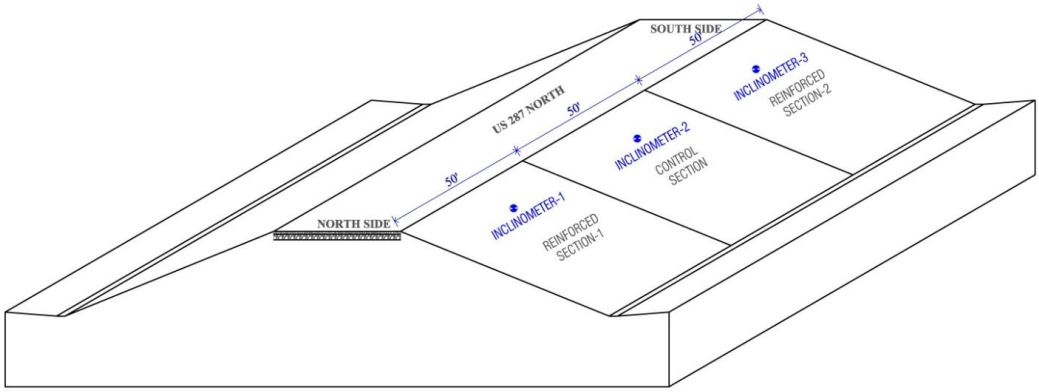


Figure 5.4 Layout of Inclinometers at US 287 Slope

Figure 5.5 Site Photos during Inclinometer Installation

*5.1.4 Topographic Survey*

A topographic survey was conducted over the US 287 slope as a part of the performance monitoring of slope stabilization. The first survey over the slope was conducted during May 2012, after the completion of RPP installation at Reinforced Section 3 and continued on monthly basis. During the survey, the cracked zones over the shoulder, as well as the RPP top at different reinforced sections, were monitored. The layout of the survey lines are presented in Figure 5.6.

During the surveying, 3 permanent points were utilized to align the periodically monitored data; whereas, 2 of the permanent points were located over the bridge near the Reinforced Section 1. Another permanent point was located over a ditch near Reinforced Section 3. The survey points, as observed during each month, were aligned, and the movement over the slope was concluded. It should be noted that during the comparison of movement, a tolerance should be allowed that ranges between ± 1 inch.

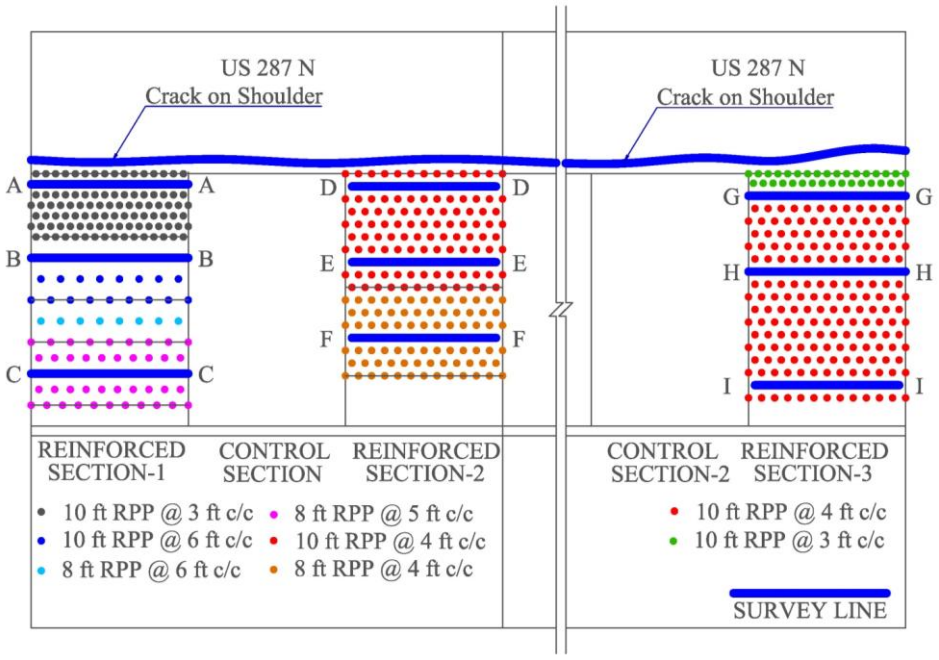


Figure 5.6 Layout of Survey Line at US 287 Slope

*5.1.5 Moisture Sensor and Matric Suction Monitoring*

Hossain, J. (2012) conducted a study on the same slope to investigate the variation of the moisture content and Matric Suction. During the study, moisture sensors and tensiometers were installed at the crest and at the middle of the slope. Results obtained from the sensors, as presented by Hossain, J (2012), is further utilized and compared with the field monitoring results.

5.1.5.1 Instrumentation Layout

The Instrumentation was carried out in the months of November and December of 2010. The layout of the sensors and details of the instrumentation are presented in Figure 5.7 and Table 5.1, respectively. There were two rows (at crest and middle of the slope) of instrumentation for the monitoring water content and soil suction. A total of 6 moisture sensors and 6 water potential probes were installed at different depths and locations of the slope. The sensors were connected to data loggers in the field to obtain continuous reading of the in-situ moisture and suction.

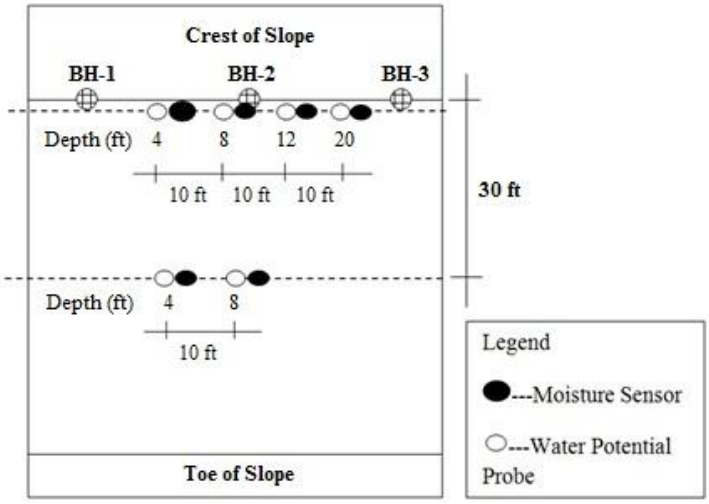


Figure 5.7 Instrumentation Layout

Table 5.1 Instrumentation Detail (According to Hossain, J. (2012))

| Location | Depth (ft.) | Sensor Type | No. of Sensors |
|---|---|---|---|
| Crest | 4 | Moisture Sensor | 4 |
| Crest | 8 | Moisture Sensor | |
| Crest | 12 | Moisture Sensor | |
| Crest | 20 | Moisture Sensor | |
| Crest | 4 | Water Potential Probe | 4 |
| Crest | 8 | Water Potential Probe | |
| Crest | 12 | Water Potential Probe | |
| Crest | 20 | Water Potential Probe | |
| Middle | 4 | Moisture Sensor | 2 |
| Middle | 8 | Moisture Sensor | |
| Middle | 4 | Water Potential Probe | 2 |
| Middle | 8 | Water Potential Probe | |

5.1.5.2 Soil Moisture Sensors

Commercially available EC-5 soil moisture sensors (manufactured by Decagon Devices, Inc.) were used to measure the volumetric water content of the soil. The overall dimension of the probes was 3.5 in x 0.7 in x 0.3 in. The sensor measures the dielectric constant of the surrounding medium in order to find the volumetric water content. The EC-5 soil moisture sensors are capable of measuring moisture content that ranged from 0% to 100% within accuracy of ±2%.

5.1.5.3 Water Potential Probes

Model MPS-1 water potential probes (manufactured by Decagon Devices, Inc.) were used to measure the matric suction of the soil. The water potential probe consisted of a porous ceramic disc. The overall dimension of the probe was 3 in x 1.3 in x 0.6 in. The sensor uses a technique that introduces a known material with static matrix of pores into the soil and allows it to come into hydraulic equilibrium according to the second law

of thermodynamics. As the two materials are in equilibrium, measuring the suction of the material gives the suction of the surrounding soil. The water potential probe uses the similar principle and measures the dielectric permittivity of the porous ceramic disc to determine its suction. The sensor MPS-1 can measure only the matric suction of the surrounding soil and is limited to suction measurements of -208.9 to 10445 psf.

5.1.5.4 Installation of the Sensors

Four moisture sensors and water potential probes were installed at depths of 4 ft, 8 ft, 12 ft and 20 ft. at the crest of the slope near the edge of the shoulder. Two more moisture sensors and water potential probes were installed at depths of 4 ft and 8 ft. at the middle of the slope. The illustrations of the sensors are presented in Figure 5.8. To install the moisture sensors, six separate boreholes of 4 in diameter were drilled using a hand auger. One moisture sensor and one water potential probe were installed in each borehole. All the boreholes were spaced 10 ft (3 m) apart at each location (Figure 3.11). After installing the sensors at the bottom of the borehole, it was backfilled with the in situ cut soil.

(a) (b)

Figure 5.8 a. EC-5 soil moisture sensors, b. MPS-1 Water Potential Probe

5.1.5.5 Data Acquisition System

After the installation of sensors, the lead wires from the sensors were connected to an automatic data acquisition system to monitor the moisture content, and matric suction a on a continuous basis. A total of 3 (three) Em-50 data logger were set up in the field to accommodate all the sensors. The Em-50 is a 5 port, self contained data logger which can measure the data in a continuous interval. The measurement interval for the current study was set to 60 minutes which allowed storing 24 data per day. The instrumented site along with the data logger is presented in Figure 5.9.

(a) (b)

Figure 5.9 Data collection a. Instrumentation locations, b. Em-50 Data logger

## 5.2 Performance Monitoring Results: US 287 Slope

The instrumented RPPs and the inclinometers at the US 287 slope were monitored on a bi-weekly basis. Besides, the topographic survey over the US 287 slope was conducted on monthly basis. The performance monitoring results for the US 287 slope are summarized in the subsequent sections.

### *5.2.1 Instrumented RPP*

During the current study, a total of 15 instrumented RPPs were installed in Reinforced Section 1, Reinforced Section 2 and Reinforced Section 3. However, some of

the strain gauges were damaged during the installation process, and a very limited number of strain gauges were sustained in the buried environment after installation. The strain gauge results are presented below.

5.2.1.1 Reinforced Section 1 and Reinforced Section 2

5.2.1.1.1 Comparison among IM3, IM5 and IM8

Instrumented RPPs IM3, IM5 and IM8 were installed at the middle of the slope in Reinforced Section 1, Control Section and Reinforced Section 2, respectively. Results obtained from these three instrumented RPPs are presented in Figure 5.10. Based on the monitoring results, no significant changes were observed in control or reinforced sections during the first 6 month after installation. However, instrumented RPPs started moving after a rainfall during September 2011. The instrumented RPP at the control section (IM5) experienced few increments and drop in strain compared to the instrumented RPPs at Reinforced section 1 and Reinforced Section 2 (IM 3 and IM8). The higher strain, as observed in the member IM5, presented the higher movement in the slope at the unreinforced zone. In addition, when compared to the control section, no significant increment in strain was observed in either of the RPPs installed in the reinforced sections, which signifies that almost no movement occurred in the reinforced sections.

The top 7 rows of the RPPs were installed at 3 ft. c/c spacing at Reinforced Section 1. The spacing of the RPP at the middle portion of the Reinforced Section 1 was 6 ft. c/c. IM3 was installed at the middle portion of the slope. Figure 5.10 indicated that there was no change in strain at IM3, compared to IM5 and IM8. There is a possibility that the 3 ft. c/c spacing at the crest of the slope might provide significant resistance and prevented initiation of the slope movement. On the other hand, the IM8 was installed at the middle section of the Reinforced Section 2, which had higher spacing of RPP 4 ft. c/c at the crest of the slope. The strain at the IM8 increased slightly during the initial period of

rainfall in November 2011, which indicated that there might be a slight movement at that location in Reinforced Section 2. Therefore, based on the monitoring results, it could be summarized that the 3 ft. c/c spacing at crest of slope provided better reinforcement than the 4 ft. c/c spacing.

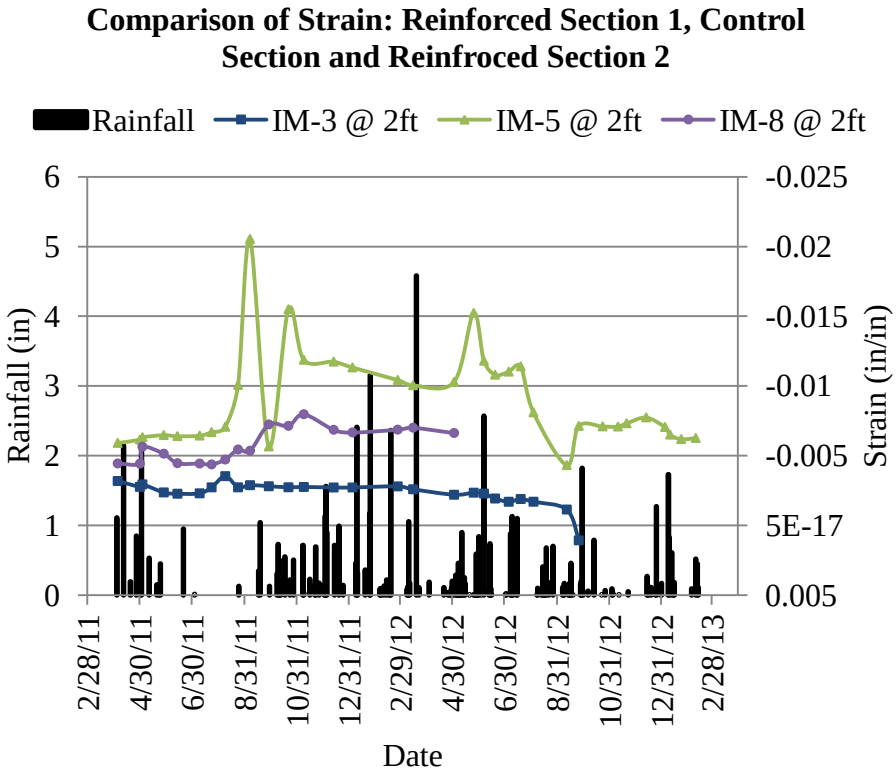


Figure 5.10 Comparison of Strain between IM3, IM5 and IM8

5.2.1.1.2 Comparison among IM4, IM6 and IM9

Instrumented members IM4, IM6 and IM9 were installed near the toe of the slope in Reinforced Section 1, Control Section and Reinforced Section 2. The overall strain distribution, with rainfall, of the three instrumented members is presented in Figure 5.11. Based on the performance monitoring result, the instrumented member installed at the control section (IM6) experienced higher strains, followed by the members at Reinforced

Section 1 and Reinforce Section 2. IM6 experienced incremental strain during September 2011 at the beginning of the wet period. IM4 and IM9 also experienced some incremental strain during the wet period that could be due to the existence of the soft soil at the toe of the slope. Figure 5.8 presented that IM9 experienced higher increment of strain compared to the strain gauge at the IM4. This variation of the strain might take place due to different spacing of RPP. The instrumented members IM4 and IM9 were installed at the 5 ft. c/c and 4 ft. c/c spacing, respectively. Due to smaller spacing, IM9 experienced less increment in strain compared to IM4, although both of them existed at the same level and in the soft soil. It can be mentioned that the higher strain represents the higher movement in the slope. Therefore, results obtained from the instrumented members indicate higher movement at the location of higher pin spacing.

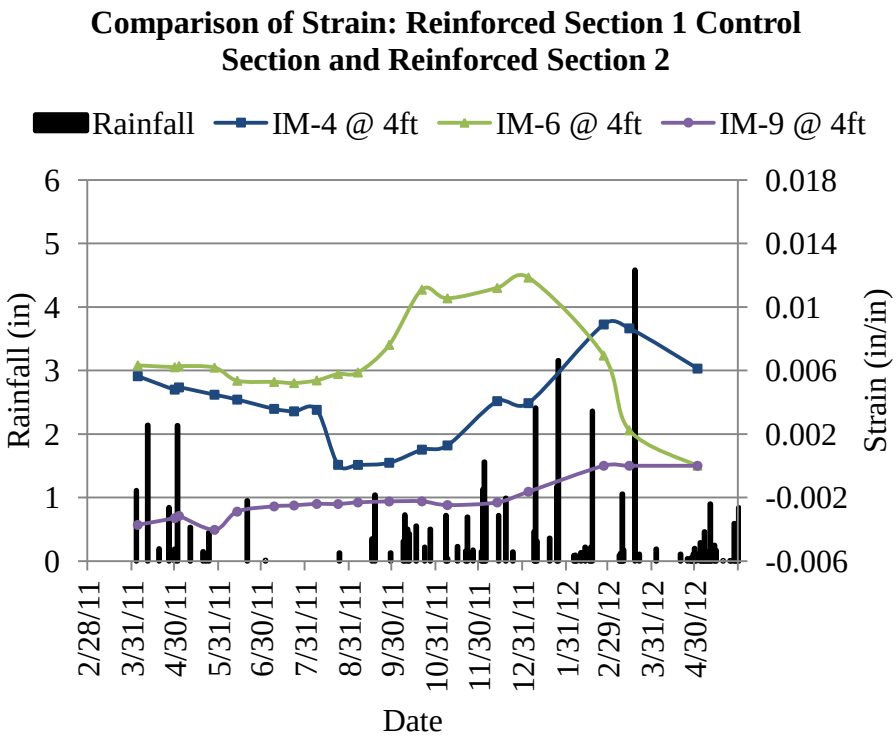


Figure 5.11 Comparison of Strain between IM4, IM6 and IM9

5.2.1.2 Reinforced Section 3

5.2.1.2.1 Comparison between IM2' and IM5'

The variation of strain between IM2' and IM5' is presented in Figure 5.12. Based on the monitoring results, no significant changes were observed in either the control or reinforced sections during the first 5 months after installation. However, instrumented RPPs started moving after a rainfall during July 2012. In addition, the observed incremental strain was higher for IM5', which was located at Control Section 2, near the crest of the slope. It should be noted that the observed behavior of the instrumented RPP IM2' and IM5' was similar to the instrumented RPP IM3, IM5 and IM8, which were installed in Reinforced Section 1, Control Section and Reinforced Section 2. The observed strain was almost constant during rest of the monitoring period.

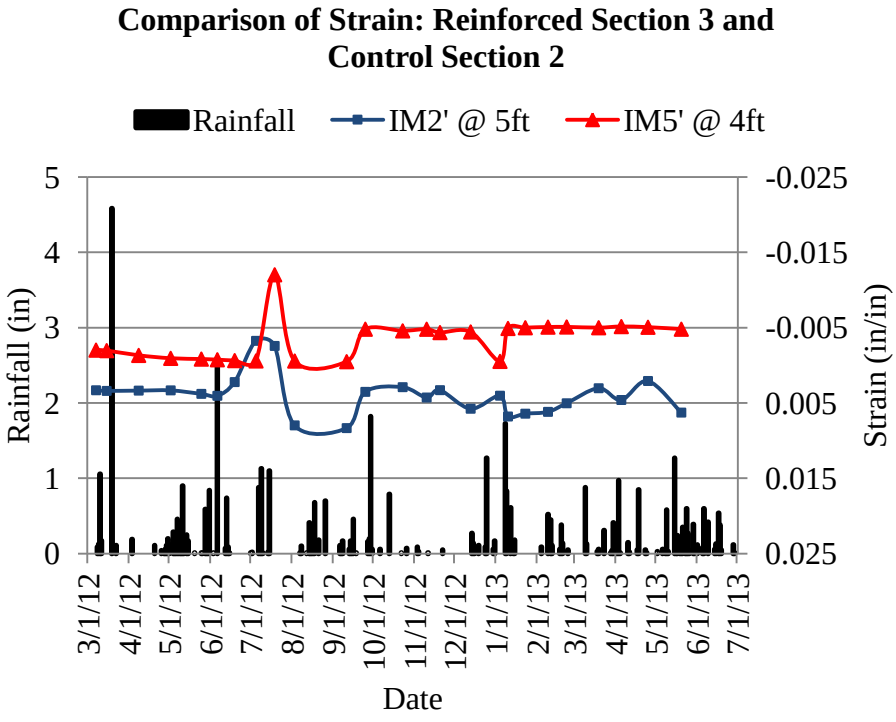


Figure 5.12 Comparison of Strain between IM2' and IM5'

5.2.1.2.2 Comparison among IM5’ and IM6’

The comparison of strain between IM5’ and IM6’, that were installed at Control Section 2, is presented in Figure 5.13. It should be noted that IM5’ was installed at the crest of the control section 2; whereas, IM6’ was installed at the middle of the slope. It was observed that both of the instrumented RPPs had almost no incremental movement for the first 5 months after installation, which could be attributed to either no movement of the slope or the stress due to slope movement may not have mobilized into the RPP. IM5’ had incremental strain at 4 ft. depth after the initial period, which could take place due to the movement of the unreinforced control section. A uniform variation of strain was observed for IM6’, which might be an indication of load mobilization over time.

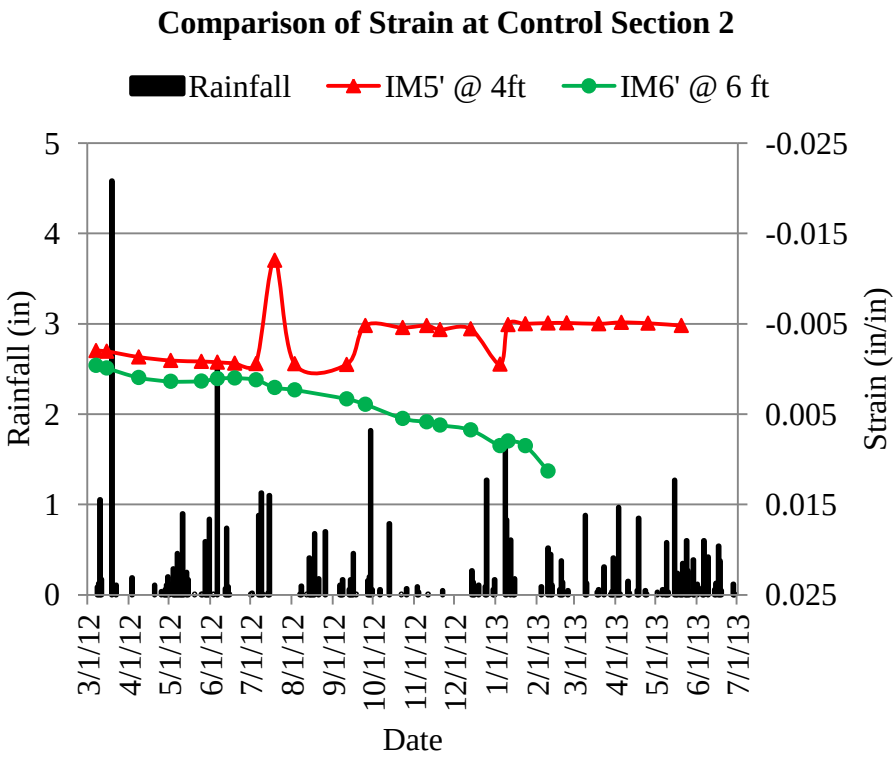


Figure 5.13 Comparison of Strain at Different Depths along IM5

*5.2.2 Topographic Survey*

The total settlement over the crest of the slope was measured during each survey and presented in Figure 5.14. The total settlement plot presented that the control sections of the slope had significant settlement at the crest when compared to the reinforced sections. The maximum settlements were 15 inches and 9 inches in the Control Section 1 and Control Section 2, respectively. On the other hand, the Reinforced Section 1 had the lowest settlement (2 inches) followed by the Reinforced Section 3 (4 inches) and Reinforced Section 2 (5 inches). It should be noted that the Reinforced Section 1 had the lowest spacing of RPP (3 ft. c/c) at the crest of the slope. Reinforced Section 2 and Reinforced Section 3 had 4 ft. c/c spacing at the crest, which was higher than Reinforced Section 1.

The instrumented RPP presented almost no movement over the Reinforced Section 1 due to the lower spacing at the crest of the slope. The total settlement plot presented the lowest settlement at the Reinforced Section 1 and was in good agreement with the instrumented RPP results. On the other hand, the high settlement of Reinforced Section 2, compared to other reinforced sections, could be attributed to the propagation effect of the crack. Since the control sections were placed at both sides of the Reinforced Section 2, the significant settlement of control sections propagated through the Reinforced Section 2 and resulted in higher settlement.

The incremental settlement plot between reinforced and control sections is presented in Figure 5.15. The increments in settlements were concluded based on the baseline settlement on May 6, 2012. The plot indicated that a total of 3 inch and 1.8 inch increments in settlement had taken place during past 1 year at control section and control section 2, respectively. However, no significant increment in settlement was observed at the reinforced sections.

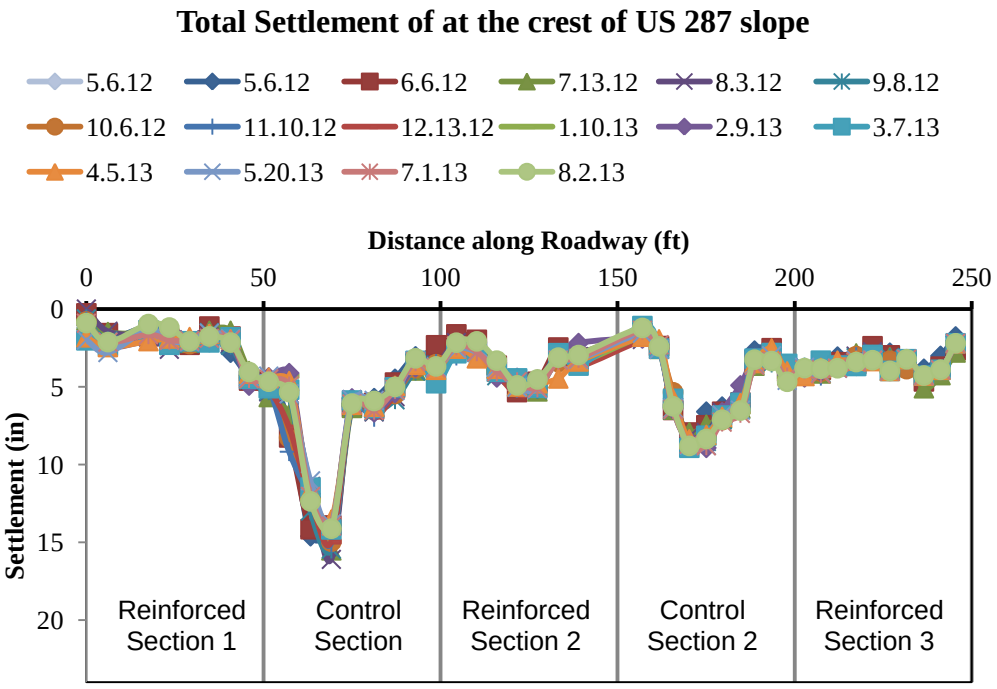


Figure 5.14 Total Settlements along the Crest of US 287 Slope

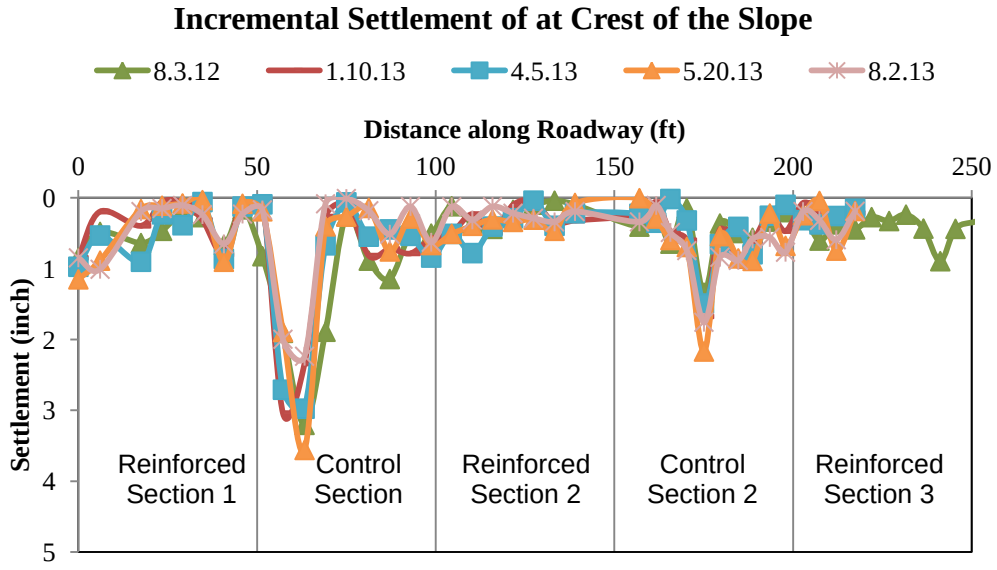


Figure 5.15 Incremental Settlements in US 287 Slope

The horizontal displacement and settlement of the 1st row of RPP at the each reinforced section is presented in Figure 5.16 to Figure 5.18. The survey results presented a horizontal movement of 3 inches over the 1st row of RPP at reinforced sections, with almost no settlement over the slope. It should be mentioned that the US 287 slope was a filled slope, constructed with high plastic clayey soil. The horizontal displacement could be attributed to be the displacement to mobilize the load. Moreover, the variation of displacement remained almost constant over the monitoring period, which indicated that additional displacement is currently taken place. On the other hand, the variation of settlement was observed over time which ranged between ±2 inches. The variation of settlement observed due to the shrinkage and swelling nature of the high plastic clay soil.

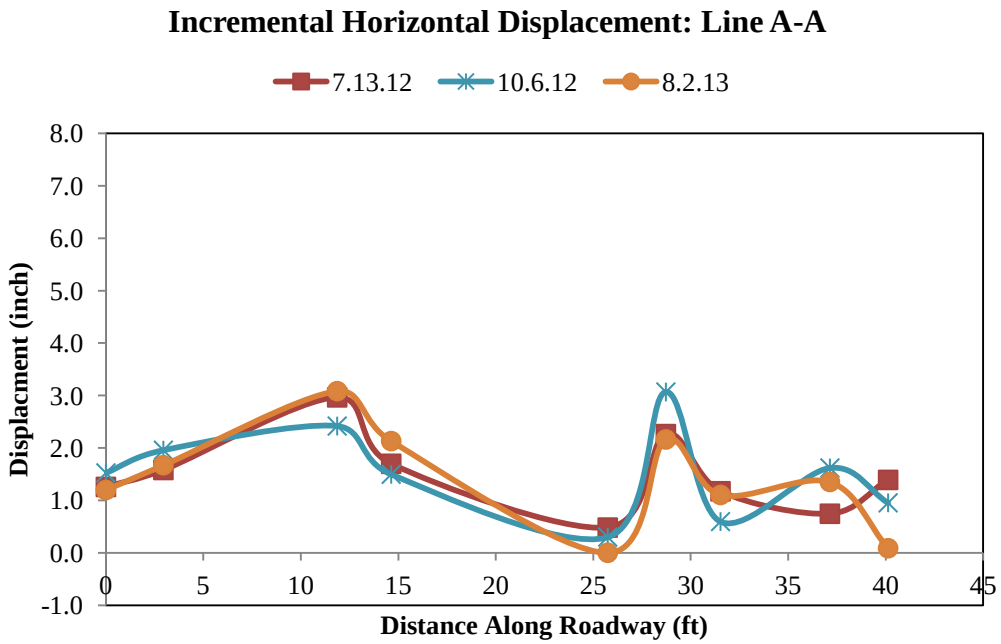


(a)

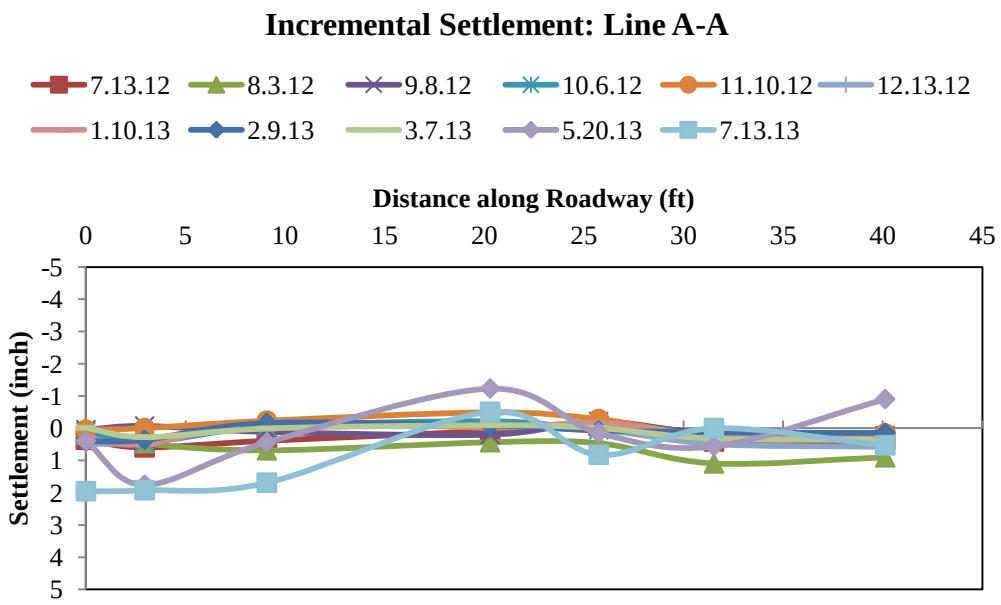


(b)

Figure 5.16 Survey Results along Line A-A, a. Incremental Horizontal Displacement, b. Incremental Settlement

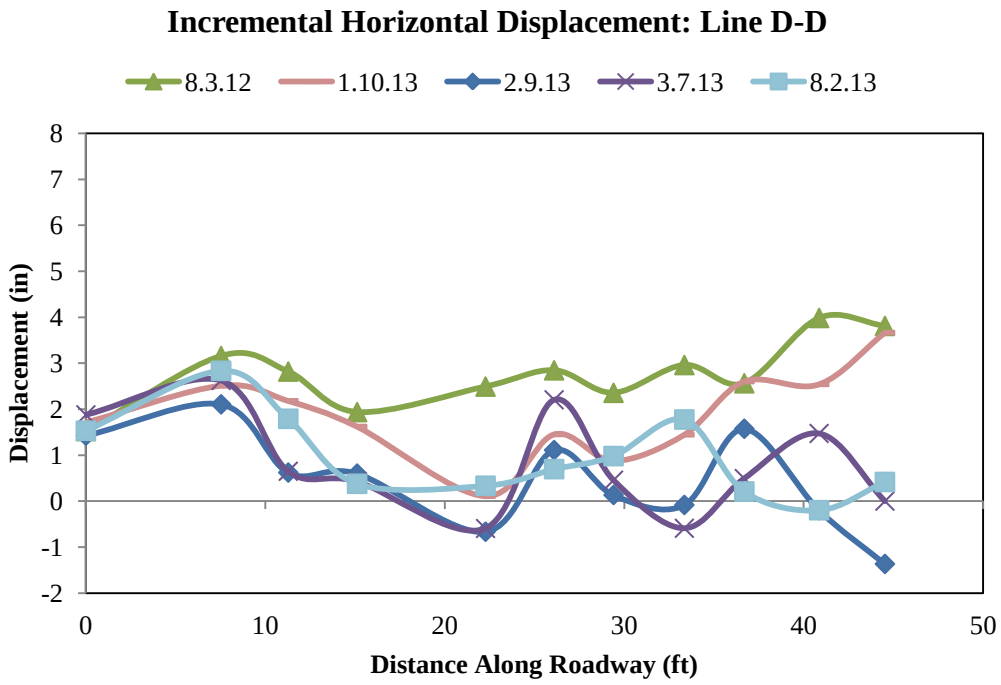


(a)

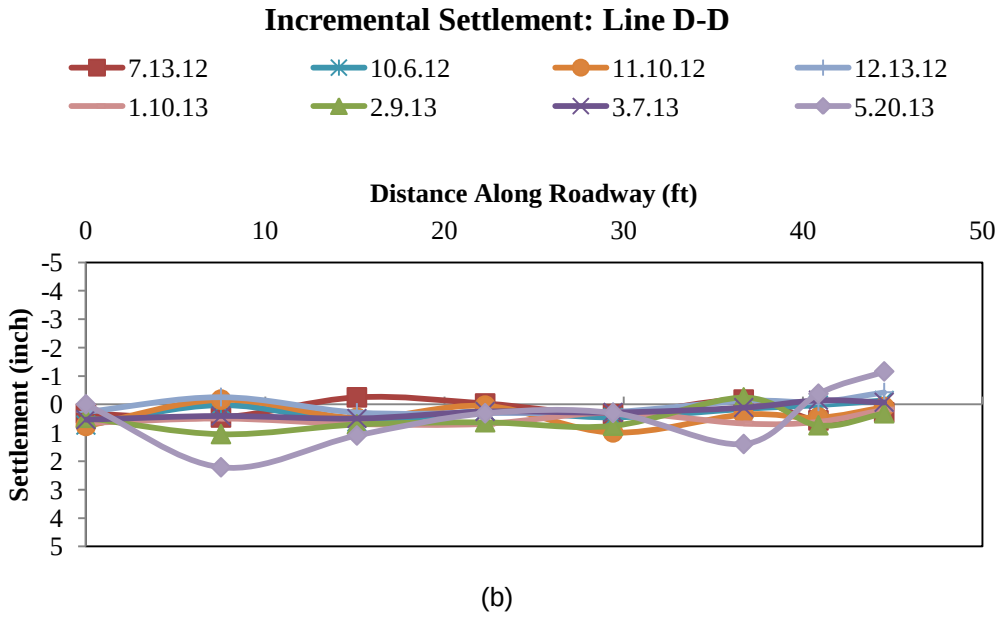


(b)

Figure 5.17 Survey Results along Line D-D, a. Incremental Horizontal Displacement, b. Incremental Settlement

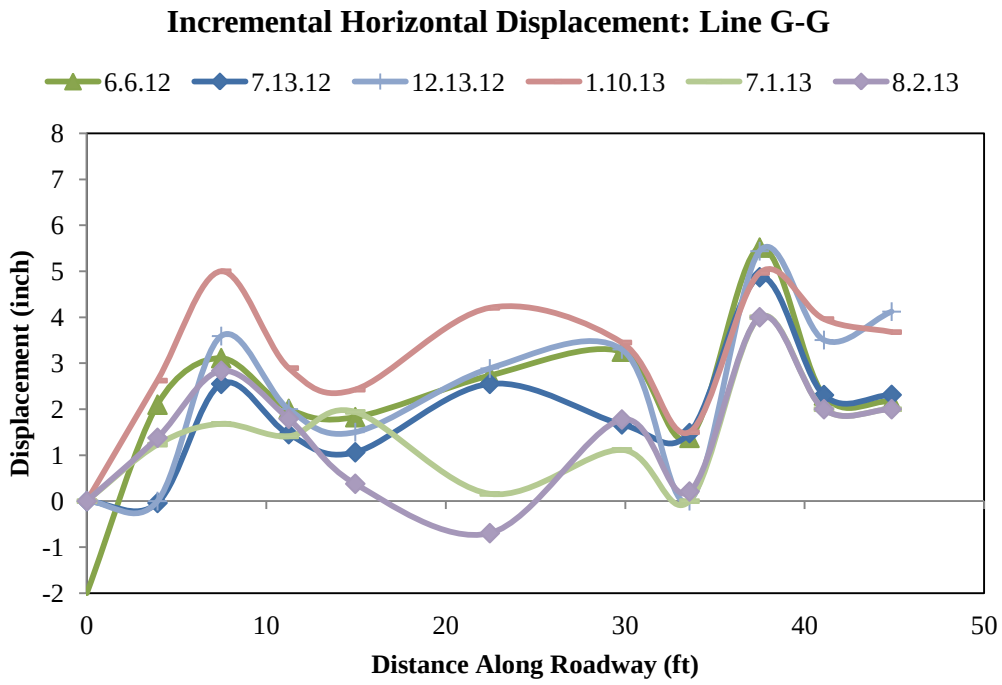


(a)

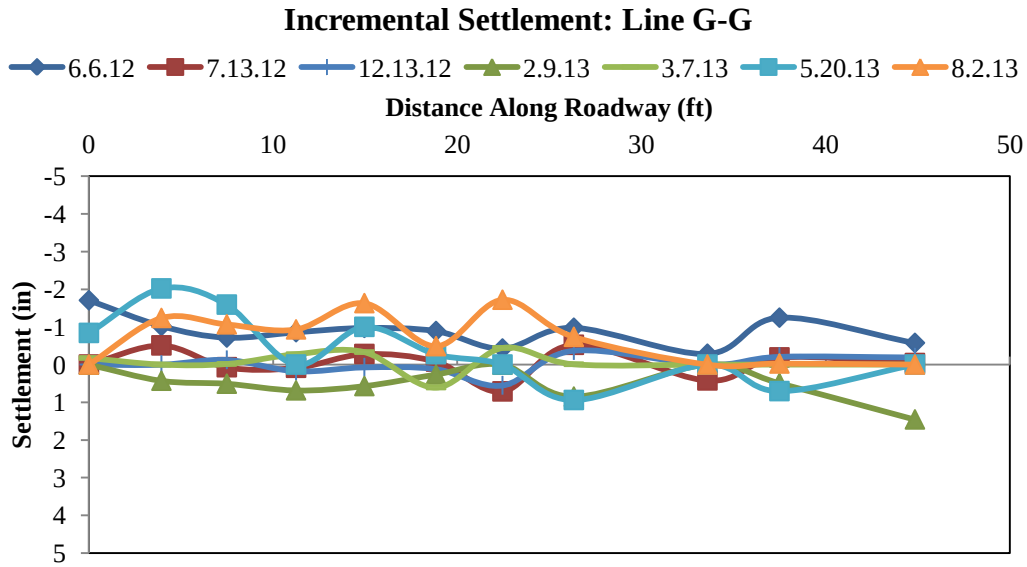


(b)

Figure 5.18 Survey Results along Line G-G, a. Incremental Horizontal Displacement, b. Incremental Settlement

*5.2.3 Inclinometer*

The inclinometers were monitored on a bi-weekly basis, and the horizontal movement of Inclinometer 1 and Inclinometer 3 is included in the current study. The data observed from Inclinometer 2 that was not in good agreement, is not presented here.

5.2.3.1 Inclinometer 1

The field monitoring results from Inclinometer 1 is presented in Figure 5.19. It was observed that Inclinometer 1 had increasing horizontal displacement during July to September 2011, the initial period after installation. However, after October 2011, the movement of the slope had dropped. The slope had similar cyclic behavior between July and Sep 2012, and increase in horizontal displacement again took place. The cyclic behavior of displacement could take place due to shrinkage and swelling behavior of high plastic clayey soil. The maximum movement of the slope, as observed from the inclinometer results, was 1.3 inches, which was observed near the surface of the slope. In addition, with the increment of the depth of the slope, the horizontal movement of the slope had dropped a depth of 20.5 ft., and almost no movement had taken place.

5.2.3.2 Inclinometer 3

The field monitoring results from inclinometer 3 are presented in Figure 5.20. The field monitoring results presented an incremental horizontal displacement of the Reinforced Section 2; whereas. the maximum movement was 1.8 inches at inclinometer 3 at the end of December 2012 and became almost constant. The maximum movement was observed near the surface of the slope, and it gradually decreased up to the depth of 20.5 ft., similar to Inclinometer 1. However, no cyclic behavior of swelling and shrinkage were observed in Inclinometer 3, similar to Inclinometer 1.

5.2.3.3 Comparison of Inclinometer 1 and Inclinometer 3

The comparisons of movement between Inclinometer 1 and Inclinometer 3 at different depths (2.5 ft. and 10.5 ft.) are presented in Figure 5.21. It was observed that Inclinometer 3 had higher horizontal movement compared to Inclinometer 1 at all depths. It should be noted that the Inclinometer 3 was installed in Reinforced Section 2, where the spacing of RPP was 4 ft. c/c. On the other hand, the inclinometer 1 was installed at Reinforced Section 1, with spacing of 3 ft. c/c. Therefore, the 4 ft. RPP spacing had higher movement than the 3ft c/c at slope crest, which was in good agreement with strain gauge and survey data.

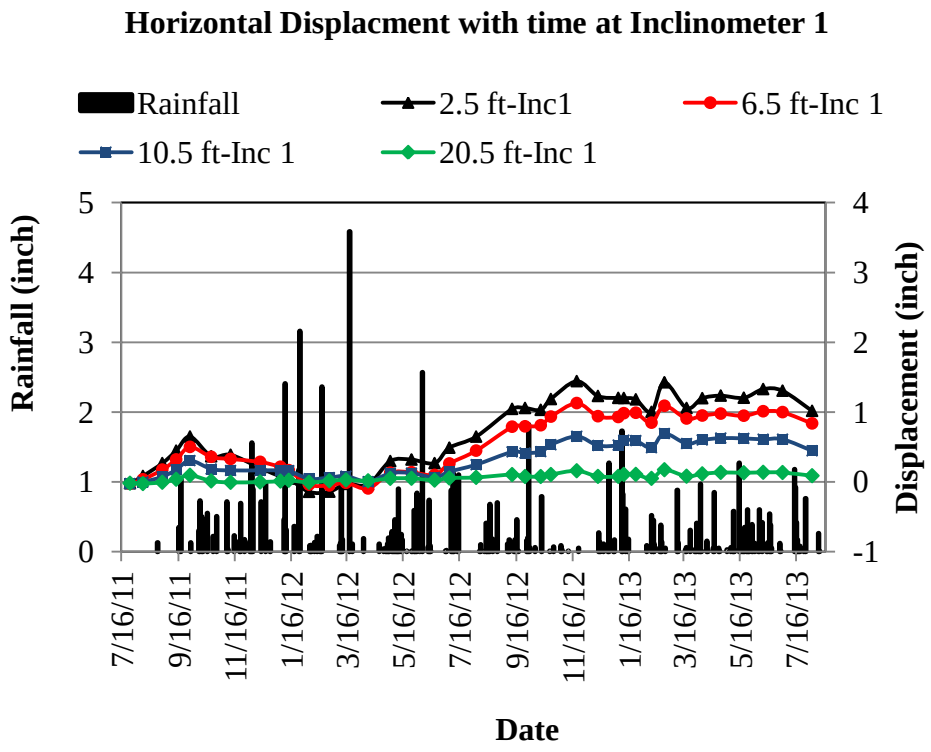


Figure 5.19 Variation of Horizontal Displacement along Inclinometer 1 at Reinforced Section 1.

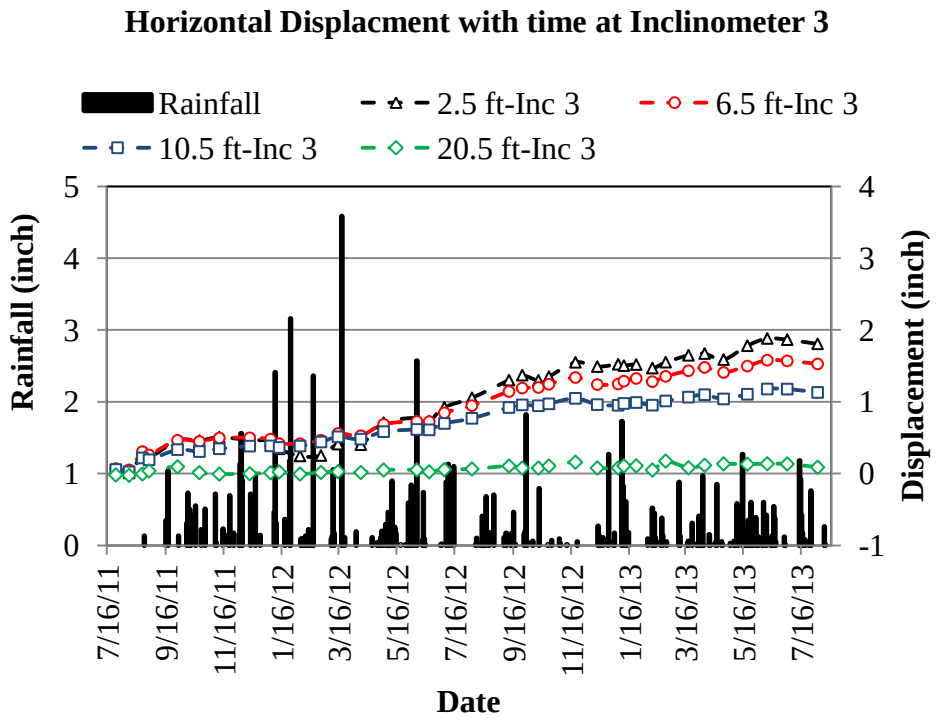


Figure 5.20 Variation of Horizontal Displacement along Inclinometer 3 at Reinforced Section 2.

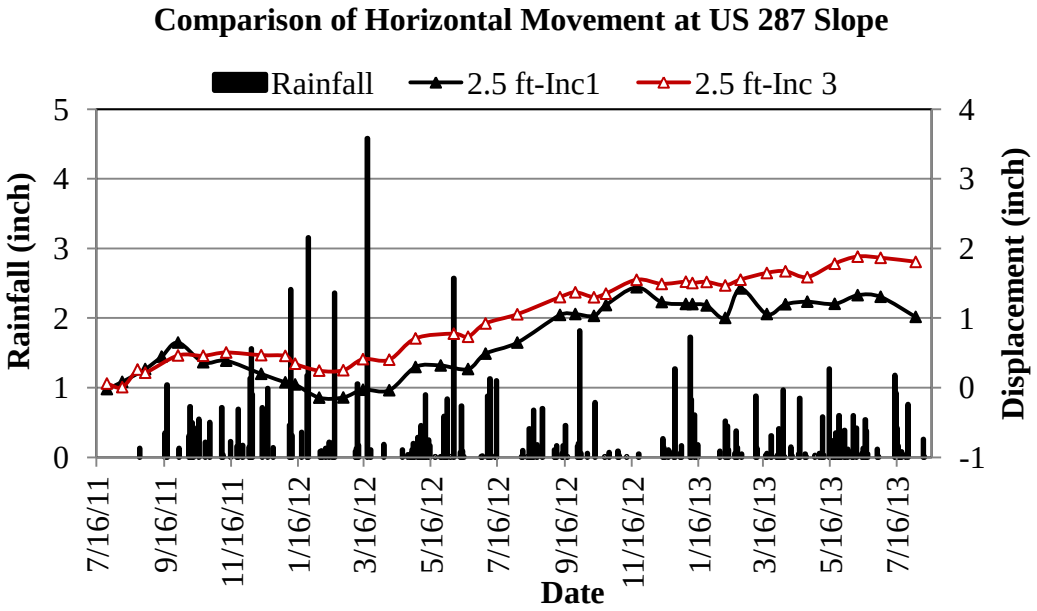


(a)

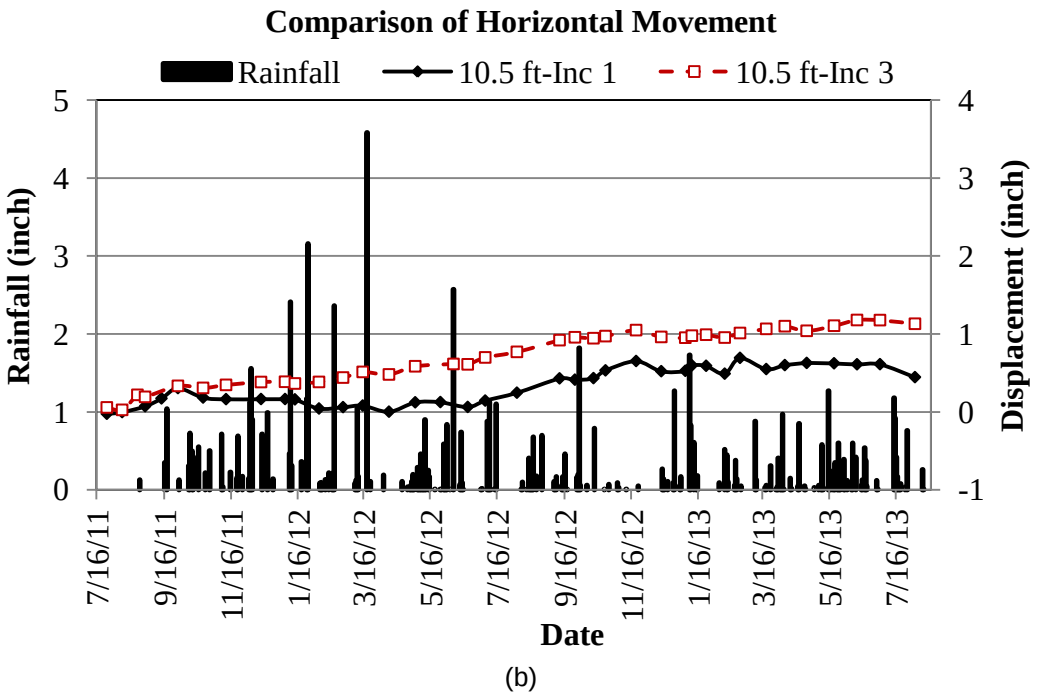


(b)

Figure 5.21 Comparison of Horizontal Displacement between Inclinometer 1 and Inclinometer 3 a. At 2.5 ft., b. At 10.5 ft.

*5.2.4 Inclinometer Displacement with the Moisture and Suction Variation*

Hossain, J. (2012) has conducted a study on the variation of moisture content and matric suction of the US 287 slope. The variation of the moisture content and matric suction data near the top soil (at 4 ft. depth) were further utilized and variation with the horizontal displacement from Inclinometer 1 and Inclinometer 3 is presented in Figure 5.22 to Figure 5.25.

After installation of RPP, the matric suction value remained almost constant up to December 2011, after that the matric suction became close to zero after few rainfall event, where the moisture content reached to its maximum value of 35%. The low matric suction signifies the fully saturated state which could be the critical condition for the slope. However, horizontal displacement was not observed at Inclinometer 1 on Reinforced Section 1 (Figure 5.22). The similar behavior was also observed for the moisture and matric suction variation at the middle of the slope as presented in Figure 6.8. It was expected that the during the high moisture period with zero suction, the shear strength of the slope decreased and went to the critical condition. However, the displacement at Reinforced Section 1 and Reinforced Section 2 was about 0.1 inch during the time period. It can be attribute that the RPP provided enough anchorage during the wet period and resisted the displacement. On the other hand, during Summer 2012 (between June and September 2012), the RPP movement was about 1 inch, as presented in Figure 5.22 and Figure 5.23. These can be explained using Figure 5.26. With the increase in temperature, the expansive soil shrink and desiccation crack took place, as explained in Figure 5.27.

The US 287 slope was constructed using high PI clay where the major dominant mineral is montmorillonite. The formation of crack at the compacted clay largely depends on the mineral content and the presence of montmorillonite make the soil highly

susceptible to the formation of desiccation cracks (Inci, G., 2008). The desiccation cracks create a loss of support condition to the RPP as illustrated in Figure 5.27. During the loss of support condition, the passive resistance for RPP reduced which resulted in higher deformation during the summer period. The desiccation cracks disappear during the wet period and RPP regained the full passive resistance.

Figure 5.26 presented that the US 287 slope had negligible movement during the next wetting and drying period (October 2012 to September 2013). The variation of horizontal displacement of the reinforced slope is illustrated against the baseline movement on October 23, 2012, as presented in Figure 5.28, which indicated that there was less than 0.1 inch movement in Reinforced Section 1 had taken place during time period (October 2012 to September 2013). This is due to the fact that the load might have been mobilized in Reinforced Section 1 and less than 0.1 inch movement had taken place during the next wetting drying period. On the other hand there was an incremental horizontal displacement up to 0.5 inch during that period at 2.5 ft depth from the slope surface at Reinforced Section 2. However, the movement was less than 0.1 inch at 10 ft depth.

The survey results presented the crest movement of the slope. The instrumented RPP and inclinometers, installed at the stabilized area, presented the displacement at a particular location. However, all the field monitoring results were in good agreement. Inclinometer 1 and Inclinometer 3 were installed at the RPP spacing of 3 ft. c/c and 4 ft. c/c, respectively and presented lower displacement at the lower RPP spacing at the crest of the slope.

As a part of slope performance monitoring, visual inspections were also conducted on regular basis. Based on the field visit, a 12 inch and 9 inch settlement was observed in control section and control section 2, respectively during June 2012. In

addition, a new cracked zone was observed over the shoulder near the pavement due to substantial settlement of the crest at the control sections. The crack was initiated centering at the control section and propagated over the certain portion of Reinforced Section 1 and Reinforced Section 2. The photos of cracked shoulder are presented in Figure 5.29. However, a new overlay over the US 287 was placed by TxDOT to repair the damage of the shoulder near the pavement.

Finally, it can be concluded that the reinforced sections are performing better than the unreinforced control sections. In addition, the spacing of RPP plays an important role in resisting crest settlement and displacement.

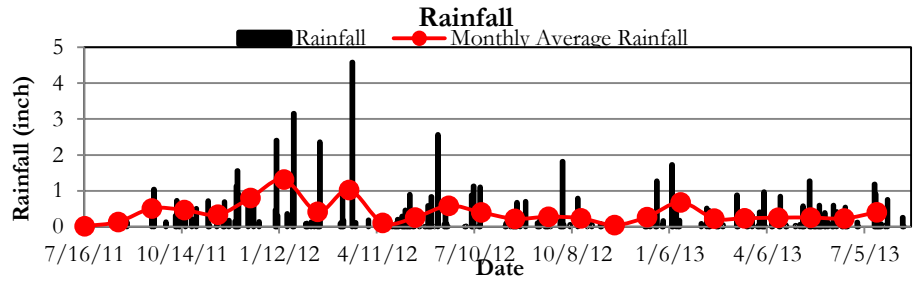


(a)

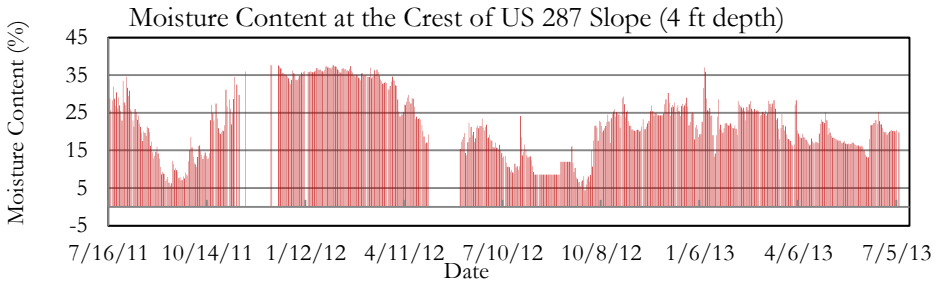


(b)

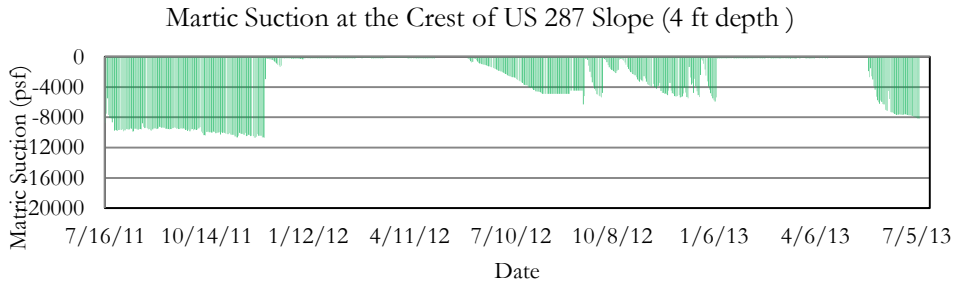


(c)

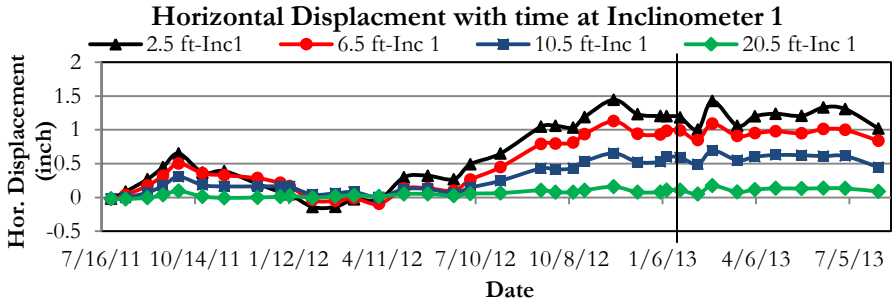


(d)

Figure 5.22 Variation of Horizontal Displacement along Inclinometer 1 at Reinforced Section 1, a. Rainfall, b. Moisture Content, c. Matric Suction and d. Hor. displacement

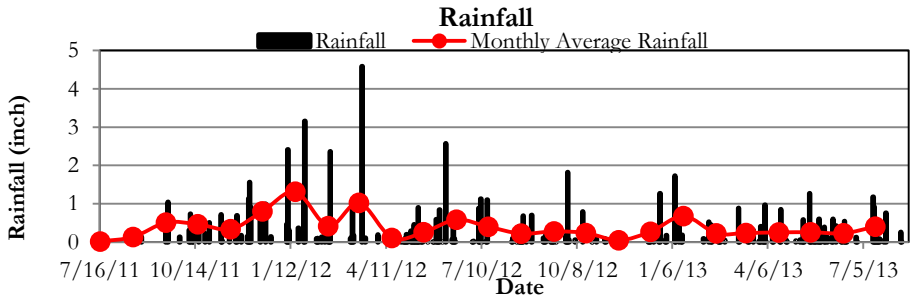


(a)

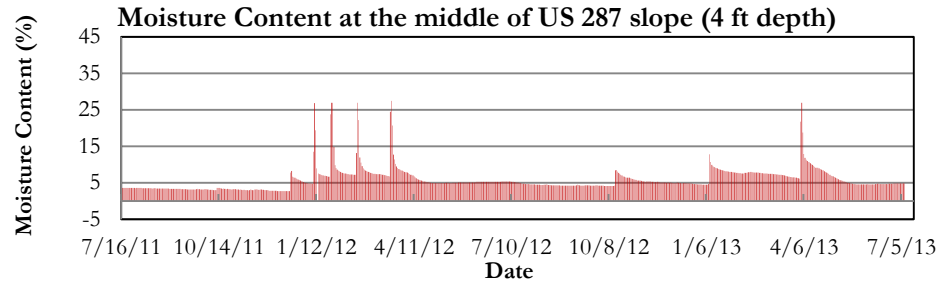


(b)

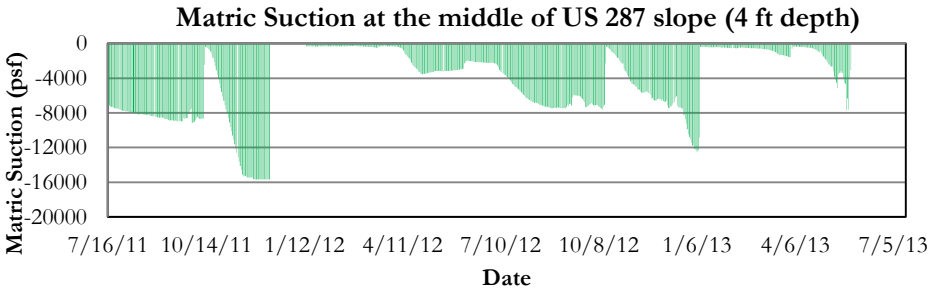


(c)

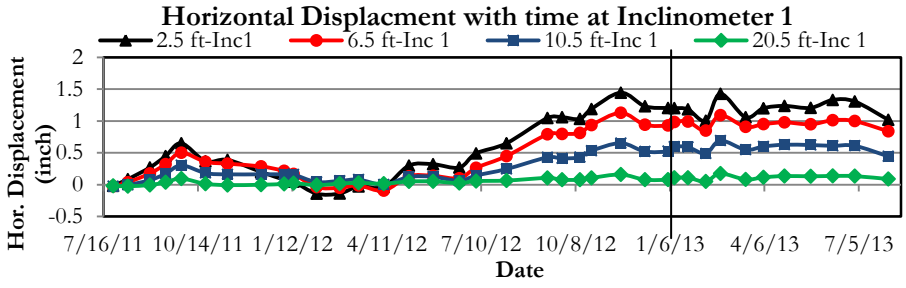


(d)

Figure 5.23 Variation of Horizontal Displacement along Inclinometer 1 at Reinforced Section 1, a. Rainfall, b. Moisture Content, c. Matric Suction and d. Hor. displacement

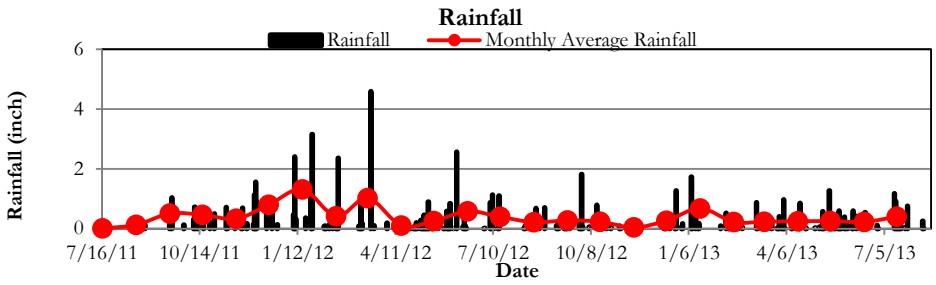


(a)

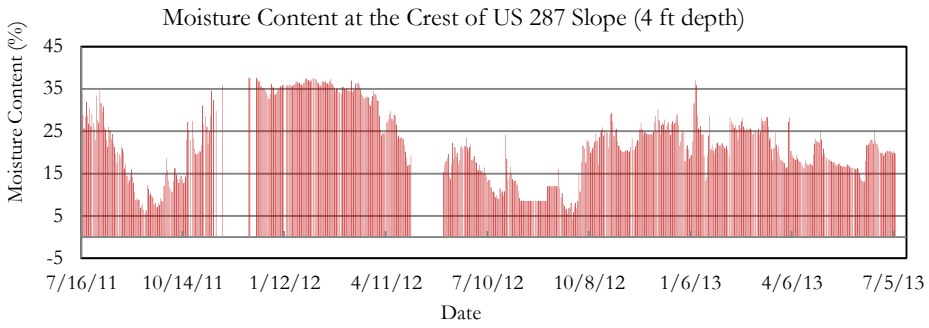


(b)

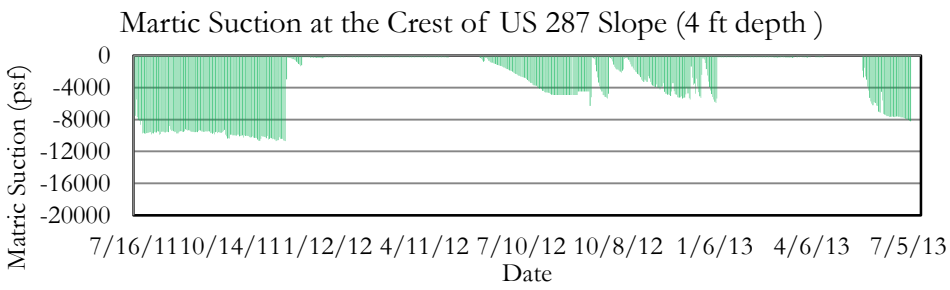


(c)

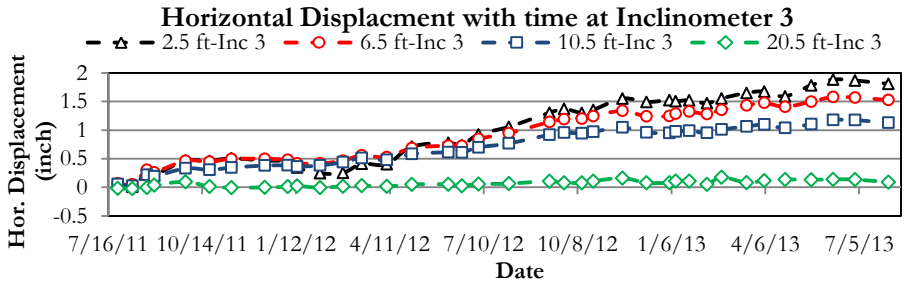


(d)

Figure 5.24 Variation of Horizontal Displacement along Inclinometer 3 at Reinforced Section 2, a. Rainfall, b. Moisture Content, c. Matric Suction and d. Hor. displacement

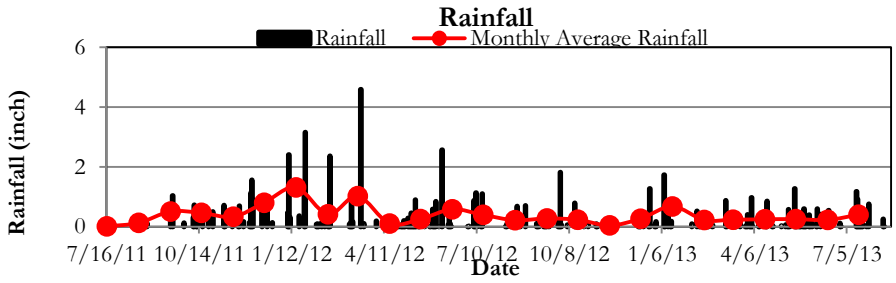


(a)

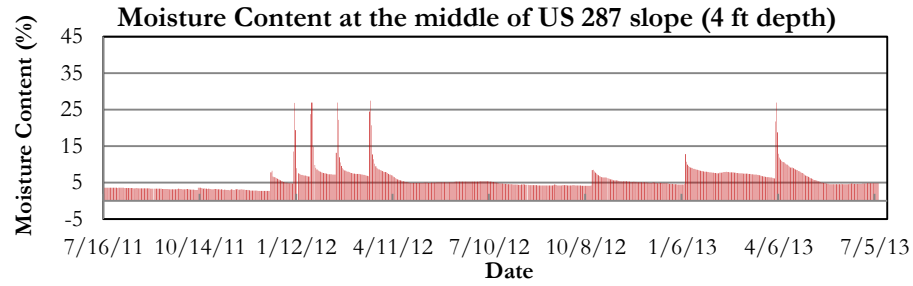


(b)

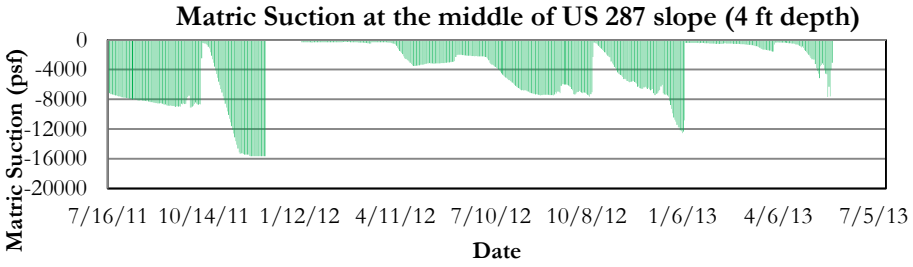


(c)

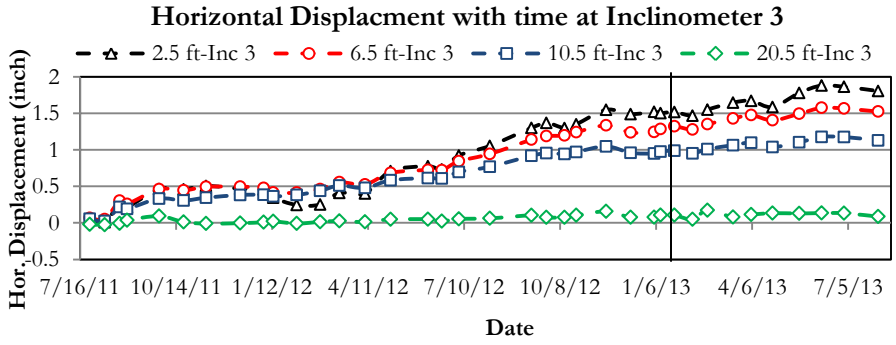


(d)

Figure 5.25 Variation of Horizontal Displacement along Inclinometer 3 at Reinforced Section 2, a. Rainfall, b. Moisture Content, c. Matric Suction and d. Hor. displacement

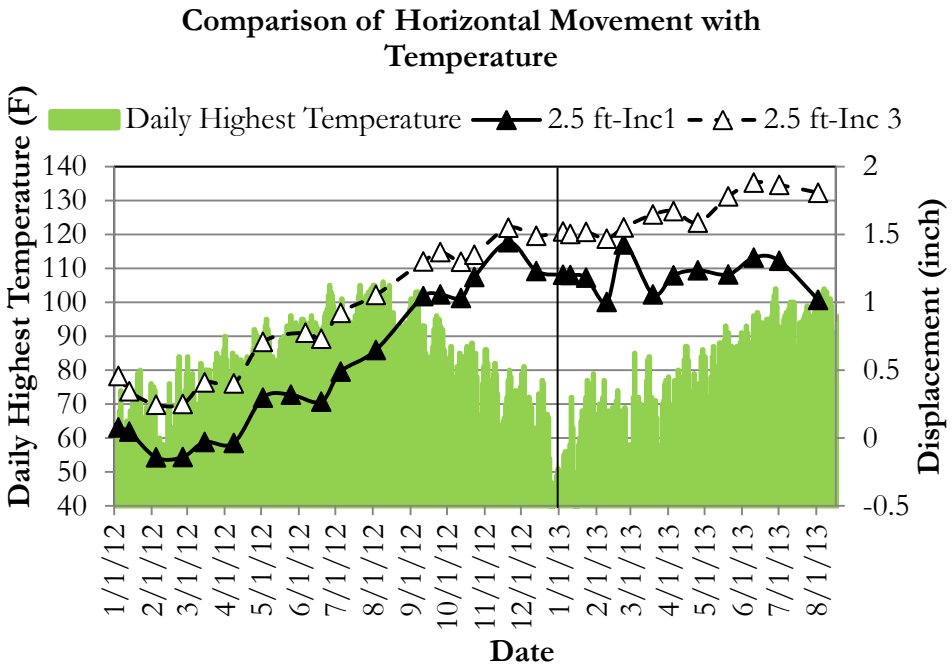


Figure 5.26 Variation of horizontal displacement with daily highest temperature

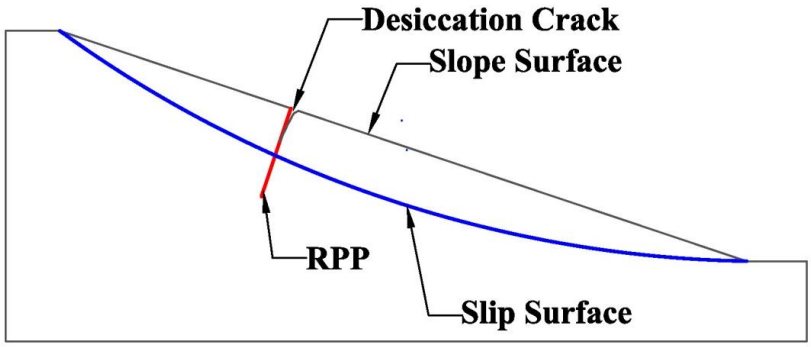


(a)

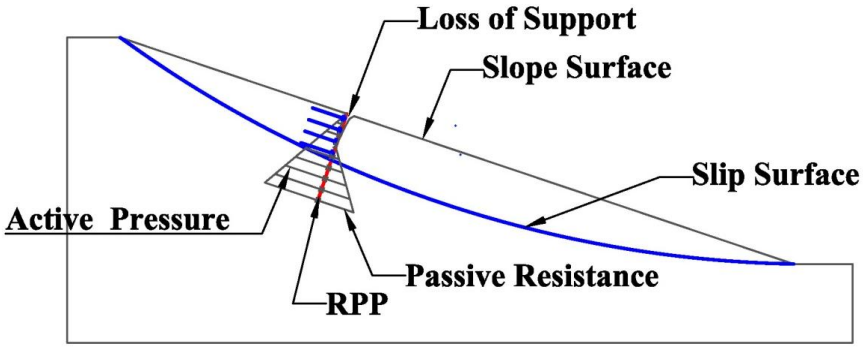


(b)

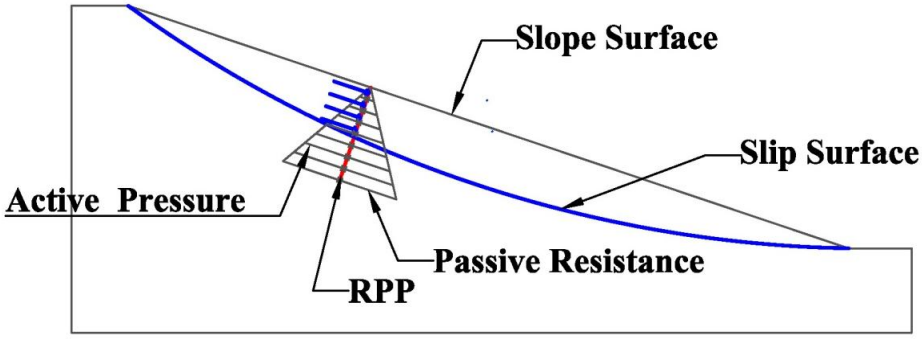


(c)

Figure 5.27 Schematic of loss of support condition for RPP during the dry period, a. Formation of desiccation crack during summer, b. Passive Resistance reduced due to loss of support, c. Desiccation crack disappear during wet period and RPP regain passive resistance.

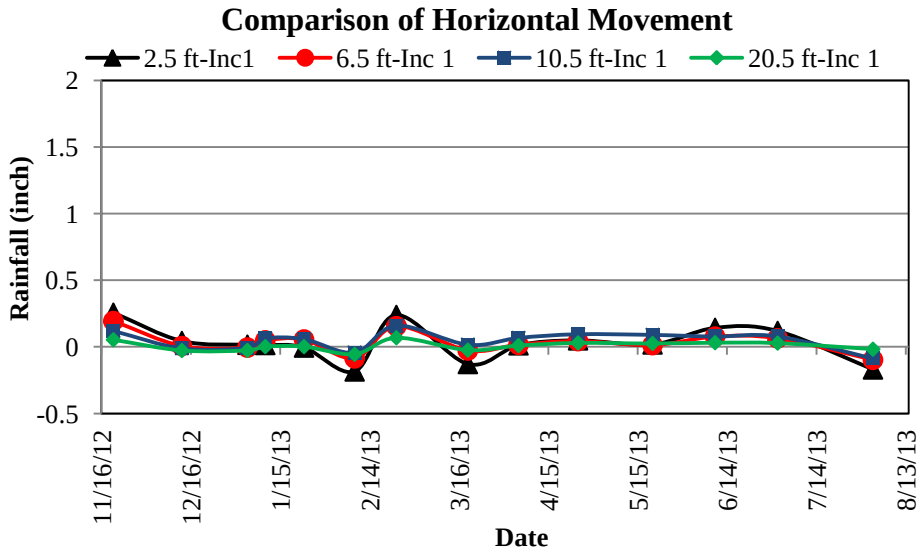


(a)

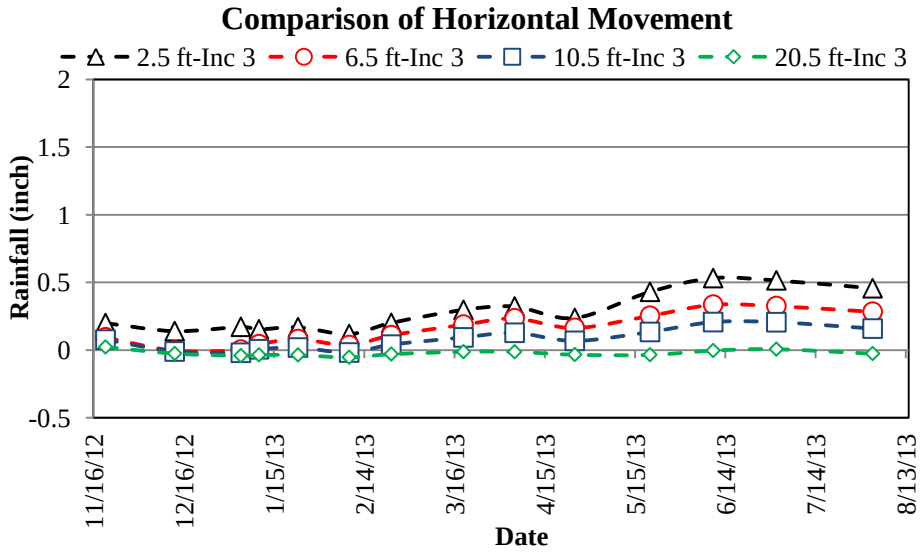


(b)

Figure 5.28 Comparison of Horizontal Movement for base line October 23, 2012, a. Inclinometer 1 at Reinforced Section 1, b. Inclinometer 3 at Reinforced Section 2

Figure 5.29 Site Photo on June 2012 a. new crack initiation from mid-width of Reinforced Section 1 toward control section, b. 12 inch settlement over control section, c. new crack over the shoulder of control section, d. new crack due to control section ends at Reinforced Section 2, e. 9 inch settlement over control section 2, f. probable crack line over roadway near control section 2.

## 5.3 Instrumentation in Loop 12 Slope

To evaluate the performance of the Loop 12 slope, instrumented RPPs were installed in both top and bottom slopes. In addition, a topographic survey was also considered to study the performance. The details of instrumentation at the Loop 12 slope are presented below.

### *5.3.1 Instrumented RPP*

A total of 3 instrumented pins were installed in the Loop 12 slope. The strain gauge IM-1 was installed at the top slope, and IM-2, IM-3 was installed at the bottom slope, along the edge of the retaining wall foundation. The RPPs were instrumented following a method similar to that presented for the US 287 slope. The layout of the instrumented RPPs at Loop 12 slopes is presented in Figure 5.30.

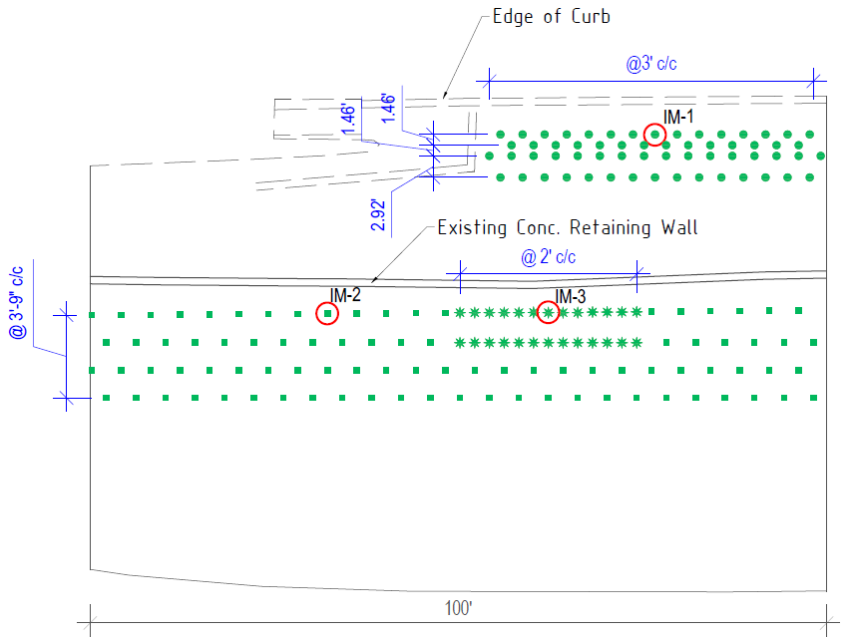


Figure 5.30 Layout of the Instrumented RPPs at Loop 12 Slope

*5.3.2 Topographic Survey*

Surveying over the Loop 12 slope was started on May, 2012 and conducted on monthly basis. Four lines over the slope were selected, designated as Line A-A, Line B-B, Line C-C and Line D-D, to monitor the movement of the reinforced slope. The layouts of the four lines are presented in Figure 5.31. The four lines are located along the curb of Loop 12 near the top slope, 1st row of RPP at the top slope, centerline of the retaining wall and 1st row of RPP at the bottom slope.

During the survey, 3 permanent points over the roadway were selected and monitored besides the survey points. The permanent points during each survey were overlapped, and the movement over the slope was concluded. The data collected during surveying may have ± 1.0 inches variation.

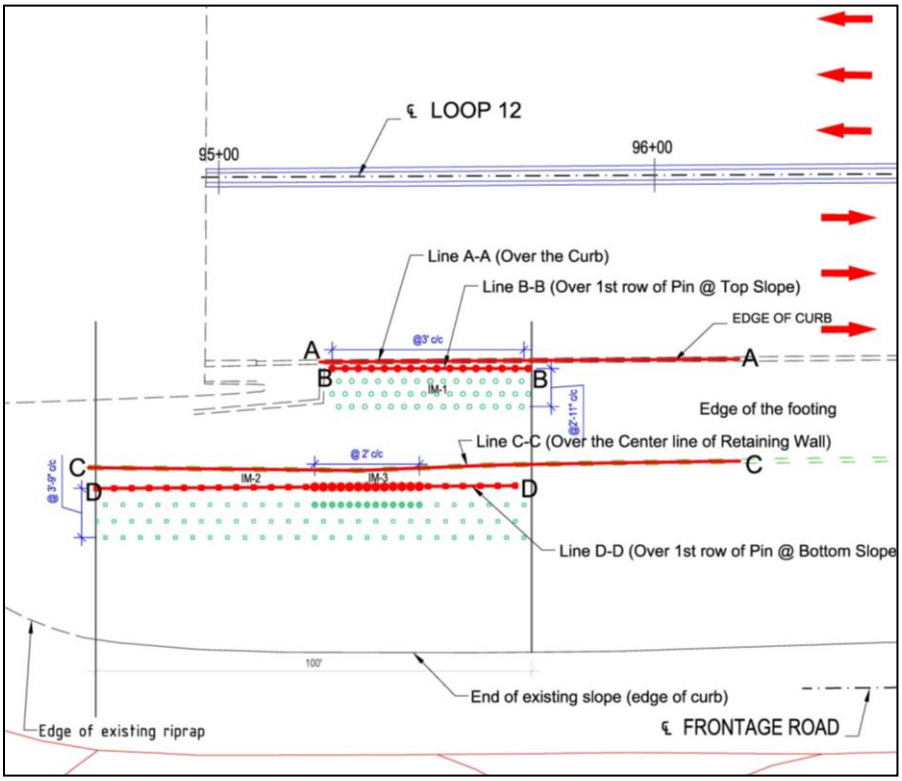


Figure 5.31 Layout of the Survey Line over Loop 12 Slope

## 5.4 Field Performance of Loop 12 Slope

The slopes over Loop 12, near the UP RR railway overpass, had been monitored periodically to evaluate the performance of the stabilized section. The monitoring of the slope included the collection of the strain gauge results from the instrumented RPP and surveying.

### *5.4.1 Strain Gauge Results of the Loop 12 Slope*

The amount of rainfall over time and the variation of strain at 4 ft. and 5 ft. depths of IM1 are presented in Figure 5.32. Based on the field monitoring results, no significant change in strain was observed on IM1 for 4-5 months after installation. However, a noticeable variation in strain was observed after a rainfall event during August 2012. The variation of strain was an indication of displacement which could take place due to the load mobilization at the top slope. After the load mobilization, no significant variation was observed at IM-1, which signified that where was almost no movement at the top slope afterwards.

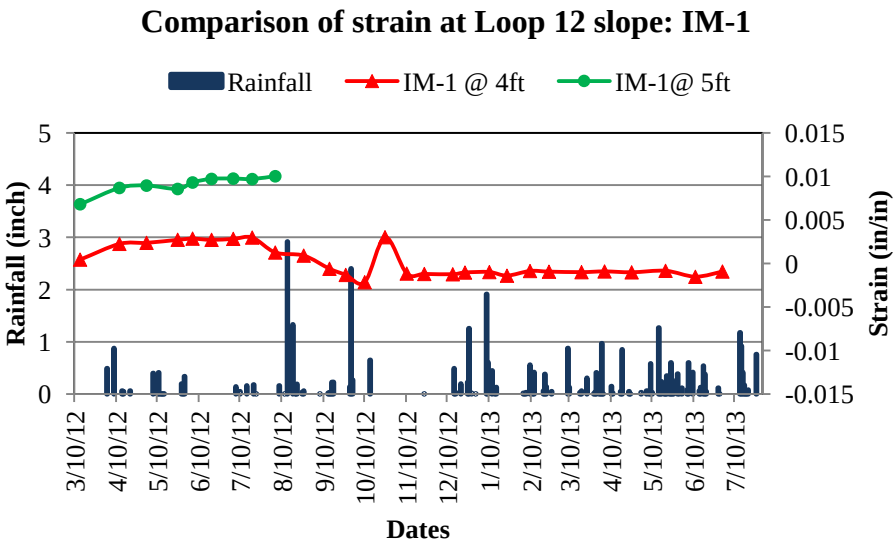


Figure 5.32 Variation of Strain with Rainfall a. IM-1 over Top Slope

*5.4.2 Surveying Results of the Loop 12 Slope*

Based on the survey results over the Loop 12 slopes, the cumulative horizontal displacement and settlement over the Line C-C to Line D-D are presented in Figure 5.33 and Figure 5.34, respectively. It should be noted that excessive horizontal movement was observed along the Line C-C over the retaining wall during the survey. The average horizontal displacement along the retaining wall observed was as much as 5 inches, where the maximum displacement was 7.5 inches at the cracked zone. On the other hand, the observed horizontal displacement along Line D-D, at the 1st row of RPP of the bottom slope, was observed as 4 inches. The variation of the cracked zone of the retaining wall is presented in Figure 5.35

The comparison of horizontal displacement at the retaining wall (Line C-C) and 1st row of RPP (Line D-D) are presented in Figure 5.36. During the design phase of slope stabilization, it was expected that the maximum movement would take place near the cracked zone of the retaining wall. Hence, to provide additional resistance, lower spacing of RPP (2 ft. c/c) was provided at the bottom slope near the cracked zone. The field monitoring result presented 4 inch horizontal movement at the 4 ft. c/c spacing of RPP; whereas, 1 to 3 inch displacement was observed at the 2 ft. c/c spacing of RPP along Line D-D. Less horizontal movement was observed at the lower spacing near the higher displacement of retaining wall at the cracked zone. It should be noted that the RPP was placed at the slope to provide temporary support, with a design period of 1-2 years. Although, the horizontal displacement of the retaining wall had taken place during the performance period, the RPP resisted the overall failure of the slope.

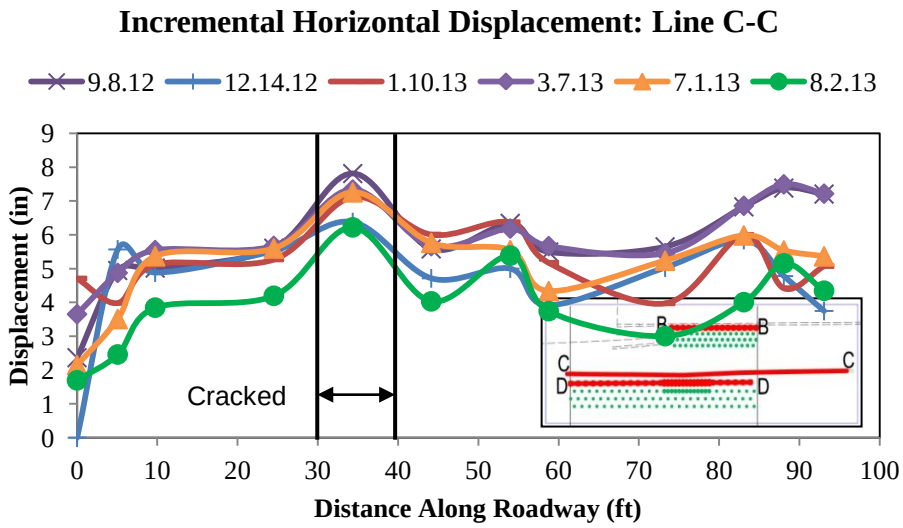


Figure 5.33 Incremental Horizontal Displacement of Retaining wall

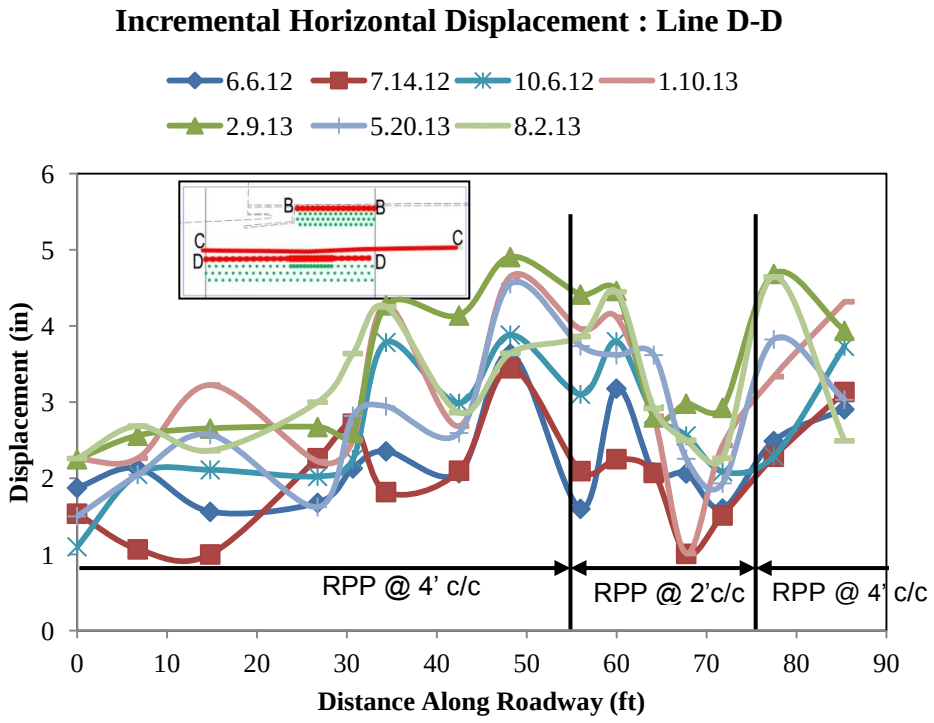


Figure 5.34 Incremental Horizontal Displacement of 1st Line of RPP at Bottom Slope

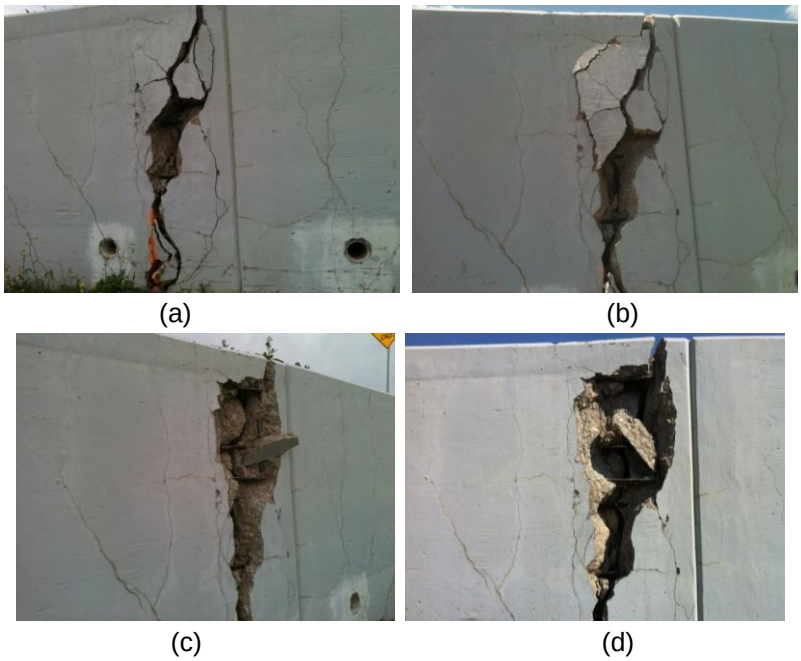


Figure 5.35 Front View of the Crack of Retaining Wall at Loop 12 Slope on a. March 14, 2012, b. August 5, 2012, c. March 19, 13, d. August 2, 13

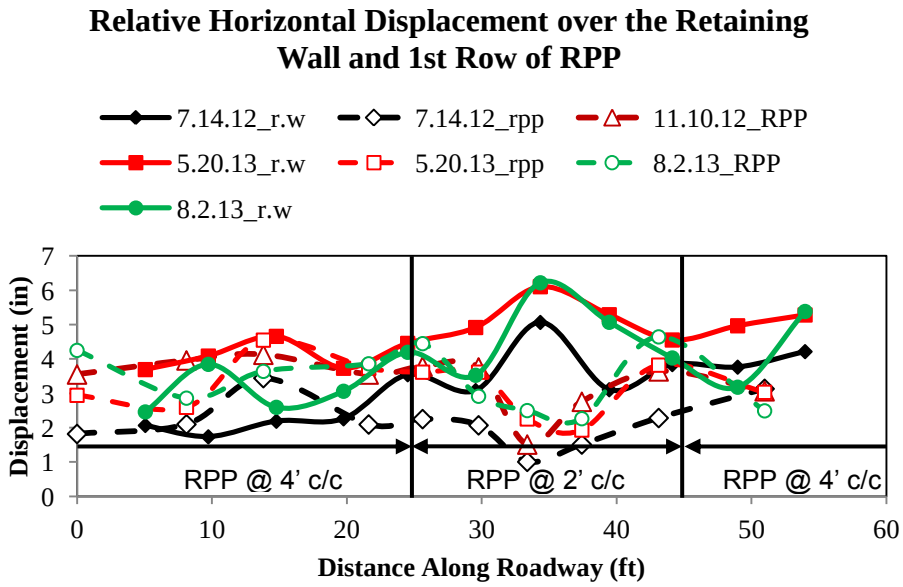


Figure 5.36 Comparison of Horizontal Displacement between Line C-C and Line D-D

## 5.5 Cost Analysis

A cost analysis was conducted for the reinforced sections of the US 287 slopes. The cost of RPP materials and cost for field installation were only considered during the cost analysis. The cost of RPP was considered using rectangular 3.5 in x 3.5 in RPP sections with 10 ft and 8 ft length. On the other hand, the cost of field installation was considered based on the cost to install RPPs over US 287 slope. The summary of the cost of slope stabilization for different slopes is presented in Table 5.2.

Table 5.2 Summary of cost of slope stabilization using recycled plastic pin in US 287 slope

| Location | Total Number of RPP | Area of Slope Stabilization (sft) | Total Cost (USD) | Cost per sft (USD/sft) |
|---|---|---|---|---|
| Reinforced Section 1 | 192 | 3000 | 13200 | 4.4 |
| Reinforced Section 2 | 216 | 3000 | 14000 | 4.7 |
| Reinforced Section 3 | 246 | 3000 | 16000 | 5.4 |

The Reinforced Section 1 and Reinforced Section 2 was stabilized with both the 10 ft and 8 ft long RPP. On the other hand, the Reinforced Section 3 was stabilized with 10 ft long RPP. With the increment in RPP length, the cost of the material (RPP) increased for Reinforced Section 3 and resulted in higher cost (5.4 USD/sft) compared to other reinforced sections.

The cost of slope stabilization using RPP depends on several factors which include the site conditions, site accessibility, the cost for site preparation, cost of the materials, mobilization and installation cost. However, on average, the slope stabilization cost using RPP ranged between 4.8 USD/sft. Sabatini et al., 1997 has conducted a study

on different earth retaining structures which represented that the cost of different retaining structures vary between 35 to 80 USD/sft, as presented in Figure 5.37. Therefore, the cost of slope stabilization using RPP is 50% to 80% less expensive compared to the cost of slope stabilization using other conventional techniques.

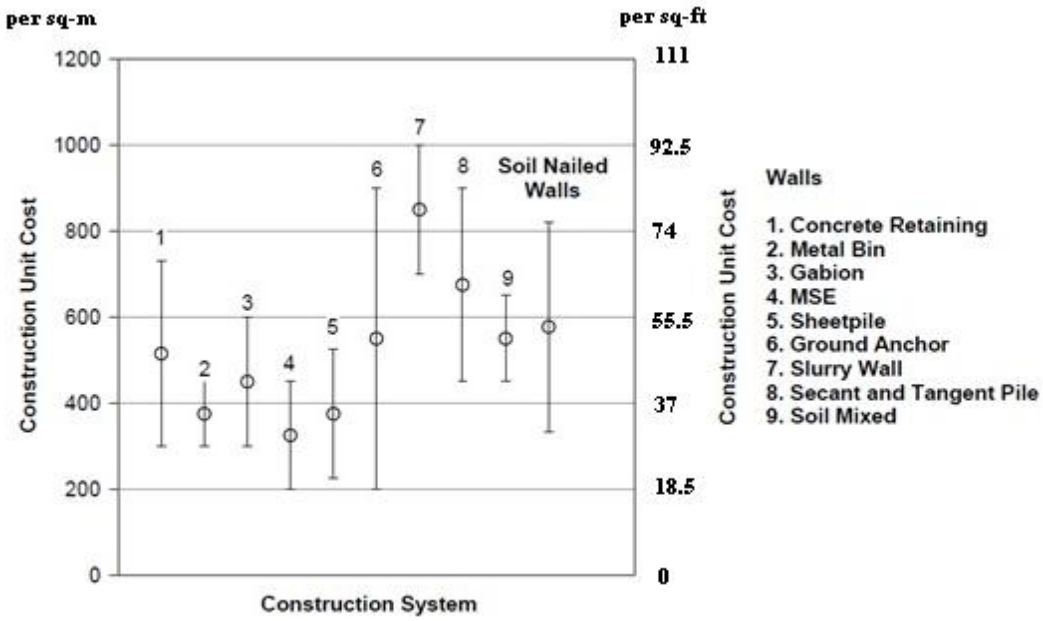


Figure 5.37 Comparison of construction cost data for various systems (Data from Sabatini et al., 1997,cited in Lazarte et al., 2003)

# Chapter 6

# Numerical Study

## 6.1 Introduction

The objective of the current study is to establish a sustainable slope stabilization method using Recycled Plastic Pin. As a part of the study, two highway slopes were stabilized using RPP and was monitored to evaluate the performance of the slope. Based on the 2 years of monitoring results, it was evident that RPP provided adequate resistance against the surficial displacement. The performances of the stabilized slopes were recalibrated in numerical study and effect of different RPP length and spacing was also evaluated.

The field study included uniform spacing of RPP (4 ft. c/c) at Reinforced Section 2 and Reinforced Section 3. In contrast, varied spacing of RPP was provided at Reinforced Section 1, where smaller spacing (3 ft. c/c) was provided at the crest, followed by 6 ft. c/c spacing at the middle of the slope and 5 ft. c/c spacing near the toe of the slope. Therefore, the total number of utilized at Reinforced Section 1 was less, compared to the number of RPP utilized in Reinforced Section 2 and Reinforced Section 3. However, the performance monitoring results presented that the smaller spacing of RPP provided higher resistance at the crest; therefore, the observed displacement was less at Reinforced Section 1, compared to Reinforced Section 2 and Reinforced Section 3. It is obvious that the closer RPP spacing at the crest provide additional resistance where the initiation of slope failure takes place.

The numerical study was conducted using two different considerations. First, the effect of length and spacing of RPP was evaluated with uniform RPP spacing throughout the slope similar to Reinforced Section 2 and Reinforced Section 3. The numerical study was further conducted to study the effect of closer spacing of RPP at the crest of the

slope, followed by wider RPP spacing similar to Reinforced Section 1. The detail of the FEM analysis is presented in this chapter.

## 6.2 Model Calibration

Slope stability analyses were performed using PLAXIS 2D, a special purpose two-dimensional finite element (FE) program used to perform deformation and stability analysis for various types of geotechnical applications (PLAXIS 2D Reference Manual, 2010). The elastic perfectly plastic Mohr-Coulomb soil model was utilized for stability analyses, using 15 node triangle elements. The FEM analysis using a 15 node triangular element is a very accurate method which produces high quality stress results for different problems (PLAXIS 2D Reference Manual, 2010). Standard fixities were applied as boundary condition. The shear strength reduction method (phi-C reduction analysis) was utilized to determine the factor of safety (FS).

During the analyses, the slope was considered to experience failure with limiting FS equal to 1.0 which incorporates the initiation of slope movement. To evaluate the soil parameters during the slope failure, back analyses were performed using PLAXIS 2D. The soil profile for the model is presented in Figure 6.1(a). The top 7 ft of soil was considered as failure zone with a fully softened strength. Besides, the other soil parameters for different soil layer were utilized from soil test results. It should be noted that the back analysis was performed in two steps considering factor of safety and anticipated deformation that was observed in the field. Several iterations were performed during numerical analyses to evaluate soil parameters. The soil parameters observed at failure from numerical modeling are presented in Table 6.1. It should be noted that the soil strength beyond the failure zone was utilized from the existing soil test report. The deformation analysis of the calibrated model was performed for the control slope. Based

on the soil parameters as presented in Table 6.1, the observed settlement were 14.6 inch which was very close to the settlement at the field.

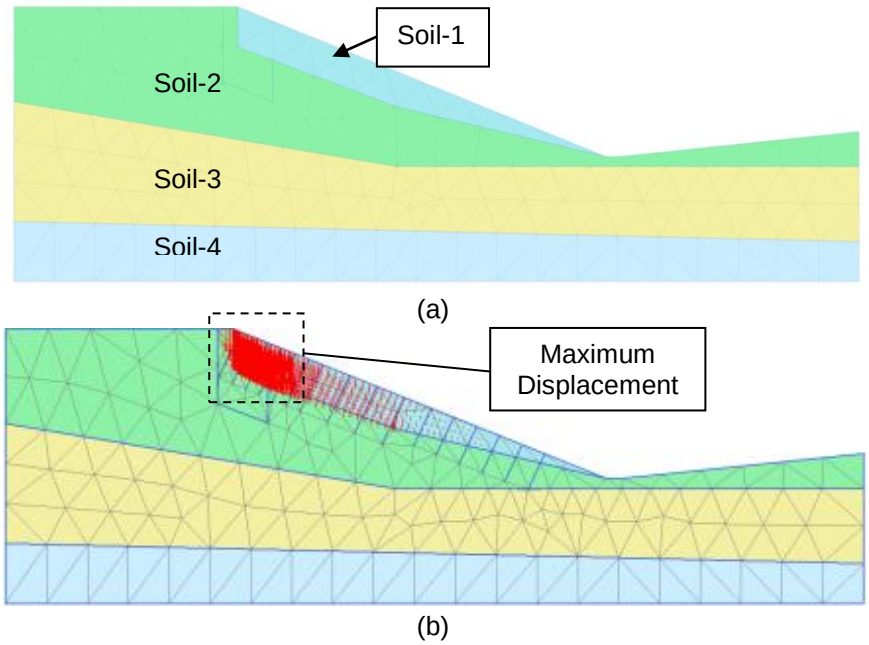


Figure 6.1 Back Analysis a. Soil model of Control section, b. Settlement at control section 14.6 in

Table 6.1 Parameters from FE analysis

| Soil Type | Friction angle φ | Cohesion c | Unit Weight γ | Elastic Modulus E | Poisson Ratio v |
|---|---|---|---|---|---|
| - | ◦ | lb/ft2 | lb/ft3 | lb/ft2 | - |
| 1 | 10 | 120 | 125 | 1122 | 0.35 |
| 2 | 23 | 120 | 125 | 10000 | 0.30 |
| 3 | 15 | 250 | 130 | 200000 | 0.25 |
| 4 | 35 | 3000 | 140 | 250000 | 0.2 |

## 6.3 Performance Evaluation of Reinforced Section 1

The identical soil parameters for the control section were utilized and the deformation analysis for Reinforced Section 1 was performed. Based on the deformation analysis, the predicated horizontal displacement and settlement was observed as 3.2 inch and 2.3 inch, respectively, as presented in Figure 6.2. It should be noted that the maximum displacement of the slope was observed at the crest and was in good agreement with the settlement at the field at Reinforced Section 1.

The horizontal displacement of the 1$^{st}$ 7 row of RPP near the crest of the slope is presented in Figure 6.3. The horizontal displacement plot presented a rotational movement similar to short pile. The short pile action generally takes place when the pile element does not get enough anchorage from the stiff foundation soil. The RPP had only 3 ft anchorage from the foundation soil and result the short pile action. However, increase in RPP length into the foundation soil may increase the resistance and reduce the deformation of RPP. The maximum horizontal displacement (3 inch) reached with 3$^{rd}$ to 4$^{th}$ row of RPP and then, the maximum horizontal displacement of RPP reduced. The site investigation program indicated that slip surface initiated at the crest of the US 287 slope. The calibrated model for the control section also presented that the maximum horizontal displacement near the crest of the slope. The closer spacing at the Reinforced Section 1 provided additional resistance at the zone (Figure 6.2a) which result the less displacement as observed from the field performance monitoring program.

The distribution of bending moment along the length of RPP of 1$^{st}$ 7 rows at Reinforced Section 1 and the percentage of moment transfer is presented in Figure 6.4. The percentage of moment transfer is calculated using the Equation 6.1.

$$\%\, Moment\ Transfer = \frac{Bending\ Moment\ M\ of\ RPP}{Maximum\ Moment\ capacing\ of\ RPP, M_{max}} \qquad (6.1)$$

Based on the Bending Moment plot along the depth of RPP, it was observed that the highest moment had taken place at the 1st row of RPP at the crest of the slope. The maximum bending moment was 300 lb-ft which was observed near the interface between the top soil and foundation soil. It is evident that the RPP got anchorage from the foundation soil which resulted in maximum bending moment near the interface between the top soil and foundation soil. The percentage of moment transfer plot at Figure 6.4 for Reinforced Section 1 presented that the maximum percentage of moment transfer is 15% which signifies only 15% of the total moment capacity of the RPP is utilized. Chen et al., (2007), presented a study to predict the life RPP for slope stabilization based on the % moment transfer. The study presented that, up to 35% moment transfer, the design life of RPP can be as much as 100 years. Nonetheless, the maximum load transfer for Reinforced Section 1 was 15% which might result in the RPP to last more than 100 years.

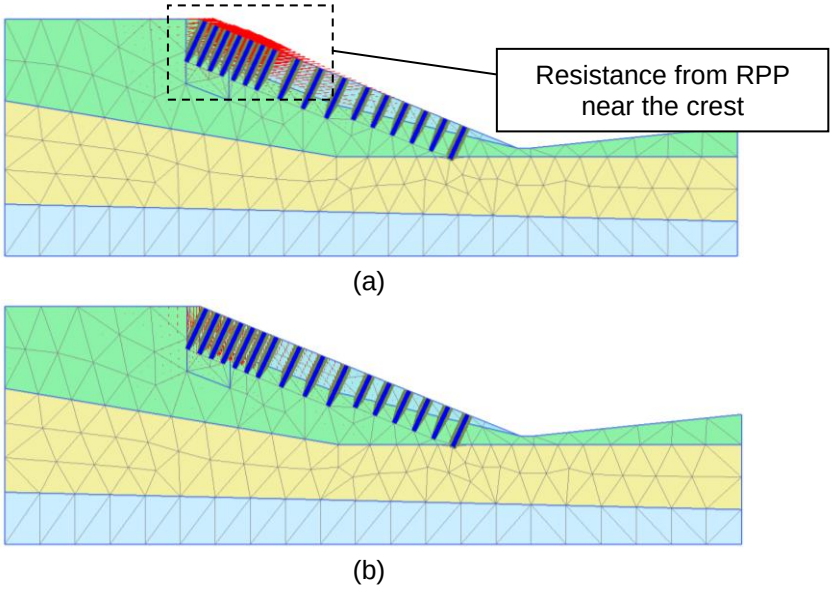


Figure 6.2 Deformation analysis at Reinfroced Secton 1, a. Horizontal Displacement at Crest = 3.2 inch, b. Settlement at the crest of the slope 2.3 inch

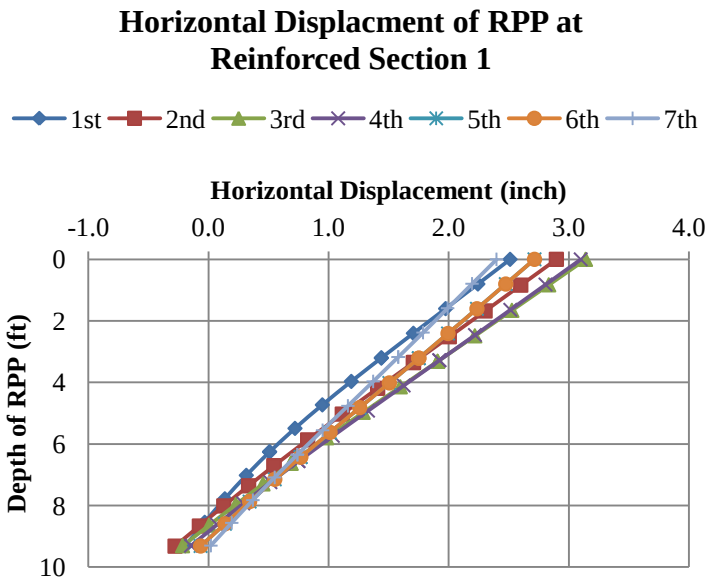


Figure 6.3 Horizontal displacement of 1st 7 row of RPP at Reinforced Section 1

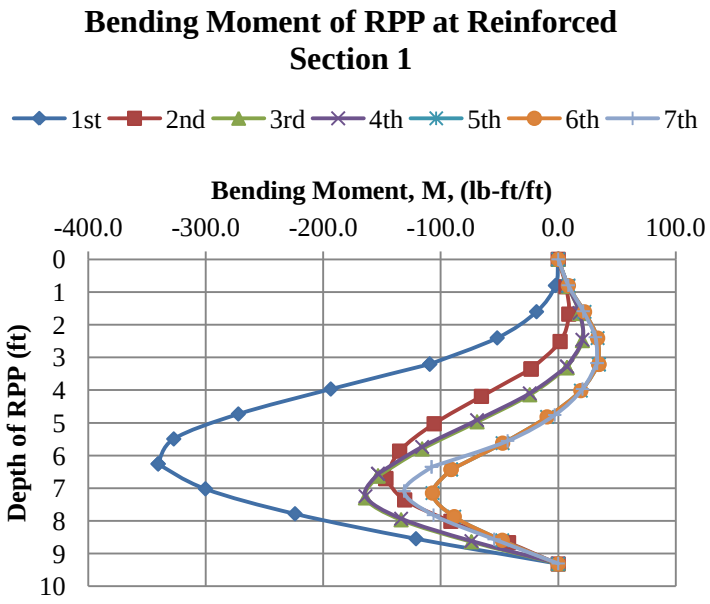


(a)

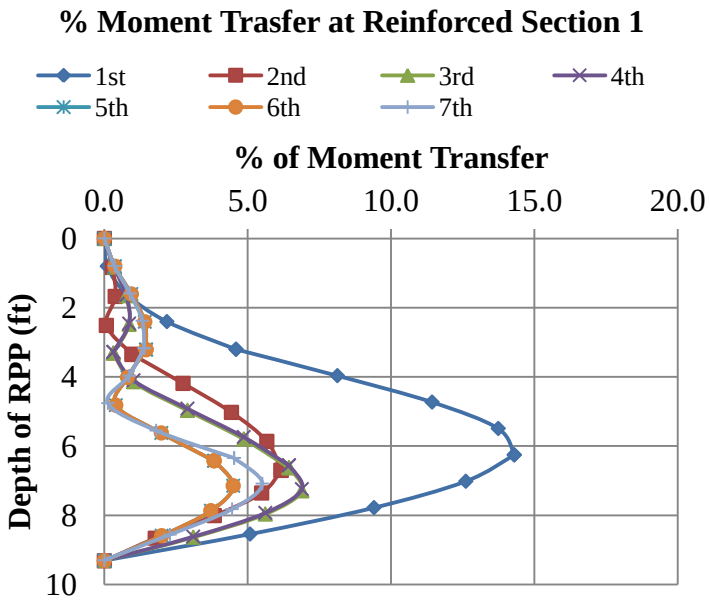


(b)

Figure 6.4 Moment along the length of RPP a. Bending moment, b. Percentage of moment transfer

## 6.4 Performance Evaluation of Reinforced Section 2

The identical soil parameters for the control section were utilized and the deformation analysis for Reinforced Section 2 was performed similar to Reinforced Section 1. Based on the deformation analysis, the predicated horizontal displacement and settlement was observed as 3.25 inch and 2.62 inch, respectively, as presented in Figure 6.5. The predicted settlement was higher compared to the settlement at Reinforced Section 1. However, the predicted settlement using the FEM analysis was less for Reinforced Section 2 compared to the observed field settlement. The variation might take place due to the propagation effect of crack at the control sections through the Reinforced Section 2 which cannot be addressed in 2D FEM analysis.

The horizontal displacement of the 1$^{st}$ 7 row of RPP near the crest of the Reinforced Section 2 is presented in Figure 6.6. The horizontal displacement plot presented a rotational movement similar to short pile behavior as described in Reinforced Section 1. However, the observed horizontal displacement was higher for Reinforced Section 2, as the resistance of 4 ft. c/c at the crest was less resulted higher deformation of Slope.

The distribution of bending moment along the length of RPP of 1$^{st}$ 7 rows at Reinforced Section 2 and the percentage of moment transfer is presented in Figure 6.7. The bending moment diagram presented that the highest bending moment (360 lb-ft) had taken place at the 1$^{st}$ row of RPP that was located at the crest of the slope, similar to Reinforced Section 1. The percentage of moment transfer plot at Figure 6.7 (b) for Reinforced Section 2 presented that the maximum percentage of moment transfer is 16% which was slightly higher compared to Reinforced Section 1. Compared with the study of Chen et al., 2007, it is evident that the RPP in Reinforced Section 2 might also survive more than 100 years.

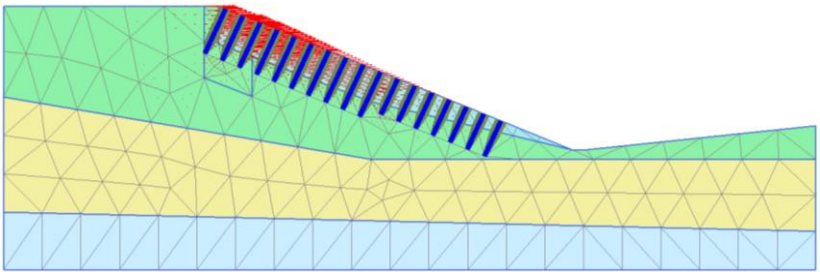

(a)

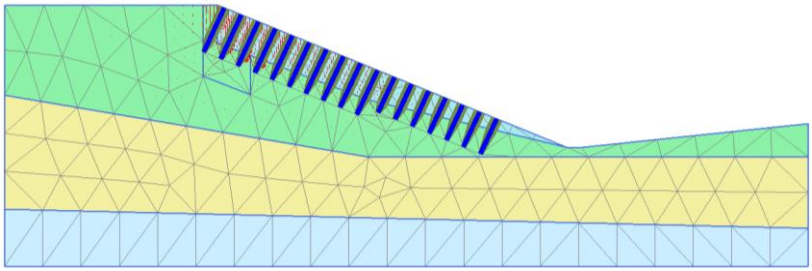

(b)

Figure 6.5 Deformation analysis at Reinfroced Secton 2, a. Horizontal Displacement at Crest = 3.25 inch, b. Settlement at the crest of the slope 2.62 inch

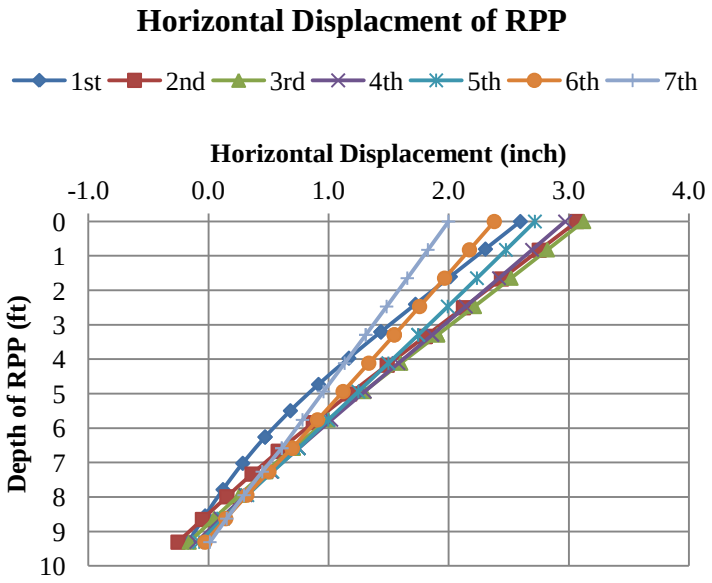


Figure 6.6 Horizontal displacement of 1st 7 row of RPP at Reinforced Section 2

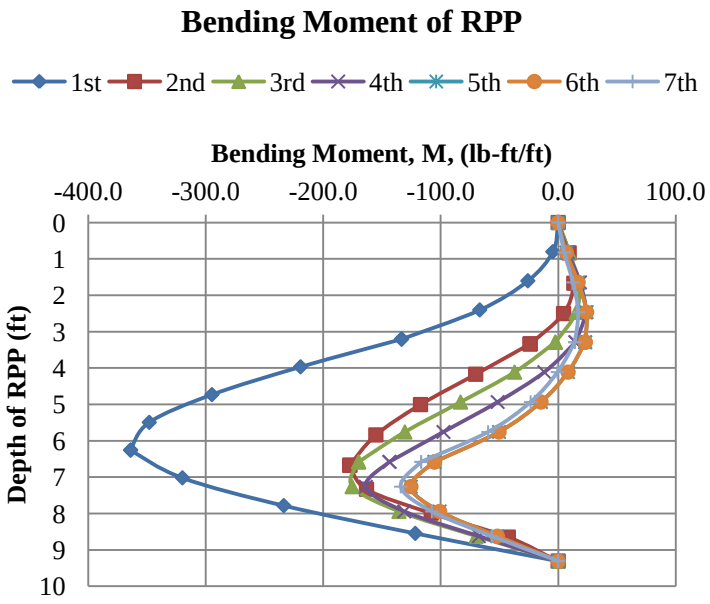


(a)

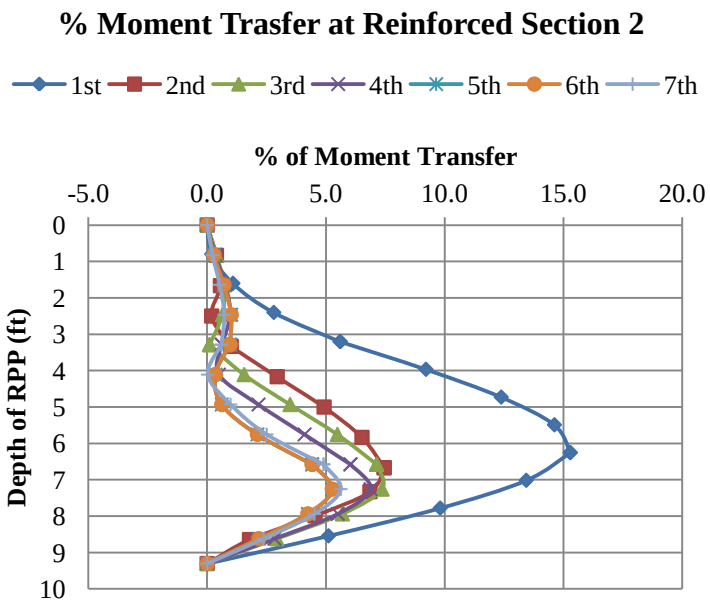


(b)

Figure 6.7 Moment along the length of RPP a. Bending moment, b. Percentage of moment transfer

## 6.5 Parametric Study: Effect of Uniform Spacing and Depth of RPP

The numerical study of the Reinforced Section 1 and Reinforced Section 2 was further evaluated using a parametric study. The parametric analysis was performed to evaluate the effect of spacing and length of RPP over the factor of safety and deformation of slope. During the current field demonstration study, 10 ft. and 8 ft. long RPP had been utilized to resist the shallow slope failure where the failure depth generally ranged between 3 ft. to 6 ft. (Loehr and Bowders, 2007). In addition, 12 ft. long RPP may be installed in the slope using the available installation method. Therefore, the 12 ft., 10 ft. and 8 ft. long RPP is selected for the parametric study.

The field study included different spacing of RPP which ranged between 3 ft. c/c and 6 ft. c/c. The current parametric study considered different spacing of RPP that ranged from 2 ft. c/c to 8 ft. c/c, with 1 ft. c/c increments. The numerical modeling matrix of the parametric study is presented in Table 6.2. The parametric study was performed using the calibrated model based on the field behavior of US 287 slope. The RPP was modeled as plate element with 0.85 interface element strength for all models.

Table 6.2 Numerical Model Matrix for Parametric Study

| Length of RPP (m) | Spacing of RPP (m) | Type of Analysis |
|---|---|---|
| 12 ft | 2 ft, 3 ft, 4 ft, 5 ft, 6 ft, 7 ft and 8 ft | Plastic Deformation |
| | | Factor of Safety |
| 10 ft | 2 ft, 3 ft, 4 ft, 5 ft, 6 ft, 7 ft and 8 ft | Plastic Deformation |
| | | Factor of Safety |
| 8 ft | 2 ft, 3 ft, 4 ft, 5 ft, 6 ft, 7 ft and 8 ft | Plastic Deformation |
| | | Factor of Safety |

## 6.6 Parametric Study Results

### *6.6.1 Factor of Safety*

The factor of safety of the reinforced slope was calculated using the strength reduction technique. The variation of factor of safety with different length and spacing of RPP is presented in Figure 6.8. The slope stability analysis for safety presented that the slipping surface goes down to a deeper depth for all the spacing, resulting in deep seated failure of the slope with factor of safety ranging between 1.61 (for RPP spacing of 2 ft. c/c) and 1.54 (for RPP spacing of 8 ft. c/c) for 12 ft. long RPP. The failure zone goes down beyond the depth of RPP at 6 ft. c/c and 3 ft. c/c spacing for 10 ft. and 8 ft. long RPP, respectively.

The factor of safety was observed almost constant at the RPP spacing from 2 ft. c/c to 5 ft. c/c. It was expected that at lower spacing, the RPP would provide higher resistance, resulting in a higher factor of safety. However, at 2 ft. c/c to 5 ft. c/c spacing, the additional resistance provided by RPP might not be mobilized to the slope that resulted in an almost constant factor of safety. At larger RPP spacing, (greater than 5 ft. c/c), the factor of safety decreased with the increment in RPP spacing. However, the rate of decrease of factor of safety was observed higher at 8 ft. long RPP than the 10 ft. and 12 ft. long RPP. It should be noted that during the analysis, the depth of the fully softened zone was 7 ft. where the soil was soft, and movement occurred at that location. As a result, RPP with 8 ft. length had smaller support from the stiff foundation than the larger length of RPP.

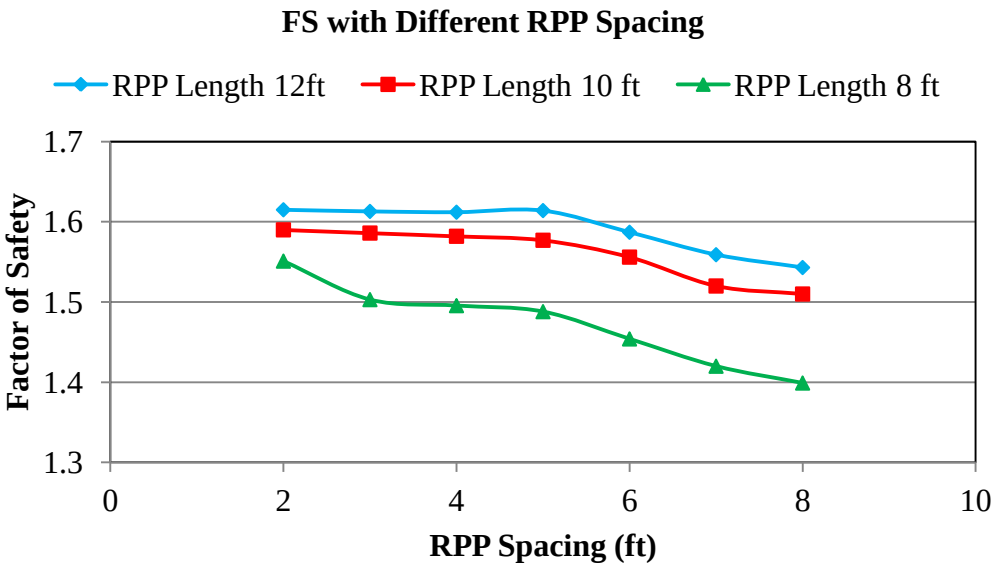


Figure 6.8 Variation of FS with RPP Length and Spacing

*6.6.2 Deformation Analysis*

Plastic calculation was performed in Plaxis 2D for deformation analysis. During the plastic calculation, the initial condition of the slope was calculated, using the gravity loading condition which is recommended for non-level ground such as slope. In gravity turn-on analysis, the vertical stress was calculated based on the weight of unstressed mesh. Horizontal stresses were then changed to be equal to $k_0$ (Earth pressure co-efficient at rest) times the calculated vertical stress (Duncan, J. M., 1996). Later, the plastic analysis was conducted by activating the RPP in the soil model. Based on the FEM analysis, the horizontal displacement of RPP at the crest of the slope was plotted with RPP spacing and length, as presented in Figure 6.9. The horizontal displacement of crest is presented in Figure 6.10

The horizontal displacement plot in Figure 6.9 presented that the 12 ft. and 10 ft. long RPP got enough resistance from the foundation soil to act as a long pile. Rotational

movement was observed for 8 ft. long RPP, which resembled the deformation profile of short pile. It was obvious that, 12 ft. and 10 ft. long RPP had enough anchorage from the foundation soil, therefore less displacement compared to 8 ft. long RPP.

Based on the deformation analysis results, it was observed that the lowest horizontal displacement was noticed at closer RPP spacing (2 ft. c/c with higher RPP length of 12 ft.) With the increment in RPP spacing, greater horizontal displacement had taken place. Moreover, at RPP spacing more than 4 ft. c/c, the increase in horizontal displacement was significant, with an increase in RPP spacing.

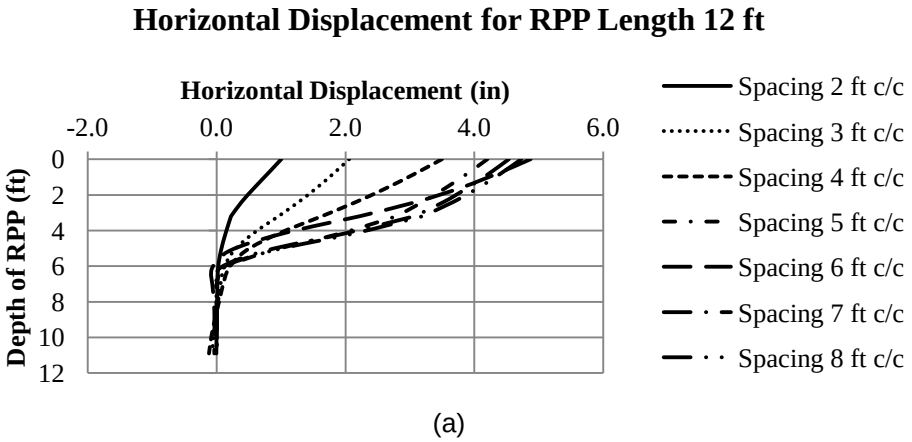


(a)

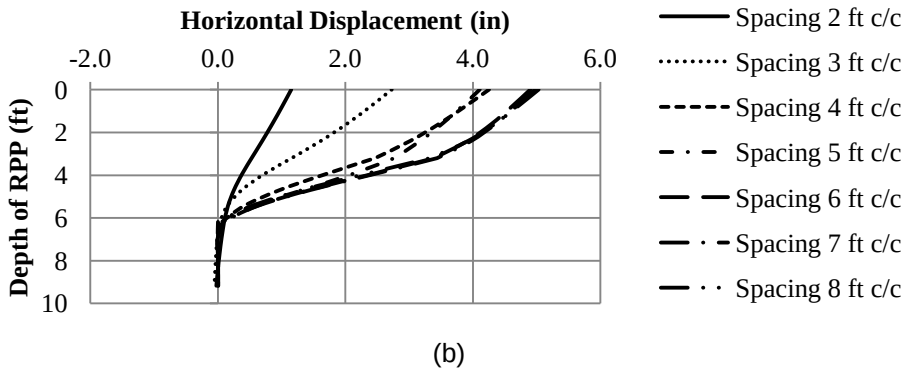


(b)

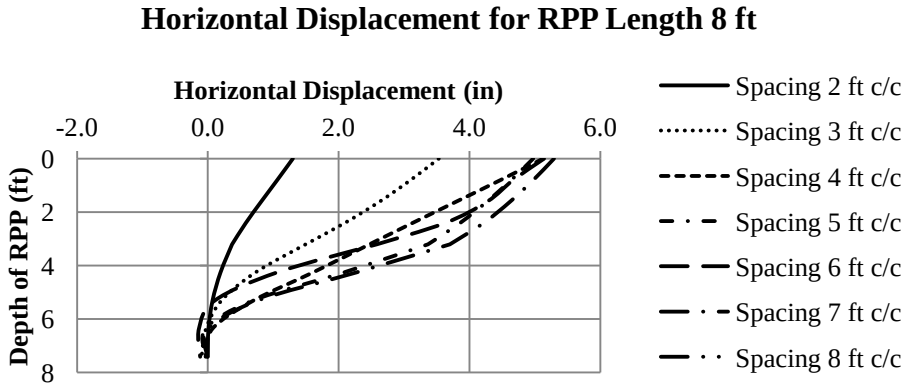


(c)

Figure 6.9 Horizontal Displacement Profile of RPP with Different Spacing a. RPP Length 12 ft, b. RPP Lengh 10 ft, c. RPP Length 8 ft.

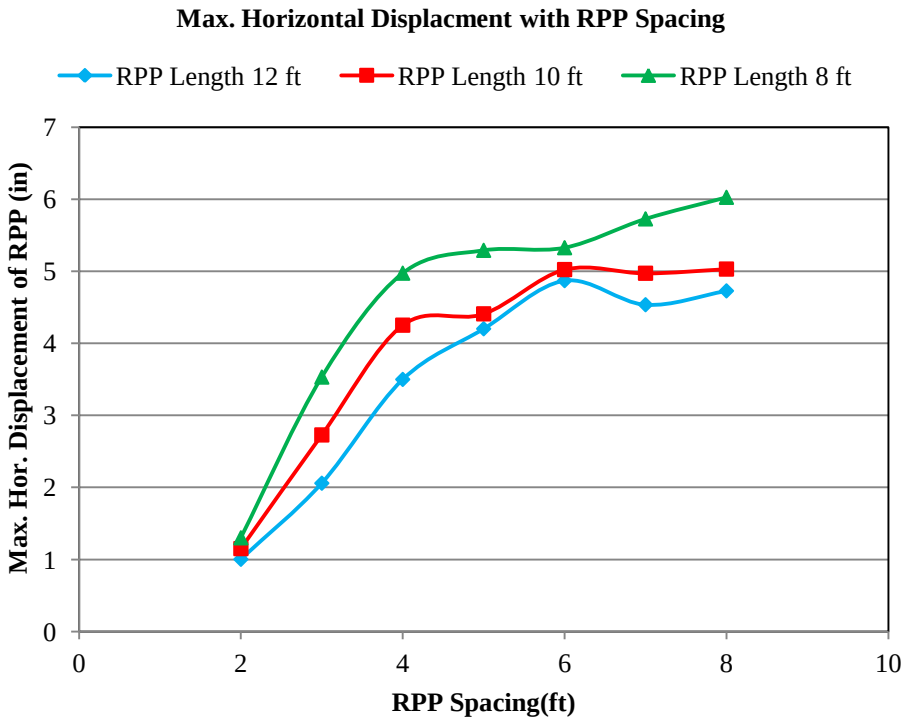


Figure 6.10 Maximum Horizontal Displacement of RPP at Crest of Slope

Finally, based on the parametric study with uniform RPP spacing throughout the slope, the factor of safety ranged between 1.61 to 1.40 with different RPP length and spacing, which might be satisfactory for different design standards. According to safety analysis, RPP might be installed with greater spacing, which would be cost effective; however, it would result higher deformation. Therefore, it is important to conduct deformation analysis, along with safety analysis, to finalize design with higher spacing of RPP.

The calibrated model, as well as the FEM analysis of the reinforced sections presented that RPP with closer spacing at the crest provide higher resistance and can reduce the deformation of the slope. On the other hand, based on the field study, it was observed that the closer RPP spacing at the crest of the slope can resist higher

horizontal deformation (Reinforced Section 1), provided high RPP spacing at the bottom part of the slope. Therefore, further study was conducted using less spacing of RPP at the crest of the slope.

## 6.7 Parametric Study: Smaller RPP Spacing at Crest

The study was conducted to investigate the effect of smaller RPP spacing on the crest to reduce the deformation of slope, provided higher spacing of RPP on the rest of the slope. As a part of the study, the slope was divided into two sections designated as the top section (1/3 length near crest) and bottom section (rest 2/3 length of the slope). The technique included closer spacing near the crest of the slope at the top section. The rest of the slope was considered with wider spacing of RPP. A total of 3 different conditions were analyzed, using RPP spacing of 2 ft., 3 ft. and 4 ft. c/c at the top section. RPP spacing that ranged between 3 ft. and 8ft c/c was considered for the remaining bottom section. FEM program PLAXIS 2D was utilized to investigate the effect of spacing on both safety and deformation of the slope.

Closer RPP spacing (2 ft., 3 ft., and 4 ft. c/c) was considered at top section during the study. RPP with 2 ft. c/c spacing at top section was investigated, with RPP spacing ranging between 3 ft. and 8 ft. c/c at bottom section. The 3 ft. and 4 ft. c/c spacing of RPP at top section had RPP spacing that ranged between 4 ft. and 8 ft. c/c at the bottom section. The arrangement of RPP spacing at both top and bottom sections during the study are summarized in Table 6.3 and Figure 6.11.

Table 6.3 Numerical Modeling Matrix

| RPP Spacing at Top Section (1/3 length of slope near crest ) | RPP Spacing at Bottom Section (rest 2/3 length of the slope) | Length of RPP |
|---|---|---|
| 2 ft | 3 ft., 4 ft., 5 ft, 6 ft., 7 ft. and 8 ft. | 12 ft., 10 ft. and 8 ft. |
| 3 ft. | 4 ft., 5 ft., 6 ft., 7 ft. and 8 ft. | 12 ft., 10 ft. and 8 ft. |
| 4 ft. | 5 ft., 6 ft., 7 ft. and 8 ft. | 12 ft., 10 ft. and 8 ft. |

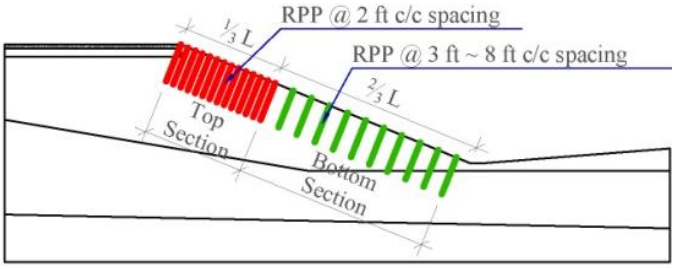


(a)

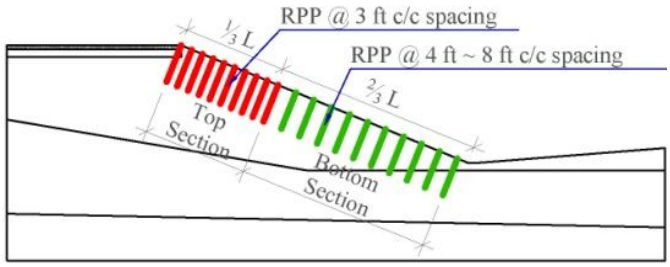


(b)

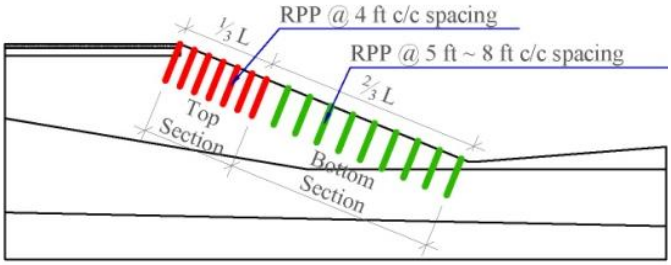


(c)

Figure 6.11 RPP Spacing at Top and Bottom Sections of Slope. a. 0.6 m c/c RPP Spacing at Top Section, b. 0.9 m c/c RPP Spacing at Top Section, c. 1.2 m c/c RPP Spacing at Top Section

## 6.8 Results of FEM Analysis with Closer RPP Spacing at Crest

### *6.8.1 Variation of Factor of Safety*

The factor of safety of the reinforced slope was calculated using the strength reduction technique. Based on the FEM analysis, the variation of factor of safety with RPP spacing is presented in Figure 6.12. The factor of safety of the slope ranged between 1.62 and 1.45 for 2 ft. c/c RPP spacing at the top section. With the increasing of RPP spacing at the top section (3 ft. and 4 ft. c/c), factor of safety of the slope reduced, ranging between 1.57 and 1.42. Figure 6.12 indicates that the factor of safety also decreased with increasing the RPP spacing at the bottom section. In contrast, the factor of safety of slope increased with longer RPP length.

The factor of safety was high for RPP spacing 2 ft. c/c compared to 3 ft. c/c and 4 ft. c/c at top section. The high factor of safety was due to additional resistance from 2 ft. c/c spacing at the crest.

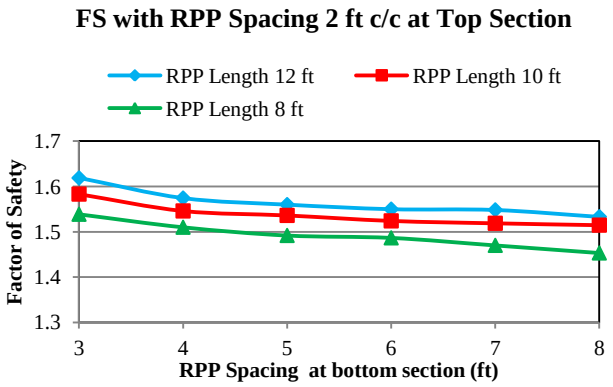


(a)

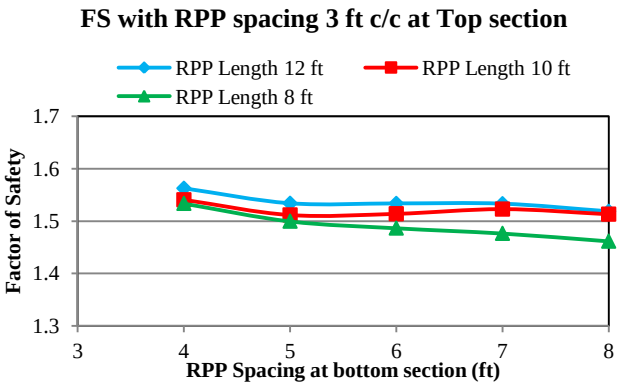


(b)

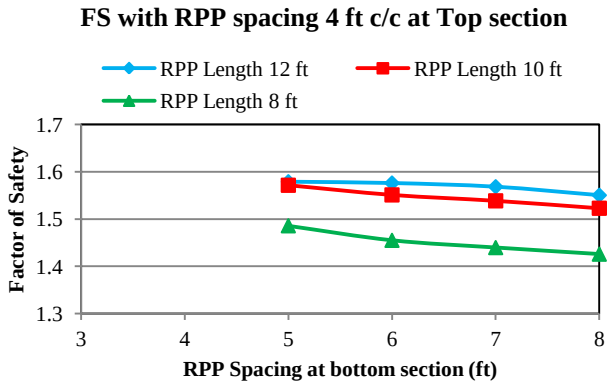


(c)

Figure 6.12 Effect of RPP Length and Spacing on Factor of Safety a. RPP Spacing 2 ft. c/c at Top Section b. RPP Spacing 3 ft. c/c at Top Section and c. RPP Spacing 4 ft. c/c at Top Section

*6.8.2 Horizontal Displacement at Crest*

The plastic calculation was performed with PLAXIS 2D for deformation analysis. The deformation analysis was conducted following the similar way as presented for the parametric study with uniform spacing throughout the slope.

Based on the FEM analysis, the lateral deformation of RPP at crest of the slope with 2 ft., 3 ft. and 4 ft. c/c RPP spacing at the top section is presented in Figure 6.13, Figure 6.14 and Figure 6.15; respectively. The horizontal displacement plots presented that the 12 ft. and 10 ft. long RPP acted as a long pile. On the other hand, rotational movement was observed for 8 ft. long RPP, which resembled with the deformation profile of a short pile. Moreover, the depth of soft soil in the FEM analysis was 7 ft. As a result, the 12 ft. and 10 ft. long RPPs had enough anchorage from the foundation soil and had less displacement than the 8 ft. long RPP. It should be noted that a similar deformation profile was observed during the parametric study, using uniform spacing of RPP throughout the slope.

During the study, only the deformation of the slope at the crest (from top section) was presented. The deformation at the bottom section (at middle and toe) of the slope was observed to be less than the displacement at the crest. Therefore, no deformation result from the bottom section of the slope is presented here.

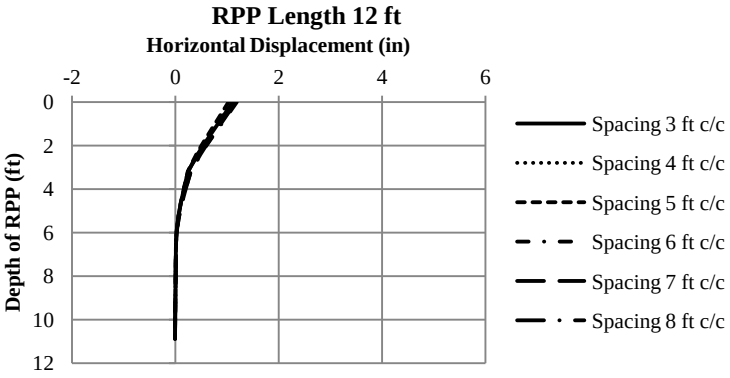


(a)

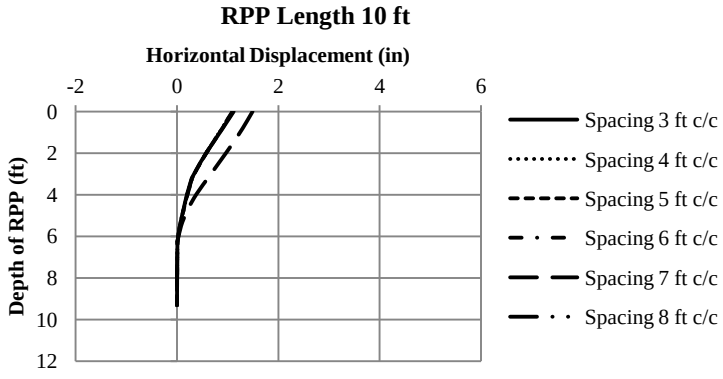


(b)

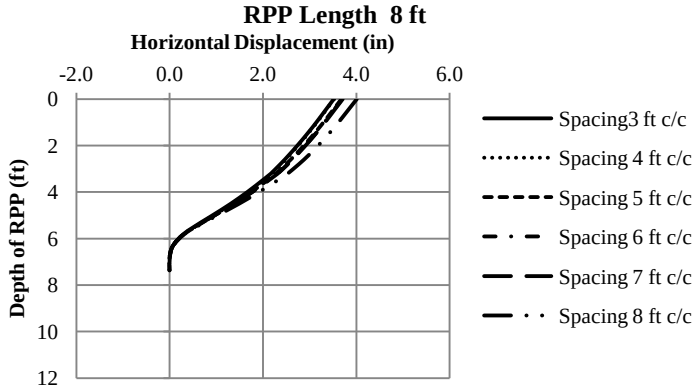


(c)

Figure 6.13 Horizontal Displacement Profile for RPP Spacing 2 ft c/c at Top Section

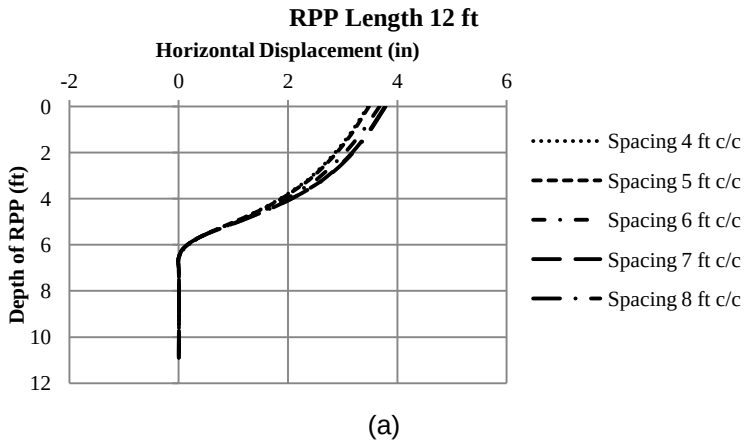


(a)

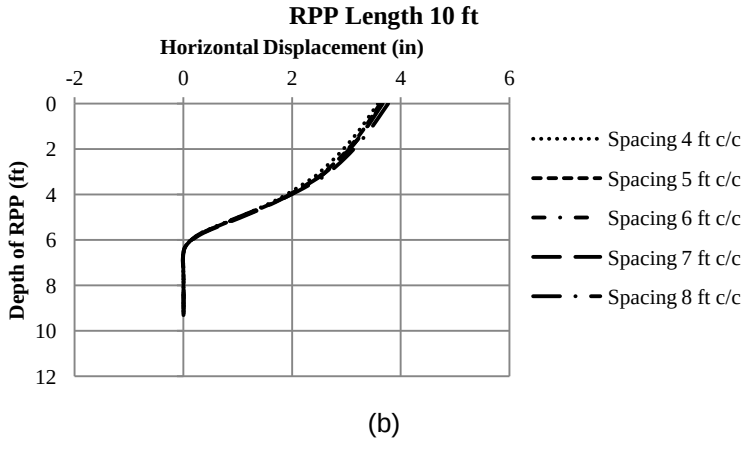


(b)

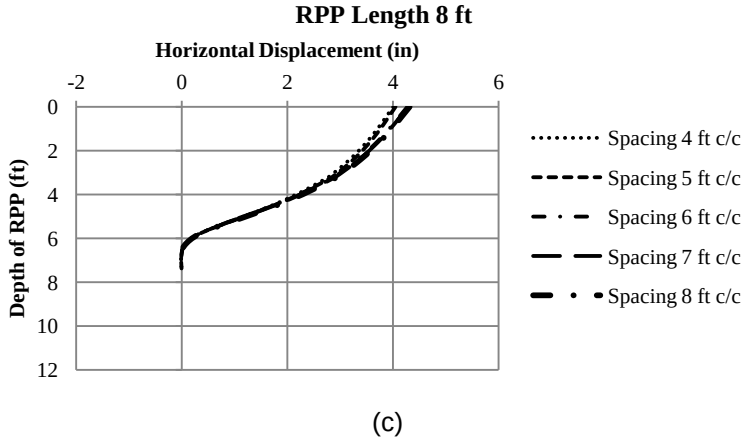


(c)

Figure 6.14 Horizontal Displacement Profile for RPP Spacing 3 ft c/c at Top Section

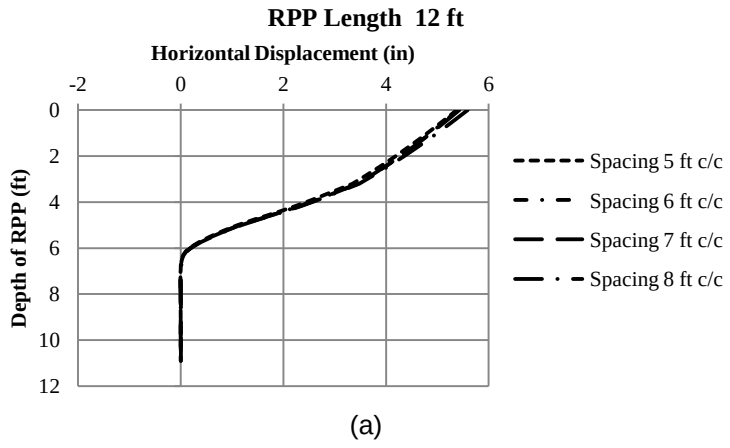


(a)

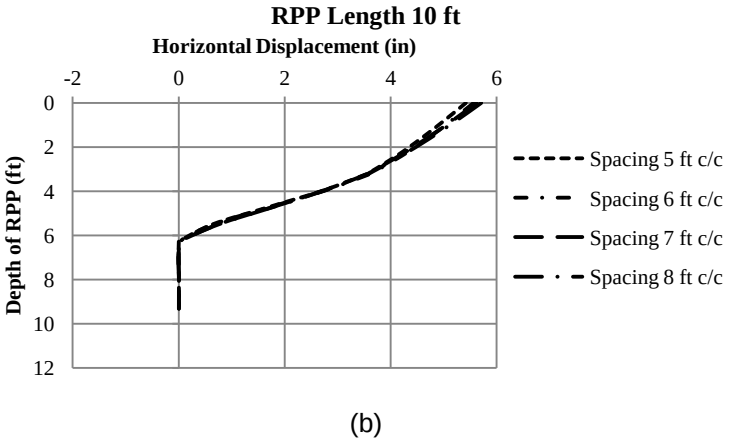


(b)

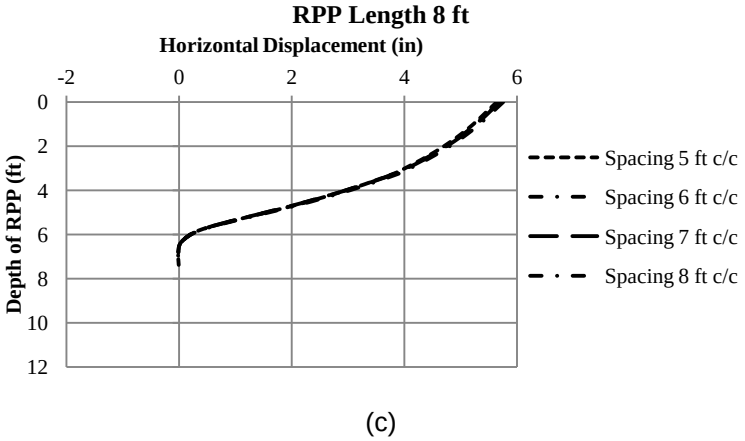


(c)

Figure 6.15 Horizontal Displacement Profile for RPP Spacing 4 ft c/c at Top Section

Based on the horizontal displacement profile, the variation of maximum horizontal displacement at the crest of slope is presented in Figure 6.16. The deformation analysis results indicated that the maximum horizontal displacement was not affected with RPP spacing at the bottom section.

The horizontal displacement was similar for 12 ft. and 10 ft. long RPPs. For 2 ft. spacing of RPP at the top section, the observed displacement was 1.18 inches. The horizontal displacement increased 3 to 4 times with RPP spacing of 3 ft. and 4 ft., compared to the displacement at RPP spacing of 2 ft. c/c at top section. The observed horizontal displacement was higher for 8 ft. long RPP than for 12 ft. and 10 ft. long RPP. The horizontal displacement was 3.54 inches for RPP spacing of 2 ft. c/c at top section. In addition, the horizontal displacement increased within 1.15 to 1.6 times with an increase in RPP spacing at the top section.

It was obvious that at closer spacing, the resistance from RPP was higher at the crest. The resistance of RPP decreased with wider spacing. Therefore, with wider RPP spacing at the top section, the horizontal displacement at the crest increased substantially. On the other hand, the 12 ft. and 10 ft. long RPPs had adequate resistance from the foundation soil. In addition, the 2 ft. c/c spacing of RPP provided substantial resistance against slope deformation. As a result, the lowest deformation had taken place.

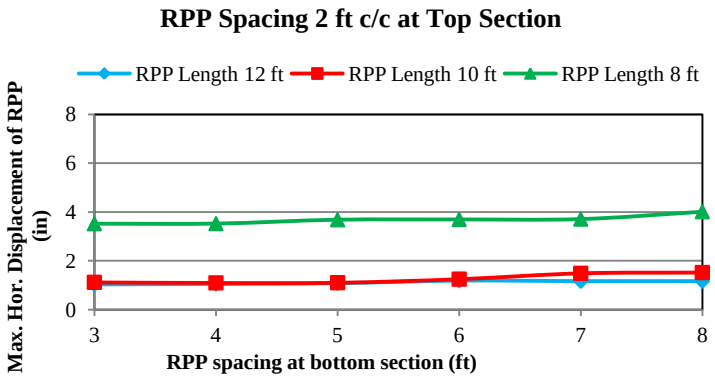


(a)

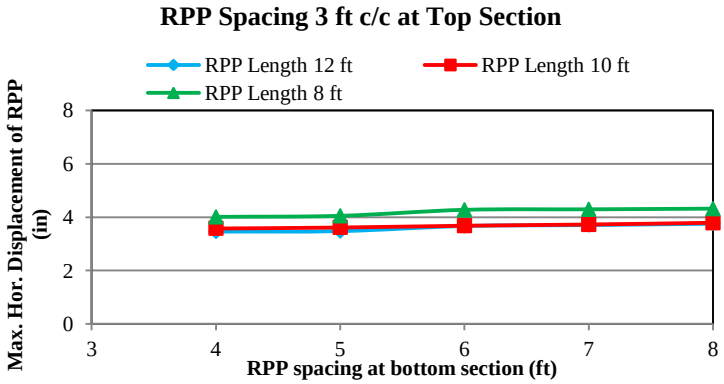


(b)

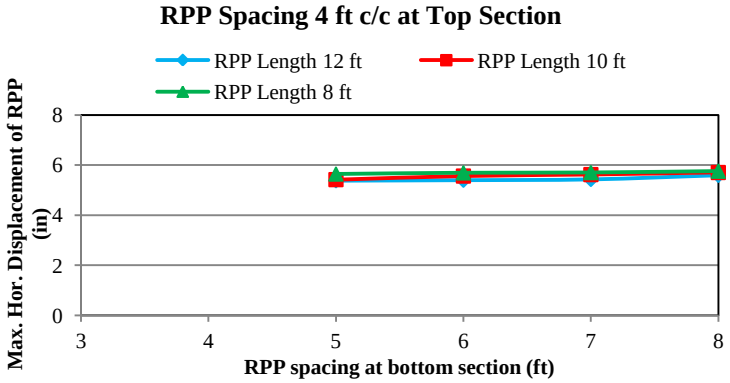


(c)

Figure 6.16 Effect of RPP Length and Spacing on Maximum Horizontal Displacement at a. RPP Spacing 2 ft. c/c at Top Section b. RPP Spacing 3 ft. c/c at Top Section and c. RPP Spacing 4 ft. c/c at Top Section

The previous section presented the factor of safety and deformation of slope that have uniform spacing of RPP throughout the slope. On the other hand, the current section presented 2 ft. c/c at the top section and wider RPP spacing at the bottom section, which resulted in fewer RPPs needed for slope stabilization. However, the observed deformation and factor of safety of the slope were similar. On the other hand, considering RPP length of 10 ft, a slope reinforced with uniform spacing of 3 ft. and 4 ft. c/c have superior performance compared to the slope reinforced with closer spacing (3 ft. and 4 ft.) at the crest, provided higher RPP spacing at the bottom section. However, the deformations of the slope remain within allowable limit recommended by Loehr and Bowders, (2007) which were around 3 in. An optimization during the design of slope stabilization can be made using the closer spacing at top section (2 ft c/c and 3 ft c/c RPP spacing), with wider spacing at bottom part, which might result in cost prohibitive design.

## 6.9 Summary

The control section of US 287 was selected as a reference slope and the performance of the control section was calibrated during the numerical study. The field performance of the reinforced sections were evaluated and compared with the FEM model. The numerical study presented that the predicated and observed performance of the Reinforced Section 1 was in good agreement. However, the predicted deformation (using FEM analysis) was lower for Reinforced Section 2 compared to the field study. The higher deformation at Reinforced Section 2 had taken place due the crack propagation through the section. However, the crack propagation phenomenon cannot be modeled using the 2D FEM package.

The calibrated FEM model was further utilized and the effect of RPP length and spacing was evaluated using parametric study. The parametric study was performed

using uniform RPP spacing throughout the slope and closer RPP spacing at the crest of the slope. Based on the parametric study, the key findings are summarized below.

RPP at uniform spacing throughout the slope

- Increase in RPP length resulted in a greater factor of safety.
- With increase in spacing of RPP, the factor of safety remained constant up to RPP spacing 5 ft. c/c, and then decreased with further increments in spacing.
- The higher RPP length had deeper depth in stiff foundation soil and resulted in less horizontal displacement.
- With incremental changes in RPP spacing, the horizontal deformation increased significantly.

RPP at closer spacing at the crest

- The spacing of RPP at the top section had significant effect on the deformation of the slope. With closer RPP spacing at the top section, the deformation of slope was low. The deformation of slope increased 3 to 4 times with wider RPP spacing at the top section.
- The effect of RPP spacing at the bottom section was not significant for the performance of the slope. However, with an increase in RPP spacing at the bottom section, the factor of safety of the slope decreased.
- The longer RPPs had higher depth in foundation soil, which resulted in additional resistance from foundation soil and improved both the performance and factor of safety of slope.

The study presented that the 2 ft. c/c RPP spacing at the top section, with high RPP spacing (such as 8 ft. c/c) at the bottom section resulted in similar performance compared to a slope reinforced with 2 ft. c/c uniform spacing of RPP. Therefore, the smaller spacing at crest can be utilized, with higher spacing at the rest of the slope to

attain better performance with lower cost. However, both deformation and safety analysis are recommended during the design of slope stabilization to evaluate the performance.

# Chapter 7

# Development of Design Chart

## 7.1 Introduction

Loehr and Bowder, (2007) presented a design approach using the limit equilibrium method to evaluate the stability of RPP reinforced slope. The general approach in limit equilibrium method, to evaluate the stability of reinforced and unreinforced slopes, is to consider a potential sliding surface, then calculate the factor of safety for the sliding surface. The factor of safety of slope is considered as

$$Factor\ of\ Safety\ (FS) = \frac{\int S}{\int \tau} \tag{7.1}$$

Where, FS is the factor of safety, s is the shear strength from soil at the sliding surface and τ is the mobilized shear stress to maintain equilibrium. The slope stability analysis is conducted using the method of slices approach with Mohr Column failure envelope, where the sliding body is divided into a number of vertical slices. The equilibrium of the individual slices determines the normal and shear stress on the sliding surface, and with an assumed sliding surface, the factor of safety is determined. The process is repeated for other potential surfaces until the lowest factor of safety is obtained. For the reinforced slope, a procedure similar to the method of slide is used. A force, due to the reinforcing member, is added to the other forces on the slide that are intersected by reinforcing members. The schematic of the equilibrium of the unreinforced and reinforced slopes is presented in Figure 7.1.

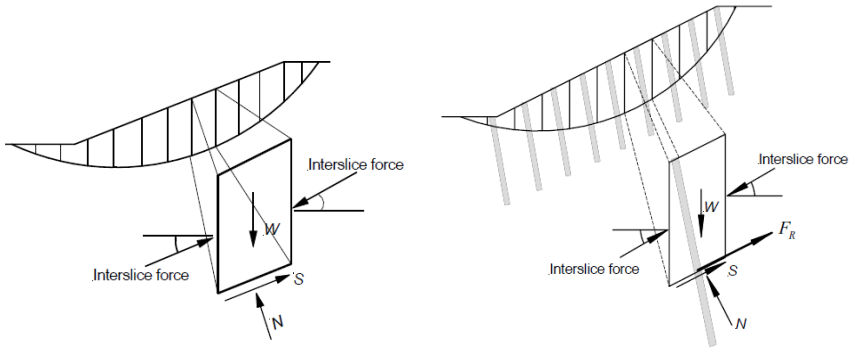


Figure 7.1 Static Equilibrium of Individual Slice in the Method of Slices a. Unreinforced Slope, b. Reinforced slope. (Loehr and Bowders, 2007)

The reinforcement force provides a direct resistance along the slip surface and increases the factor of safety. Loehr and Bowders (2007) referred to the reinforcement force as the limit resistance, which varies along the depth of RPP. The author considered two soil failure mechanisms and two structural failure modes to establish the limit resistance curve for RPP. Based on the failure modes of soil and RPP, Loehr and Bowders (2007) proposed a combined limit resistance curve, as presented in Figure 7.2.

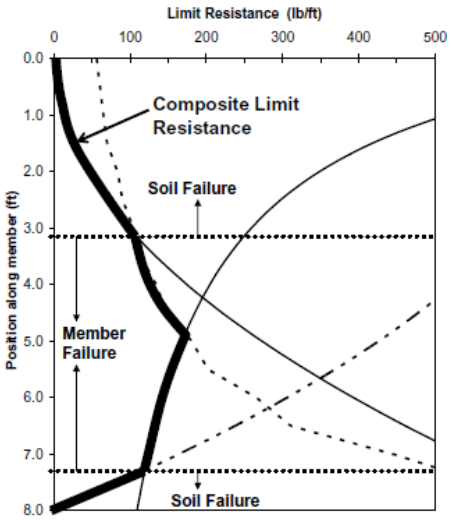


Figure 7.2 Combined Limit Resistance Curve (Loehr and Bowders, 2007).

Once the combined limit resistance curve is developed for a particular condition and slope, the FS of the reinforced slope can be determined using the limit resistance slope stability analysis software, including the resistance from the RPP. The design approach considered by Loehr and Bowders (2007) was simple and very straight forward. However, to utilize the design procedure, a designer needs to develop the combined limit resistance curve for the specific condition, which is time consuming. On the other hand, the design approach considers the failure modes for the structural failure of RPP; however, it lacks to explain the deformation of the reinforced slope.

Chen et al., (2007) performed a study on the creep behavior of RPP. Due to the variety of manufacturing processes and constituents, the engineering properties of commercially available materials vary substantially. The polymeric materials are durable in terms of environmental degradation; however, they can exhibit higher creep rates compared to other structural materials such as timber, concrete or steel. Therefore, it is also important to consider the creep criteria in the design of RPP stabilized slope.

The current study presented a design approach for slope stabilization using RPP. The design approach considered the similar limit resistance approach for the failure mode of soil, as presented by Loehr and Bowders (2007); however, it incorporated the performance of the slope instead of using the limiting criteria of the structural failure of RPP. The current approach considered the limit resistance based on the adjacent soil and the limiting resistance of RPP based on the deformation of RPP as well as the limiting criteria for creep. The detail of the design approach is presented below.

## 7.2 Limiting Criteria

### *7.2.1 Limit Failure of Adjacent Soil of RPP*

The limit lateral soil pressure is the maximum lateral pressure that the soil adjacent to the Recycled Plastic Pin (RPP) can sustain before failure, either by flowing

around or between reinforcing members. Loehr and Bowders (2007) proposed two different soil failure modes, referred to as Failure Mode 1 and Failure Mode 2, as presented in Table 7.1. In Failure Mode 1, it is considered that the soil above the sliding surface fails by flowing between or around the reinforcing members. On the other hand, in Failure Mode 2, the soil below the sliding surface adjacent to the reinforcing member is assumed to fail, which results in the reinforcing member passing through the soil. The limit resistance corresponding to each of these failure modes is computed based on the limit soil pressure.

Table 7.1 Summary of Soil Failure Mode for Establishing Limit Lateral Resistance of RPP

| Failure Mode | Description |
|---|---|
| Failure Mode 1 | Failure of soil above sliding surface or between reinforcing member |
| Failure Mode 2 | Failure of soil below sliding surface due to insufficient anchorage length |

The limit soil pressures (a stress) and limit lateral resistance (a force) act on a reinforcing member for an assumed sliding depth, as presented in Figure 7.3. The limit resistance (a force) is computed by integrating the limit soil pressure over the length of the reinforcing member above the depth of sliding, considering that the limit soil pressure is fully mobilized along the entire length of the member above the sliding surface.

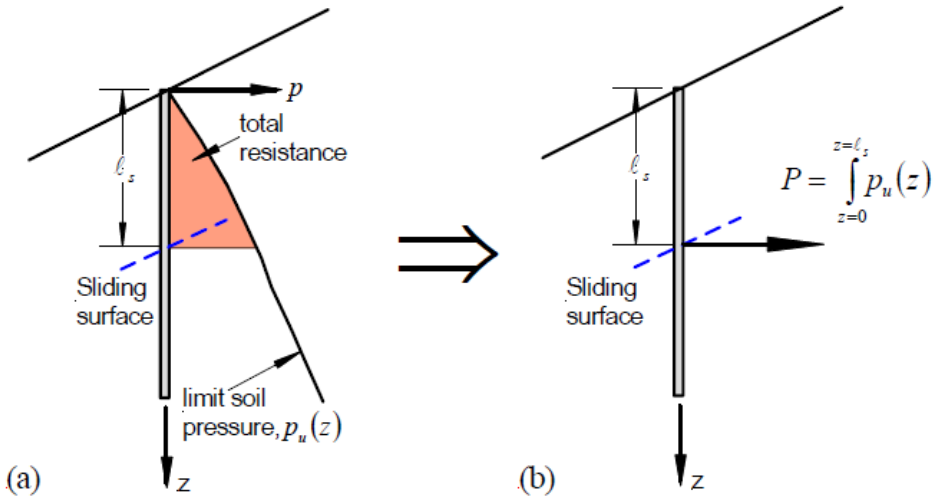


Figure 7.3 Schematic Diagram of Calculation of Limit Resistance Force: a. Limit Soil Pressure and b. Equivalent Lateral Resistance Force (Loehr and Bowders, 2007)

*7.2.2 Limit Resistance of RPP*

During this current study, the limit resistance of RPP is evaluated using the performance criteria. Since, the modulus of elasticity of RPP is low compared to other structural materials, it is important to consider the anticipated displacement due to the applied soil pressure. In addition, the creep criteria should be considered for the limit resistance of RPP. Therefore, the limit resistance of RPP should be evaluated based on the limit horizontal displacement, as well as the maximum allowed flexural stress on RPP. The limit resistance of RPP is presented below.

7.2.2.1 Limit Horizontal Displacement of RPP

RPP is subjected to active pressure and passive resistance of soil when it is installed as slope reinforcement. In addition, due to sliding of the slope, RPP is subjected to an additional soil pressure above the slip surface. The schematic of the load over the RPP is illustrated in Figure 7.4. RPPs get anchorage from the foundation soil below the slipping plane, work as a lateral support and resist the movement of soil above the slip

surface. However, during this interaction, a displacement takes place which depends on the additional pressure due to slope movement, the depth of the soft soil over the slipping plane, the active and passive pressure of soil and the anchorage from the foundation. Based on the displacement of RPP during this interaction, the overall displacement of the slope should take place. It is important to limit the displacement of the RPP as slope reinforcement to limit the overall displacement of the slope. Therefore, the current study considered the limit horizontal displacement approach where the capacity of RPP was evaluated based on the anticipated displacement due to the soil movement.

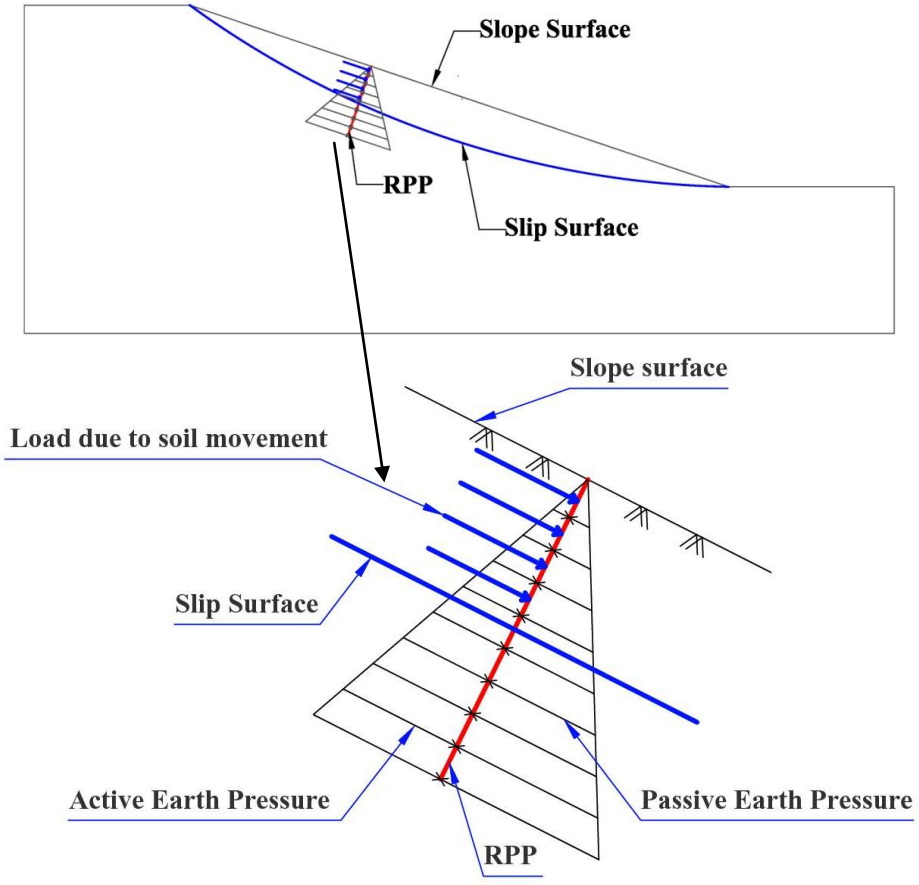


Figure 7.4 Schematic of load over RPP as slope reinforcement

7.2.2.2 Limit Maximum Flexure for Prolonged Creep Life

Chen et al., (2007) presented a study on the creep behavior of RPP. The author studied the flexural creep responses on scaled RPP at different temperature such as 21°, 35°, 56°, 68°, and 80°C. The study considered the Arrhenious method to estimate the long term creep behavior. Based on the study, Chen et al. (2007) observed that, as the temperature increased, the time to reach failure decreased for the same load condition. In addition, the loading levels, along with temperature, affect the creep behavior of the recycled plastic specimens. The study presented that at higher load levels, closer to the ultimate strength of the material, the creep rate was faster and it required shorter time to reach failure. Based on the study, the author presented a method to investigate the design life of RPP based on % load mobilization, as presented in Figure 7.5.

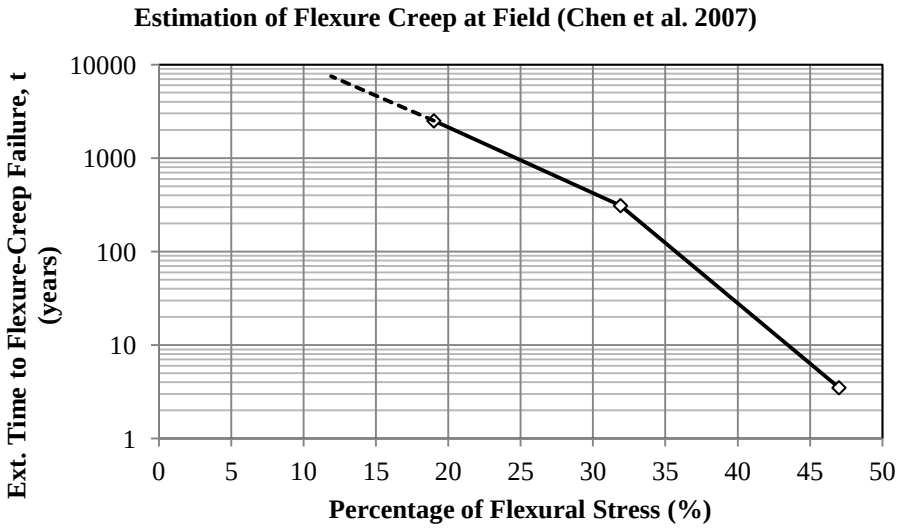


Figure 7.5 Flexural Creep at Field Condition (Chen et al., 2007)

Figure 7.5 indicated that at the higher mobilized loads, the design life of RPP become susceptible to creep failure. Therefore, it is important to limit the percentage of flexural stress in RPP to limit the creep failure time. It should be noted that at 35% of

flexural stress, the estimated time to flexure-creep failure should be 100 years, which is higher than the average design life of a highway slope. Therefore, during this current design procedure, a RPP should be restricted to 35% of flexural stress to its ultimate capacity.

## 7.3 Determination of Limit Soil Pressure

### *7.3.1 Calculation of Limit Soil Pressure*

Ito and Matsui (1975) proposed a method to determine the limit of lateral force on stabilizing piles in a slope. The method was established based on soil failure between piles, assuming the soil between the piles to be in a plastic state, according to the Mohr-Coulomb failure criterion. The assumed region of plastic behavior is shown in Figure 7.6. This method is referred to as the “theory of plastic deformation.” The limit soil pressure of RPP is calculated using the Equation 7.2 and Equation 7.3. Sample soil parameter, as presented in Table 7.2, was utilized to determine the limit soil pressure for RPP which is illustrated in Figure 7.7.

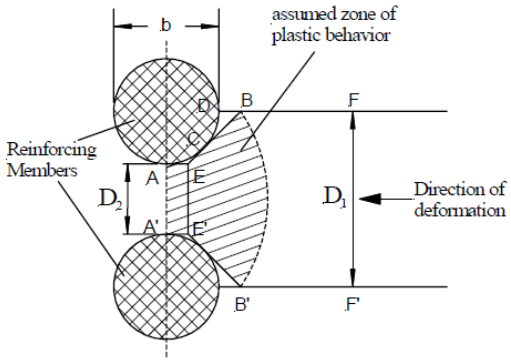


Figure 7.6 Assumed Region of Plastic Deformation for Theory Proposed by Ito and Matsui (1975)

$$P(z) = cD_1\left(\frac{D_1}{D_2}\right)^{N_\varphi{}^{\frac{1}{2}}tan\varphi+N_\varphi-1}\left[\frac{1}{N_\varphi tan\varphi}\left\{\exp\left(\frac{D_1-D_2}{D_2}\right)N_\varphi tan\varphi * \tan\left(\frac{\pi}{8}+\frac{\varphi}{4}\right) - 2N_\varphi{}^{\frac{1}{2}}tan\varphi - 1\right\} + \frac{2tan\varphi + 2N_\varphi{}^{\frac{1}{2}} + N_\varphi{}^{-\frac{1}{2}}}{N_\varphi{}^{\frac{1}{2}}tan\varphi + N_\varphi - 1}\right] - c\left\{D_1\frac{2tan\varphi + 2N_\varphi{}^{\frac{1}{2}} + N_\varphi{}^{-\frac{1}{2}}}{N_\varphi{}^{\frac{1}{2}}tan\varphi + N_\varphi - 1} - 2D_2N_\varphi{}^{-\frac{1}{2}}\right\} + \frac{\gamma z}{N_\varphi}\left\{D_1\left(\frac{D_1}{D_2}\right)^{N_\varphi{}^{\frac{1}{2}}tan\varphi+N_\varphi-1} * \exp\left(\frac{D_1-D_2}{D_2}\right)N_\varphi tan\varphi * \tan\left(\frac{\pi}{8}+\frac{\varphi}{4}\right) - D_2\right\} \quad (7.2)$$

Where,

$$N_\varphi = \tan^2\left(\frac{\pi}{4}+\frac{\varphi}{2}\right) \quad (7.3)$$

And,

$c =$ cohesion intercept, $\varphi = friction\ angle, \gamma =\ unit\ weight\ of\ soil$

$D_1 =$ center to center pile spacing and $D_2 = inner\ distance\ between\ piles$

Table 7.2 Parameters for Estimating Limit Soil Pressure

| RPP Properties | | Soil Parameter | |
|---|---|---|---|
| Size (inch) (Rectangular) | 3.5 x 3.5 | c (psf) | 200 |
| Length (ft) | 10 | φ | 10 |
| Spacing (ft) | 3 | ϒ (pcf) | 125 |

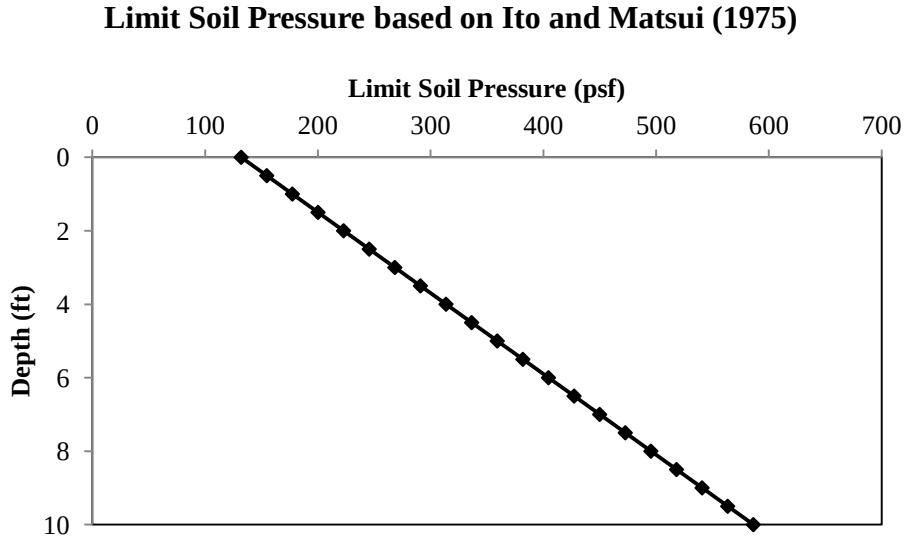


Figure 7.7 Limit Soil Pressure with Depth of RPP

*7.3.2 Calculation of Limit Soil Resistance*

In Failure Mode 1, the soil above the sliding surface is assumed to fail by flowing between or around the reinforcing members. RPP is assumed sufficiently anchored into stable soil below the sliding surface. The schematic diagram of Failure Mode 1 is presented in Figure 7.8. The limit resistance for Failure Mode 1 is determined by integrating the limit soil pressure (as presented in Figure 7.7) along the RPP up to the depth of the sliding surface, considering that the limit soil pressure is fully mobilized along the length of RPP below the sliding surface. This calculation is repeated for varying depths of sliding to develop a curve describing the magnitude of the limit resistance along the length of the RPP, as presented in Figure 7.9.

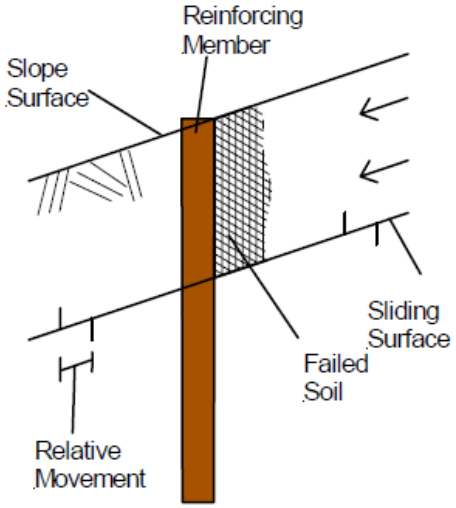


Figure 7.8 Schematic Diagram of Failure Mode-1 (Loehr and Bowders, 2007)

**Limit Soil Pressure based on Ito and Matsui (1975)**

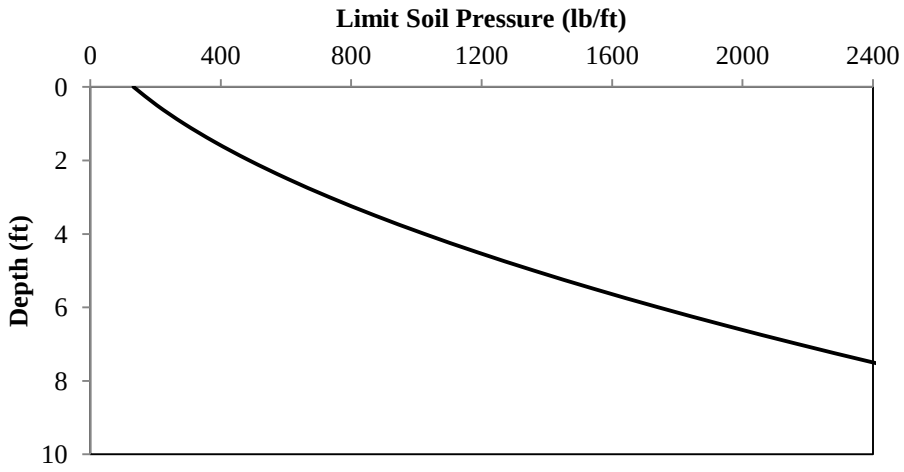


Figure 7.9 Limit Soil Resistance based on Failure Mode-1

The limit soil resistance for Failure Mode-2 is also calculated through the similar process for Failure Mode-1, except that the soil below the sliding surface adjacent to the RPP is assumed to fail while the member is sufficiently anchored in the moving soil

above the sliding surface. The reinforcing RPP is essentially flowing through the soil below the sliding surface, as illustrated in Figure 7.10.

The limit resistance for Failure Mode-2 is determined by integrating the limit soil pressure along the RPP, below the depth of the sliding surface, considering that the limit soil pressure is fully mobilized along the length of member below the sliding surface. This calculation is repeated for varying depths of sliding to develop a curve describing the magnitude of the limit resistance along the length of the reinforcing member for Failure Mode-2, as presented in Figure 7.11.

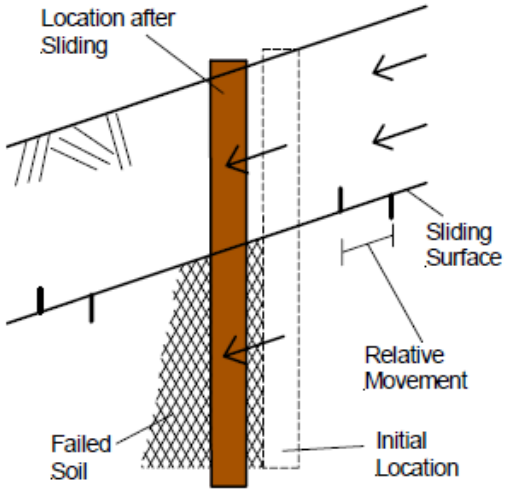


Figure 7.10 Schematic Diagram of Failure Mode-2 (Loehr and Bowders, 2007)

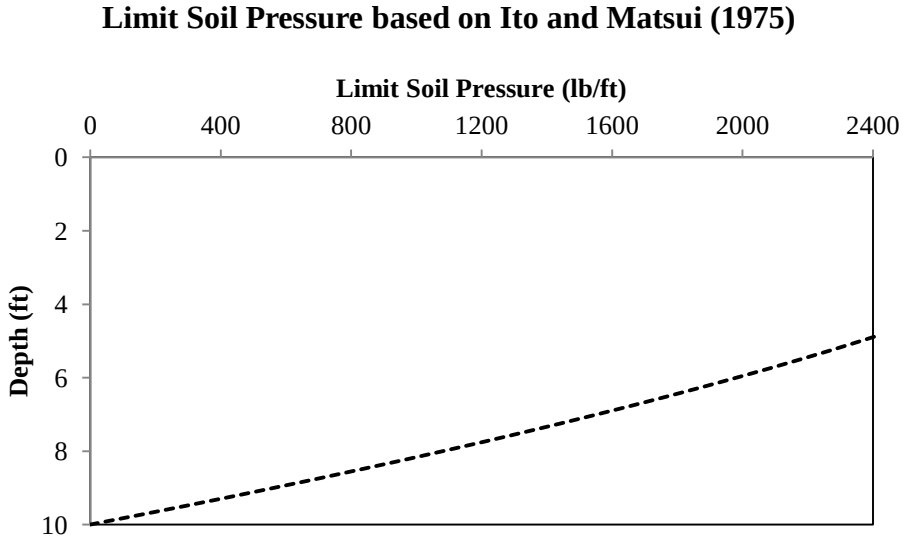


Figure 7.11 Limit Soil Resistance based on Failure Mode-2

Combining the two soil failure modes, a composite curve is developed by taking the least resistance of the two failure modes to produce the limit resistance along the length of the RPP, as presented in Figure 7.12. The limit resistance is suitable for cases where failure of the soil completely controls the resistance.

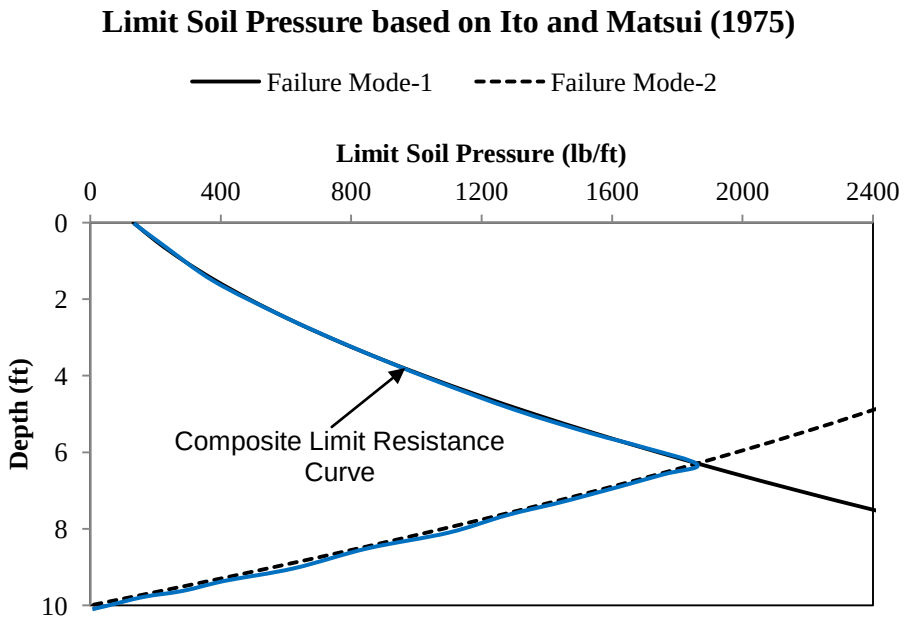


Figure 7.12 Composite limit resistance curve of Failure Modes 1 and 2

## 7.4 Limit Horizontal Displacement and Maximum Flexure of RPP

The elasto-plastic finite element method (FEM) is an accurate, robust and simple method. Previous studies indicated that the shear strength reduction finite element method had been successfully used to evaluate the stability and deformation of slopes reinforced with piles and anchors (Wei and Cheng, 2009; Yang et al., 2011, Cai and Ugai, 2003). This technique was utilized to evaluate the stability of slopes reinforced with piles or anchors under a general frame, where soil-structure interactions are considered, using zero thickness elasto plastic interface element. During this study, the finite element method was utilized to evaluate the resistance of RPP.

The objective of the current design approach was to develop a design chart to evaluate the load capacity of RPP based on limiting horizontal displacement and maximum flexural stress. A series of loads were applied over the RPP and the

corresponding horizontal displacement, as well as the maximum bending moment determined for each case. RPP is utilized to stabilize shallow slope failure. Loehr and Bowders, (2007) presented that the extent of shallow failures ranged between 3 ft. and 7 ft. deep for moderate to steep slopes where the geometry of slope varied between 2H:1V to 4H:1V. It is also important to consider the soil strength, which should cover a wide range for shallow slope failures. The current study considered wide range to failure depth, loading and slope ratio, as well as soil strength parameters, as presented in Table 7.3 and Table 7.4. The flow chart for the development of design chart is presented in Figure 7.13

Table 7.3 Consideration for the Development of Design Chart

| Slope Inclination | Depth of Slip Surface (ft) | Lateral Pressure on RPP ($lb/ft^2$) |
|---|---|---|
| 2H:1V, 3H:1V, 4H:1V | 3, 4, 5, 6, 7 | 10, 20, 30, 40, 50, 60, 70, 80, 90, 100, 200, 300, 400, 500 |

Table 7.4 Soil Parameters

| Cohesion (psf) | Friction Angle φ | | | |
|---|---|---|---|---|
| 100 | 0 | 10 | 20 | 30 |
| 200 | 0 | 10 | 20 | 30 |
| 300 | 0 | 10 | 20 | 30 |
| 400 | 0 | 10 | 20 | 30 |
| 500 | 0 | 10 | 20 | 30 |

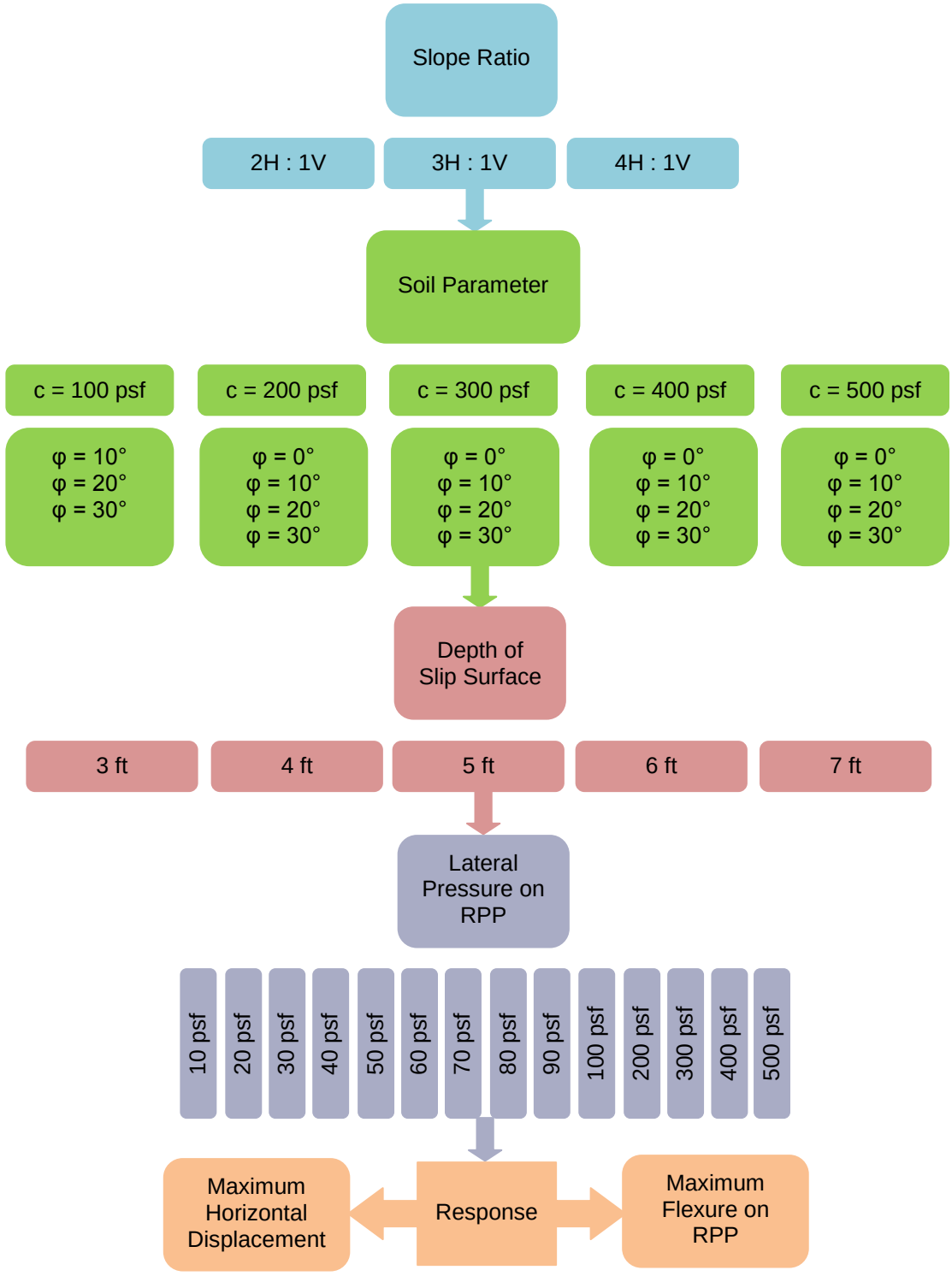


Figure 7.13 Flow Chart for development of design charts

The deformation analysis was performed using PLAXIS 2D. The RPP was considered as elastic material and modeled as plate element. The elastic perfectly plastic Mohr-Coulomb soil model was utilized for stability analyses, using 15 node triangular elements. The 15-node element provides a fourth order interpolation for displacements and numerical integration that involves twelve stress points. The 15-node triangle is a very accurate element and has produced high quality stress results for different problems (Plaxis Reference Manual, 2011). Standard fixities were applied as boundary condition where the two vertical boundaries were free to move vertically and were considered fixed in the horizontal direction. The bottom boundary was modeled as fixed boundary.

The FEM analysis was performed using the soil model as presented in Figure 7.14. It should be noted that two layers of soil were considered in the soil model. During the current analysis, the depth of the slipping surface varied between 3 ft. and 7 ft., with different slope rations 2H:1V to 4H:1V. The top layer above the slipping surface was considered as soft soil. On the other hand, the bottom layer was considered stiff foundation soil. The analysis was conducted with different soil strengths at the top soil, as presented earlier in Table 7.4. The deformation analysis was conducted by applying uniform load over the RPP throughout the sliding depth and the corresponding maximum horizontal deformation and the maximum bending moment was determined, as presented in Figure 7.15. Based on the applied load, the total resistance of RPP with corresponding horizontal deformation and maximum flexure stress is summarized for a given soil strength (for example cohesion c = 200 psf and friction angle $\phi$ =10˚, detail parameters for FEM analysis are presented in Table 7.5), with varied depth of slip surface, as presented in Figure 7.16.

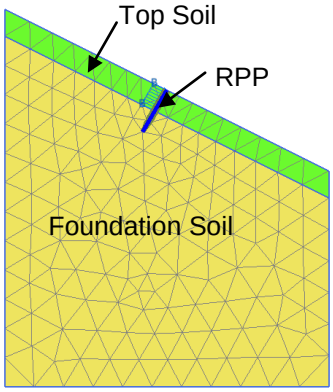


(a)

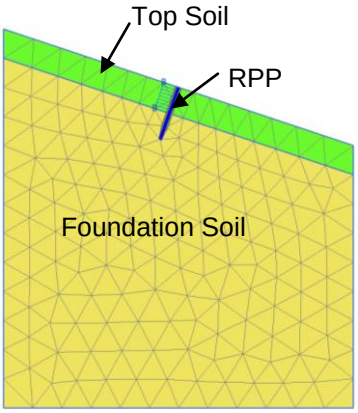


(b)

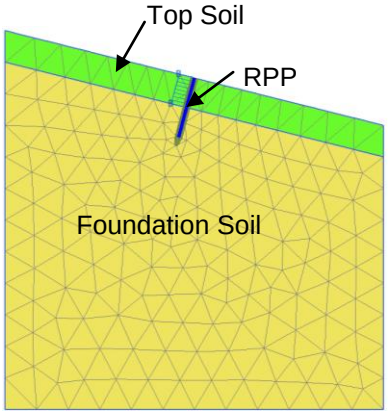


(c)

Figure 7.14 Soil Model for determination of horizontal displacment with applied load, a. Slope Ratio 2H:1V, b. Slope Ratio 3H:1V, c. Slope Ratio 4H:1V

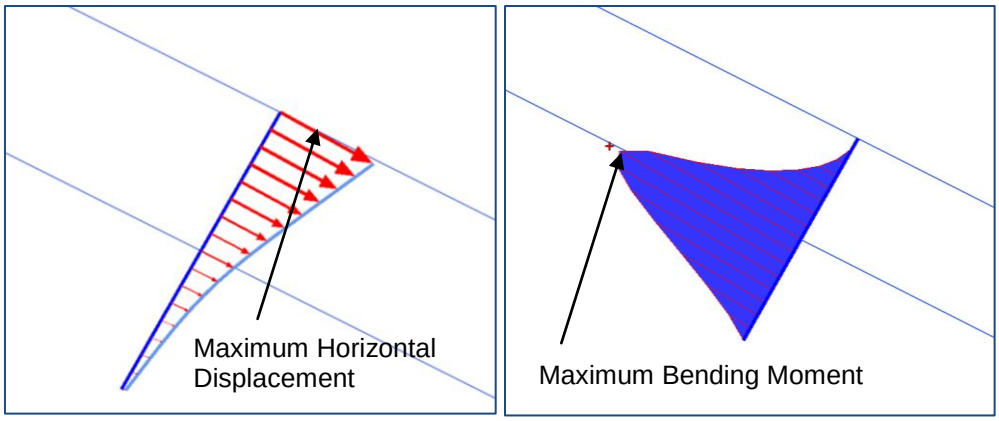


(a) (b)

Figure 7.15 Determination of Response of RPP due to Applied Load, a. Maximum Horizontal Displacement, b. Maximum Bending Moment

Table 7.5 Parameters from FE analysis

| Soil Type | Friction angle φ | Cohesion c | Unit Weight γ | Elastic Modulus E | Poisson Ratio v | RPP properties | Unit | Parameters |
|---|---|---|---|---|---|---|---|---|
| - | ◦ | psf | pcf | psf | - | | | |
| Top Soil | 10 | 200 | 125 | 2025 | 0.35 | EA | lb/ft | 857500 |
| | | | | | | EI | $lbft^2/ft$ | 255300 |
| Foundation Soil | 30 | 500 | 125 | 37140 | 0.30 | d | ft | 1.89 |
| | | | | | | w | lb/ft/ft | 4.4 |

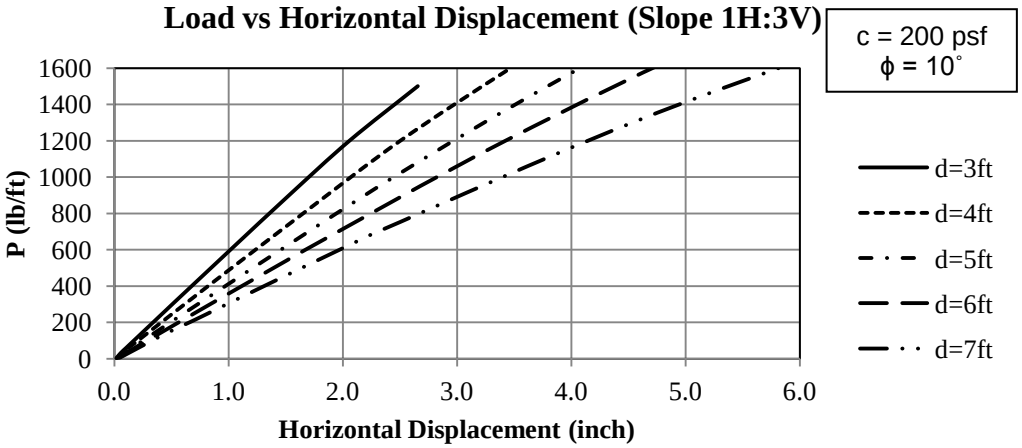


(a)

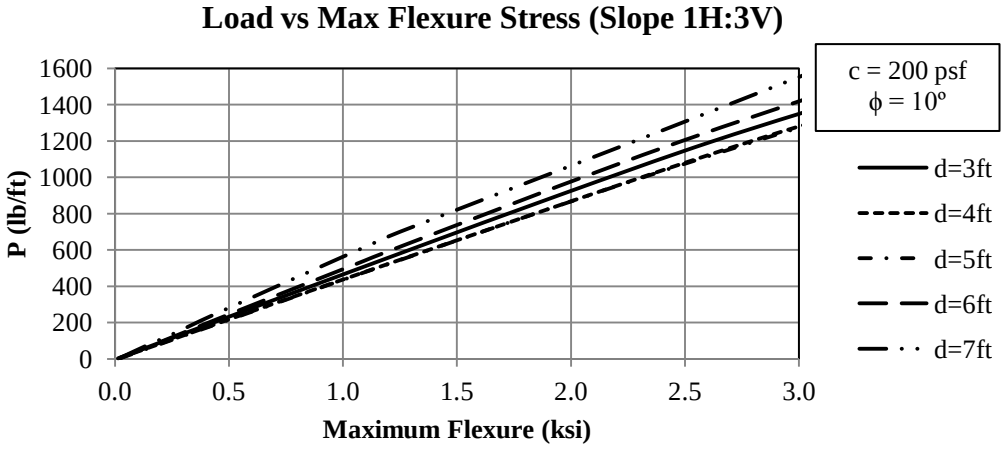


(b)

Figure 7.16 Limit Resistance Curve for RPP for c = 200 psf and ϕ = 10˚, a. Load vs Horizontal Displacement for Slope 3H:1V, b. Load vs Maximum Flexure for Slope 3H:1V

## 7.5 Finalizing Design Chart

The study was further continued and a series of design charts (Limit soil failure, limit horizontal displacement and limit maximum flexure), were developed, based on different soil strength parameters. The design charts are attached in Appendix B.

## 7.6 Calculation of Factor of Safety

The developed design chart for limit resistance of RPP can be utilized in most of the commercial slope stability analysis software to determine the factor of safety of the reinforced slope where the resistance of RPP can be applied as a pile resistance. Moreover, the design chart can be utilized and slope stability analysis can be performed using hand calculation. During this study, two different approaches to perform the hand calculation, which included the conventional method of slices and infinite slope approach, is presented.

### *7.6.1 Approach 1: Conventional Method of Slices*

The conventional method of slices is also known as the ordinary method of slices which can be explained using the Figure 7.17, where arc AC is a trial failure surface, centering at point O. The soil above the trial surface is divided into several vertical slices. Considering a unit length perpendicular cross section below, the active forces that act on a typical slice are also presented in Figure 7.17, where W is weight of the n th slice. The force N and T, respectively are the normal and tangential components of the reaction R. Pn and Pn+1 are the normal forces that act on the side of the slice. Similarly, the shearing forces that act on the sides are Tn and Tn+1. During the method of slices, the pore pressure is considered as zero. Moreover, an approximate assumption is made where the Pn and Tn are equal in magnitude to the resultants of Pn+1 and Tn+1 and that their line of action coincide.

For Equilibrium condition,

$$N = WCos\alpha \tag{7.4}$$

And the resisting shear force,

$$T = \tau_d * b = \frac{\tau_f * \Delta L}{FS} = \frac{1}{FS}\,(c' + \sigma' \tan\varphi') * \Delta L \tag{7.5}$$

The normal stress, σ' can be determined as,

$$\sigma' = \frac{N}{\Delta L} = \frac{WCos\alpha}{\Delta L} \tag{7.6}$$

For equilibrium of the trial wedge, ABC, the moment of the driving force about the center point O equals to the moment of the resisting force about O, as presented below.

$$\sum_{n=1}^{n=p} W * r * Sin\alpha = \sum_{n=1}^{n=p} \frac{1}{FS}\left(c' + \frac{WCos\alpha}{\Delta L}\tan\varphi'\right) * \Delta L * r \tag{7.7}$$

Therefore, the factor of safety (FS) of the unreinforced slope can be determined as,

$$FS = \frac{\sum_{n=1}^{n=p} (c'\Delta L + WCos\alpha \tan\varphi')}{\sum_{n=1}^{n=p} W * r * Sin\alpha} \tag{7.8}$$

On the other hand, for reinforced slope, RPP provided an additional resistance, P, along the slipping plane and increase the resisting force, as presented in Figure 7.18. Therefore, for the reinforced slope,

$$T = \tau_d * b = \frac{\tau_f * \Delta L}{FS} = \frac{1}{FS}\left[\left(c' + \frac{WCos\alpha}{\Delta L}\tan\varphi'\right) * \Delta L + P\ \right] \tag{7.9}$$

For equilibrium of the trial wedge, ABC, the moment of the driving force about the center point O equals to the moment of the resisting force about O, as presented below.

$$\sum_{n=1}^{n=p} W * r * Sin\alpha = \frac{1}{FS}\left[\sum_{n=1}^{n=p}\left(c' + \frac{WCos\alpha}{\Delta L}\tan\varphi'\right) * \Delta L * r + \sum_{n=1}^{n=q} P * r\right] \tag{7.10}$$

And, the factor of safety of the reinforced slope can be determined as,

$$FS = \frac{\sum_{n=1}^{n=p}\left(c'\Delta L + \frac{WCos\alpha}{\Delta L}\tan\varphi'\right) + \sum_{n=1}^{n=q} P}{\sum_{n=1}^{n=p} W * r * Sin\alpha} \tag{7.11}$$

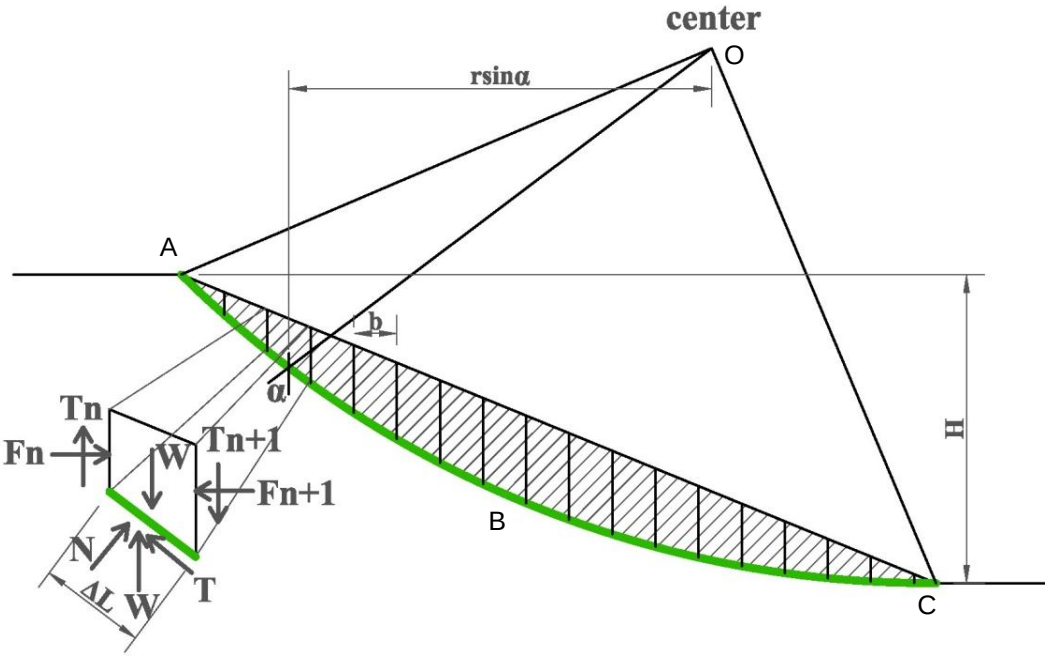


Figure 7.17 Schematic of ordinary method of slice

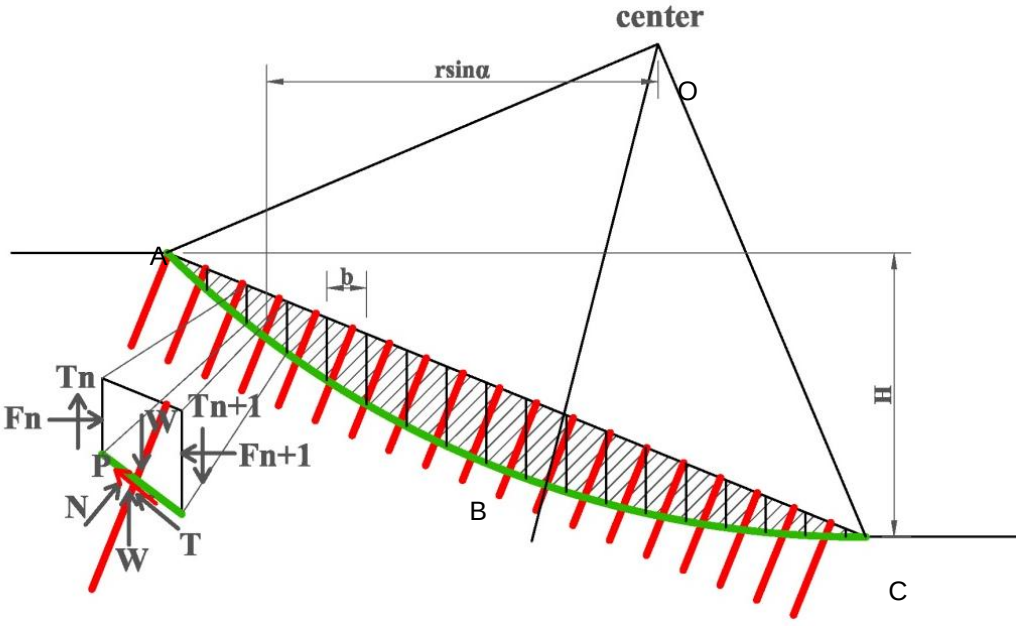


Figure 7.18 Schematic of Reinforced Slope using Ordinary Method of Slice

The composite limit resistance curve can be utilized to determine the design chart of RPP (P) as presented in Appendix B.

7.6.1.1 Design Steps for Approach 1

To design a slope using RPP, any commercial available slope stability analysis program, such as GSTABLE, UTEXAS or GEO-SLOPE, can be utilized to determine the critical slip surface with minimum factor of safety. Once the critical slip surface is obtained, the reinforcement design can be performed with the following steps:

- The failure surface of the slope should be divided into small segments of slides according to conventional method of slice approach.
- A spacing of RPP should be considered and plotted along the critical slip surface.
- Based on the plot of RPP, the depth of the critical slip surface (d) that it crossed the individual RPP can be determined.
- Using the depth of critical slip surface d, the limit resistance of individual RPP 'P' should be determined from the design charts attached in Appendix B. The design chart should be utilized to determine the lowest resistance based on the limit soil resistance, limit horizontal displacement and maximum flexure criteria, considering the soil parameters and structural parameters of RPP.
- Finally, the Factor of Safety of reinforced slopes can be determined using Equation 7.11.
- If the factor of safety of reinforced slopes is lower than the target factor of safety, it is suggested to reduce the spacing of RPP to increase the factor of safety of the reinforced slope.

*7.6.2 Approach 2: Infinite Slope*

The factor of safety of the surficial failure can also be conducted using the infinite slope approach, with seepage parallel to the slope face. The schematic of infinite slope failure for c-ϕ soil with parallel seepage is presented in Figure 7.19.

Let's consider that seepage through the soil and water level coincides with the ground surface. The shear strength of the surface is given by,

$$\tau = c' + \sigma' \tan \varphi' \quad (7.12)$$

Considering the slope element ABCD, the forces that act on the vertical faces AB and CD are equal and opposite. The total weight of the slope element of unit length is

$$W = \gamma_{sat} * L * h \quad (7.13)$$

Where, $\gamma_{sat}$ is the saturated unit weight of soil.

The components of W in the direction of normal and parallel to plane AB are,

$$N_a = N_r = WCos\beta = \gamma_{sat} * L * h * Cos\beta \quad (7.14)$$

And

$$T_a = T_r = WCos\beta = \gamma_{sat} * L * h * Cos\beta \quad (7.15)$$

The total stress and the shear stress at the base of the element are,

$$\sigma = \frac{N_r}{\left(\frac{L}{Cos\ \beta}\right)} = \gamma_{sat} * h * Cos^2\beta \quad (7.16)$$

And,

$$\tau = \frac{T_r}{\left(\frac{L}{Cos\ \beta}\right)} = \gamma_{sat} * h * Cos\beta * Sin\beta \quad (7.17)$$

The resistive shear stress developed at the base of the element for unreinforced slope is,

$$\tau_d = c'_d + \sigma' \tan \varphi'_d \quad (7.18)$$

$$\tau_d = c'_d + (\sigma - u) \tan \varphi'_d \quad (7.19)$$

Where,

$$u = \gamma_w * hcos^2\beta \quad (7.20)$$

Therefore, combining Equation 7.16, 7.19 and 7.20,

$$\tau_d = c'_d + (\gamma_{sat} * h * Cos^2\beta - \gamma_w * hcos^2\beta\ ) \tan \varphi'_d \quad (7.21)$$

$$\tau_d = c'_d + \gamma' * h * Cos^2\beta \tan \varphi'_d \quad (7.22)$$

Considering, $c'_d = \frac{c'}{FS}\ and,\ \tan \varphi'_d = \frac{\tan \varphi}{FS}$ and combing Equation 7.22 with Equation 7.17

$$FS = \frac{c' + h\,\gamma' cos^2\beta * tan\varphi'}{\gamma_{sat} * h * sin\beta * cos\beta} \quad (7.23)$$

For reinforced slope, RPP provided additional resistance P, as presented in Figure 7.19, along the base and increase the shear resistance as follows

$$\tau_d = c'_d + \gamma' * h * Cos^2\beta \tan \varphi'_d + P/L \quad (7.24)$$

Therefore, for reinforced Slope, combining equation 7.24 with equation 7.17, the factor of safety can be determined as,

$$FS = \frac{c'L + hL\,\gamma' cos^2\beta * tan\varphi' + \left(\frac{L}{S} + 1\right) * P}{\gamma_{sat} * hL * sin\beta * cos\beta} \quad (7.25)$$

Where,

L = Length (parallel to slope face)

S = RPP spacing

P = Limit resistance of RPP

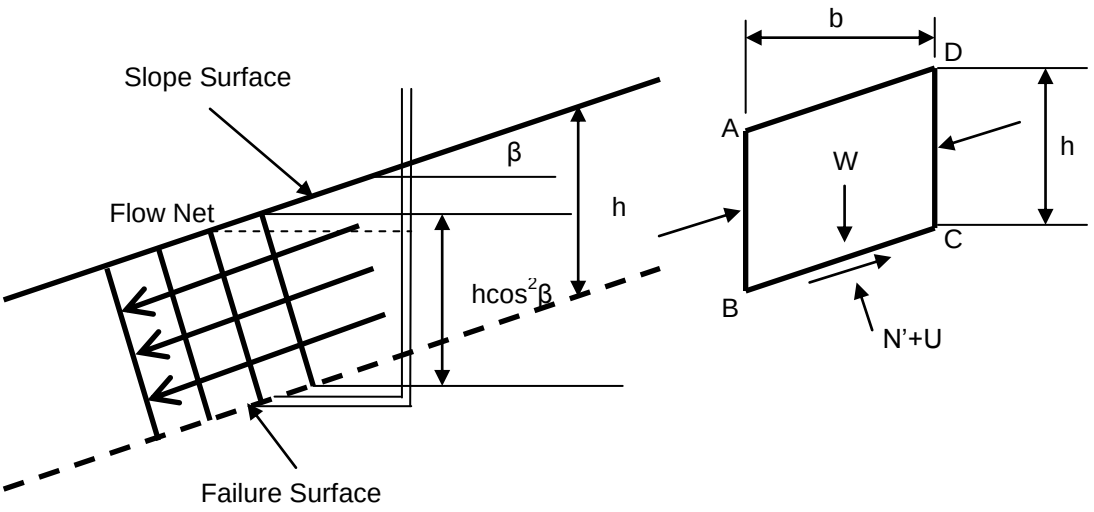


(a)

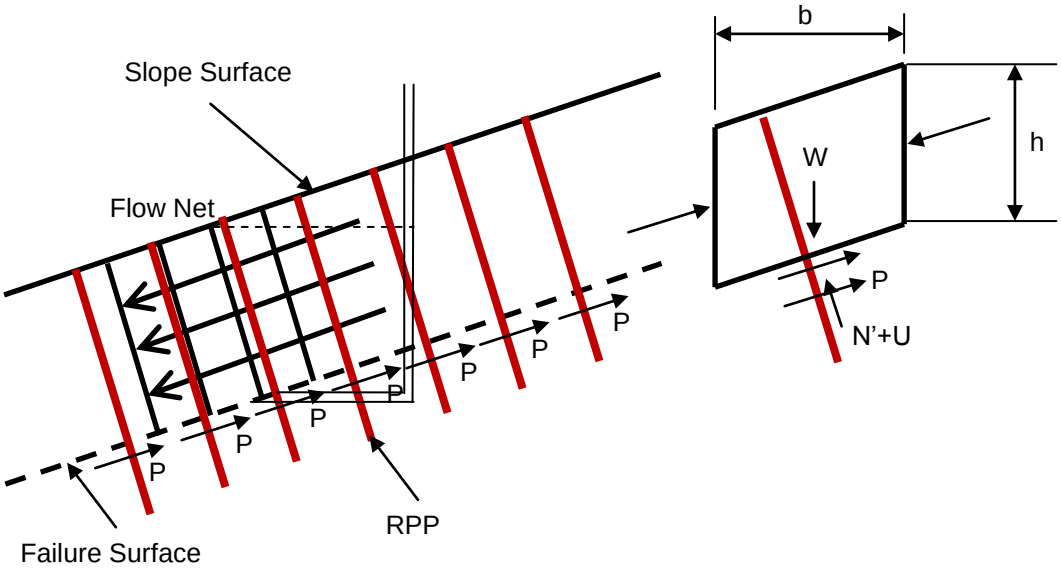


(b)

Figure 7.19 Schematic of Infinite Slope approach, a. Unreinforced Slope, b. Reinforced Slope

7.6.2.1 Design Steps for Approach 2

The Infinite slope is the simplest approach to determine the factor of safety of both the unreinforced and reinforced slope and can be performed using a simple excel spreadsheet. The design can be performed with the following steps:

- The factor of safety of the unreinforced slope should be determined using the soil parameters and depth of surficial failure. If no data is available on the depth of surficial failure, it is suggested to use maximum failure depth of 7 ft.
- Using the depth of failure, the limit resistance 'P' should be determined from the design chart attached in Appendix B. The design chart should be utilized to determine lowest resistance based on the limit soil resistance, limit horizontal displacement and maximum flexure criteria considering the soil parameters and structural parameters of RPP.
- A spacing of RPP should be considered.
- Finally, the factor of safety of reinforced slope can be determined using Equation 7.25.
- If the factor of safety of reinforced slope is lower than the target factor of safety, it is suggested to reduce the spacing of RPP to increase the factor of safety of the reinforced slope.

## 7.7 Validation

A total of 3 slopes, designated as Slope 1, Slope 2 and Slope 3, were utilized to determine the factor of safety of the reinforced slope, using the current design approach. The slopes were considered identical in terms of the height of the slope and the soil properties; however, the inclination was considered different. The soil properties of the slope are presented in Table 7.6. Each of the slopes is divided into two layers: a soft soil

layer at the top of the slope and a stiff foundation layer at the bottom. The depth of the soft layer was considered as 7 ft.

*7.7.1 Unreinforced Slope*

The factor of safety of the unreinforced slope was determined using 3 different approaches, a. Numerical Modeling, b. Method of slices and c. Infinite slope approach. Based on the slope stability analysis, the slip surface and factor of safety of the unreinforced slope is presented in Figure 7.20, Figure 7.21 and Table 7.7. The lowest factor of safety was observed from the infinite slope approach, followed by the FEM analysis and Method of Slices. It should be noted that the infinite slope approach considered the slip surface parallel to the slope face. A similar failure trend was observed in the FEM analysis (Figure 7.20). On the other hand, the circular slip surface was considered using the Ordinary method of slice method; however, the factor of safety was close compared to the other two methods. Each of the unreinforced slopes was considered for the design of the reinforced slope.

Table 7.6 Soil Properties and Geometry for Validation of Design Method

| Slope Type | Slope Height ft | Slope Inclination | Top Soil | | | Foundation Soil | | |
|---|---|---|---|---|---|---|---|---|
| | | | c psf | φ deg | ϒ pcf | c psf | φ deg | ϒ pcf |
| Slope 1 | 40 | 2H:1V | 250 | 10 | 125 | 300 | 20 | 125 |
| Slope 2 | 40 | 3H:1V | 250 | 10 | 125 | 400 | 10 | 125 |
| Slope 3 | 40 | 4H:1V | 250 | 10 | 125 | 400 | 10 | 125 |

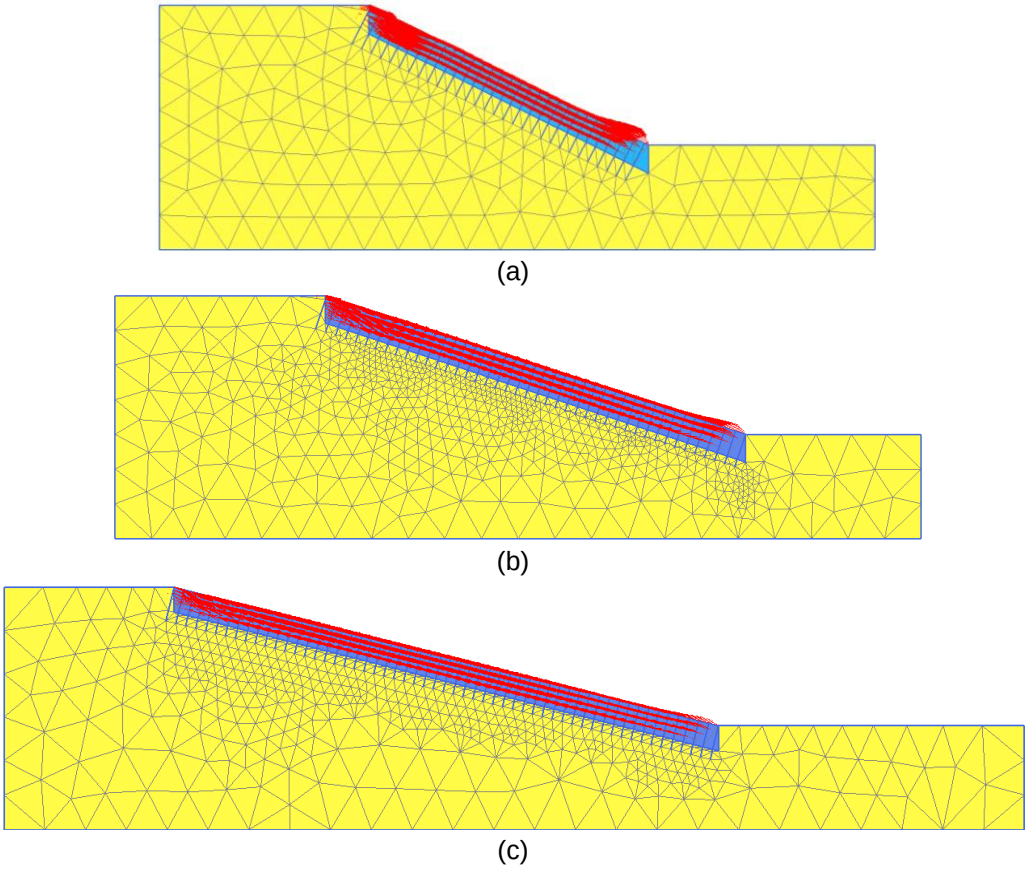

(a)

(b)

(c)

Figure 7.20 Failure Surface of Unreinforced Slope using FEM Analysis, a. Slope 1, b. Slope 2 and c. Slope 3.

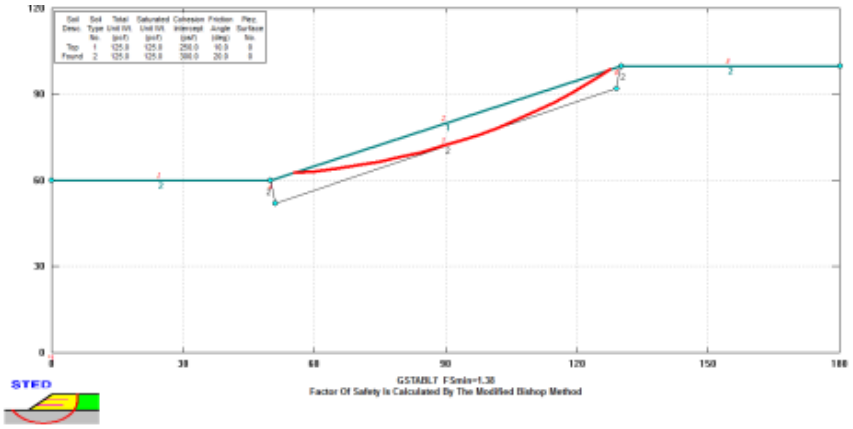


(a)

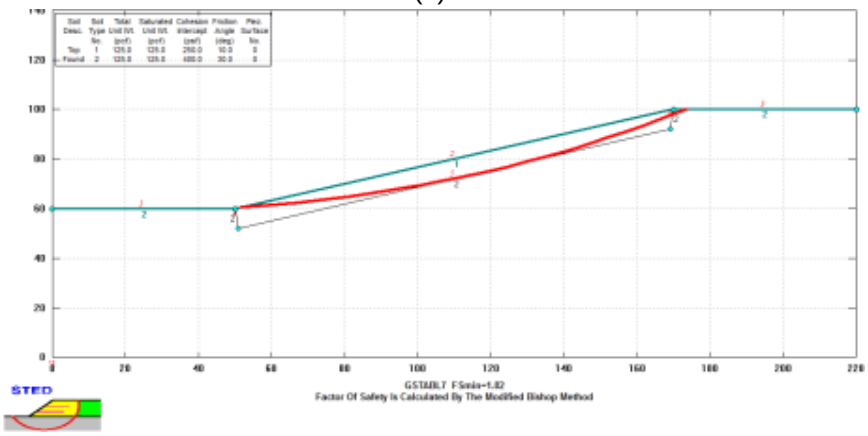


(b)

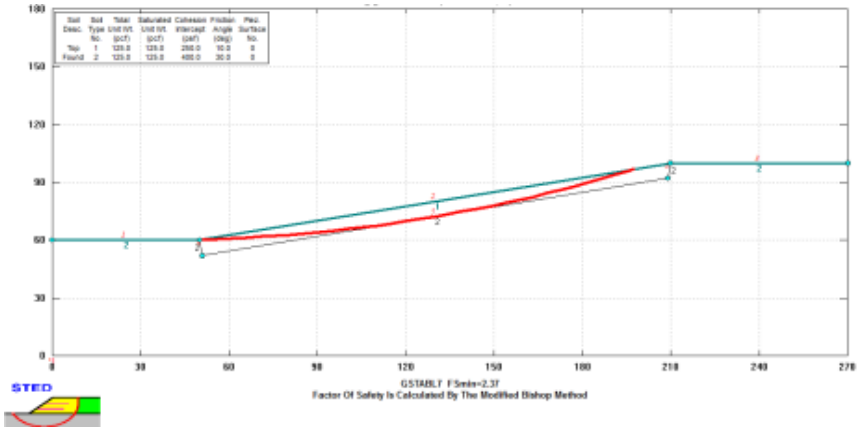


(c)

Figure 7.21 Failure Surface of Unreinforced Slope using Modified Bishop Method, a. Slope 1, b. Slope 2 and c. Slope 3.

Table 7.7 Factor of Safety of Unreinforced Slope using Different Methods

| Slope Type | FEM Analysis | Method of Slice | Infinite Slope |
|---|---|---|---|
| Slope 1 | 1.23 | 1.2 | 1 |
| Slope 2 | 1.66 | 1.69 | 1.45 |
| Slope 3 | 2.21 | 2.12 | 1.88 |

*7.7.2 Reinforced Slope*

The factor of safety of the reinforced slope was determined using three different approaches, a. Finite Element analysis, b. Ordinary Method of Slice and c. Infinite Slope Approach with RPP spacing of 3 ft c/c. At the beginning, the factor of safety of the slope for the reinforced slope was determined using the FEM analysis in Plaxis. Later, the factor of safety from the FEM analysis is compared with the other methods. The failure surface of the reinforced slope in Plaxis is presented in Figure 7.22.

The factor of safety for the method of slice and infinite slope approach was determined based on the limit resistance of RPP determined from Appendix B. It is important for a designer to select maximum horizontal displacement value and failure depth for the selection of limit resistance curve. Based on the field study conducted by Loehr and Boweders (2007), it was suggested that the maximum allowable horizontal displacement is 3 inches. During the current study, the limit resistance of RPP was determined using 1 inch and 2 inch horizontal displacement. Moreover, the allowable flexure is considered as the 35% of its maximum capacity which is 1.4 ksi. The depth of slipping surface was considered as 7 ft. The average limit resistances of RPP for different slopes are presented in Table 7.8. The limit resistances of RPP were utilized to calculate the factor of safety of the reinforced slopes and are summarized in Table 7.9 and Table

7.10. A sample detail analysis to calculate the factor of safety of the reinforced slope is attached in Appendix C.

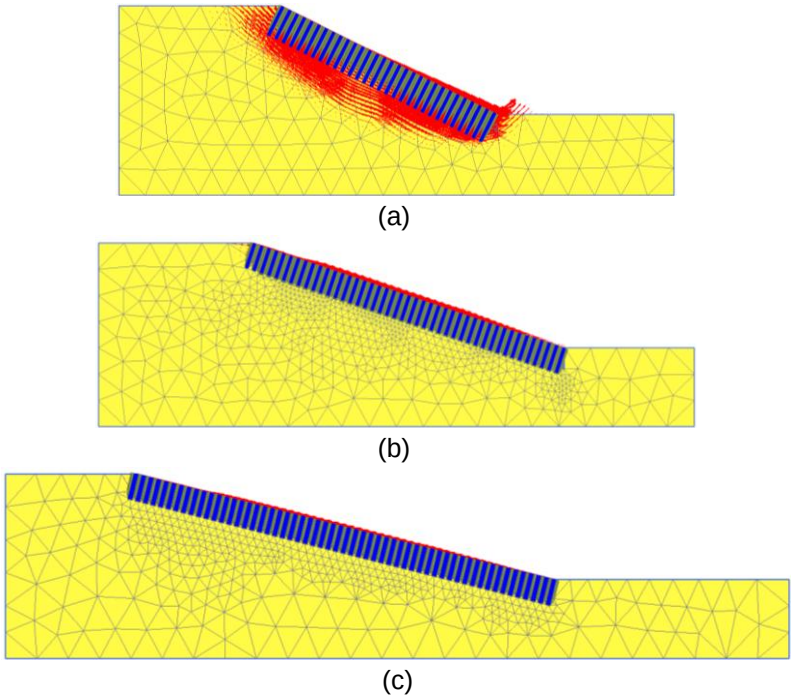


Figure 7.22 Failure Surface of Unreinforced Slope using Modified Bishop Method, a. Slope 1, b. Slope 2 and c. Slope 3.

Table 7.8 Limit Resistance of RPP

| Slope Type | Slope Inclination | Soil Parameters | | | RPP Properties Flexure | Allowable RPP Properties for Flexure | Average Limit Resistance | |
|---|---|---|---|---|---|---|---|---|
| | | c | φ | ϒ | | | 1” dis. | 2” dis. |
| | | psf | deg | pcf | ksi | ksi | Lb/ft | Lb/ft |
| Slope 1 | 2H:1V | 250 | 10 | 125 | 4 | 1.4 | 350 | 560 |
| Slope 2 | 3H:1V | 250 | 10 | 125 | 4 | 1.4 | 360 | 540 |
| Slope 3 | 4H:1V | 250 | 10 | 125 | 4 | 1.4 | 330 | 525 |

Table 7.9 Factor of Safety of Unreinforced and Reinforced Slope for Allowed Horizontal Displacement 1 inch

| Slope Type | PLAXIS | | Method of Slice | | Infinite Slope | |
|---|---|---|---|---|---|---|
| | Unreinforced Slope | Reinforced Slope | Unreinforced Slope | Reinforced Slope | Unreinforced Slope | Reinforced Slope |
| Slope 1 | 1.23 | 1.55 | 1.2 | 1.58 | 1 | 1.27 |
| Slope 2 | 1.66 | 2.27 | 1.69 | 2.24 | 1.45 | 1.86 |
| Slope 3 | 2.21 | 3.14 | 2.12 | 2.72 | 1.88 | 2.44 |

Table 7.10 Factor of Safety of Unreinforced and Reinforced Slope for Allowed Horizontal Displacement 2 inch

| Slope Type | PLAXIS | | Method of Slice | | Infinite Slope | |
|---|---|---|---|---|---|---|
| | Unreinforced Slope | Reinforced Slope | Unreinforced Slope | Reinforced Slope | Unreinforced Slope | Reinforced Slope |
| Slope 1 | 1.23 | 1.55 | 1.2 | 1.88 | 1 | 1.52 |
| Slope 2 | 1.66 | 2.27 | 1.69 | 2.55 | 1.45 | 2.35 |
| Slope 3 | 2.21 | 3.14 | 2.12 | 3.14 | 1.88 | 3.05 |

Based on Table 7.9 and Table 7.10, the factor of safety of the reinforced slope calculated using the ordinary method of slices was in good agreement with the calculated factor of safety using the FEM analysis. However, the calculated factor of safety was lower using infinite slope approach as the initial factor of safety was lower. Moreover, during the infinite slope approach, the limit resistance of RPP was determined using the depth of failure surface equals to 7 ft, which resulted in very low resistance from RPP and low factor of safety. On the other hand, during the ordinary method of slice, the failure depth varied within different slices and resulted in higher resistance from RPP (failure depth ranged between 3 ft and 6 ft) at the crest and toe of the slope with the failure depth

of 7 ft. at the middle of the slope. Therefore, the total resistance from RPP is higher using the ordinary method of slices and resulted in higher factor of safety.

The factor of safety of the reinforced slope using 2 inch allowable horizontal displacement result in higher factor of safety compared to the limit resistance of RPP for 1 inch horizontal displacement. During the 2 inch horizontal displacement, the limit resistance of RPP is higher (Table 7.8) which consequence higher factor of safety. It should be noted that, the calculated factor of safety was in good agreement using the ordinary method of slice with FEM analysis, for allowable horizontal displacement of 1 inch with the slope ratio of 2H:1V and 3H:1V. On the other hand, the 2 inch horizontal displacement, the calculated factor of safety using the Ordinary method of slices was in good agreement with FEM analysis for gentle slopes with slope ratio of 4H: 1V.

Finally, the infinite slope approach presented the lowest factor of safety and resulted in conservative design. It is recommended to use the infinite slope approach, limiting horizontal displacement equal to 1 inch.

## 7.8 Limitation of the Design Method

The current study presented the design chart based on the interaction of RPP with the top soil, foundation soil due to the applied loading. However the design charts underestimate the resistance of RPP when it is installed in group. It should be noted that the current study considered the capacity of single RPP. However, in actual case the RPP should be installed in group which will have higher lateral resistance resulting higher factor of safety. It is suggested to consider future study to incorporate the lateral resistance due to the group effect of RPP into the design method.

# Chapter 8

# Conclusions and Recommendations

## 8.1 Summary and Conclusion

The current study summarized the remediation of shallow slope failure using recycled plastic pin. Two highway slopes located over US 287 near the St. Paul overpass in Midlothian, and over Loop 12, near the UP RP rail overpass in Dallas, Texas were stabilized using RPP. Three 15.25 m (50 ft.) sections were selected and reinforced using RPP after a crack, caused by slope movement, was observed over the shoulder in the US 287 slope. On the other hand, two 15.25 m (50 ft) control sections were placed between the reinforced sections to compare the performances of the slope. Moreover, a total of 50 ft. sections over top slope and 100 ft. sections at the bottom slope at Loop 12 were reinforced with RPP as a temporary solution. The field performance of the slope was monitored, using instrumented RPPs, inclinometers and surveying.

The site investigation results indicated that the slopes were constructed by using high plastic clay, which is susceptible to shrinkage and swelling behavior. The presence of shoulder cracks at US 287 slope works as potential passage of rain water intrusion. During rainfall, water might get into the slope through the crack, which would eventually lead to saturation of soils near the crest of the slope and subsequent reduction in shear strength. To resist any further failure of the slope, it was essential to take remedial measures of the US 287 slope. On the other hand, during and after rainfall, the soil at the top slope of Loop 12 became saturated due to moisture intrusion and created a perched water zone due to low permeability of the high plastic clay. The presence of the perched water zone resulted increased lateral pressure and failure of the Loop 12 slope.

The field installation program revealed that a crawler-mounted rig, equipped with a mast-mounted pseudo vibratory hammer, worked effectively to install RPPs. The

driving rate of RPP depends on the length and spacing of RPP, stiffness of soil and efficiency of the installation team. The observed overall driving rate, considering all the reinforced sections at the US 287 slope was, 2.66 ft./min, which represented that on average, a single RPP can be installed within 4 minutes, and a total of 100 to 120 RPPs can be installed in a single day.

The performance monitoring results of the US 287 slope indicated that the unreinforced control sections had significant settlement, (as much as 15 inches), at the crest of the slope. In addition, a total of 3 inch increments in settlement had taken place during the year. In contrast, almost no increment in settlement was observed at the reinforced section in US 287 slopes. Moreover, the total settlement in the reinforced section was negligible compared to the unreinforced section. The instrumented RPP and inclinometer result indicated less horizontal displacement in Reinforced Section 1 compared to Reinforced Section 2 and Reinforced Section 3. Less settlement at the Reinforced Section 1 had taken place due to the lower spacing at the crest.

The comparison of horizontal displacement of the Reinforced Section 1 and Reinforced Section 2 with the variation of the rainfall, moisture content and matric suction results indicated that, RPP provided enough anchorage during the wet period when the shear strength of soil was low due to low matric suction. However, the movement of the reinforced slope had taken place during dry season due to the presence of desiccation cracks which resulted in lack of support condition for RPP. The horizontal displacement was 1.5 inch which had taken place during the 1$^{st}$ year after construction; however, it became less than 0.1 inch after 1$^{st}$ year. It should be noted that the horizontal displacement had taken place due to the load mobilization at the presence of desiccation cracks during the 1$^{st}$ year.

The performance monitoring results of Loop 12 presented that the top of the retaining wall is still moving after the installation of RPP. However, RPP installed adjacent to the footing provided lateral resistance and restricted the sliding of the wall. The maximum resistance was observed with higher RPP spacing. It should be noted that the RPP was placed at the slope to provide temporary support with a design period of 1-2 years. Although, the horizontal displacement of the retaining wall had taken place during the performance period, the RPP resisted the overall failure of the slope.

The cost of slope stabilization using RPP depends on several factors such as the site conditions, site accessibility, the cost for site preparation, cost of the materials, mobilization and installation cost. However, on average, the slope stabilization cost using RPP ranged between 4.8 USD/sft. On the other hand, the cost of different retaining structures and conventional stabilization technique vary between 35 and 80 USD/sft. Therefore, the cost of slope stabilization using RPP is around 50% to 80% less expensive compared to the cost of slope stabilization using other conventional techniques.

The performance of the control section of US 287 slope was calibrated in Plaxis, and further deformation analysis was performed for the reinforced sections. The FEM analysis results were in good agreement with the field performance of reinforced section 1. On the other hand, the FEM analysis indicated less settlement compared to the actual field settlement in Reinforced Section 2. The deformation analysis presented that only 16% of load transfer had taken place compared to the ultimate capacity of RPP.

The calibrated FEM model was further utilized and a parametric study was performed to investigate the effect of spacing and length of RPP on the factor of safety and deformation of slope. The parametric study indicated that the factor of safety of slope remained constant up to RPP spacing of 5 ft. c/c and then increased with further increment in RPP spacing. On the other hand, deformation of slope is low at closer RPP

spacing and deformation increase with higher RPP spacing. Moreover, a further study to evaluate the effect of closer RPP spacing at crest presented that, with closer RPP spacing near the crest and wider RPP spacing at the rest of slope perform better compared to the slope reinforced with uniform spacing at the entire portion.

The field performance of the slope was further utilized to develop a performance-based design method for slope stabilization, using RPP. A design chart was developed using 3 different limiting criteria (limit soil failure, limit horizontal displacement of RPP and limit maximum flexure) to determine the limit resistance of RPP. The limit resistance of RPP can be utilized to determine the factor of safety of reinforced slopes, using any commercially available slope stability software, as well as the infinite slope approach. The comparison between the design approaches presented that the infinite slope approach had the lowest factor of safety and resulted in conservative design. It is recommended to use the infinite slope approach, using limiting horizontal displacement equal to 1 inches.

## 8.2 Recommendation for Future Studies

Based on the current study, the following recommendations are proposed for future studies:

- The study presented the field demonstration study of few sections. However, no large scale studies on the actual slope stabilization were performed. It is recommended to perform a study on the actual slope remediation using RPP at larger scale.
- The performance results included in the current study were based on the short term monitoring period. However, the study should be continued to evaluate the long term performance of the stabilized slope.
- During the study, only the rectangular RPP sections were utilized. However, different RPP sections are commercially available such as in circular and in H-

pile form. A study using different RPP cross sections (different shape) can be performed to determine the useful sections for slope stabilization.

- During this study, the 2D numerical modeling was performed using Plaxis. However, the 2D numerical analysis cannot explain the crack propagation between the control section and control section 2 through the Reinforced Section 2, which resulted in higher deformation of the reinforced section. On the other hand, the 3D deformation analysis has the capability to consider the lateral extent of cracks and can be utilized to explain the additional deformation of the Reinforced Section 2 compared to the other reinforced sections. Therefore, it is suggested to conduct the 3D numerical analysis of the control slopes as well as the reinforced sections.
- During the current study, a design method was developed for the slope stabilization using RPP. The design method was developed based on the field performance results at the US 287 slope. It is suggested to evaluate the design method based on the performance results obtained from other slope sites.
- The design method in this study was developed considering the resistance of a single RPP. However, the RPPs are installed in groups in the field. It is well understood that the lateral resistance of the RPP in group should be higher than single RPP. Therefore, a further study is recommended to develop a factor considering the group action.

Appendix A

Borehole Log: US 287 Slope

| Project: Slope Stabiliy Analysis<br>Project Location: US 287 (North), Mansfield, TX.<br>Project Number: | **Log of Boring BH-1**<br>Sheet 1 of 1 |
|---|---|

| | | | | | |
|---|---|---|---|---|---|
| Date(s) Drilled | 10/28/10 - 10/28/10 | Logged By | UTA | Checked By | UTA |
| Drilling Method | | Drill Bit Size/Type | | Total Depth of Borehole | 20.0 |
| Drill Rig Type Hollow stem | | Drilling Contractor | Alpha Testing, Inc. | Surface Elevation | |
| Groundwater Level(s) | | Sampling Method(s) | Shelby Tube | Hammer Data | |
| Borehole Backfill | Moisture Sensor installed at the bore hole. | Comments | | | |

| Elevation feet | Depth, feet | SAMPLES Type | SAMPLES Number | SAMPLES Sampling Resistance, Blows / 6 in. | SAMPLES SPT N-Value Blows/ ft. | SAMPLES Pocket Penetrometer, tsf | Graphic Log | MATERIAL DESCRIPTION | Water Content, % | ATTERBERG LIMITS Liquid Limit | ATTERBERG LIMITS Plastic Limit | ATTERBERG LIMITS Plasticity Index | REMARKS/ OTHER TESTS |
|---|---|---|---|---|---|---|---|---|---|---|---|---|---|
| | 0 | | | | | | | Gray, Medium Plastic Clay, Traces of Pebbles. | | | | | |
| | | | | | | | | Dark Brown, High Plastic Clay. | | | | | |
| | 5 | | | | | 1.5 | | | 22.2 | 48 | 23 | 25 | Texas Cone Penetrometer: 3(6) 3(6) |
| | | | | | | | | Tan, High Plastic Clay. | | | | | |
| | 10 | | | | | 1.75 | | Light Tan, High Plastic Clay. | 28.6 | 60 | 27 | 33 | Texas Cone Penetrometer: 5(6) 6(6) |
| | 15 | | | | | 1 | | | 32.6 | 72 | 24 | 48 | Texas Cone Penetrometer: 5(6) 3(6) |
| | 20 | | | | | 2.5 | | | 29.4 | 64 | 26 | 38 | Texas Cone Penetrometer: 8(6) 12(6) |
| | 25 | | | | | | | | | | | | |
| | 30 | | | | | | | | | | | | |

UTA

Figure A 1 Log of BH-1

| Project: Slope Stabiliy Analysis<br>Project Location: US 287 (North), Mansfield, TX.<br>Project Number: | **Log of Boring BH-2**<br>Sheet 1 of 1 |
|---|---|

| | | | | | |
|---|---|---|---|---|---|
| Date(s) Drilled | 10/28/10 - 10/28/10 | Logged By | UTA | Checked By | UTA |
| Drilling Method | | Drill Bit Size/Type | | Total Depth of Borehole | 25.0 |
| Drill Rig Type Hollow stem | | Drilling Contractor | Alpha Testing, Inc. | Surface Elevation | |
| Groundwater Level(s) | | Sampling Method(s) | Shelby Tube | Hammer Data | |
| Borehole Backfill | Cement Grout | Comments | | | |

| Elevation feet | Depth, feet | SAMPLES Type | SAMPLES Number | Sampling Resistance, Blows / 6 in. | SPT N-Value Blows/ ft. | Pocket Penetrometer, tsf | Graphic Log | MATERIAL DESCRIPTION | Water Content, % | ATTERBERG LIMITS Liquid Limit | ATTERBERG LIMITS Plastic Limit | ATTERBERG LIMITS Plasticity Index | REMARKS/ OTHER TESTS |
|---|---|---|---|---|---|---|---|---|---|---|---|---|---|
| | 0 | | | | | | | Gray, Medium Plastic Clay, Traces of Pebbles. | | | | | |
| | 5 | | | | | | | Dark Tan, High Plastic Clay. | 18.8 | 49 | 26 | 23 | Texas Cone Penetrometer: 3(6) 2(6) |
| | 10 | | | | | 1.75 | | | 34.0 | 67 | 29 | 38 | Texas Cone Penetrometer: 3(6) 3(6) |
| | 15 | | | | | 3.25 | | | 36.6 | 73 | 45 | 28 | Texas Cone Penetrometer: 5(6) 5(6) |
| | 20 | | | | | | | Dark Tan, High Plastic Clay. | 25.7 | 61 | 35 | 26 | Texas Cone Penetrometer: 6(6) 9(6) |
| | 25 | | | | | | | | 27.5 | 62 | 25 | 37 | Texas Cone Penetrometer: 10(6) 8(6) |
| | 30 | | | | | | | | | | | | |

UTA

Figure A2 Bore hole log for BH-2

| Project: Slope Stabiliy Analysis<br>Project Location: US 287 (North), Mansfield, TX.<br>Project Number: | **Log of Boring BH-3**<br>Sheet 1 of 1 |
|---|---|

| | | | | | |
|---|---|---|---|---|---|
| Date(s) Drilled | 10/28/10 - 10/28/10 | Logged By | UTA | Checked By | UTA |
| Drilling Method | | Drill Bit Size/Type | | Total Depth of Borehole | 25.0 |
| Drill Rig Type | Hollow stem | Drilling Contractor | Alpha Testing, Inc. | Surface Elevation | |
| Groundwater Level(s) | | Sampling Method(s) | Shelby Tube | Hammer Data | |
| Borehole Backfill | Cement Grout | Comments | | | |

| Elevation feet | Depth, feet | SAMPLES Type | SAMPLES Number | Sampling Resistance, Blows / 6 in. | SPT N-Value Blows/ ft. | Pocket Penetrometer, tsf | Graphic Log | MATERIAL DESCRIPTION | Water Content, % | ATTERBERG LIMITS Liquid Limit | ATTERBERG LIMITS Plastic Limit | ATTERBERG LIMITS Plasticity Index | REMARKS/ OTHER TESTS |
|---|---|---|---|---|---|---|---|---|---|---|---|---|---|
| | 0 | | | | | | | Gray, Medium Plastic Clay, Traces of Pebbles. | | | | | |
| | | | | | | | | Dark tan, High Plastic Clay. | 15.0 | | | | |
| | 5 | | | | | 2 | | | 20.2 | 52 | 25 | 27 | Texas Cone Penetrometer: 3(6) 4(6) |
| | | | | | | | | Tan, High Plastic Clay. | | | | | |
| | 10 | | | | | 1.5 | | | 29.9 | 61 | 27 | 34 | Texas Cone Penetrometer: 3(6) 3(6) |
| | | | | | | | | Dark Tan, High Plastic Clay. | | | | | |
| | 15 | | | | | 2 | | | 33.3 | 79 | 28 | 51 | Texas Cone Penetrometer: 4(6) 5(6) |
| | 20 | | | | | | | | 28.7 | 58 | 26 | 32 | Texas Cone Penetrometer: 7(6) 8(6) |
| | | | | | | | | Dark Brown, High Plastic Clay. | | | | | |
| | 25 | | | | | | | | 27.3 | 65 | 25 | 40 | Texas Cone Penetrometer: 7(6) 6(6) |
| | 30 | | | | | | | | | | | | |

UTA

Figure A3 Borehole Log for BH-3

# Appendix B

## Design Charts

List of Figures

| Figure No | c | φ | Slope Ratio |
|---|---|---|---|
| B1 | 100 | 10 | 1:3 |
| B2 | 100 | 10 | 1:4 |
| B3 | 100 | 20 | 1:2 |
| B4 | 100 | 20 | 1:3 |
| B5 | 100 | 20 | 1:4 |
| B6 | 100 | 30 | 1:2 |
| B7 | 100 | 30 | 1:3 |
| B8 | 100 | 30 | 1:4 |
| B9 | 200 | 0 | 1:2 |
| B10 | 200 | 0 | 1:3 |
| B11 | 200 | 0 | 1:4 |
| B12 | 200 | 10 | 1:2 |
| B13 | 200 | 10 | 1:3 |
| B14 | 200 | 10 | 1:4 |
| B15 | 200 | 20 | 1:2 |
| B16 | 200 | 20 | 1:3 |
| B17 | 200 | 20 | 1:4 |
| B18 | 200 | 30 | 1:2 |
| B19 | 200 | 30 | 1:3 |
| B20 | 200 | 30 | 1:4 |
| B21 | 300 | 0 | 1:2 |
| B22 | 300 | 0 | 1:3 |
| B23 | 300 | 0 | 1:4 |
| B24 | 300 | 10 | 1:2 |
| B25 | 300 | 10 | 1:3 |
| B26 | 300 | 10 | 1:4 |
| B27 | 300 | 20 | 1:2 |
| B28 | 300 | 20 | 1:3 |
| B29 | 300 | 20 | 1:4 |
| B30 | 300 | 30 | 1:2 |
| B31 | 300 | 30 | 1:3 |
| B32 | 300 | 30 | 1:4 |
| B33 | 400 | 0 | 1:2 |
| B34 | 400 | 0 | 1:3 |
| B35 | 400 | 0 | 1:4 |
| B36 | 400 | 10 | 1:2 |
| B37 | 400 | 10 | 1:3 |
| B38 | 400 | 10 | 1:4 |
| B39 | 400 | 20 | 1:2 |

| Figure No | c | φ | Slope Ratio |
|---|---|---|---|
| B40 | 400 | 20 | 1:3 |
| B41 | 400 | 20 | 1:4 |
| B42 | 400 | 30 | 1:2 |
| B43 | 400 | 30 | 1:3 |
| B44 | 400 | 30 | 1:4 |
| B45 | 500 | 0 | 1:2 |
| B46 | 500 | 0 | 1:3 |
| B47 | 500 | 0 | 1:4 |
| B48 | 500 | 10 | 1:2 |
| B49 | 500 | 10 | 1:3 |
| B50 | 500 | 10 | 1:4 |
| B51 | 500 | 20 | 1:2 |
| B52 | 500 | 20 | 1:3 |
| B53 | 500 | 20 | 1:4 |
| B54 | 500 | 30 | 1:2 |
| B55 | 500 | 30 | 1:3 |
| B56 | 500 | 30 | 1:4 |

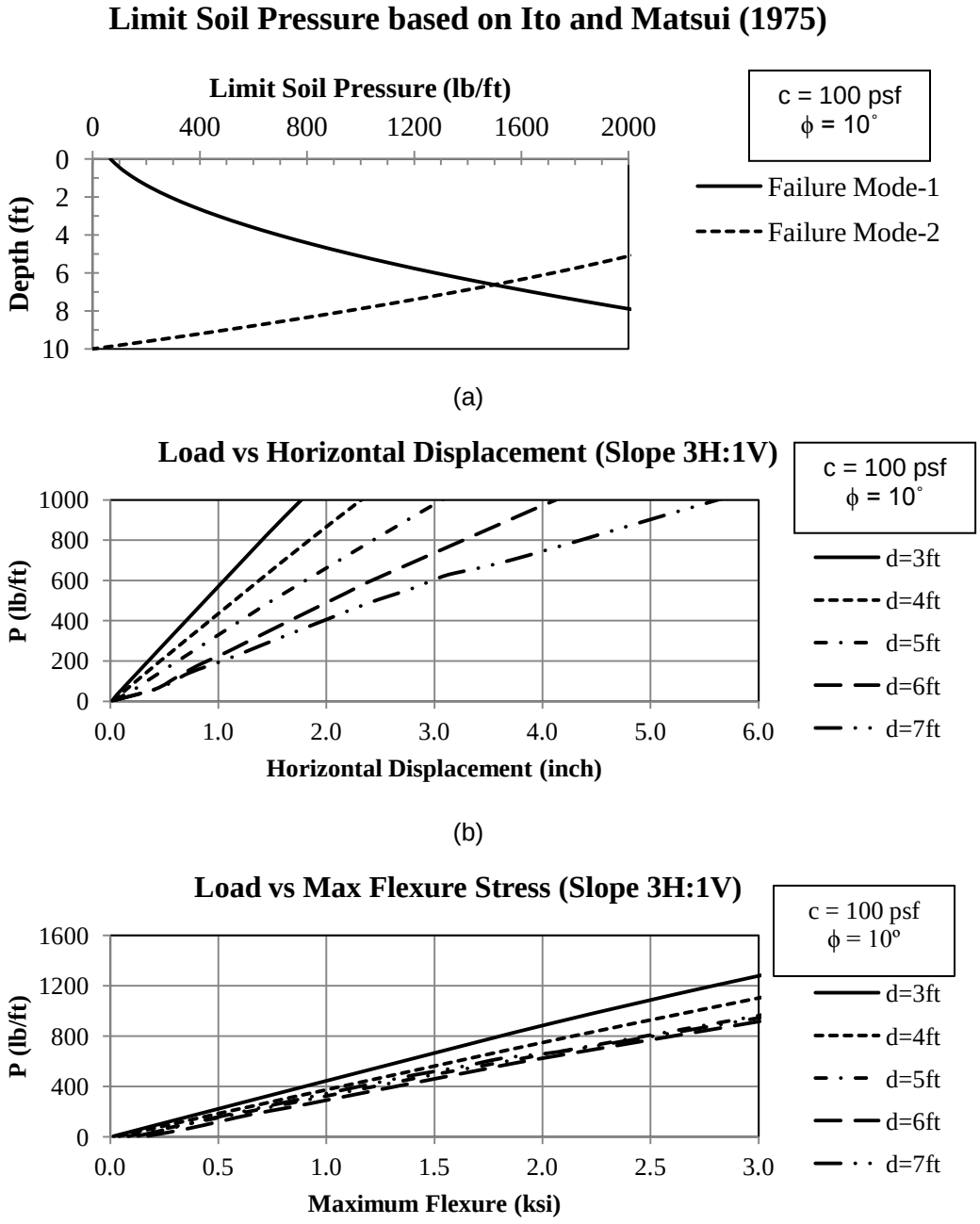


Figure B1 Design Chart for c = 100 psf and ϕ = 10˚, a. Limit soil curve, b. Load vs Horizontal Displacement for slope 3H:1V, c. Load vs Maximum Flexure for slope 3H:1V

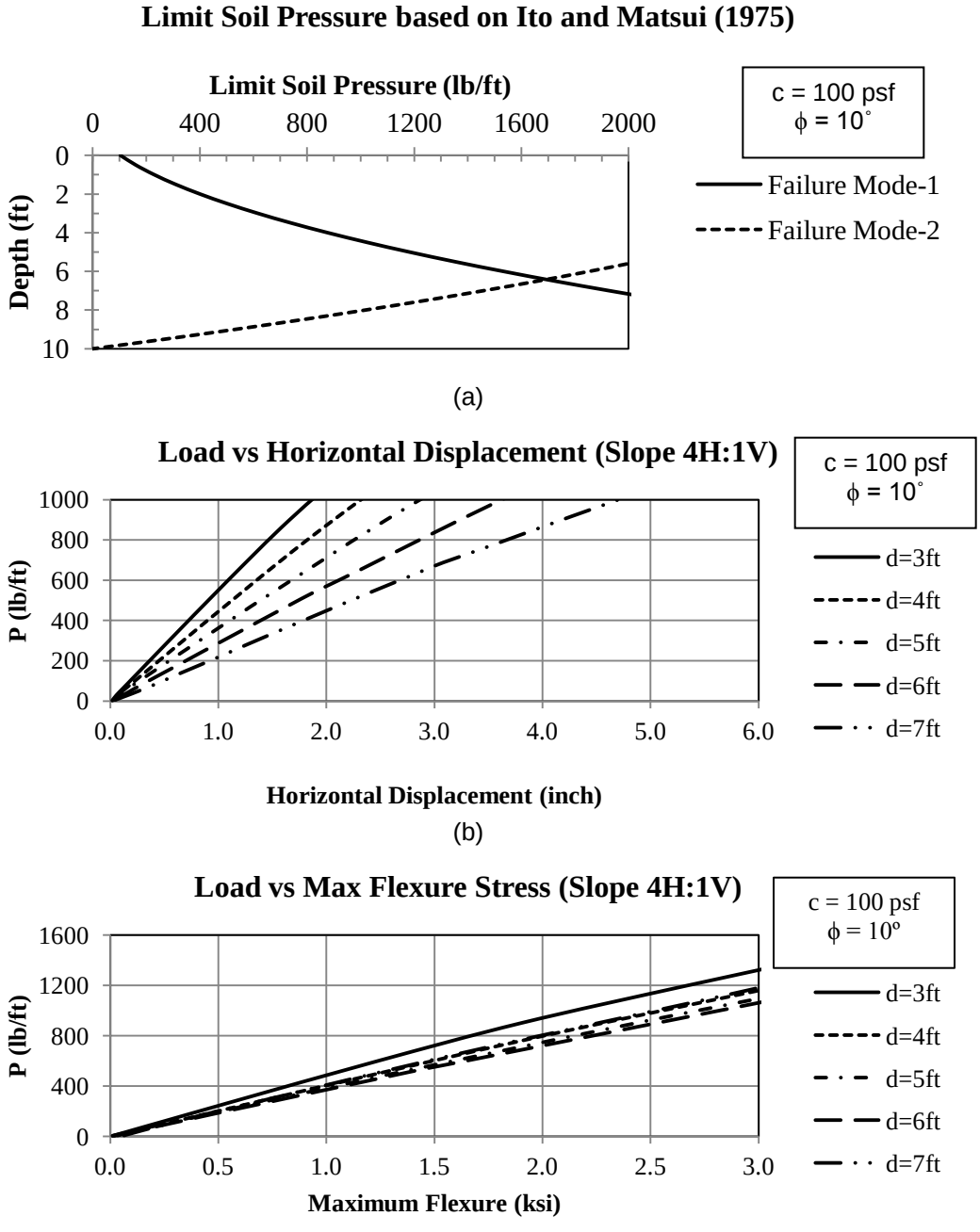


Figure B2 Design Chart for c = 100 psf and $\phi = 10^{\circ}$, a. Limit soil curve, b. Load vs Horizontal Displacement for slope 4H:1V, c. Load vs Maximum Flexure for slope 4H:1V

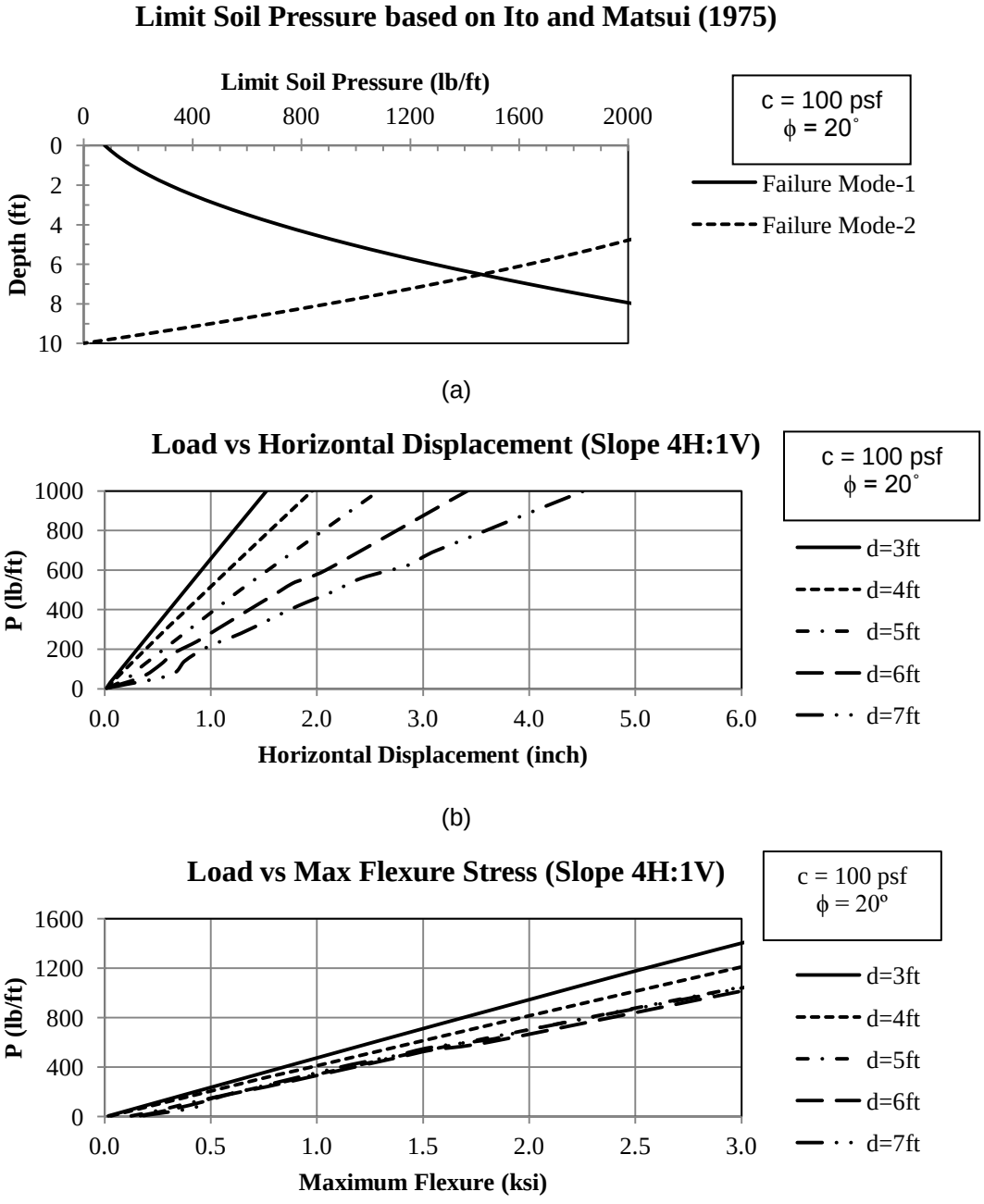


Figure B3 Design Chart for c = 100 psf and $\phi = 20^{\circ}$, a. Limit soil curve, b. Load vs Horizontal Displacement for slope 2H:1V, c. Load vs Maximum Flexure for slope 2H:1V

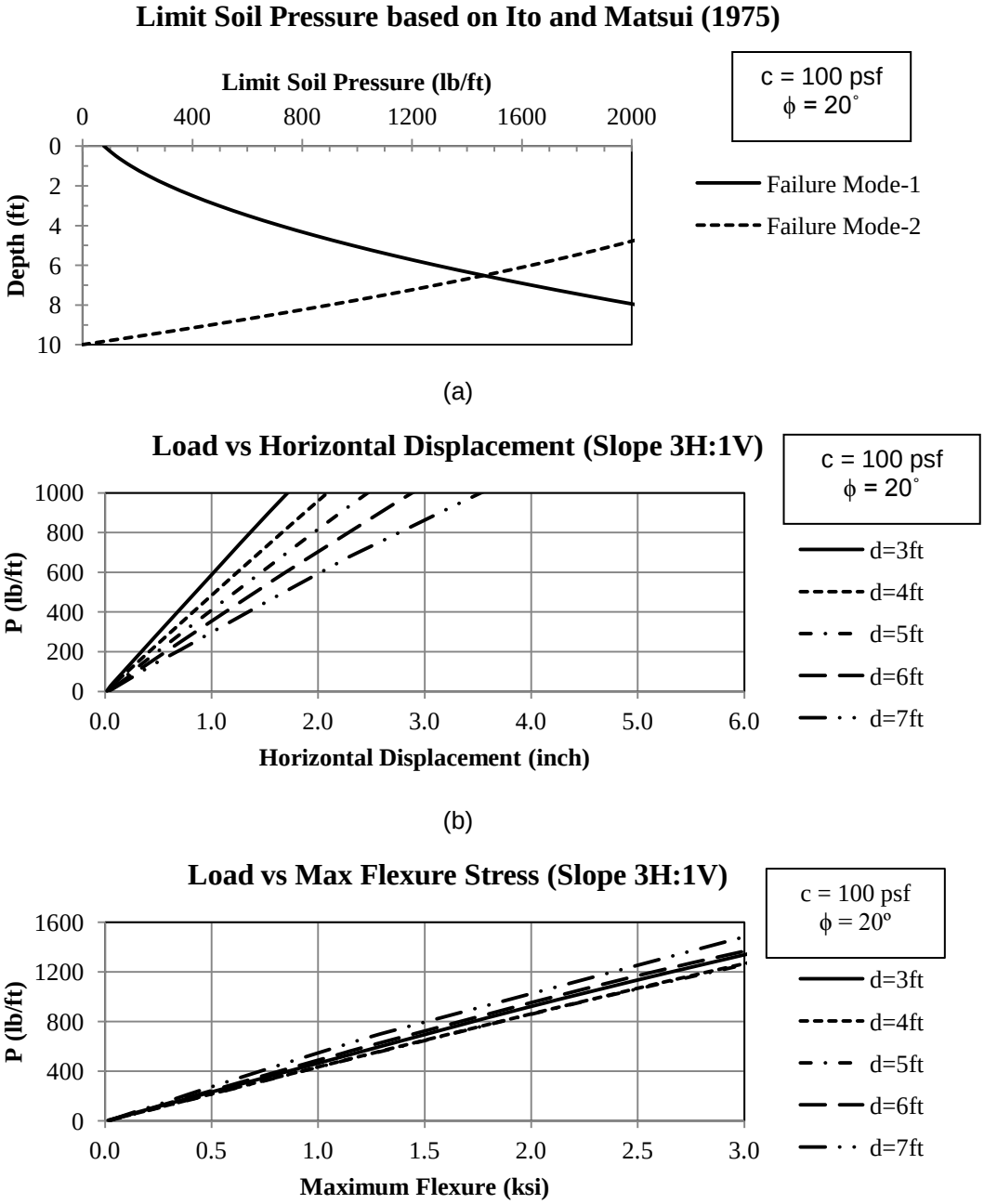


Figure B4 Design Chart for c = 100 psf and ϕ = 20˚, a. Limit soil curve, b. Load vs Horizontal Displacement for slope 3H:1V, c. Load vs Maximum Flexure for slope 3H:1V

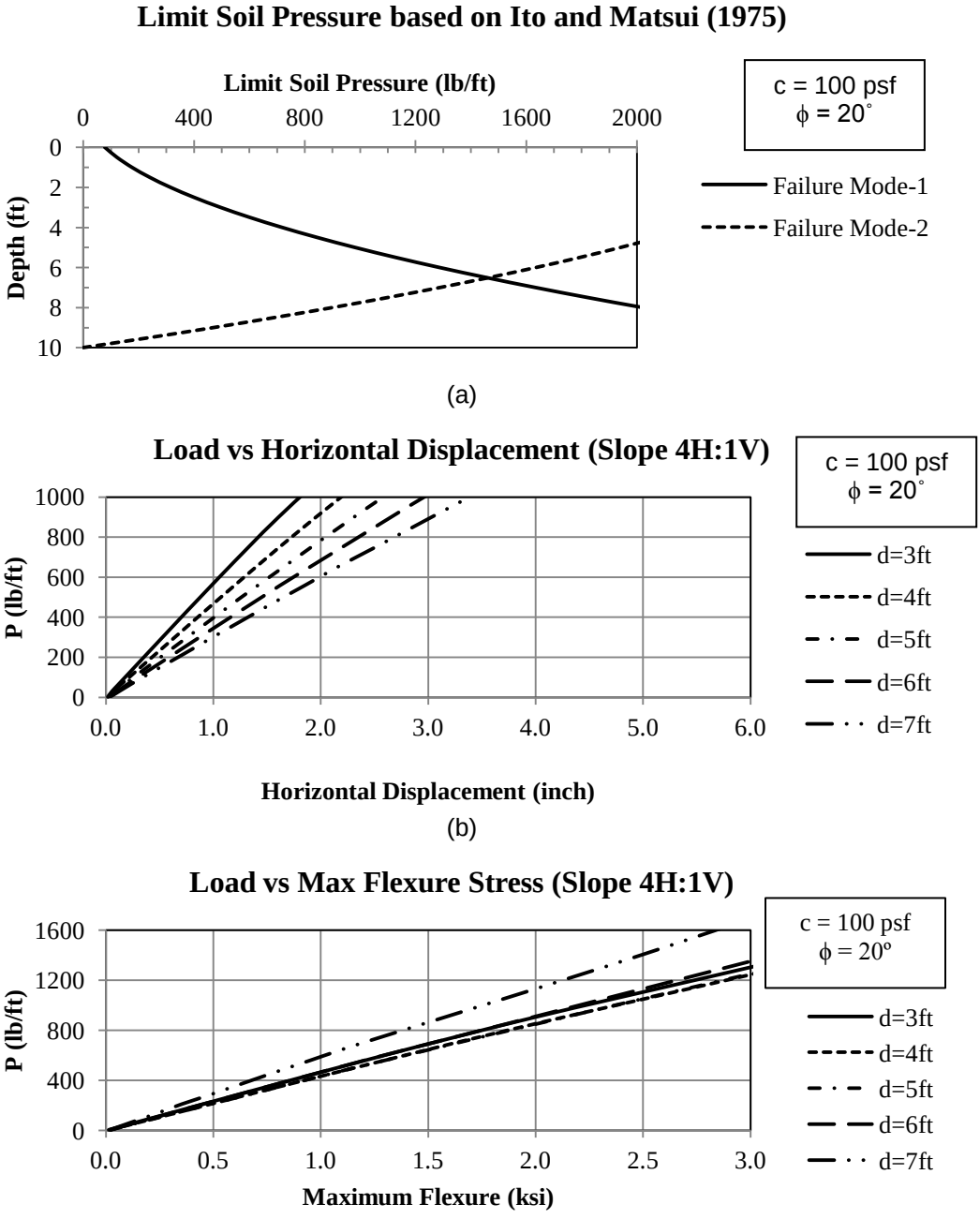


Figure B5 Design Chart for c = 100 psf and $\phi = 20^{\circ}$, a. Limit soil curve, b. Load vs Horizontal Displacement for slope 4H:1V, c. Load vs Maximum Flexure for slope 4H:1V

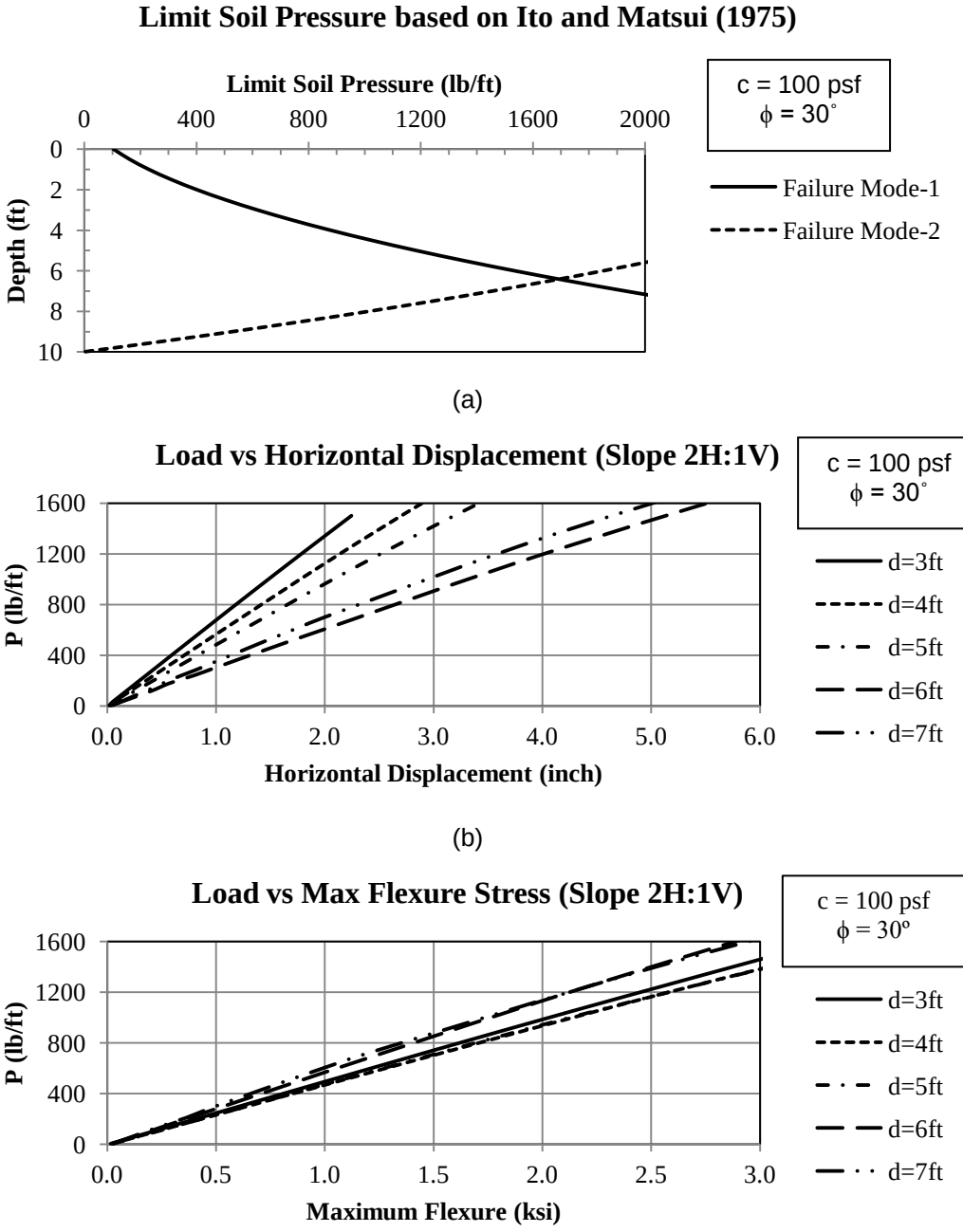


Figure B6 Design Chart for c = 100 psf and $\phi = 30^{\circ}$, a. Limit soil curve, b. Load vs Horizontal Displacement for slope 2H:1V, c. Load vs Maximum Flexure for slope 2H:1V

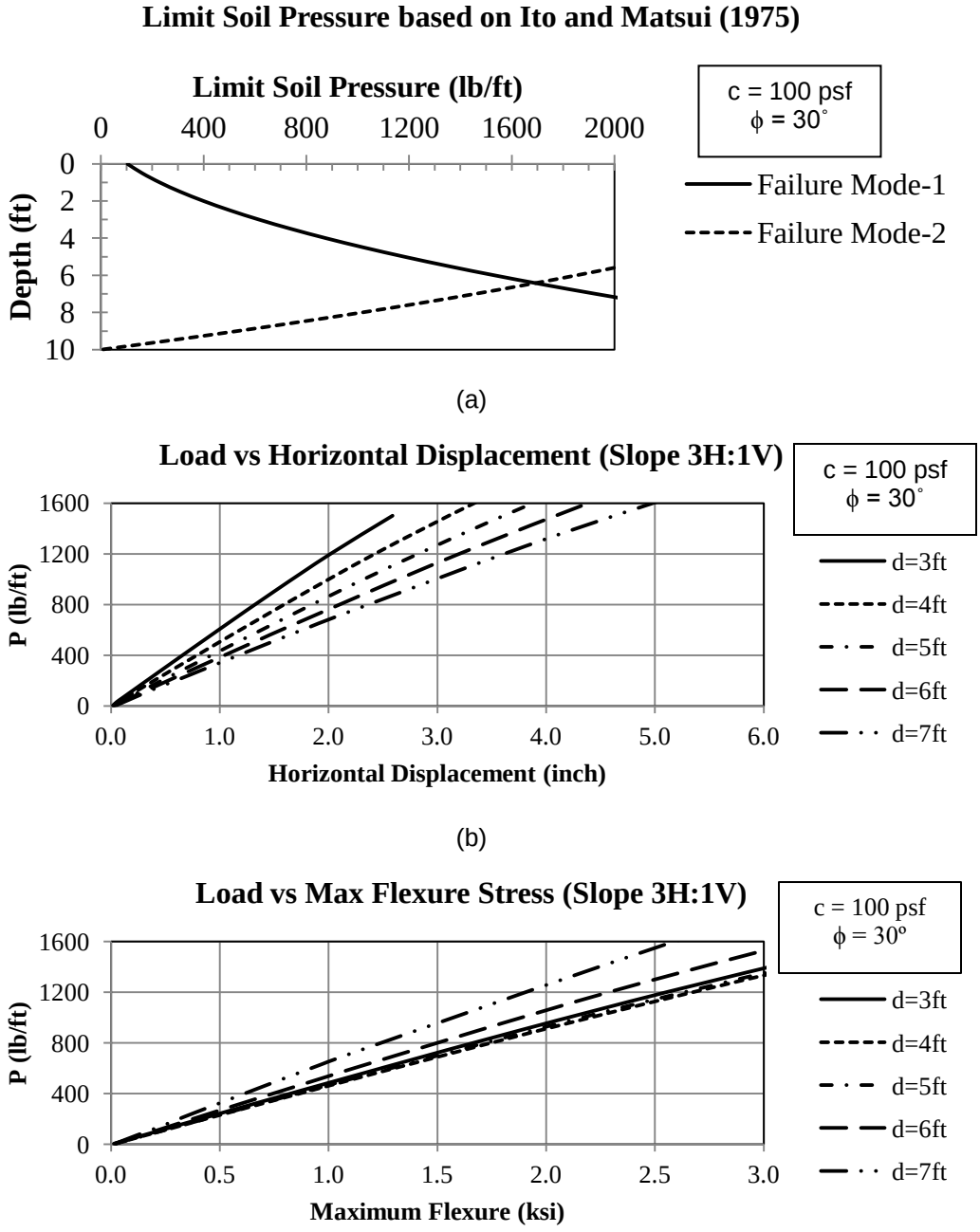


Figure B7 Design Chart for c = 100 psf and ϕ = 30˚, a. Limit soil curve, b. Load vs Horizontal Displacement for slope 3H:1V, c. Load vs Maximum Flexure for slope 3H:1V

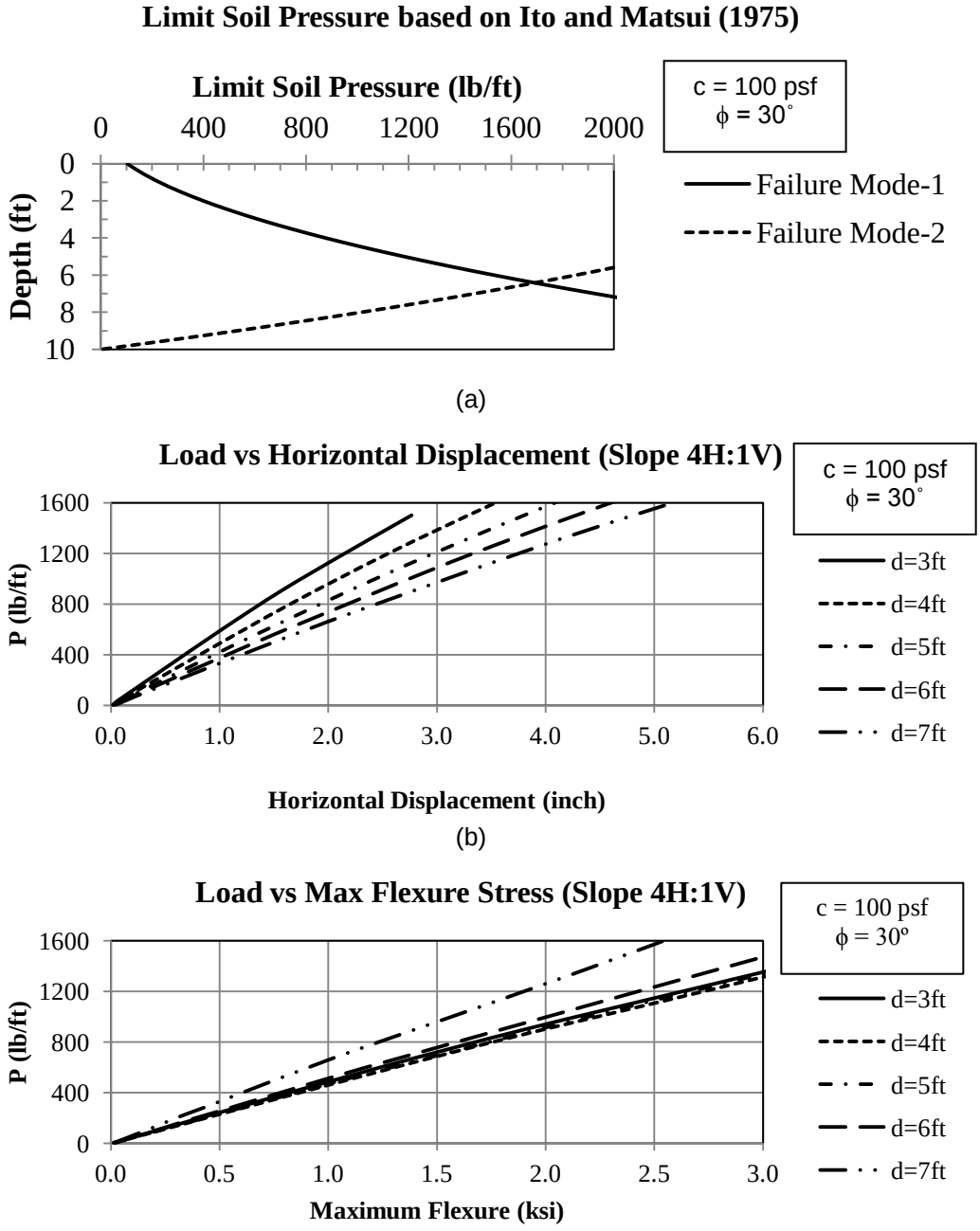


Figure B8 Design Chart for c = 100 psf and $\phi = 30^{\circ}$, a. Limit soil curve, b. Load vs Horizontal Displacement for slope 4H:1V, c. Load vs Maximum Flexure for slope 4H:1V

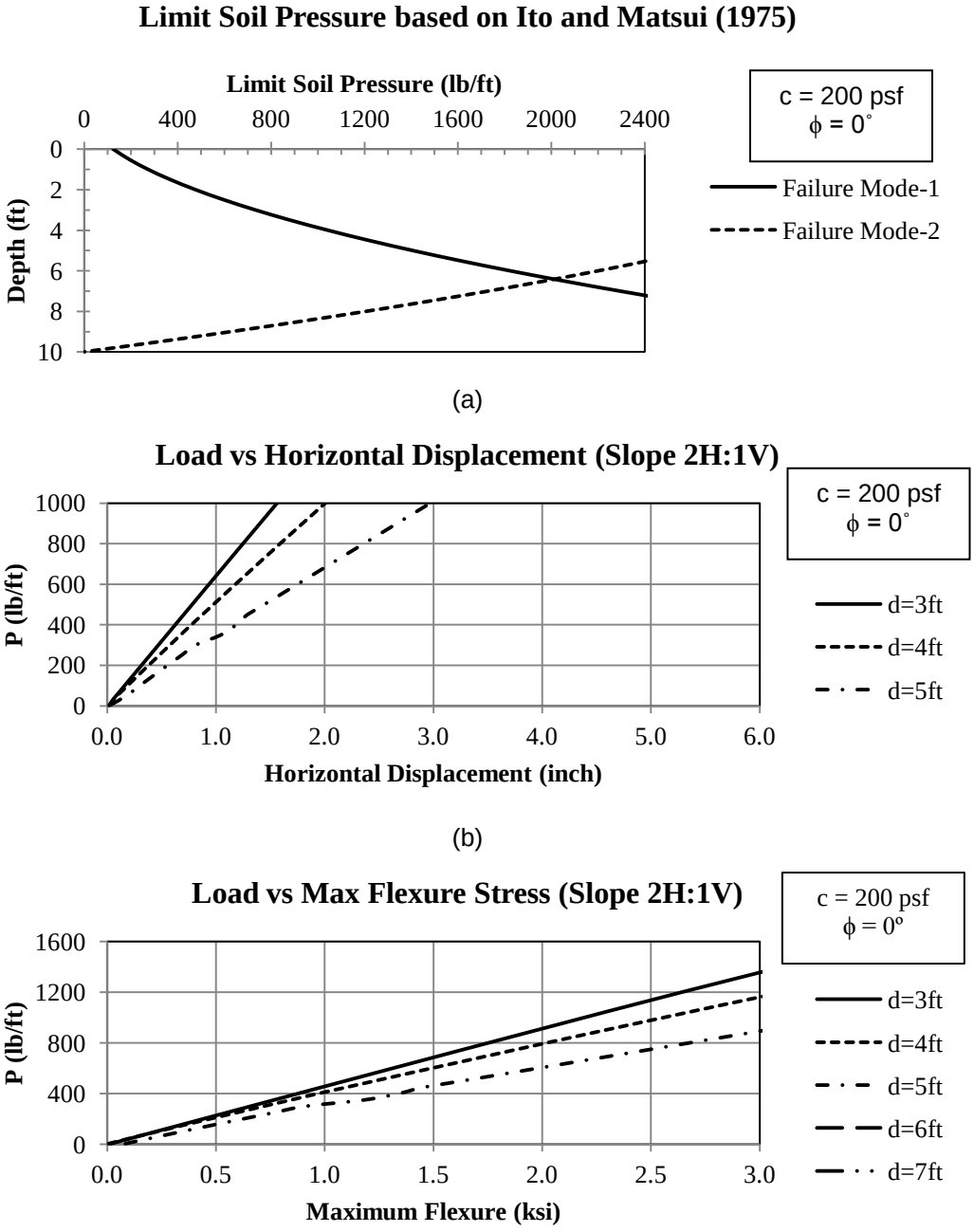


Figure B9 Design Chart for c = 200 psf and ϕ = 0˚, a. Limit soil curve, b. Load vs Horizontal Displacement for slope 2H:1V, c. Load vs Maximum Flexure for slope 2H:1V

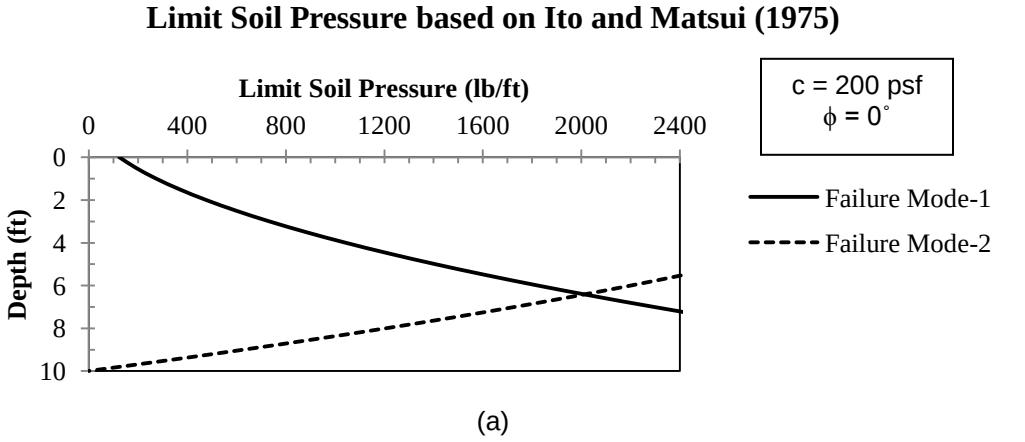


(a)

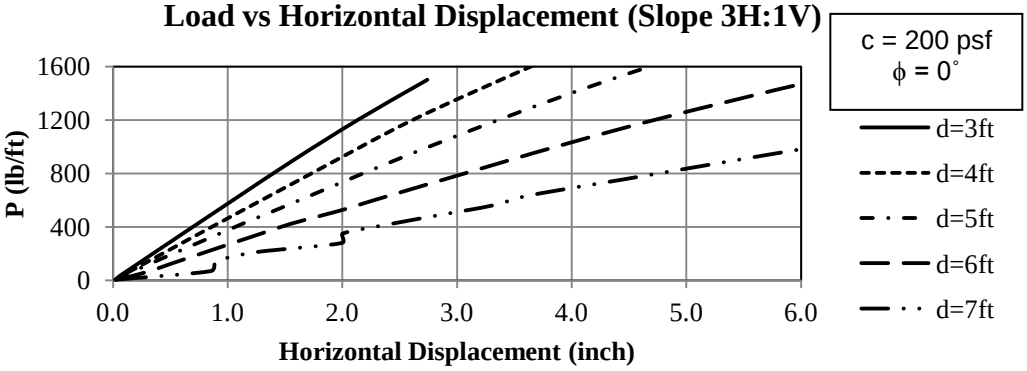


(b)

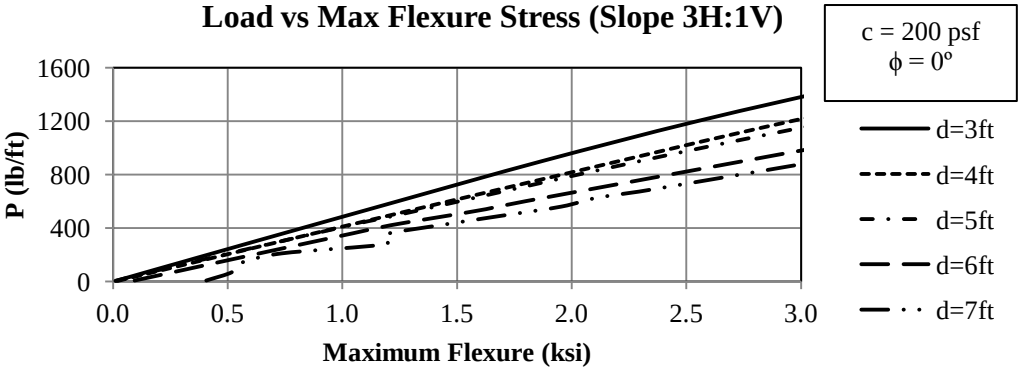


(c)

Figure B10 Design Chart for c = 200 psf and ϕ = 0˚, a. Limit soil curve, b. Load vs Horizontal Displacement for slope 3H:1V, c. Load vs Maximum Flexure for slope 3H:1V

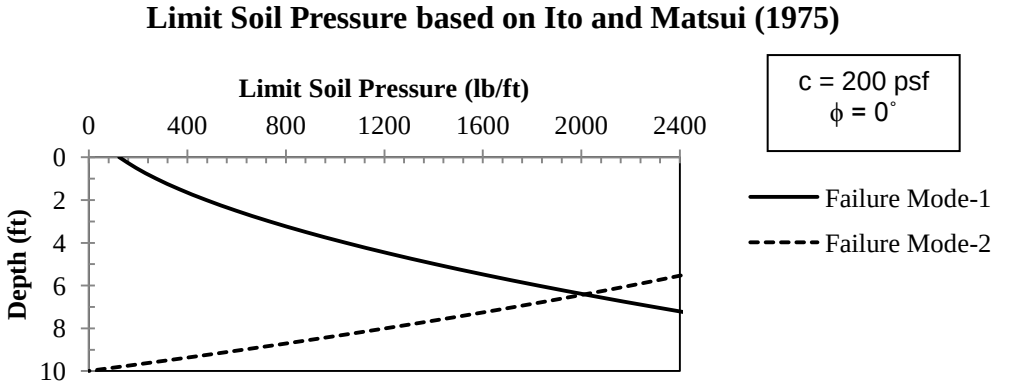


(a)

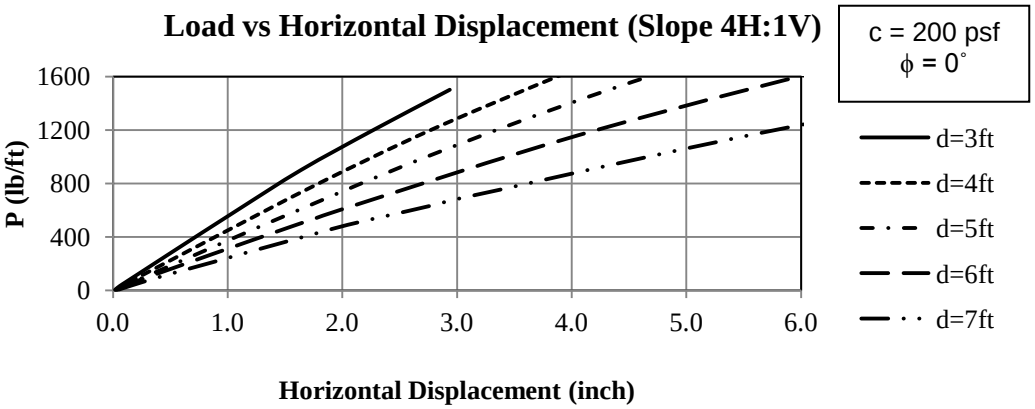


(b)

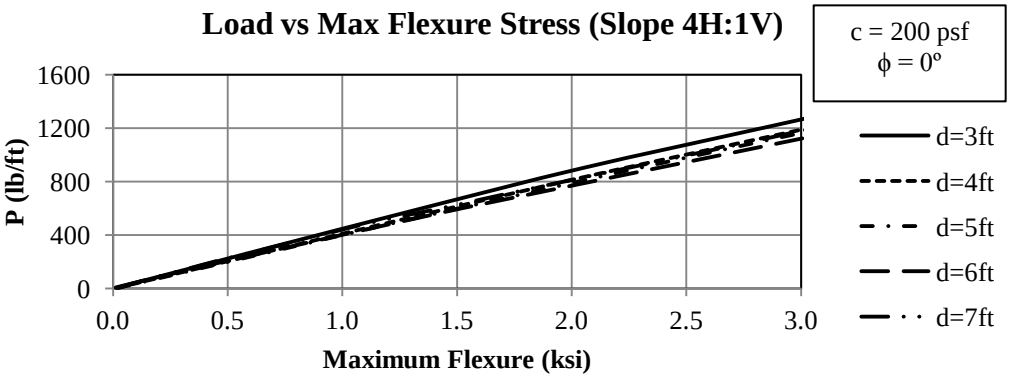


(c)

Figure B11 Design Chart for c = 200 psf and ϕ = 0˚, a. Limit soil curve, b. Load vs Horizontal Displacement for slope 4H:1V, c. Load vs Maximum Flexure for slope 4H:1V

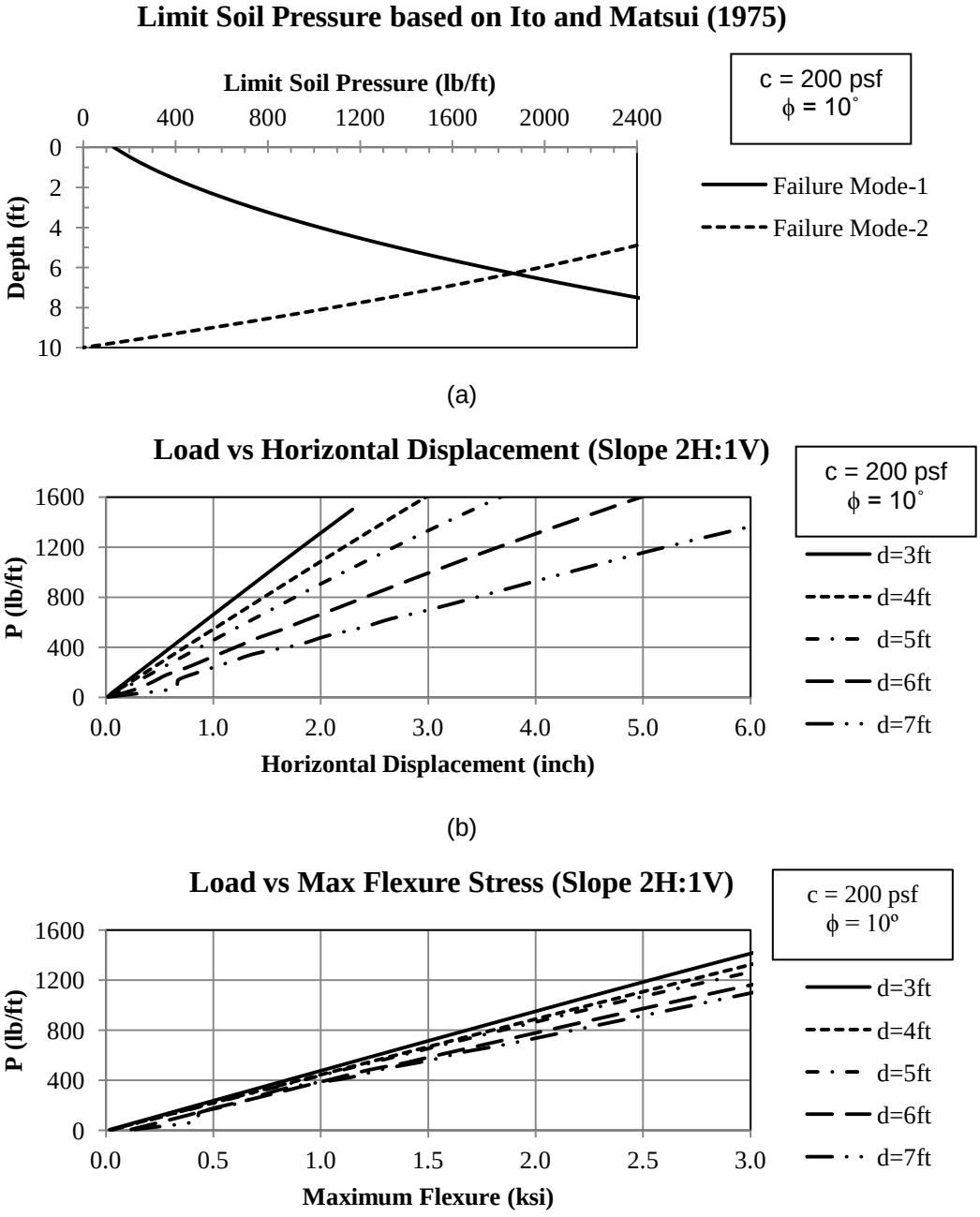


Figure B12 Design Chart for c = 200 psf and ϕ = 10˚, a. Limit soil curve, b. Load vs Horizontal Displacement for slope 2H:1V, c. Load vs Maximum Flexure for slope 2H:1V

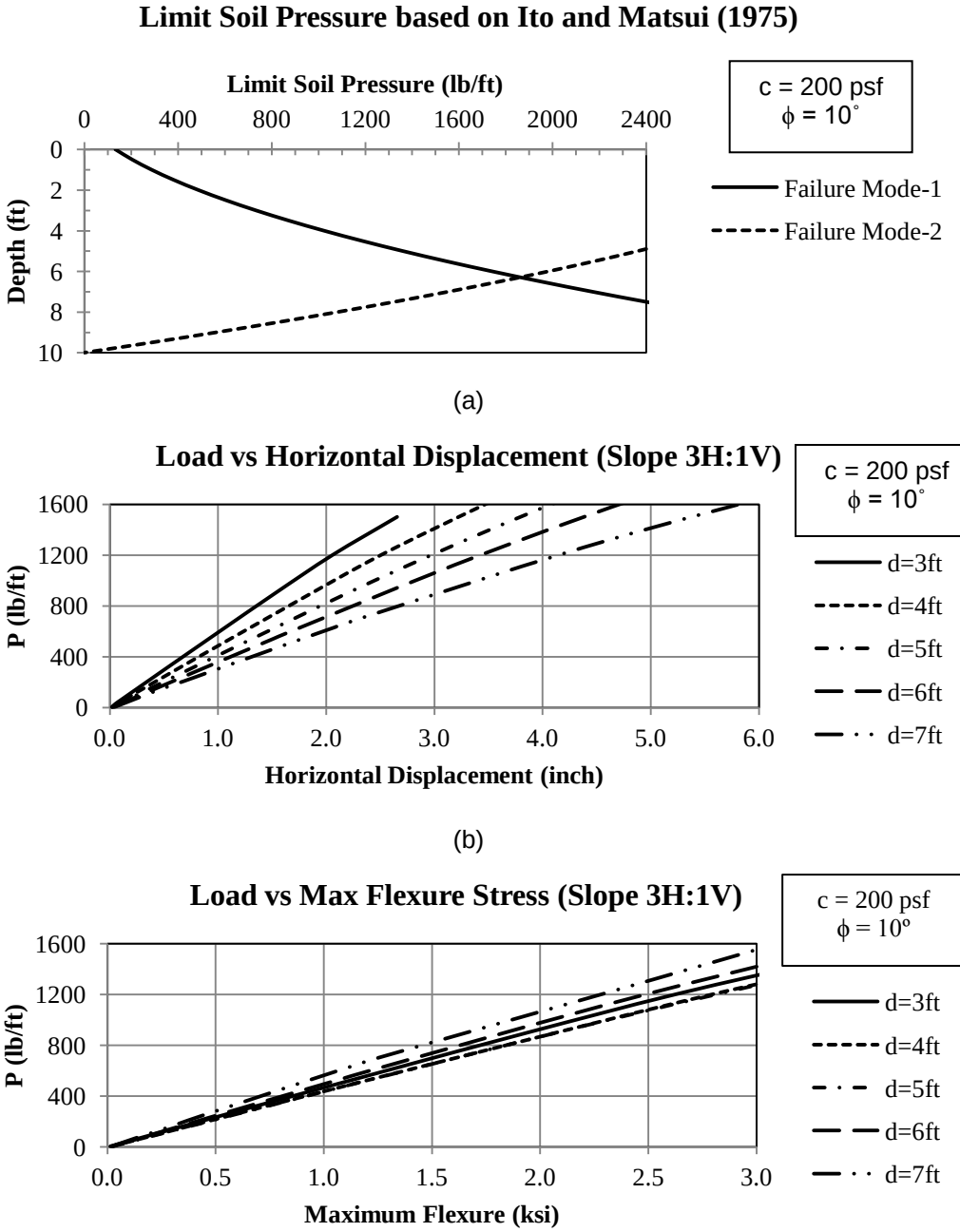


Figure B13 Design Chart for c = 200 psf and ϕ = 10˚, a. Limit soil curve, b. Load vs Horizontal Displacement for slope 3H:1V, c. Load vs Maximum Flexure for slope 3H:1V

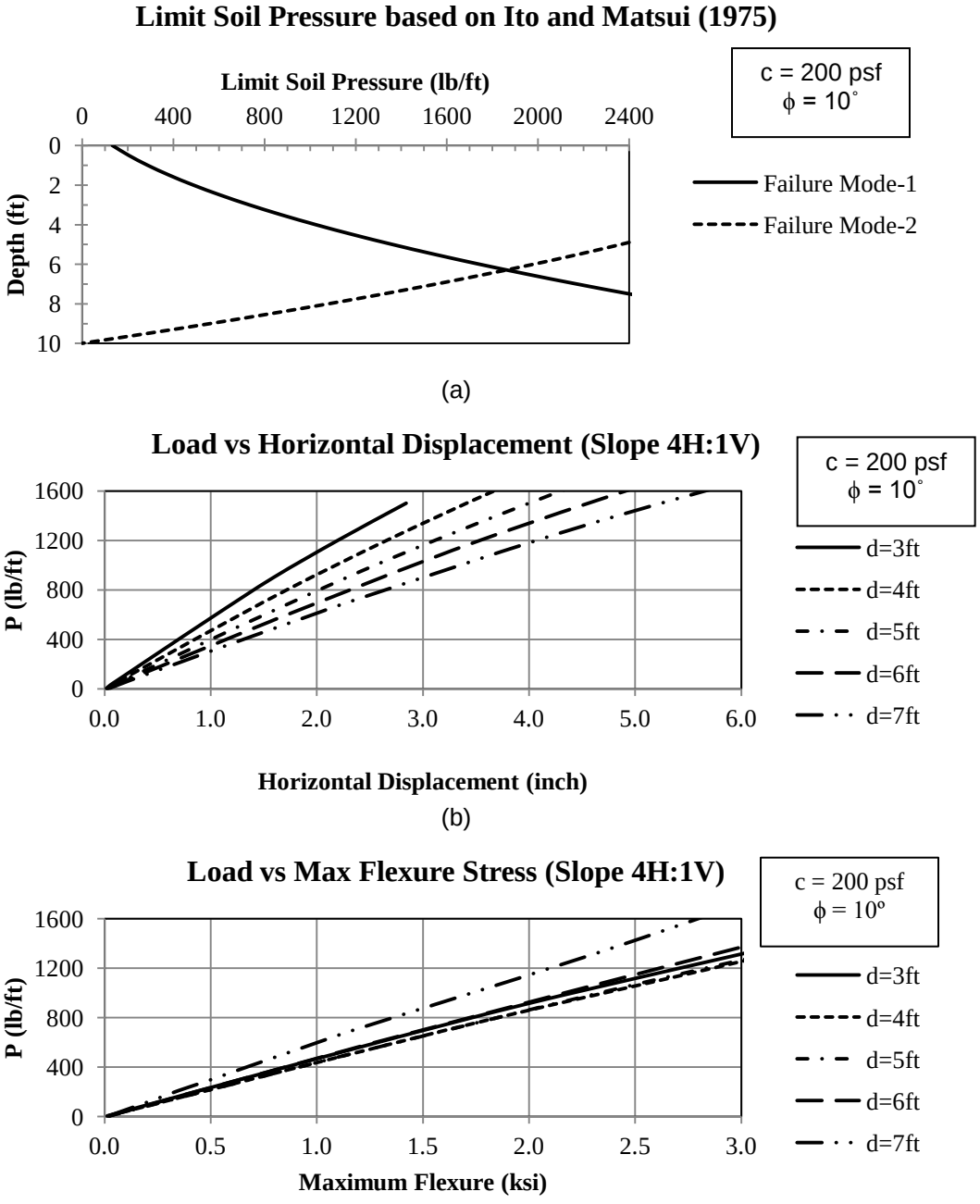


Figure B14 Design Chart for c = 200 psf and ϕ = 10˚, a. Limit soil curve, b. Load vs Horizontal Displacement for slope 4H:1V, c. Load vs Maximum Flexure for slope 4H:1V

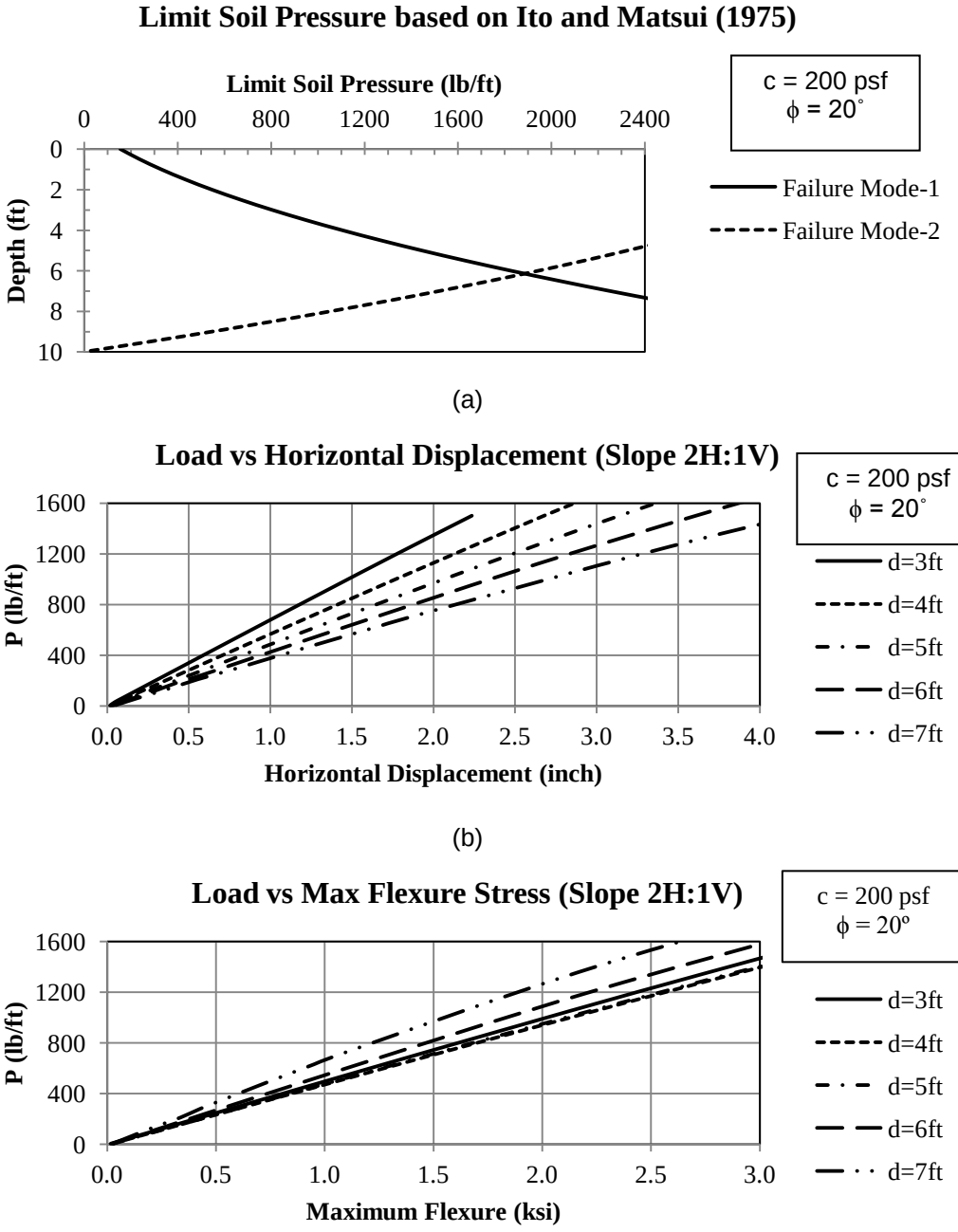


Figure B15 Design Chart for c = 200 psf and ϕ = 20˚, a. Limit soil curve, b. Load vs Horizontal Displacement for slope 2H:1V, c. Load vs Maximum Flexure for slope 2H:1V

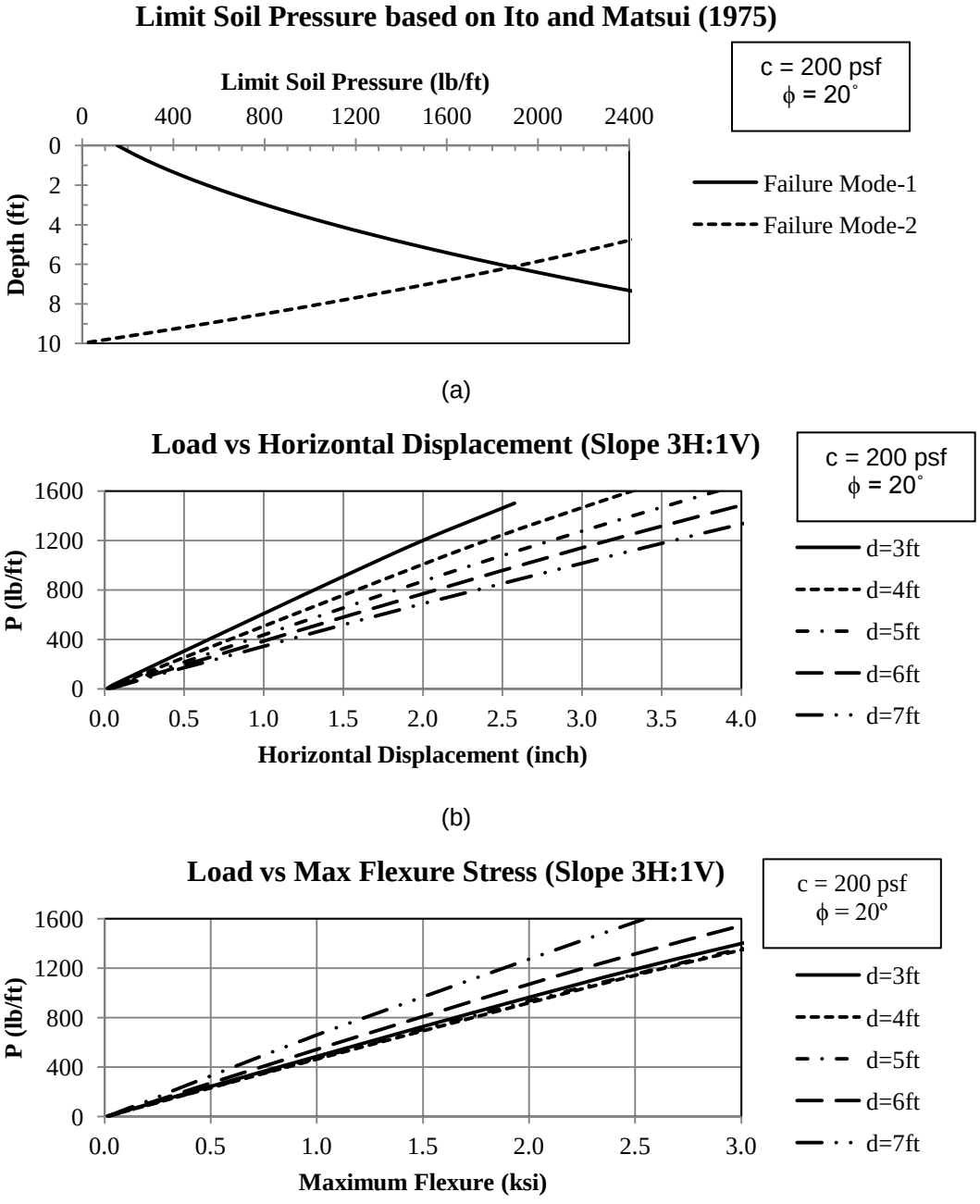


Figure B16 Design Chart for c = 200 psf and ϕ = 20˚, a. Limit soil curve, b. Load vs Horizontal Displacement for slope 3H:1V, c. Load vs Maximum Flexure for slope 3H:1V

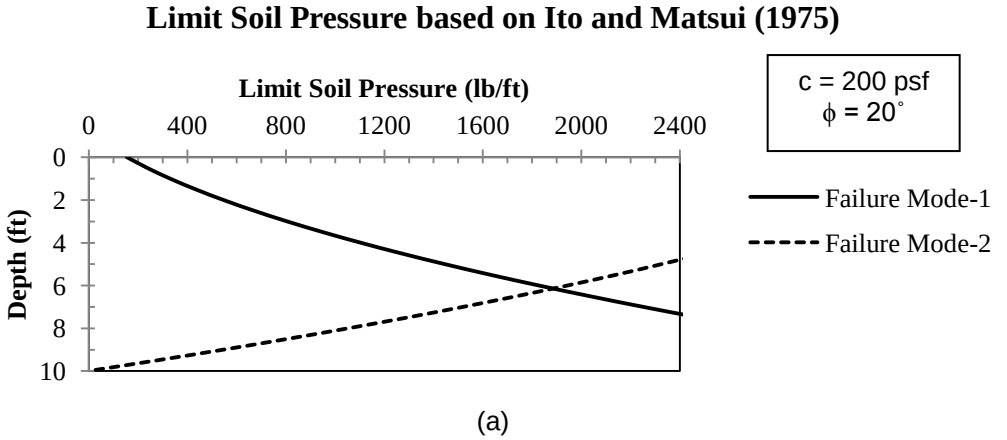


(a)

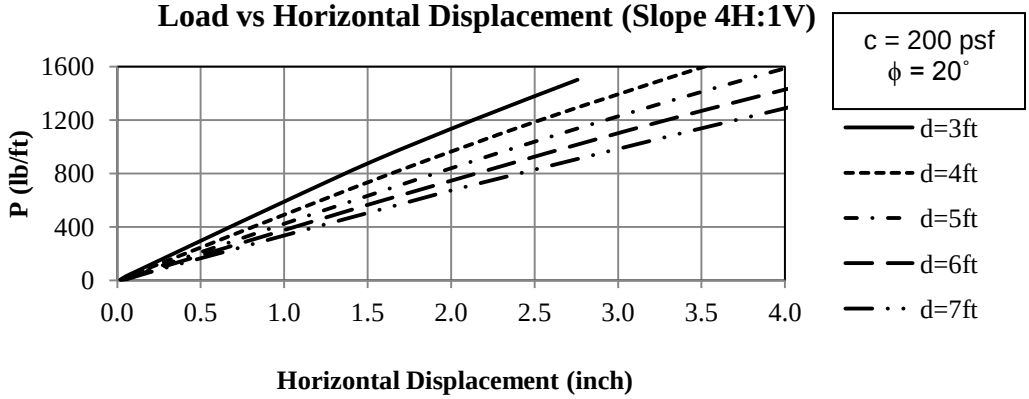


(b)

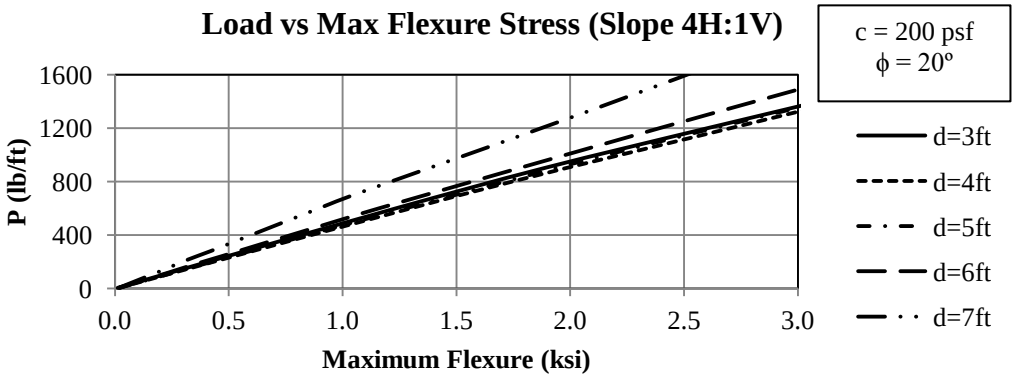


(c)

Figure B17 Design Chart for c = 200 psf and ϕ = 20˚, a. Limit soil curve, b. Load vs Horizontal Displacement for slope 4H:1V, c. Load vs Maximum Flexure for slope 4H:1V

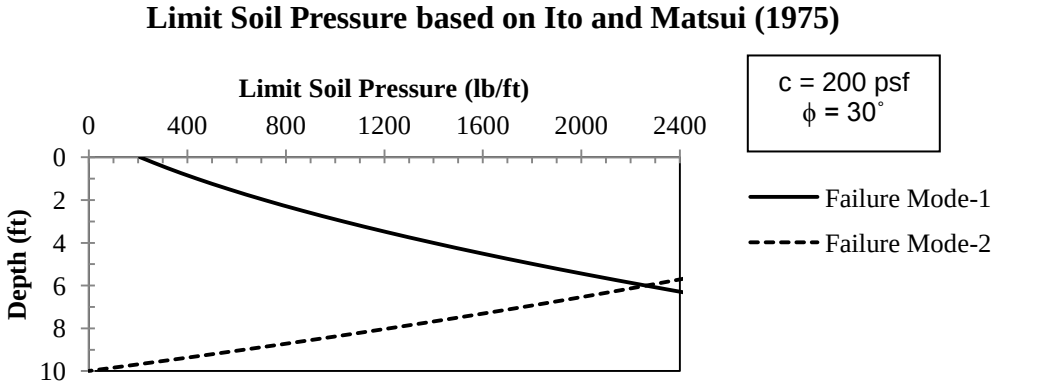


(a)

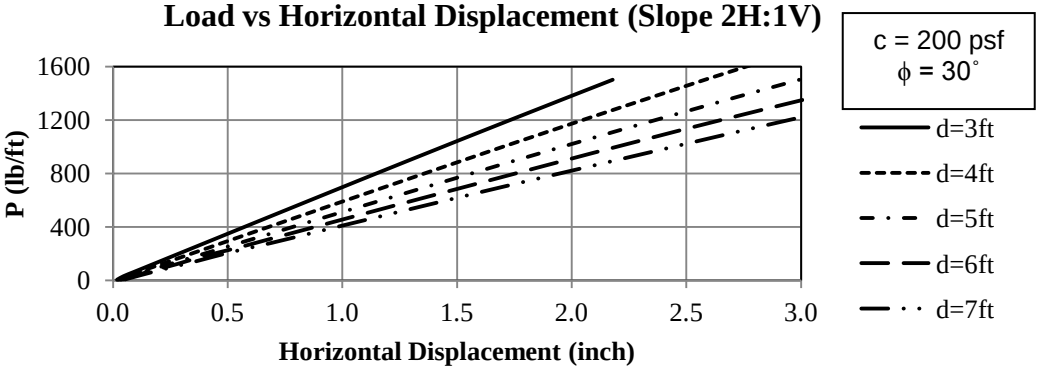


(b)

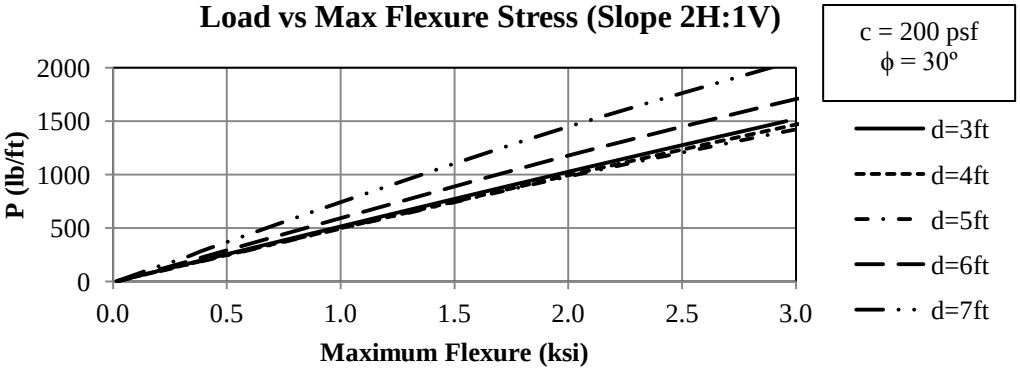


(c)

Figure B18 Design Chart for c = 200 psf and ϕ = 30˚, a. Limit soil curve, b. Load vs Horizontal Displacement for slope 2H:1V, c. Load vs Maximum Flexure for slope 2H:1V

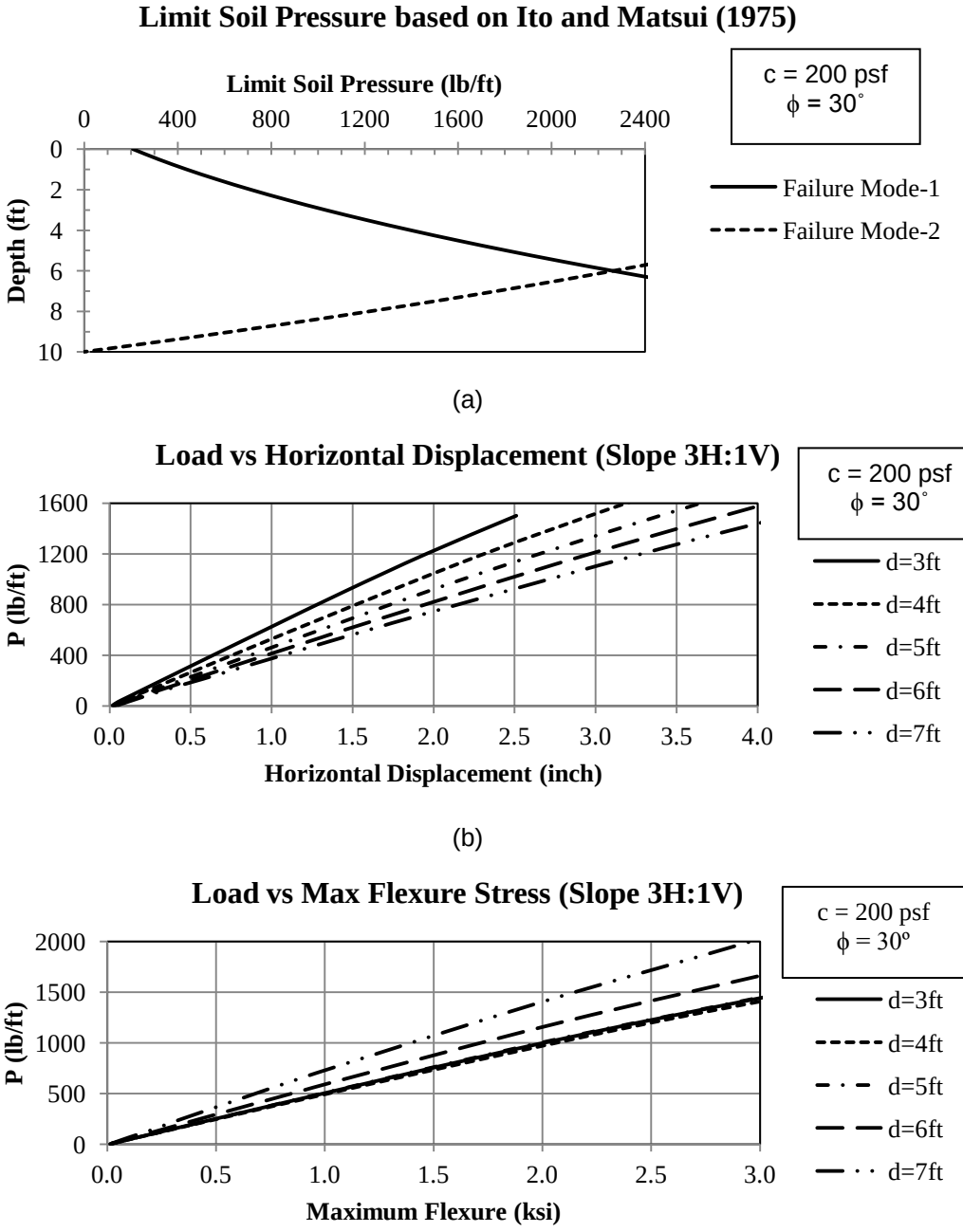


Figure B19 Design Chart for c = 200 psf and ϕ = 30˚, a. Limit soil curve, b. Load vs Horizontal Displacement for slope 3H:1V, c. Load vs Maximum Flexure for slope 3H:1V

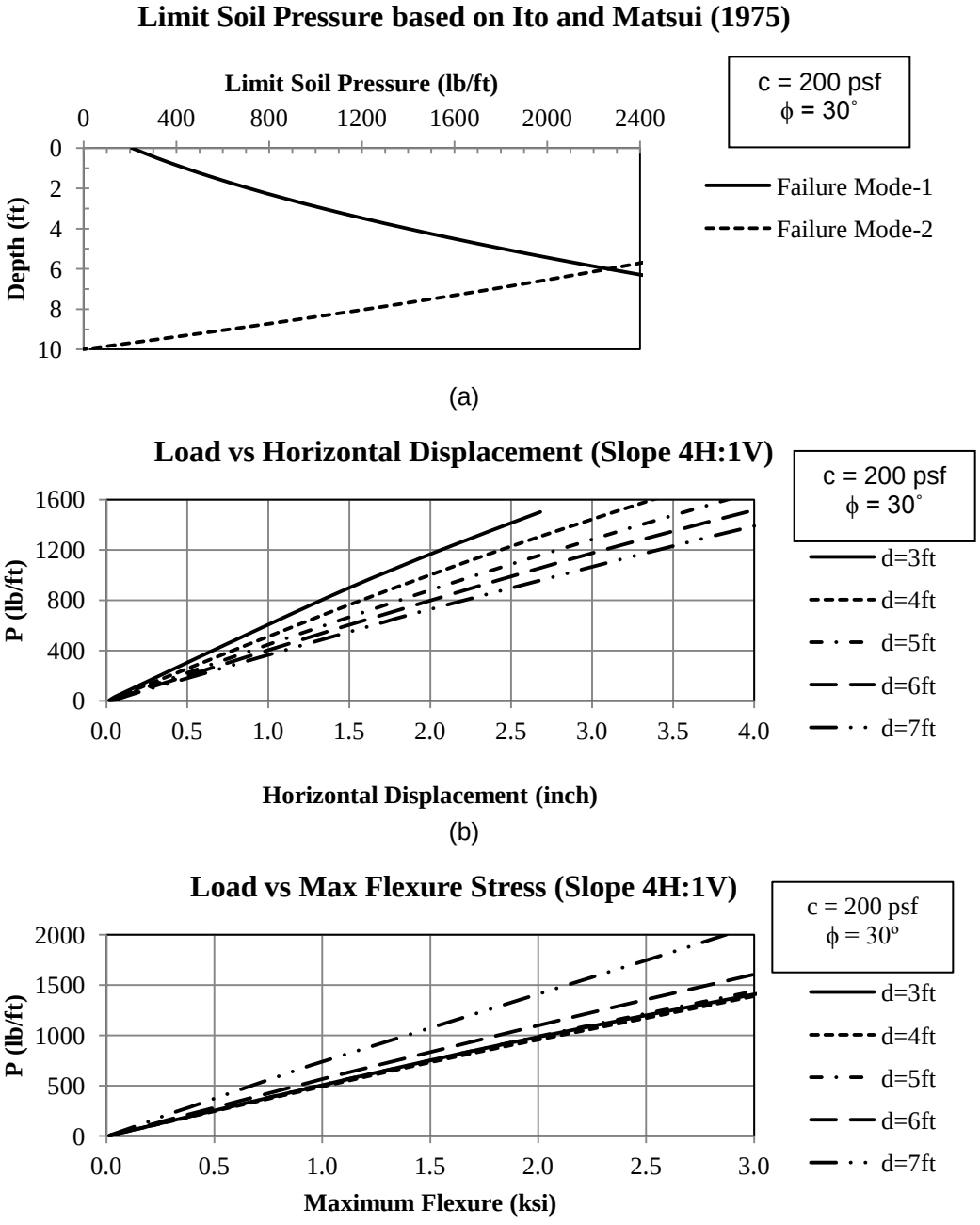


Figure B20 Design Chart for c = 200 psf and ϕ = 30˚, a. Limit soil curve, b. Load vs Horizontal Displacement for slope 4H:1V, c. Load vs Maximum Flexure for slope 4H:1V

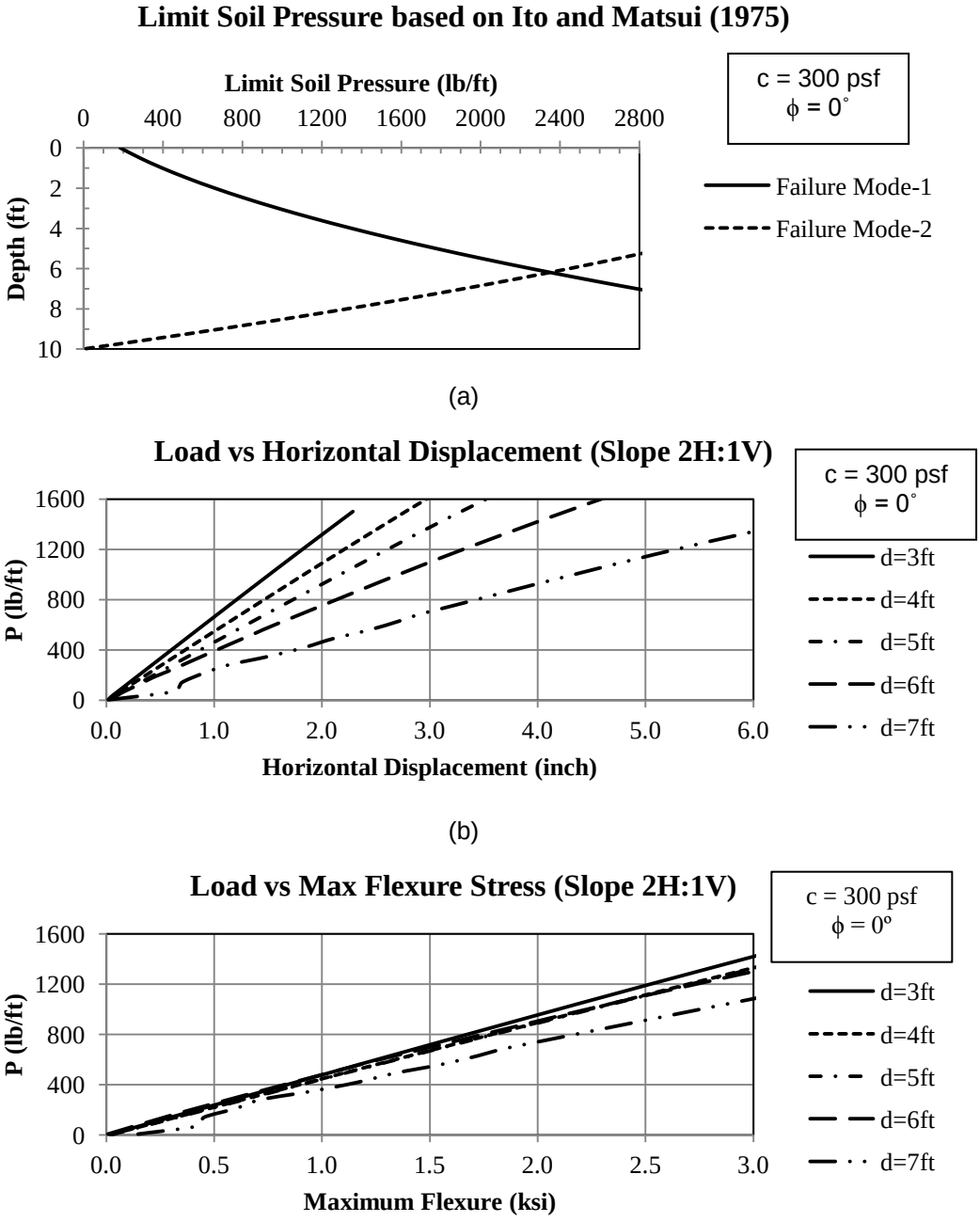


Figure B21 Design Chart for c = 300 psf and $\phi = 0^{\circ}$, a. Limit soil curve, b. Load vs Horizontal Displacement for slope 2H:1V, c. Load vs Maximum Flexure for slope 2H:1V

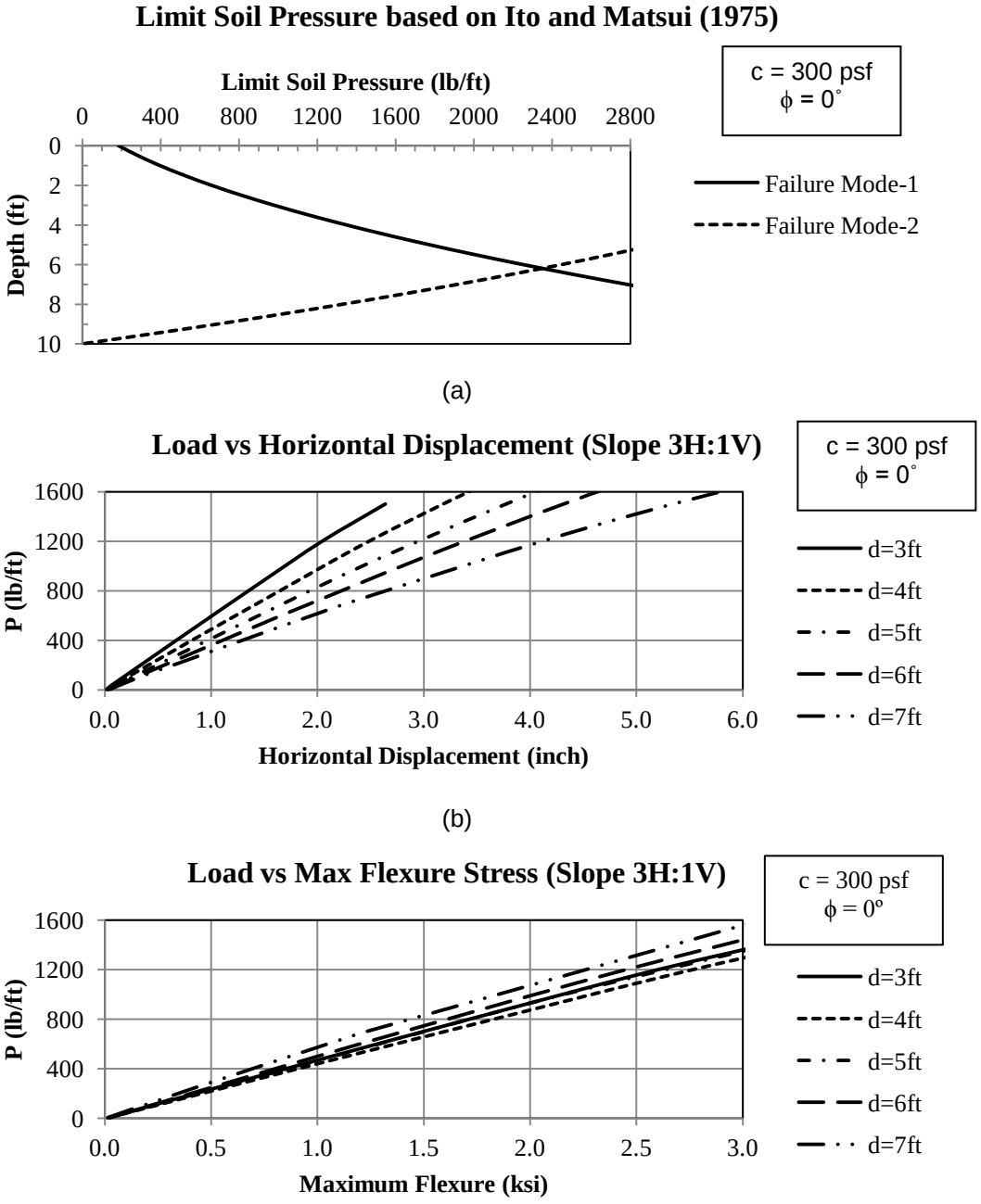


Figure B22 Design Chart for c = 300 psf and $\phi = 0^{\circ}$, a. Limit soil curve, b. Load vs Horizontal Displacement for slope 3H:1V, c. Load vs Maximum Flexure for slope 3H:1V

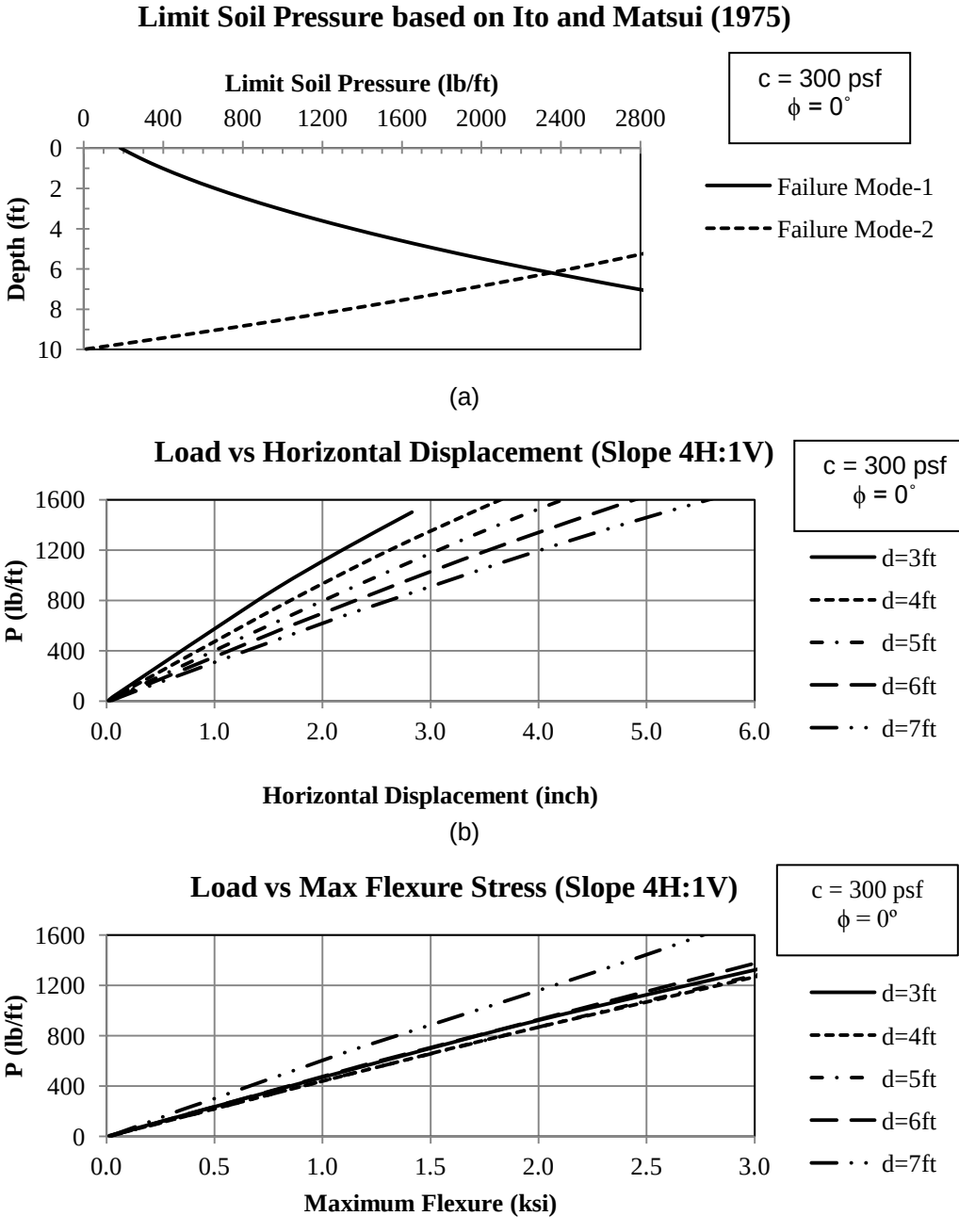


Figure B23 Design Chart for c = 300 psf and $\phi = 0^{\circ}$, a. Limit soil curve, b. Load vs Horizontal Displacement for slope 4H:1V, c. Load vs Maximum Flexure for slope 4H:1V

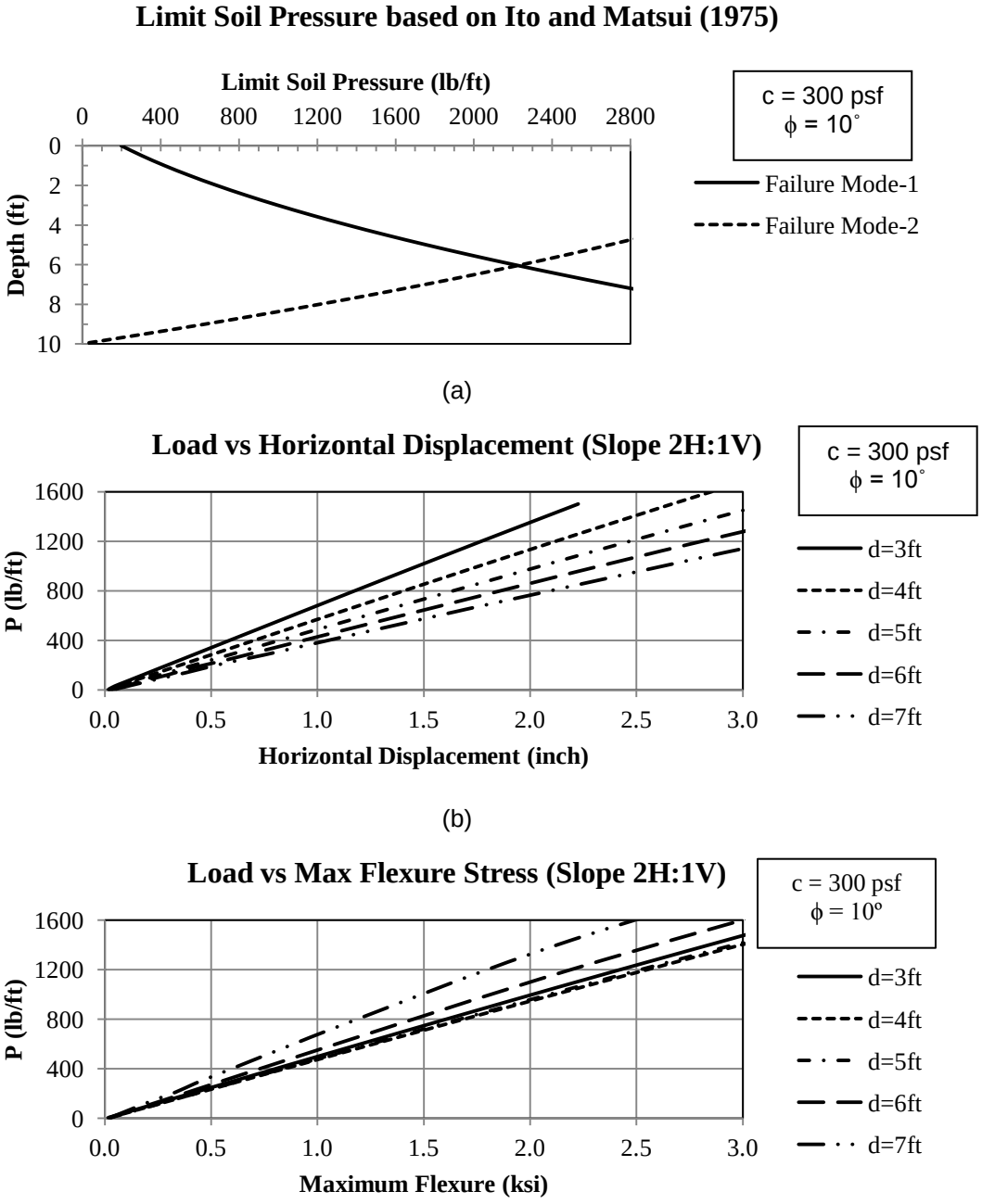


Figure B24 Design Chart for c = 300 psf and ϕ = 10˚, a. Limit soil curve, b. Load vs Horizontal Displacement for slope 2H:1V, c. Load vs Maximum Flexure for slope 2H:1V

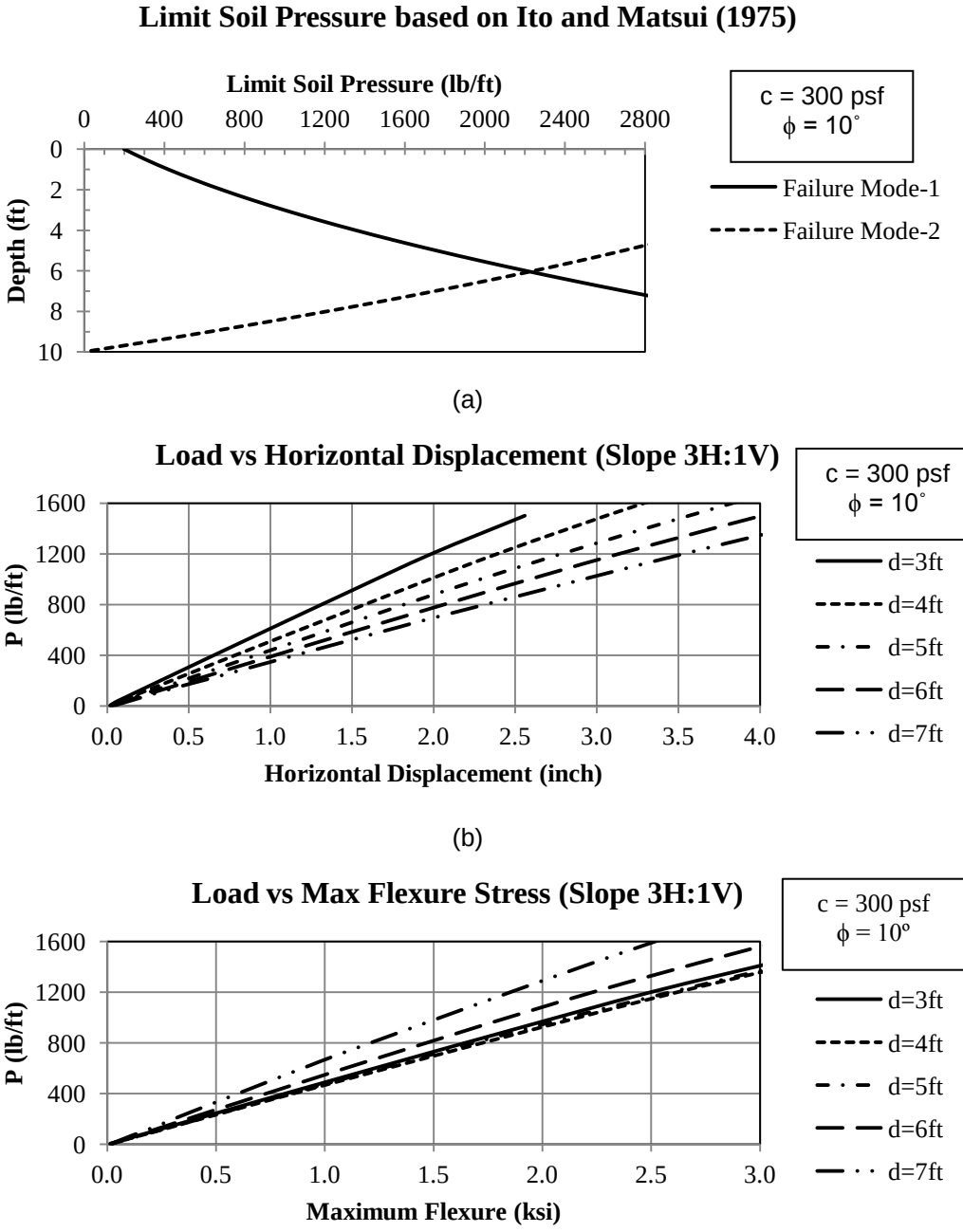


Figure B25 Design Chart for c = 300 psf and ϕ = 10˚, a. Limit soil curve, b. Load vs Horizontal Displacement for slope 3H:1V, c. Load vs Maximum Flexure for slope 3H:1V

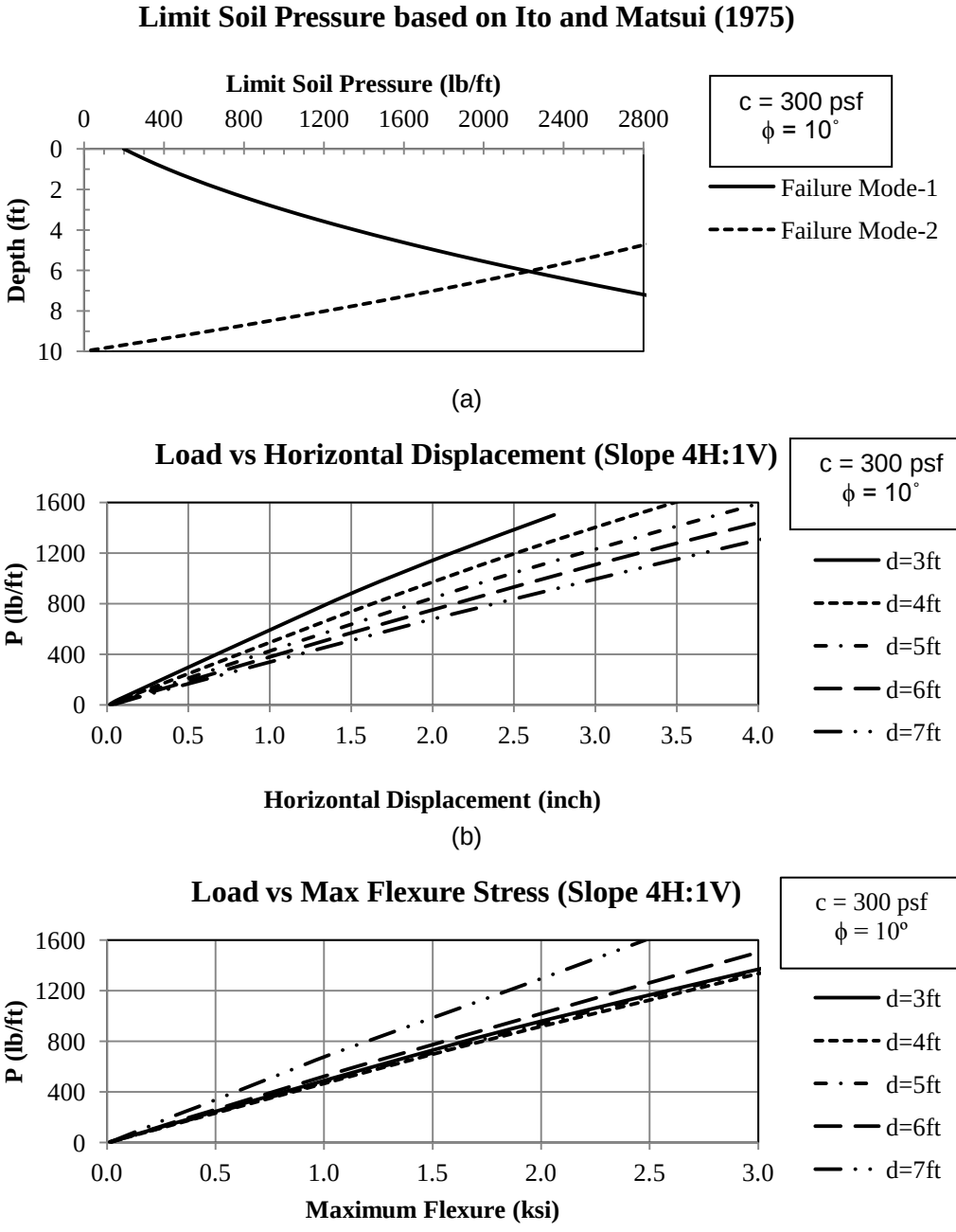


Figure B26 Design Chart for c = 300 psf and $\phi = 10^{\circ}$, a. Limit soil curve, b. Load vs Horizontal Displacement for slope 4H:1V, c. Load vs Maximum Flexure for slope 4H:1V

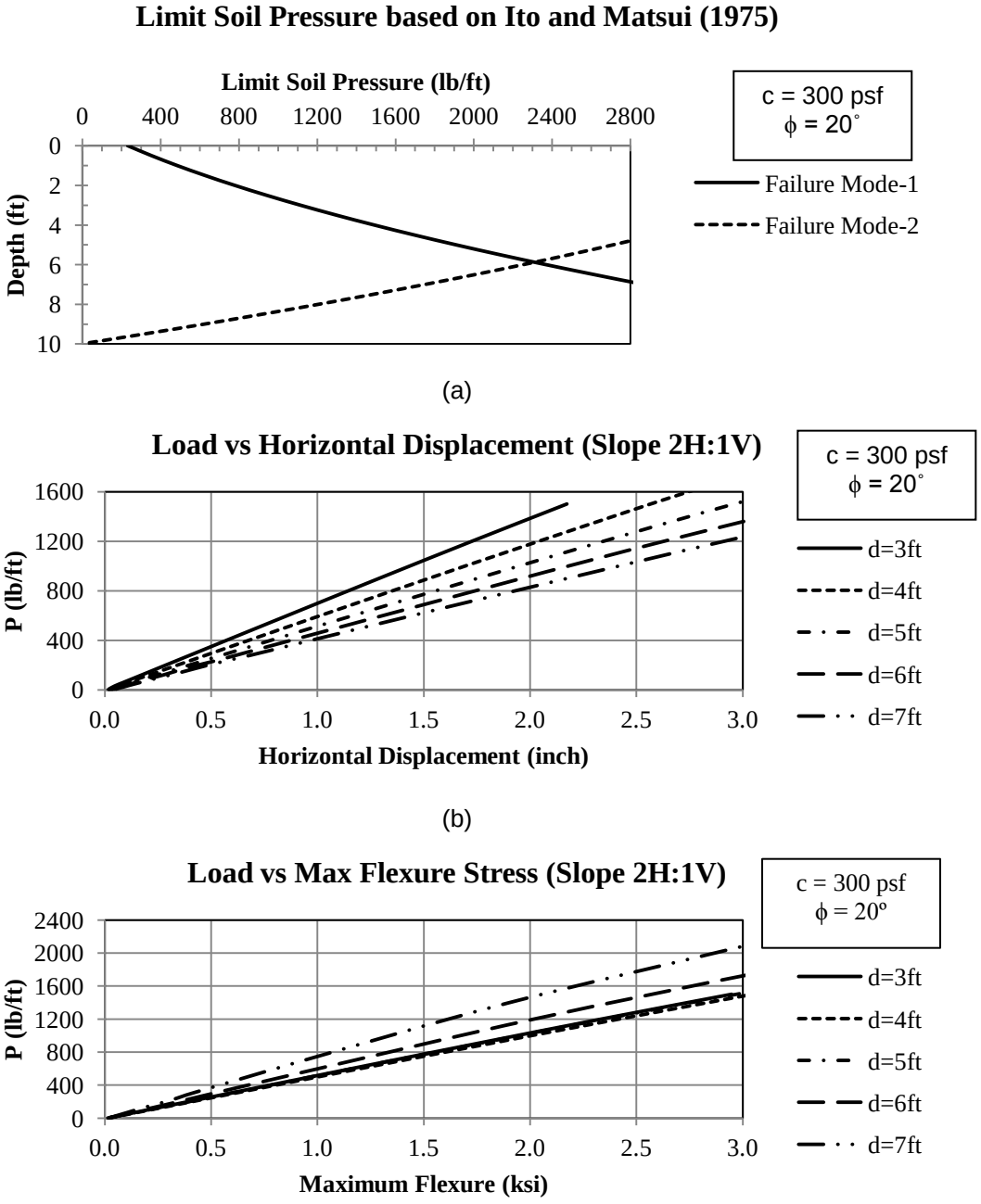


Figure B27 Design Chart for c = 300 psf and $\phi = 20^{\circ}$, a. Limit soil curve, b. Load vs Horizontal Displacement for slope 2H:1V, c. Load vs Maximum Flexure for slope 2H:1V

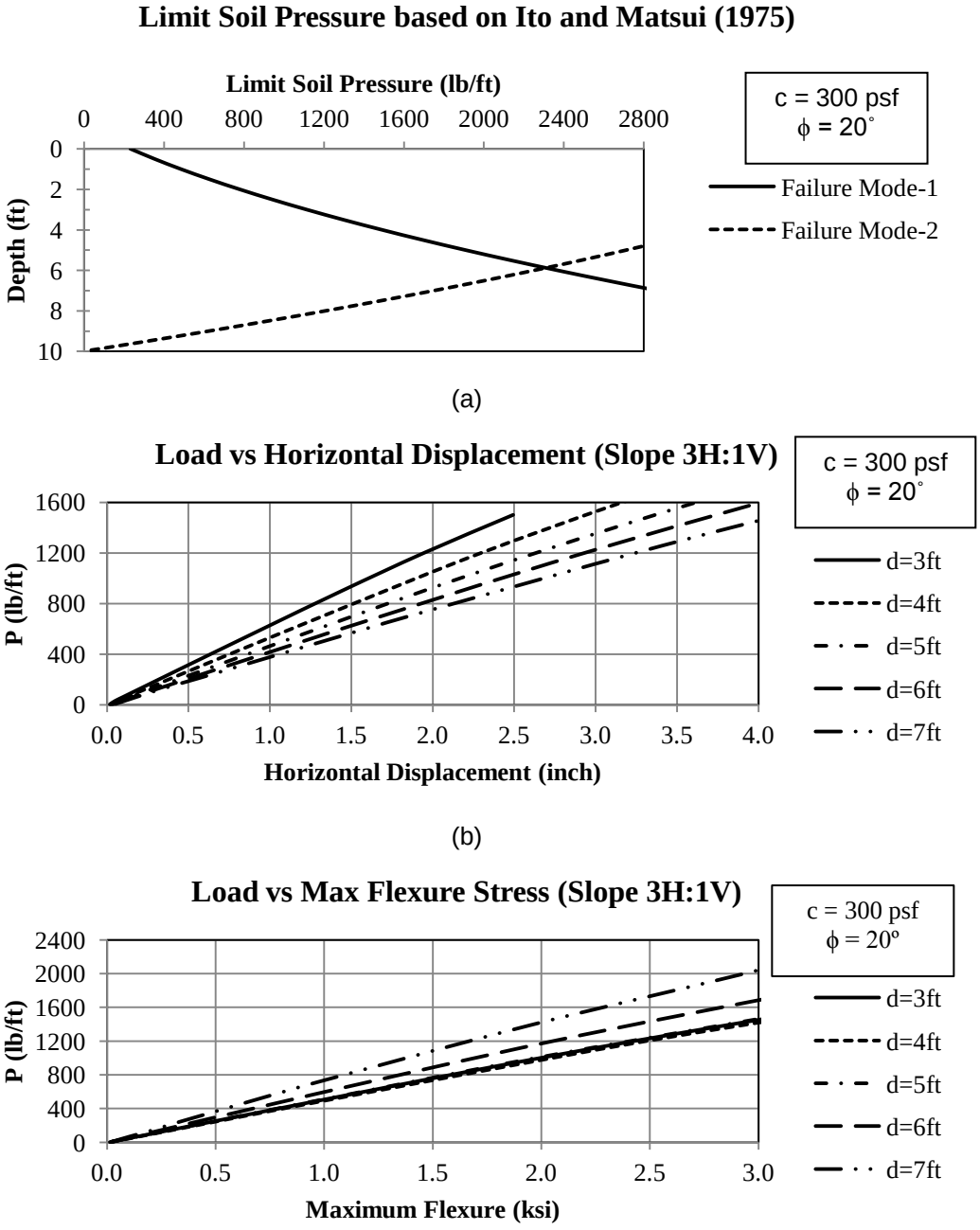


Figure B28 Design Chart for c = 300 psf and ϕ = 20˚, a. Limit soil curve, b. Load vs Horizontal Displacement for slope 3H:1V, c. Load vs Maximum Flexure for slope 3H:1V

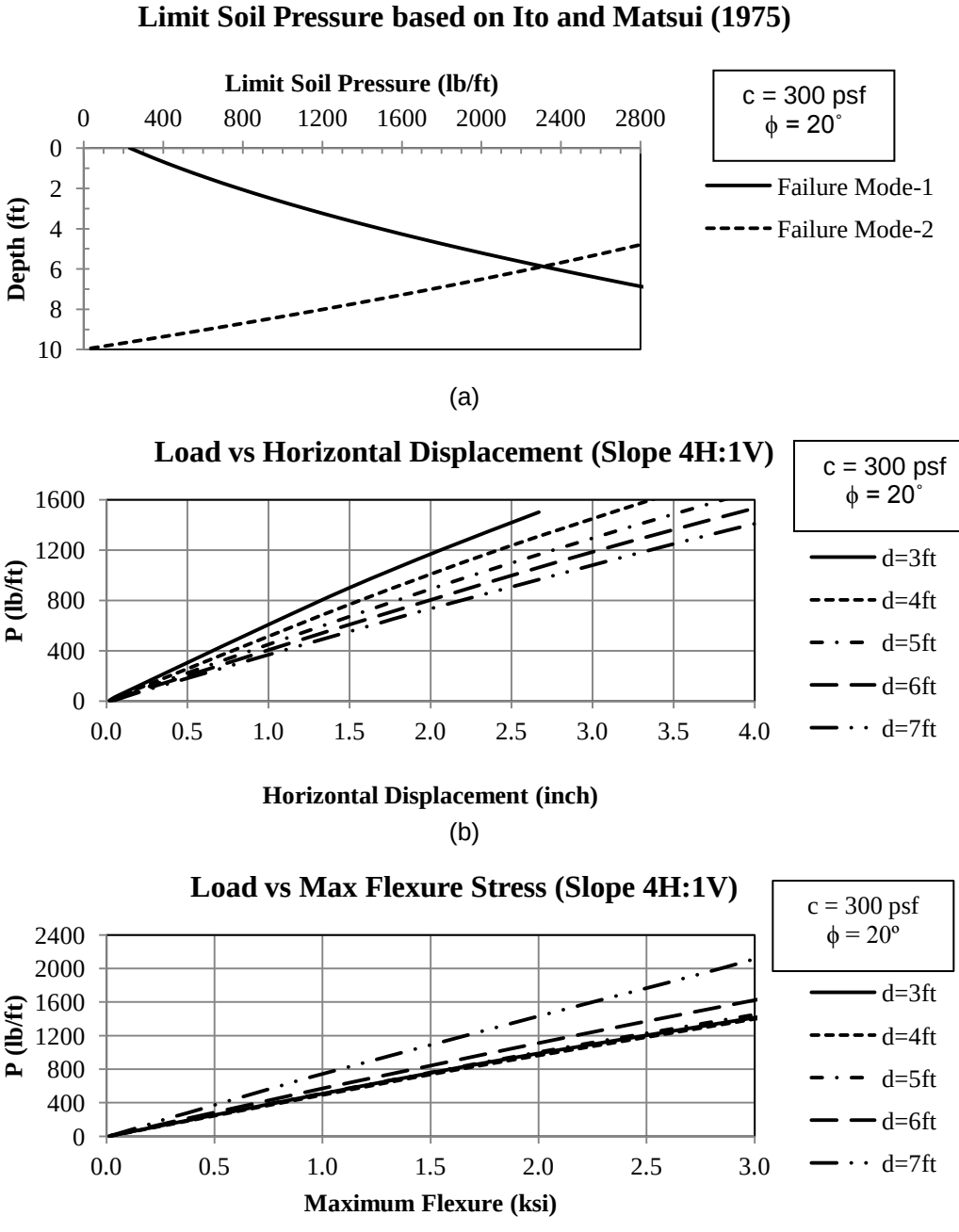


Figure B29 Design Chart for c = 300 psf and ϕ = 20˚, a. Limit soil curve, b. Load vs Horizontal Displacement for slope 4H:1V, c. Load vs Maximum Flexure for slope 4H:1V

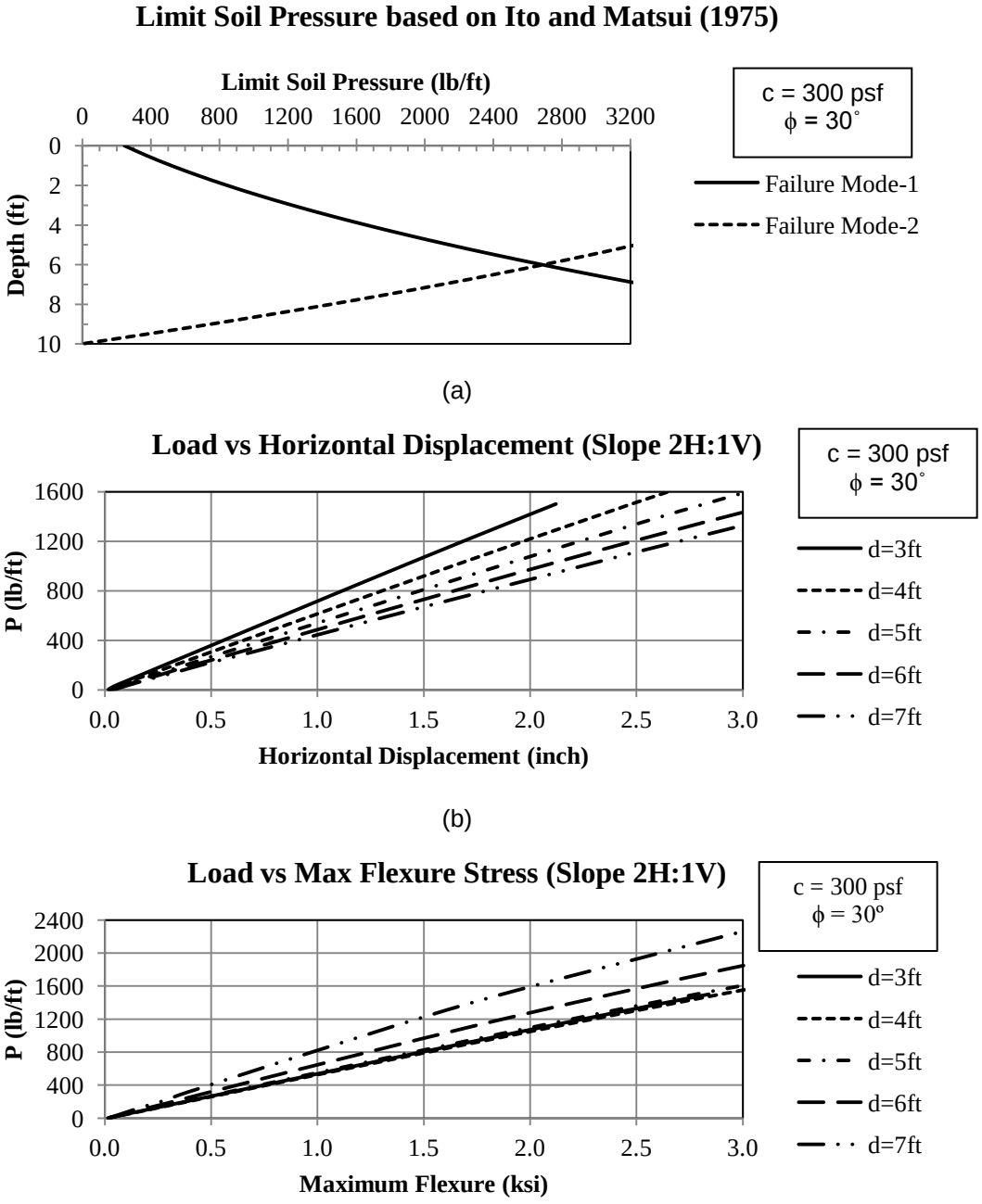


Figure B30 Design Chart for c = 300 psf and ϕ = 30˚, a. Limit soil curve, b. Load vs Horizontal Displacement for slope 2H:1V, c. Load vs Maximum Flexure for slope 2H:1V

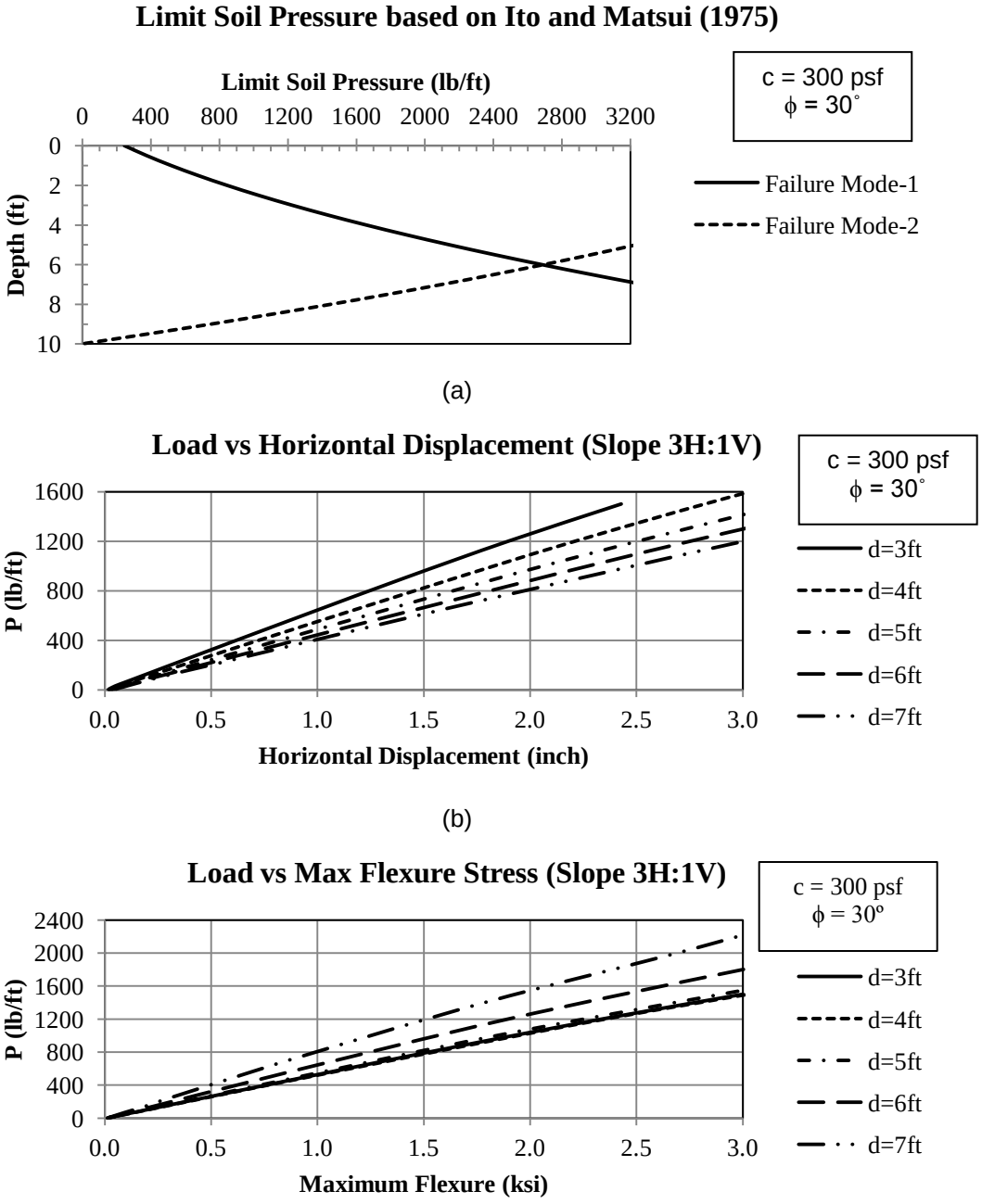


Figure B31 Design Chart for c = 300 psf and ϕ = 30˚, a. Limit soil curve, b. Load vs Horizontal Displacement for slope 3H:1V, c. Load vs Maximum Flexure for slope 3H:1V

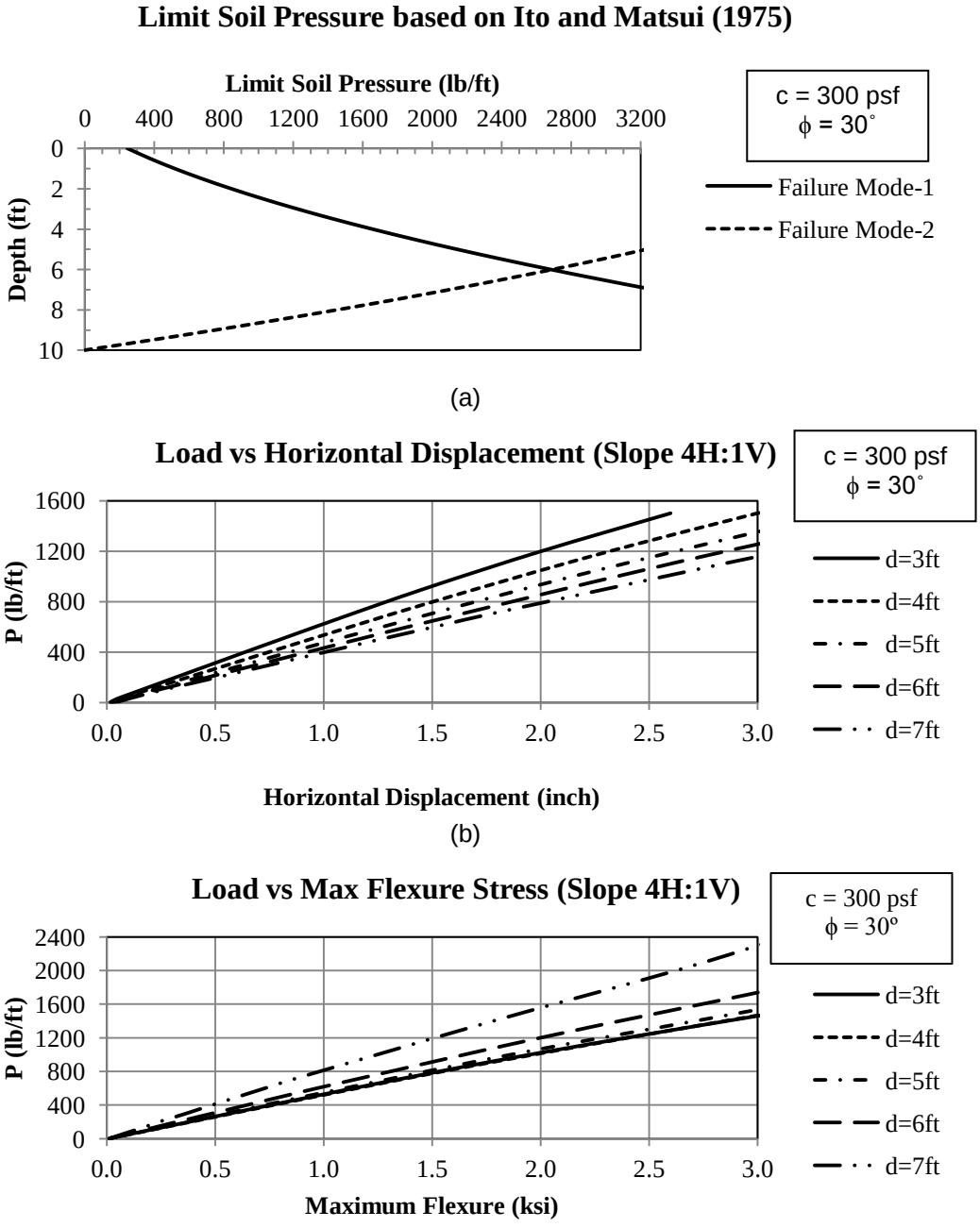


Figure B32 Design Chart for c = 300 psf and ϕ = 30˚, a. Limit soil curve, b. Load vs Horizontal Displacement for slope 4H:1V, c. Load vs Maximum Flexure for slope 4H:1V

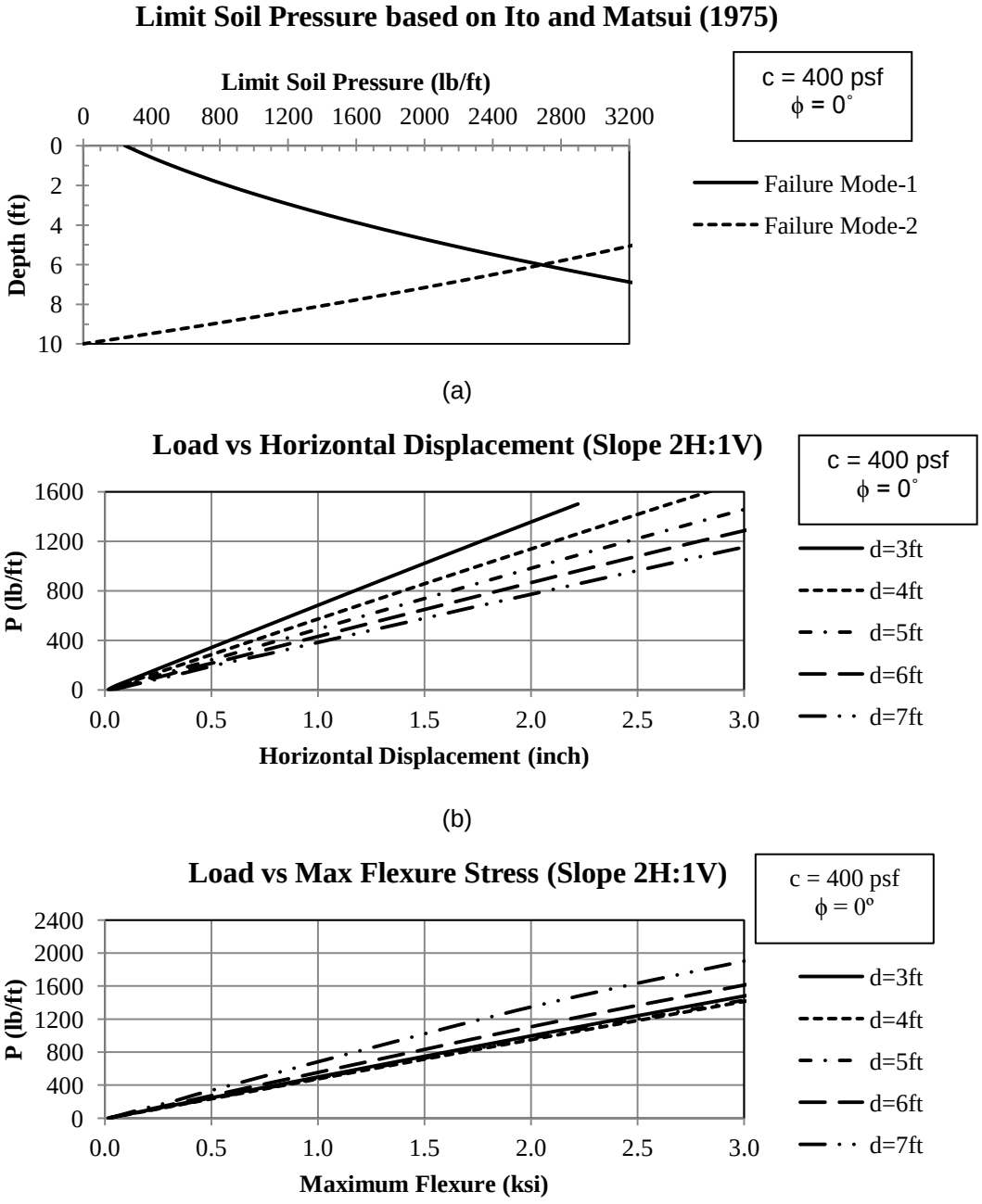


Figure B33 Design Chart for c = 400 psf and $\phi = 0^{\circ}$, a. Limit soil curve, b. Load vs Horizontal Displacement for slope 2H:1V, c. Load vs Maximum Flexure for slope 2H:1V

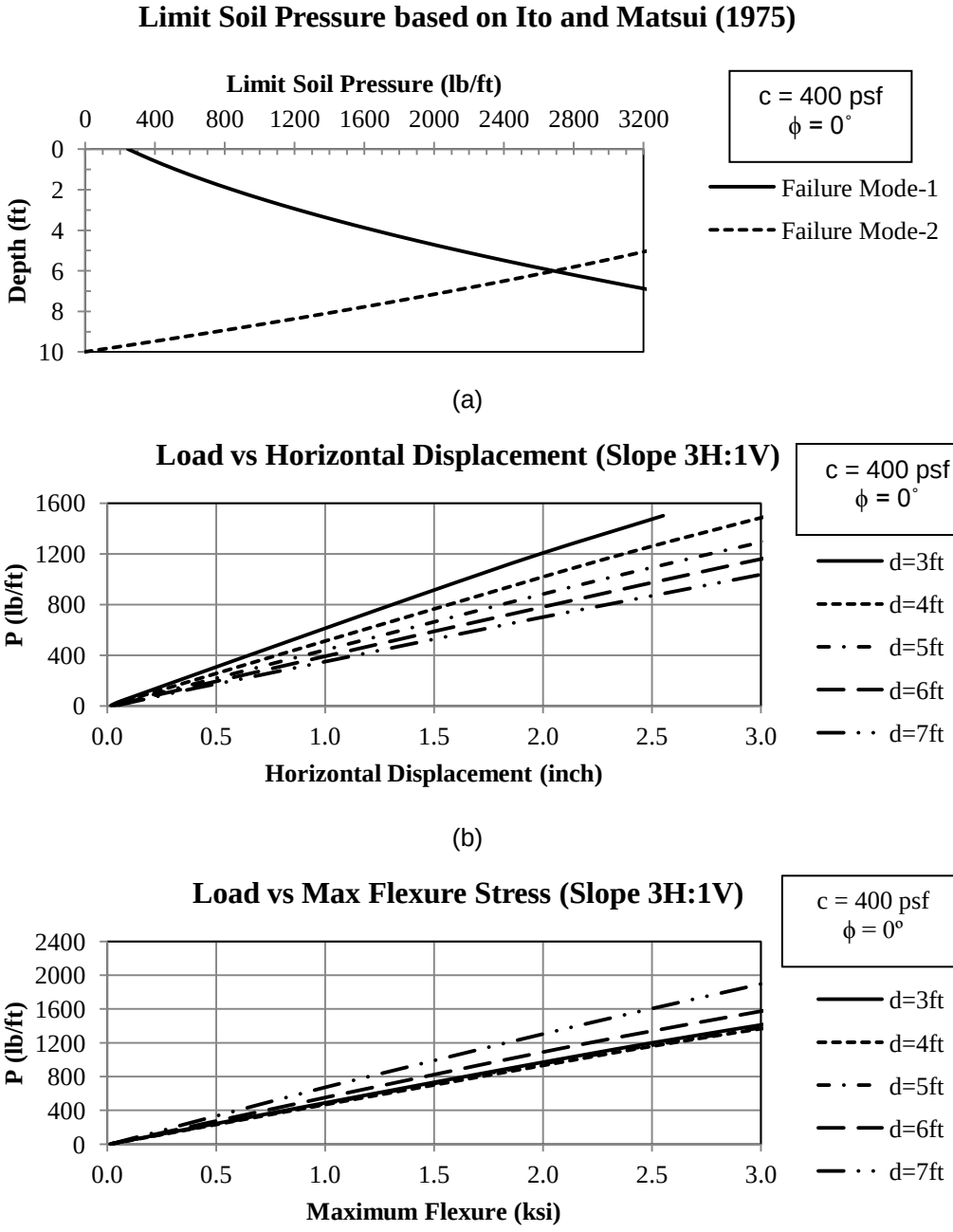


Figure B34 Design Chart for c = 400 psf and $\phi = 0^{\circ}$, a. Limit soil curve, b. Load vs Horizontal Displacement for slope 3H:1V, c. Load vs Maximum Flexure for slope 3H:1V

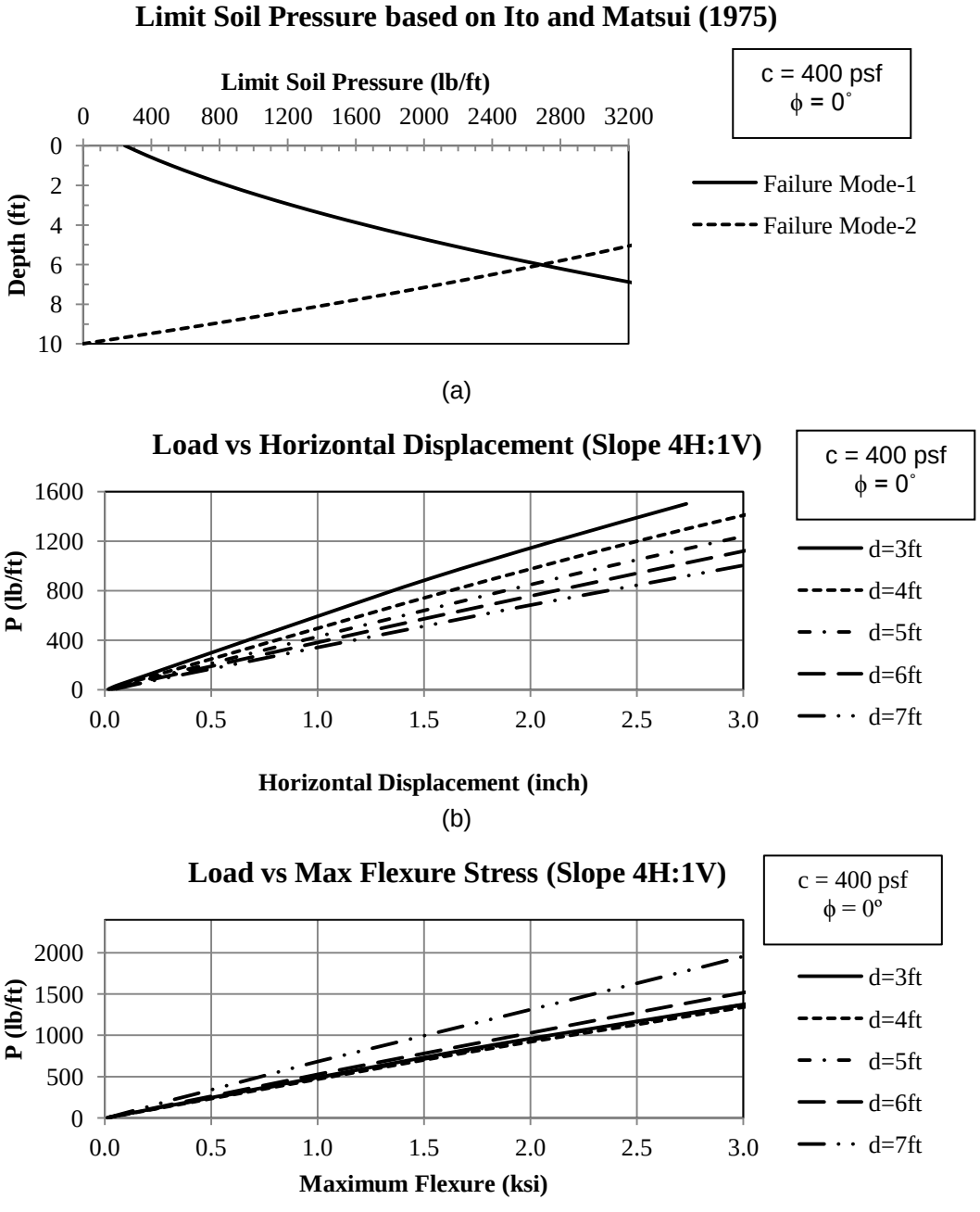


Figure B35 Design Chart for c = 400 psf and $\phi = 0^{\circ}$, a. Limit soil curve, b. Load vs Horizontal Displacement for slope 4H:1V, c. Load vs Maximum Flexure for slope 4H:1V

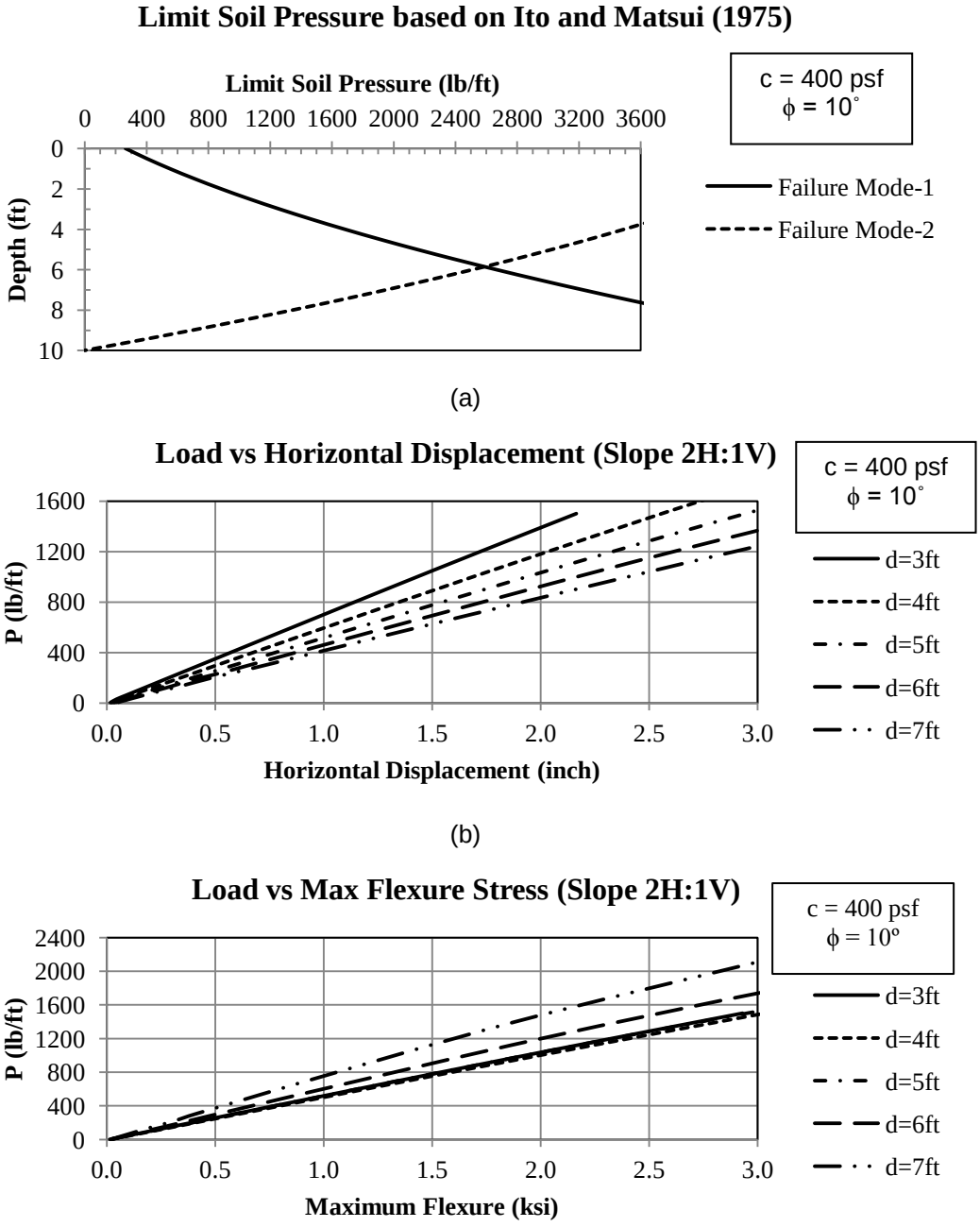


Figure B36 Design Chart for c = 400 psf and ϕ = 10˚, a. Limit soil curve, b. Load vs Horizontal Displacement for slope 2H:1V, c. Load vs Maximum Flexure for slope 2H:1V

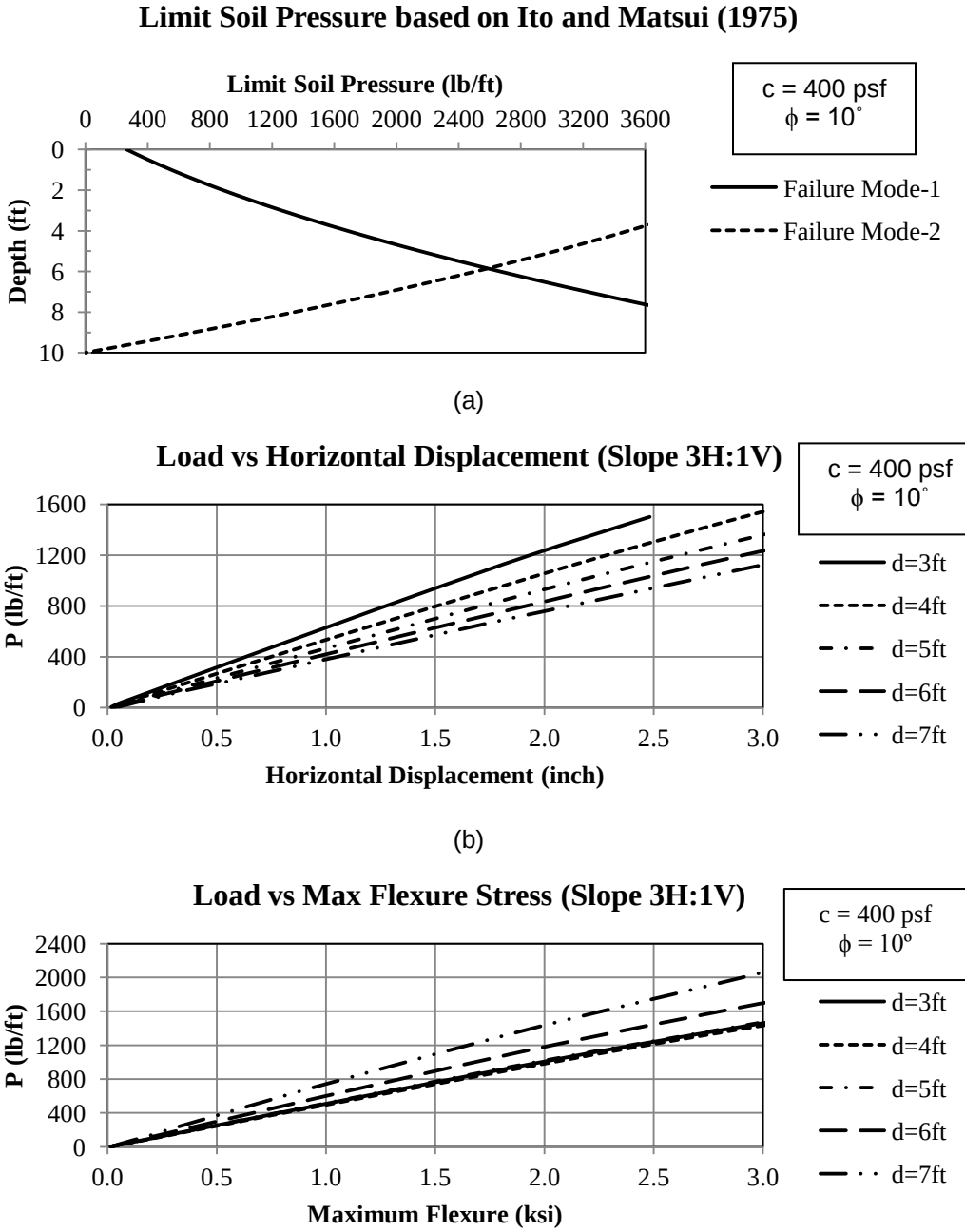


Figure B37 Design Chart for c = 400 psf and ϕ = 10˚, a. Limit soil curve, b. Load vs Horizontal Displacement for slope 3H:1V, c. Load vs Maximum Flexure for slope 3H:1V

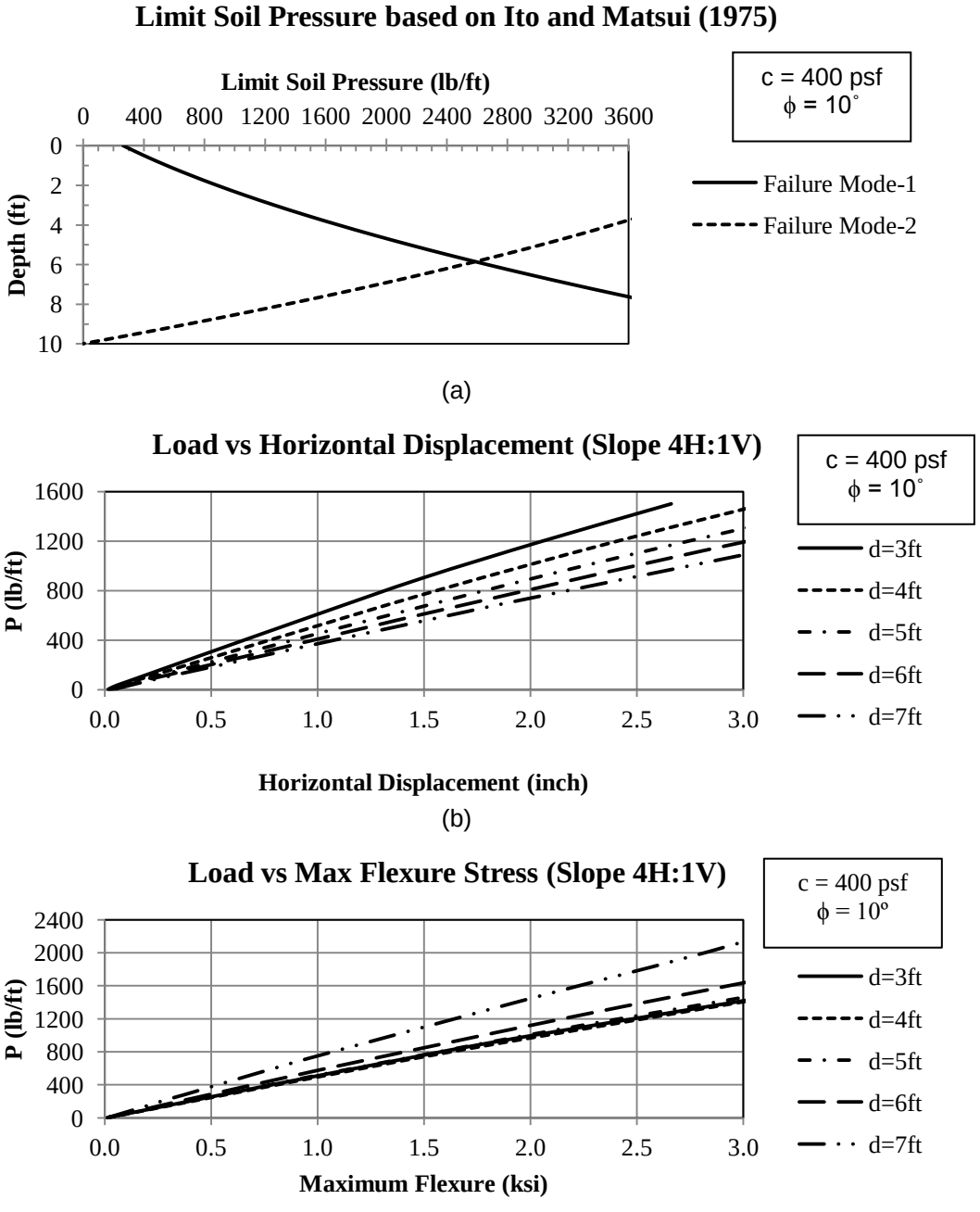


Figure B38 Design Chart for c = 400 psf and ϕ = 10˚, a. Limit soil curve, b. Load vs Horizontal Displacement for slope 4H:1V, c. Load vs Maximum Flexure for slope 4H:1V

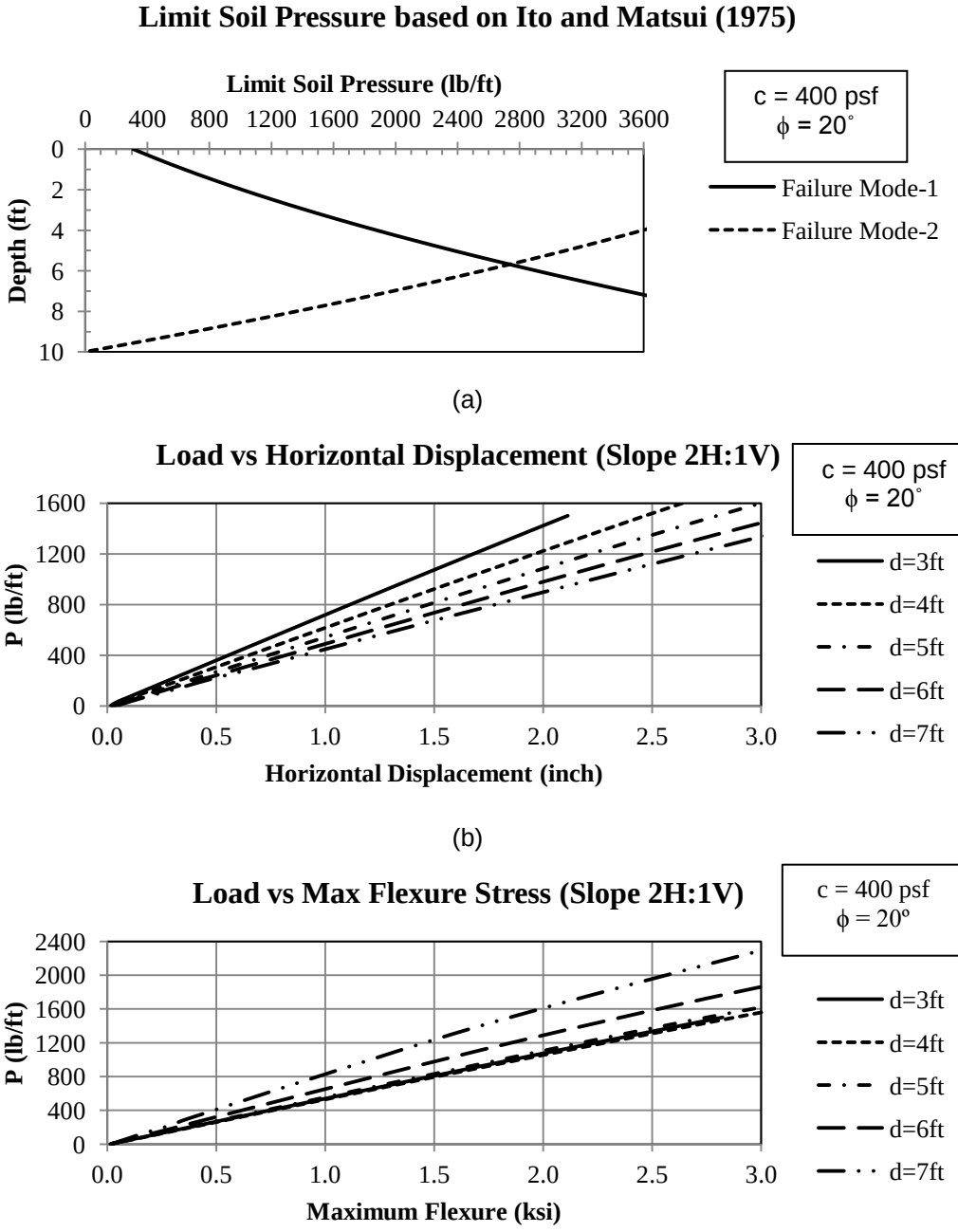


Figure B39 Design Chart for c = 400 psf and ϕ = 20˚, a. Limit soil curve, b. Load vs Horizontal Displacement for slope 2H:1V, c. Load vs Maximum Flexure for slope 2H:1V

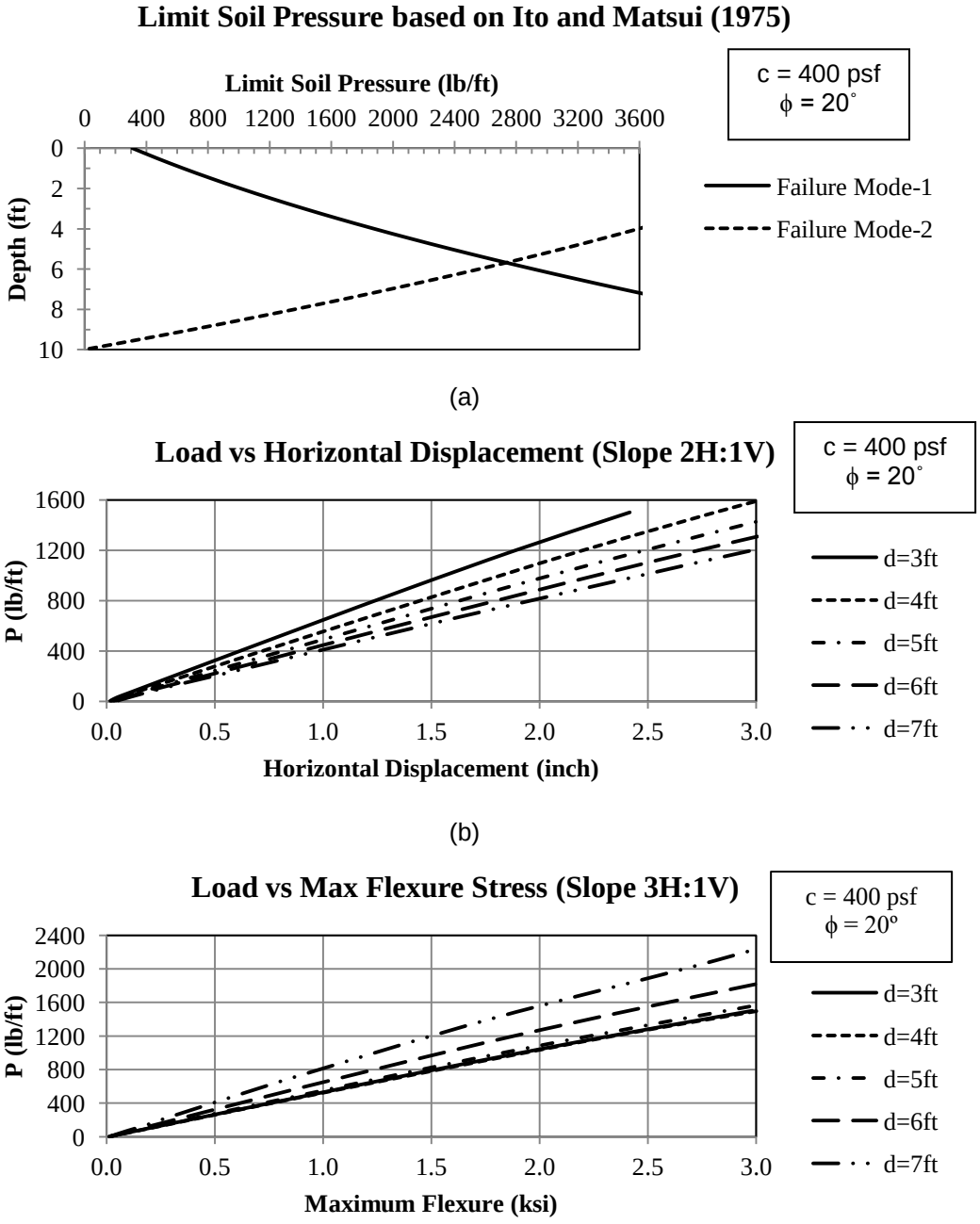


Figure B40 Design Chart for c = 400 psf and ϕ = 20˚, a. Limit soil curve, b. Load vs Horizontal Displacement for slope 3H:1V, c. Load vs Maximum Flexure for slope 3H:1V

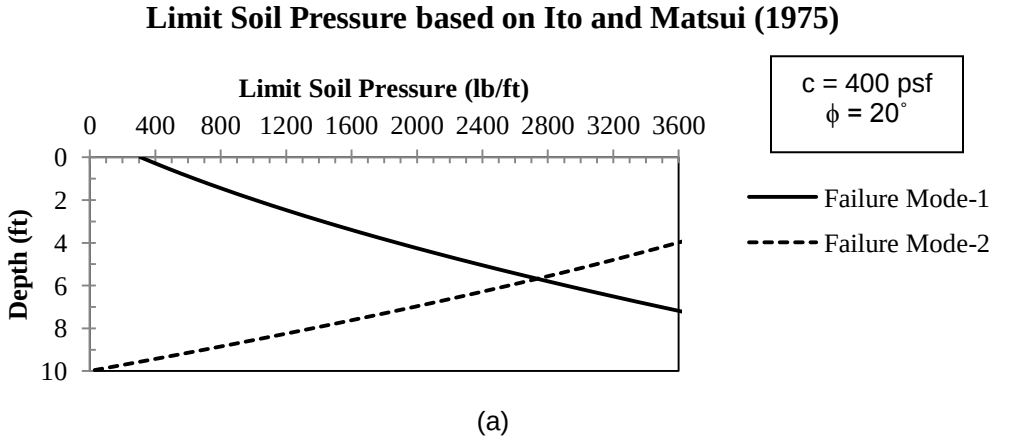


(a)

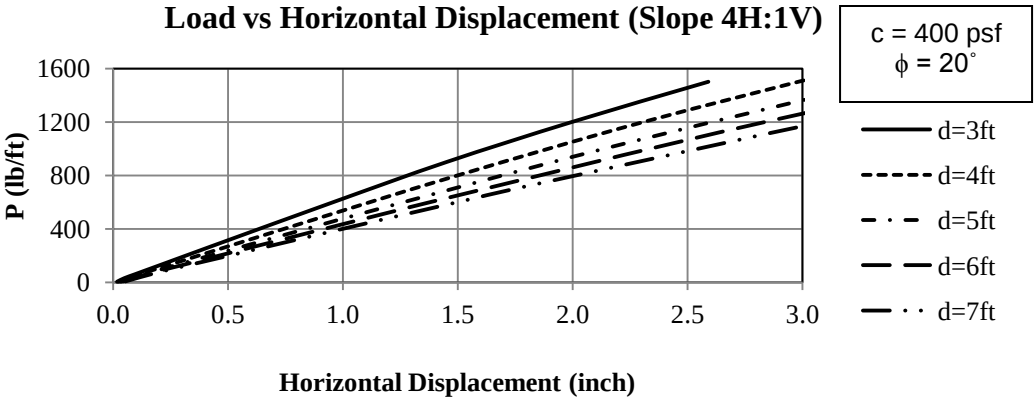


(b)

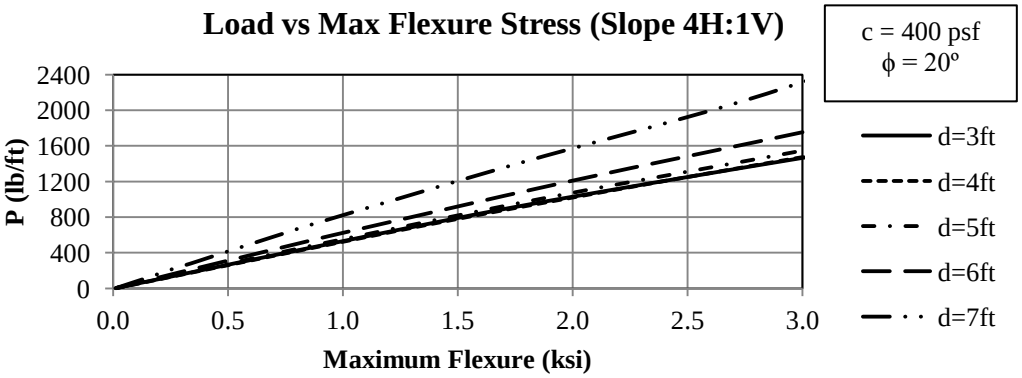


(c)

Figure B41 Design Chart for c = 400 psf and ϕ = 20˚, a. Limit soil curve, b. Load vs Horizontal Displacement for slope 4H:1V, c. Load vs Maximum Flexure for slope 4H:1V

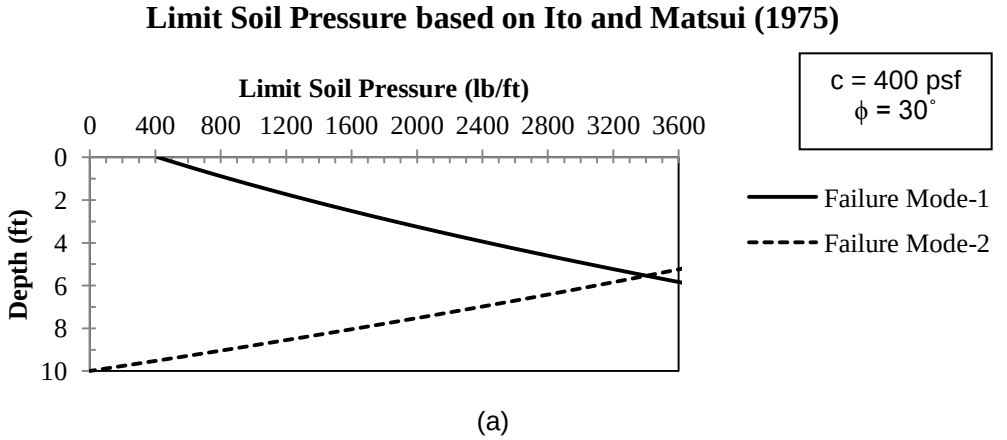


(a)

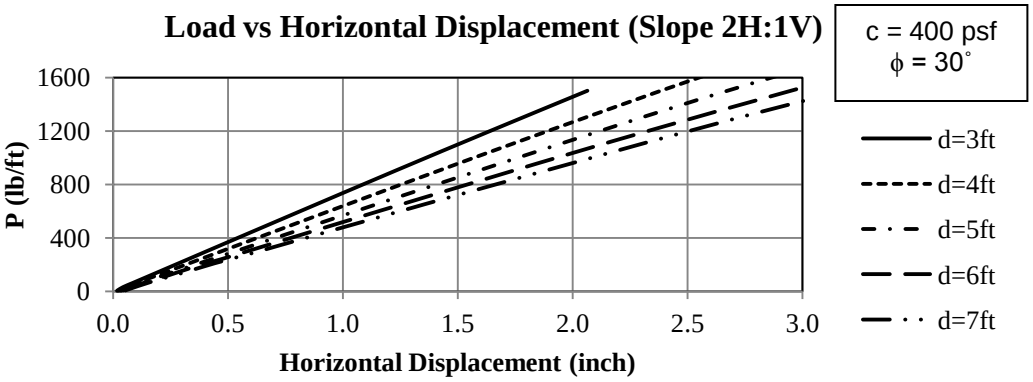


(b)

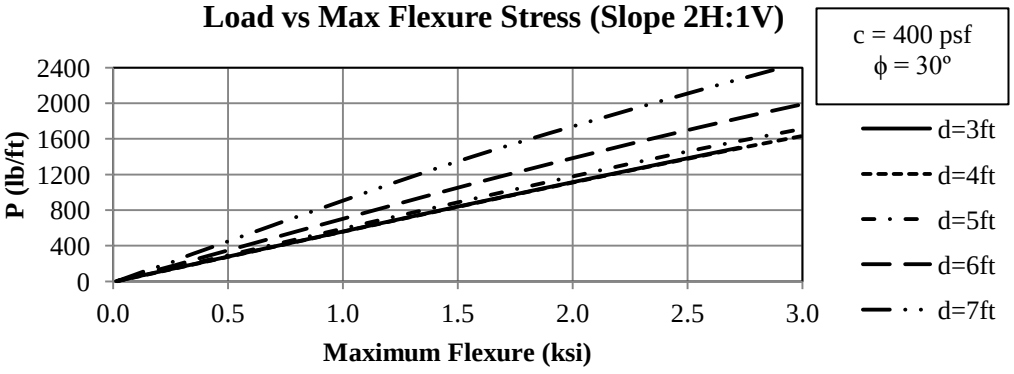


(c)

Figure B42 Design Chart for c = 400 psf and ϕ = 30˚, a. Limit soil curve, b. Load vs Horizontal Displacement for slope 2H:1V, c. Load vs Maximum Flexure for slope 2H:1V

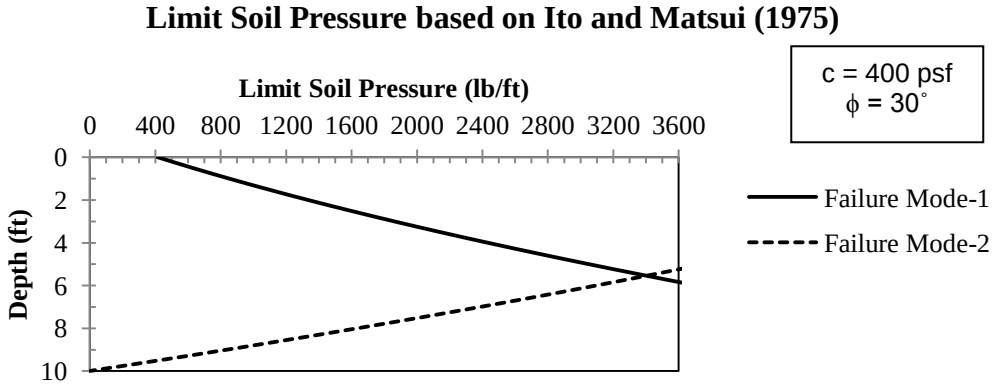


(a)

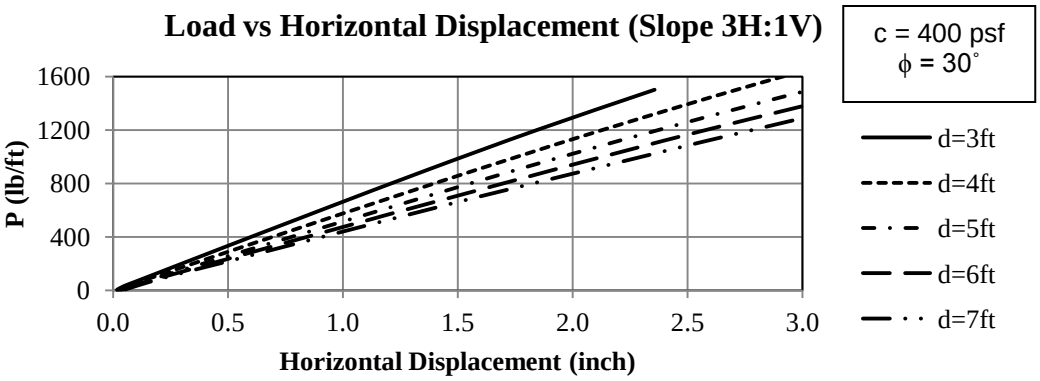


(b)

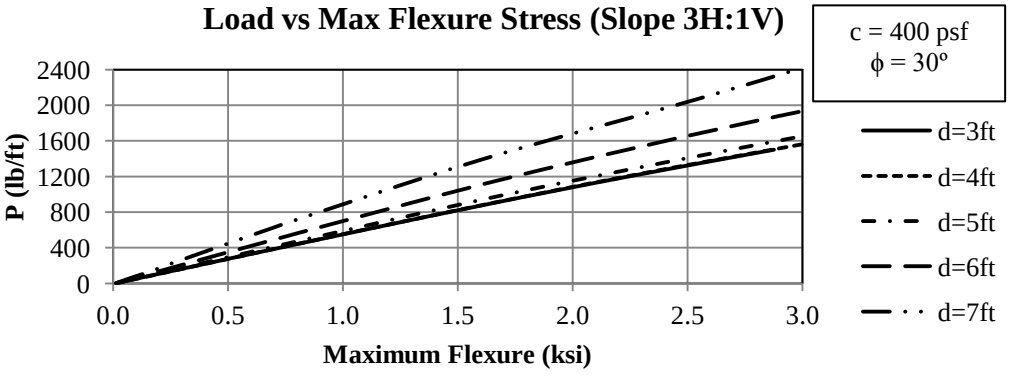


(c)

Figure B43 Design Chart for c = 400 psf and ϕ = 30˚, a. Limit soil curve, b. Load vs Horizontal Displacement for slope 3H:1V, c. Load vs Maximum Flexure for slope 3H:1V

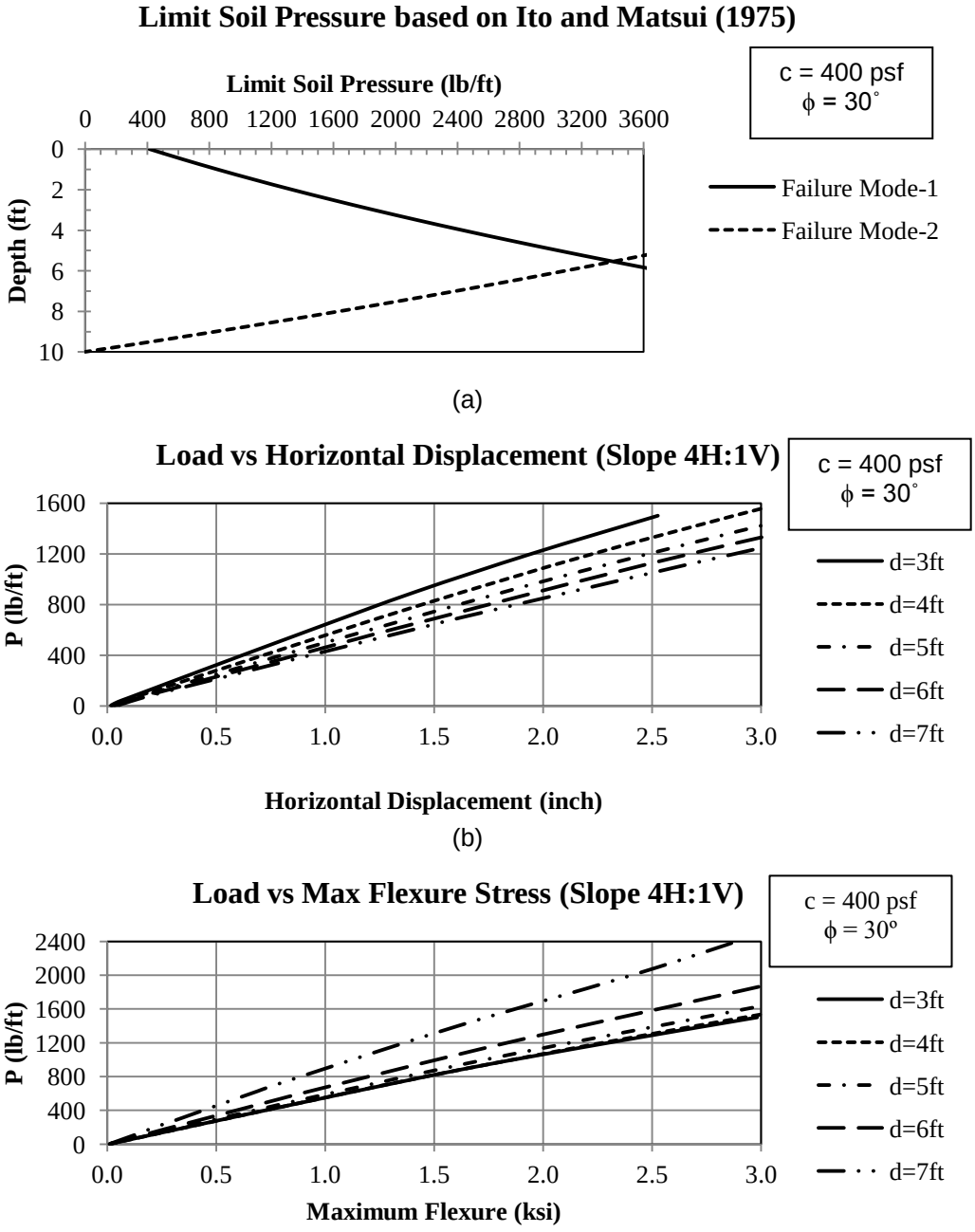


Figure B44 Design Chart for c = 400 psf and ϕ = 30˚, a. Limit soil curve, b. Load vs Horizontal Displacement for slope 4H:1V, c. Load vs Maximum Flexure for slope 4H:1V

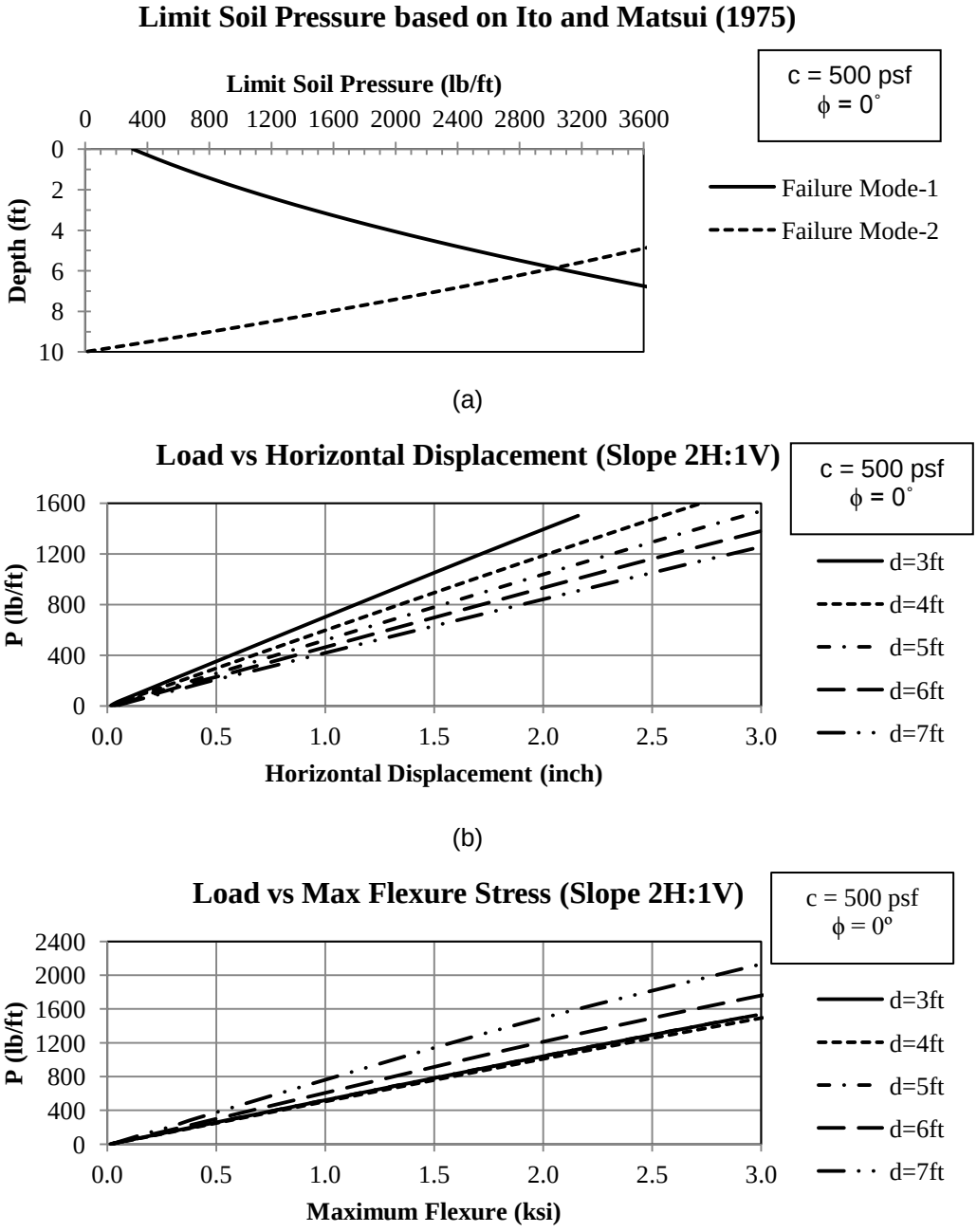


Figure B45 Design Chart for c = 500 psf and $\phi = 0^{\circ}$, a. Limit soil curve, b. Load vs Horizontal Displacement for slope 2H:1V, c. Load vs Maximum Flexure for slope 2H:1V

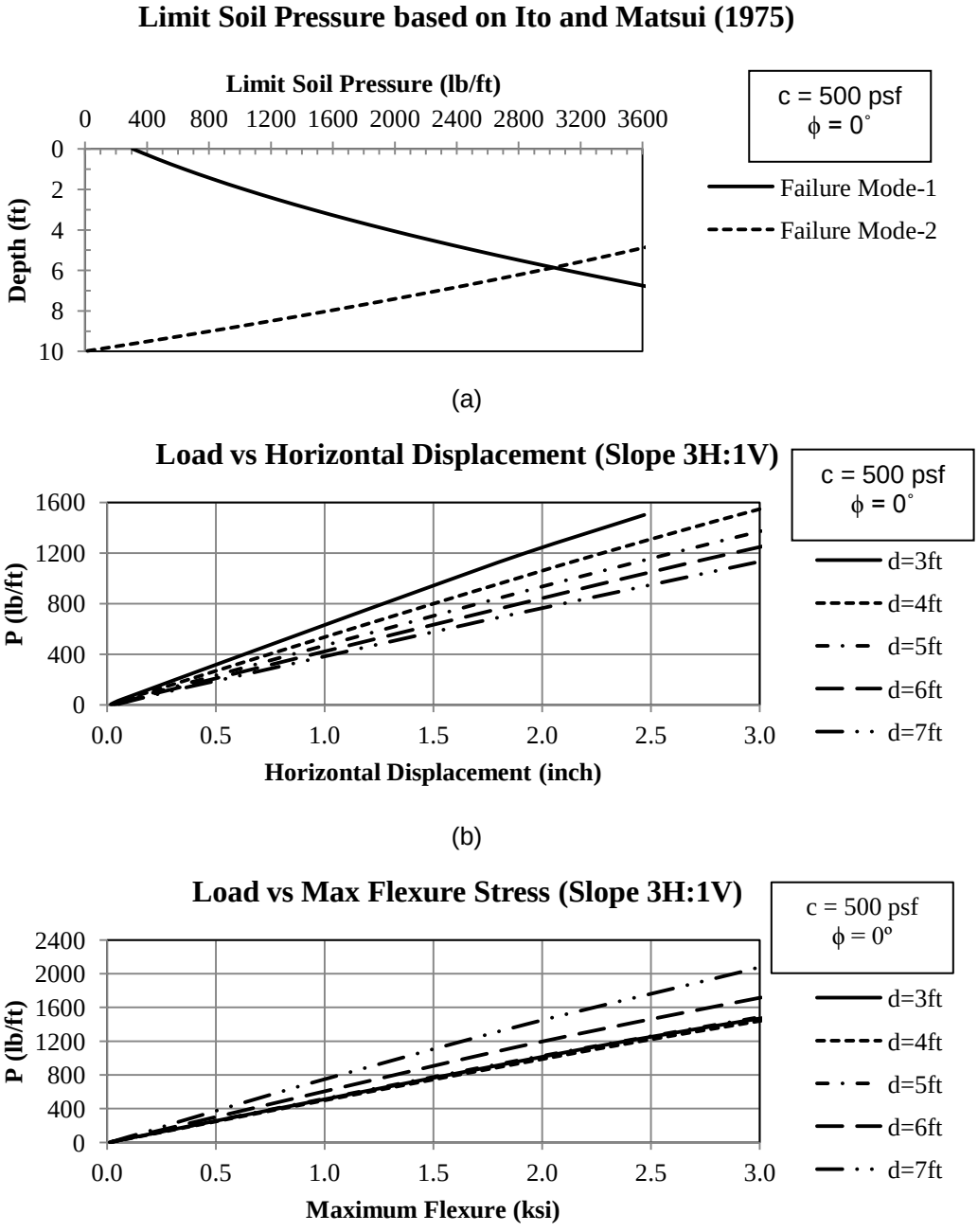


Figure B46 Design Chart for c = 500 psf and $\phi = 0^{\circ}$, a. Limit soil curve, b. Load vs Horizontal Displacement for slope 3H:1V, c. Load vs Maximum Flexure for slope 3H:1V

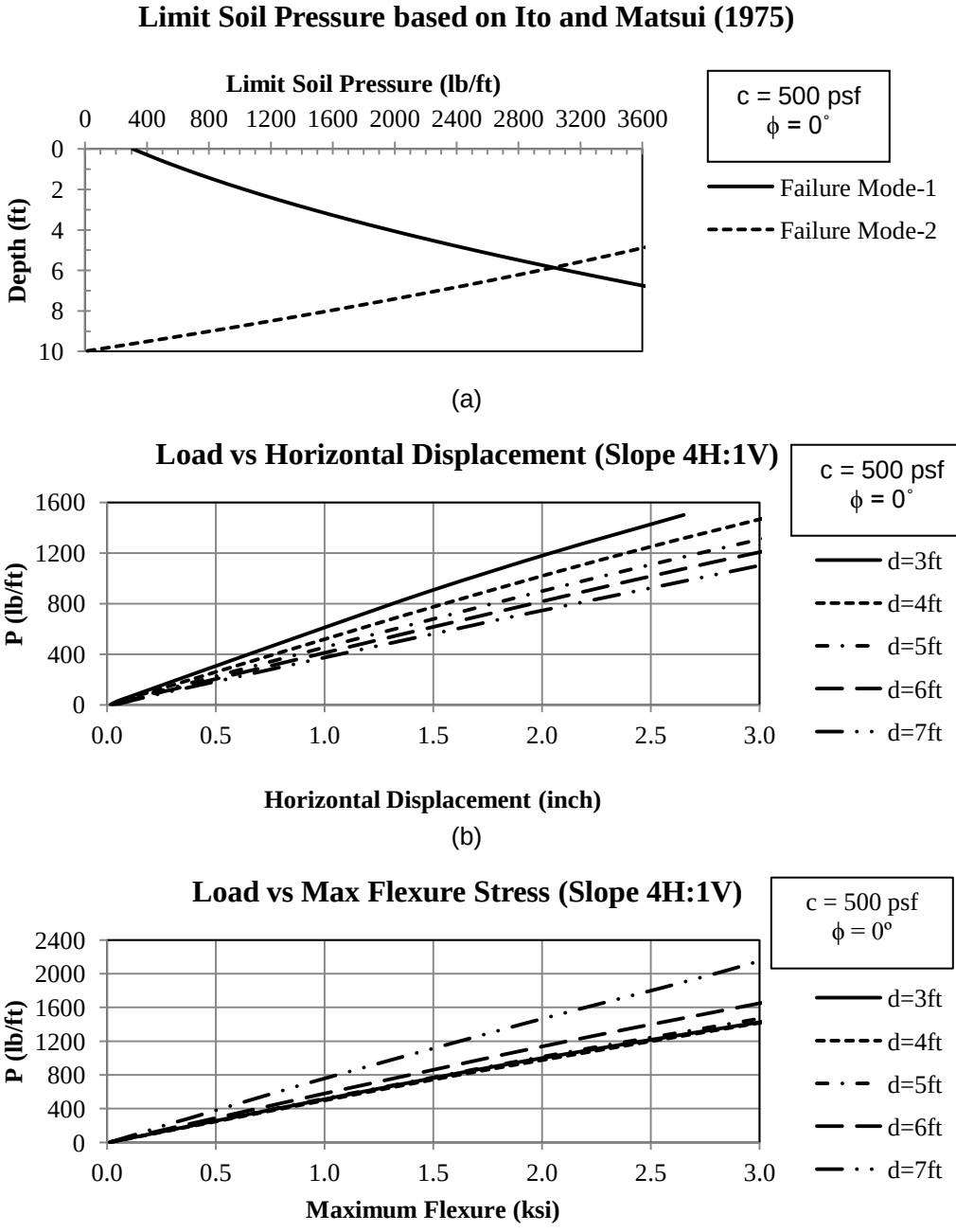


Figure B47 Design Chart for c = 500 psf and $\phi = 0^{\circ}$, a. Limit soil curve, b. Load vs Horizontal Displacement for slope 4H:1V, c. Load vs Maximum Flexure for slope 4H:1V

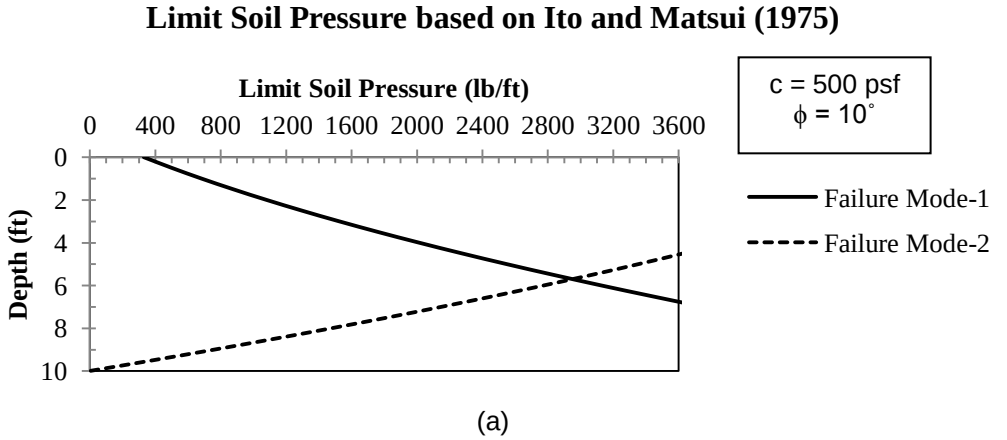


(a)

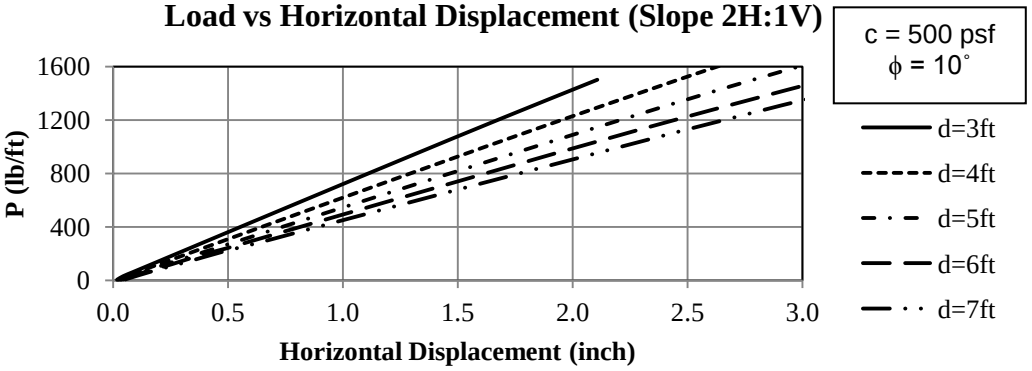


(b)

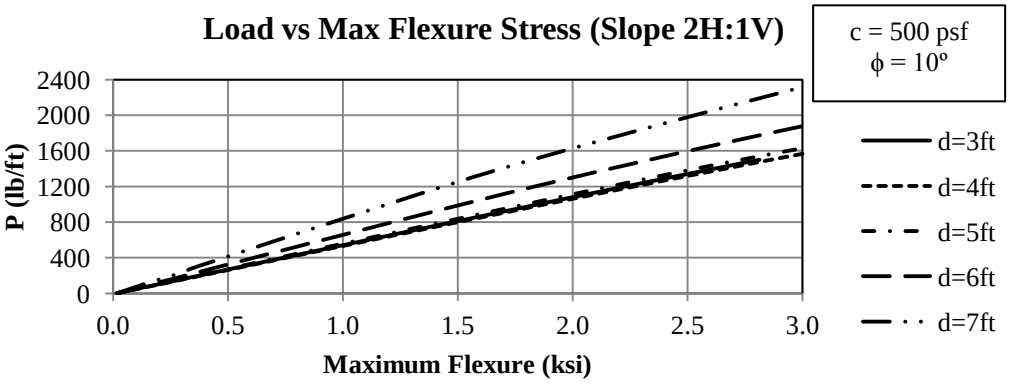


(c)

Figure B48 Design Chart for c = 500 psf and ϕ = 10˚, a. Limit soil curve, b. Load vs Horizontal Displacement for slope 2H:1V, c. Load vs Maximum Flexure for slope 2H:1V

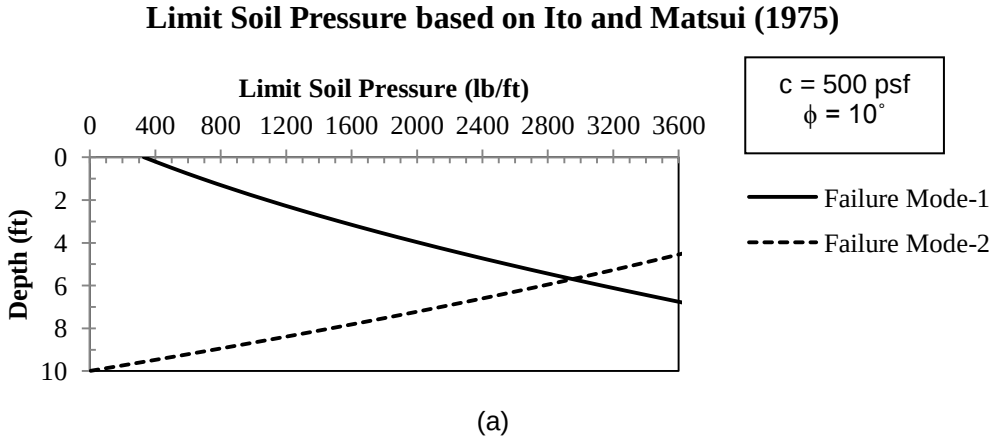


(a)

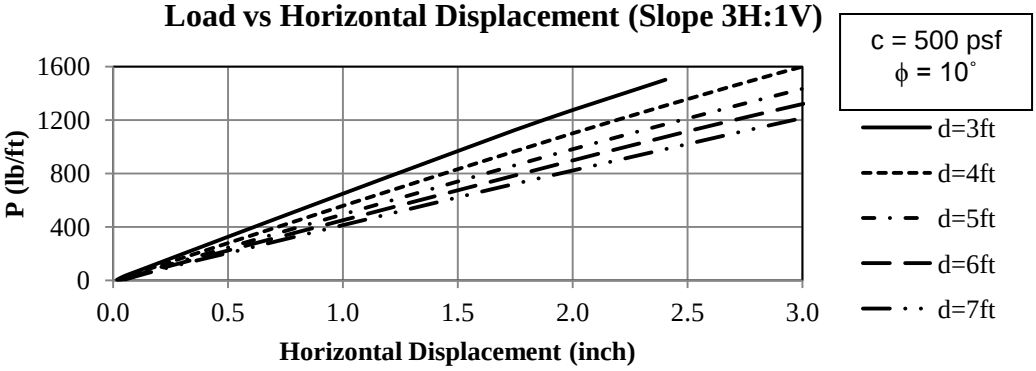


(b)

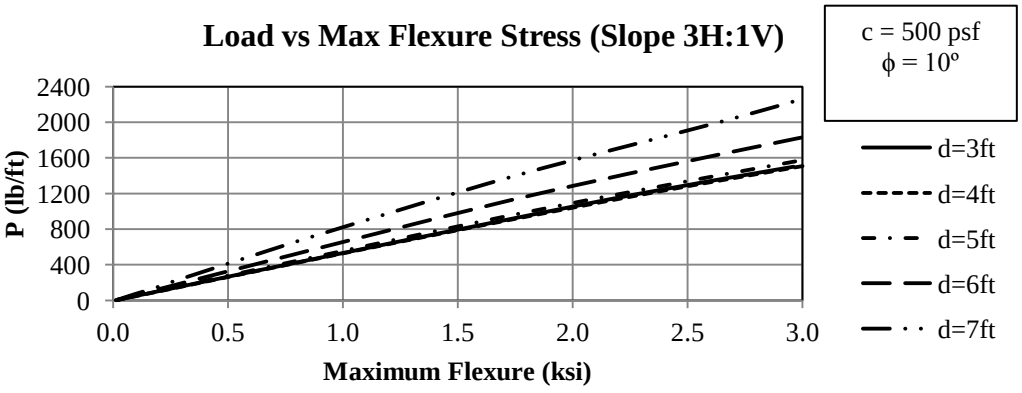


(c)

Figure B49 Design Chart for c = 500 psf and ϕ = 10˚, a. Limit soil curve, b. Load vs Horizontal Displacement for slope 3H:1V, c. Load vs Maximum Flexure for slope 3H:1V

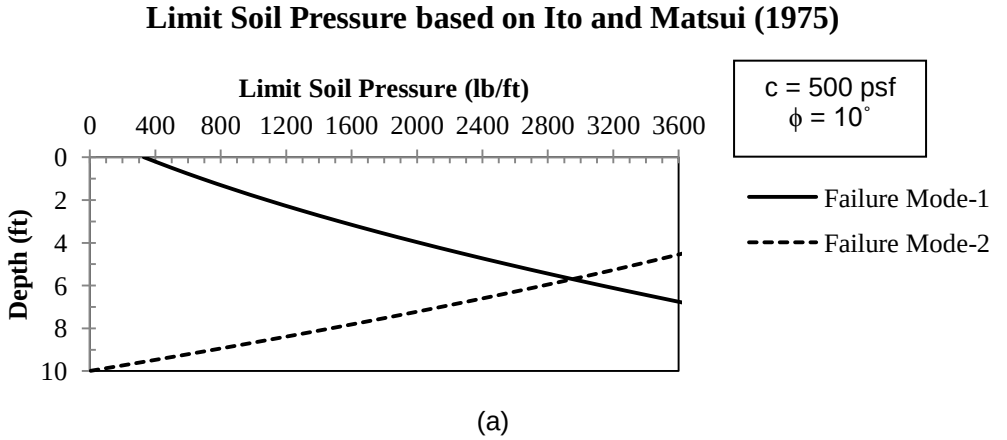


(a)

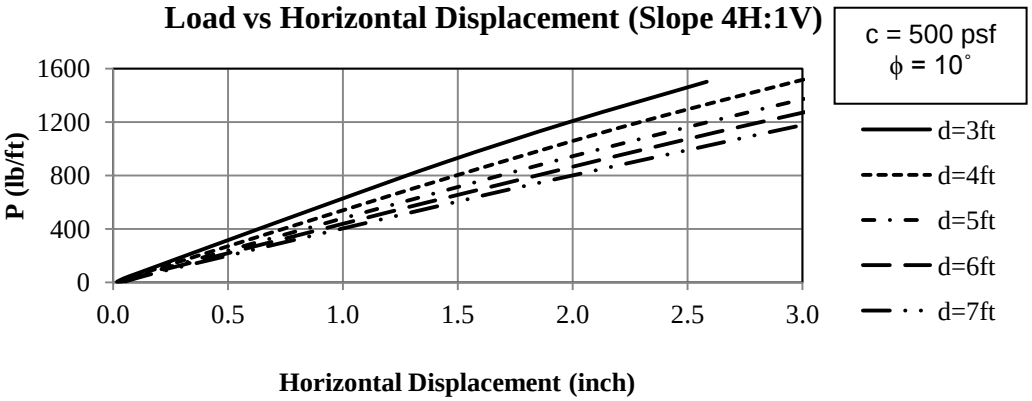


(b)

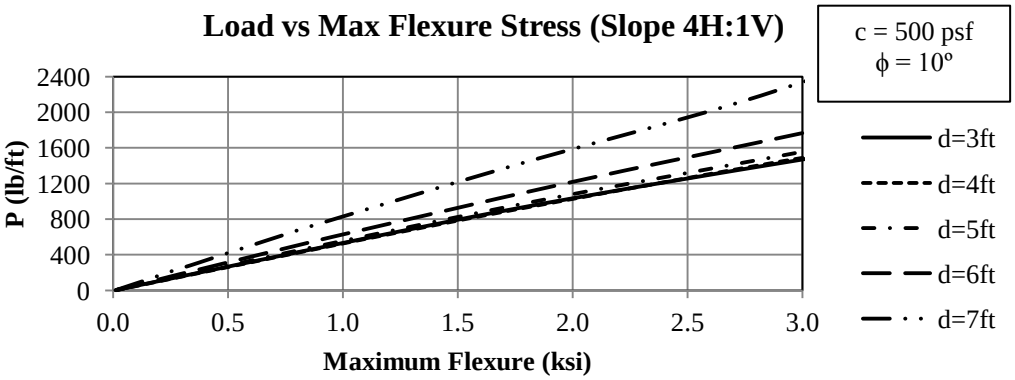


(c)

Figure B50 Design Chart for c = 500 psf and ϕ = 10˚, a. Limit soil curve, b. Load vs Horizontal Displacement for slope 4H:1V, c. Load vs Maximum Flexure for slope 4H:1V

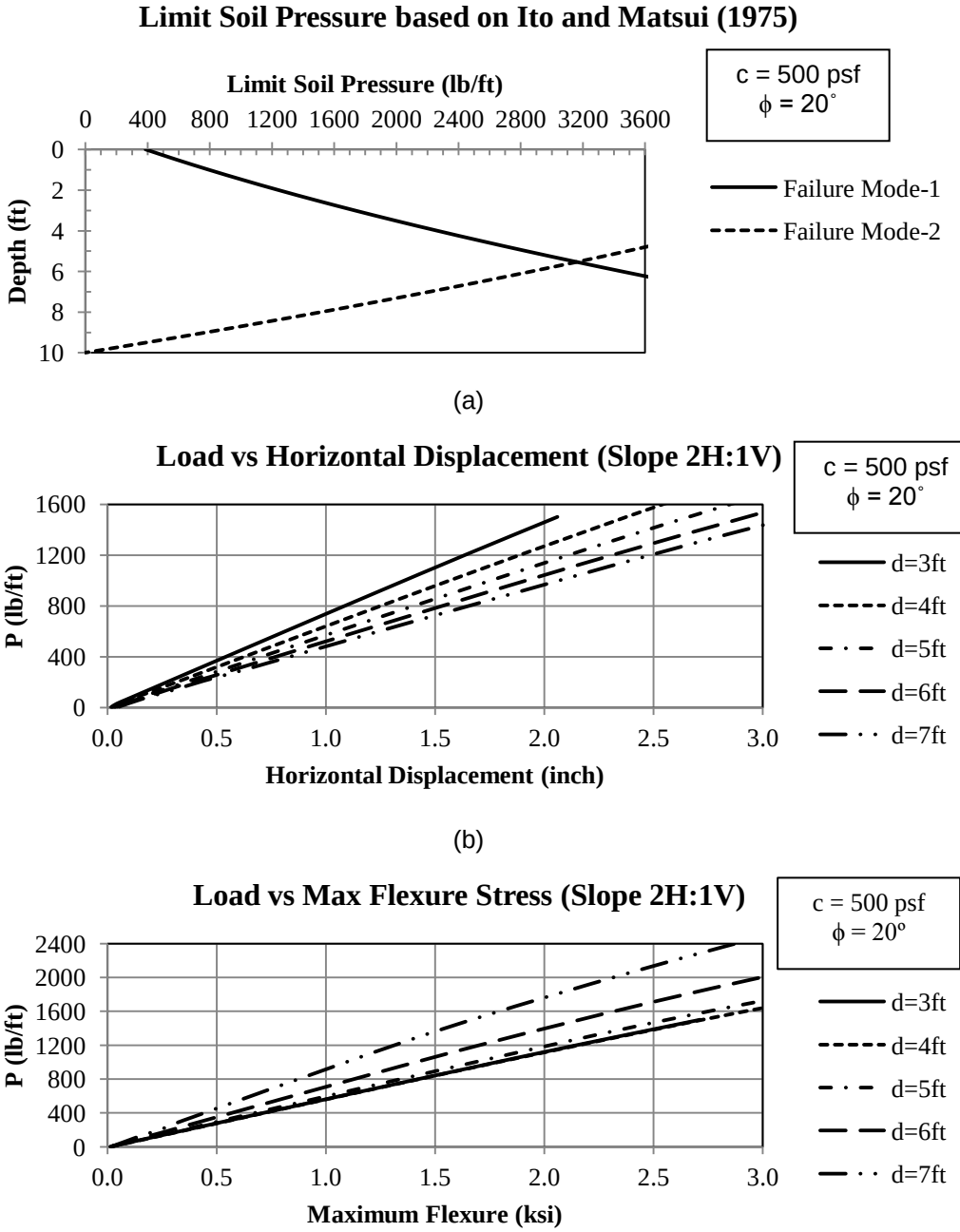


Figure B51 Design Chart for c = 500 psf and ϕ = 20˚, a. Limit soil curve, b. Load vs Horizontal Displacement for slope 2H:1V, c. Load vs Maximum Flexure for slope 2H:1V

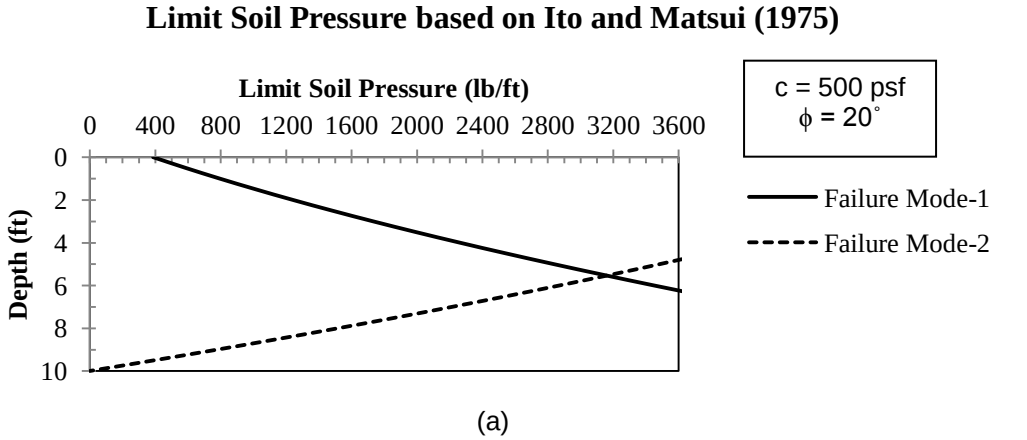


(a)

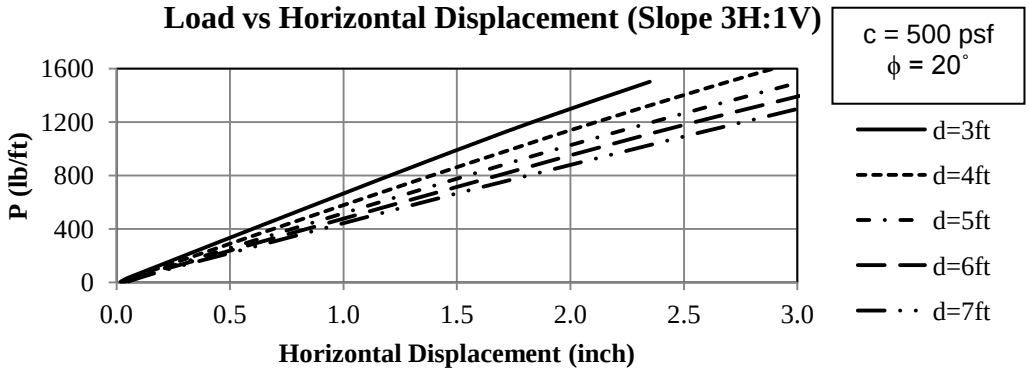


(b)

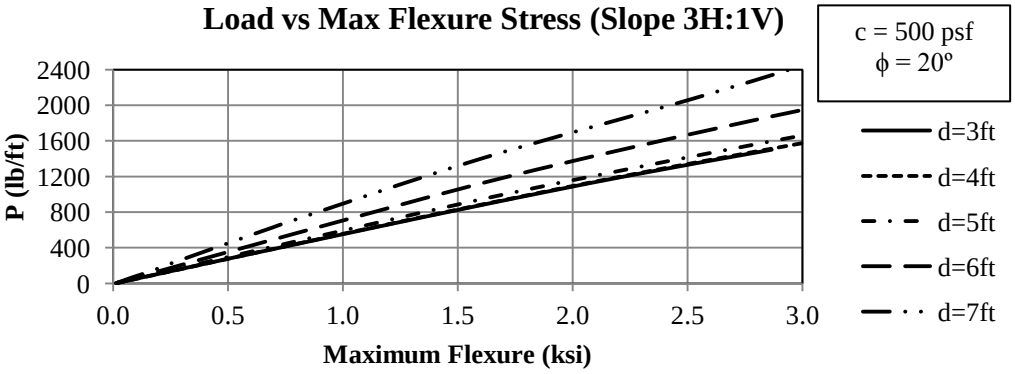


(c)

Figure B52 Design Chart for c = 500 psf and ϕ = 20˚, a. Limit soil curve, b. Load vs Horizontal Displacement for slope 3H:1V, c. Load vs Maximum Flexure for slope 3H:1V

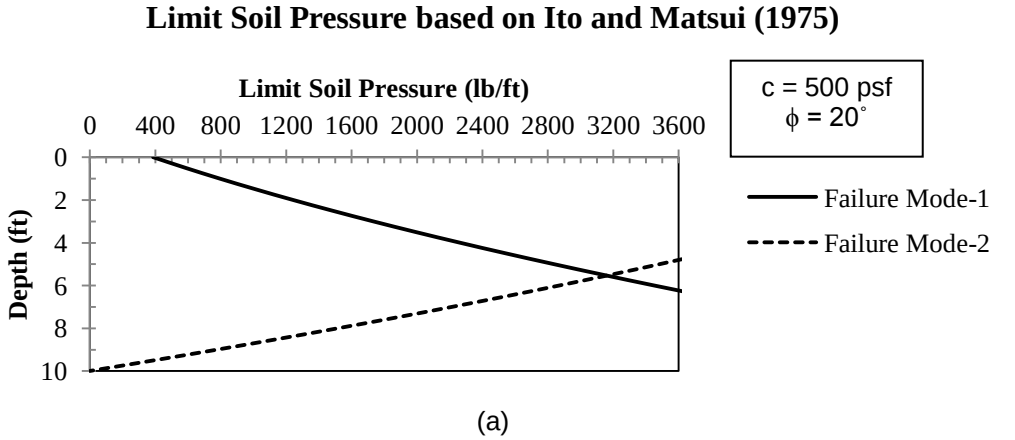


(a)

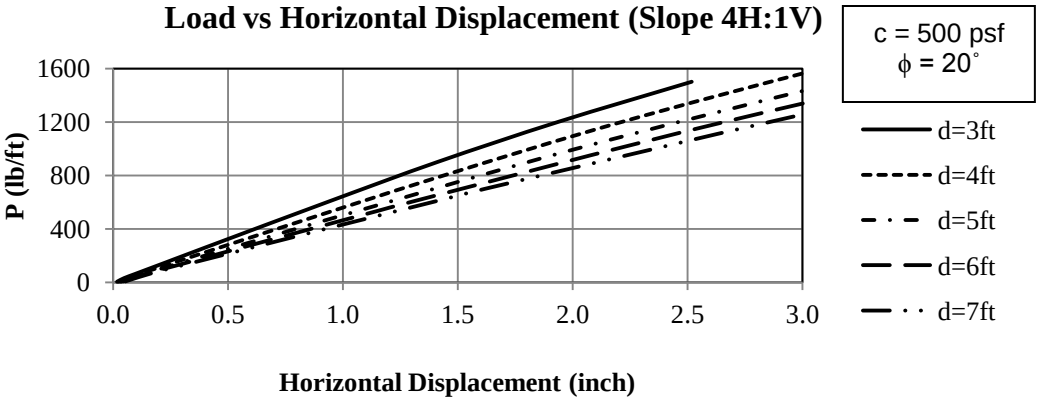


(b)

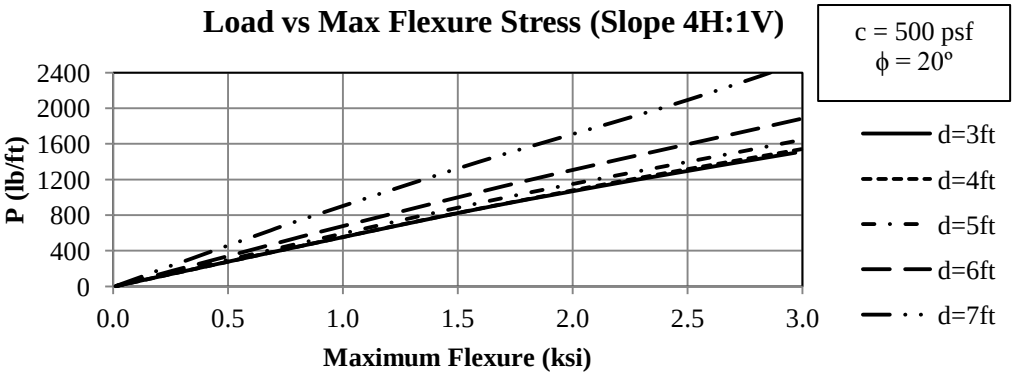


(c)

Figure B53 Design Chart for c = 500 psf and ϕ = 20˚, a. Limit soil curve, b. Load vs Horizontal Displacement for slope 4H:1V, c. Load vs Maximum Flexure for slope 4H:1V

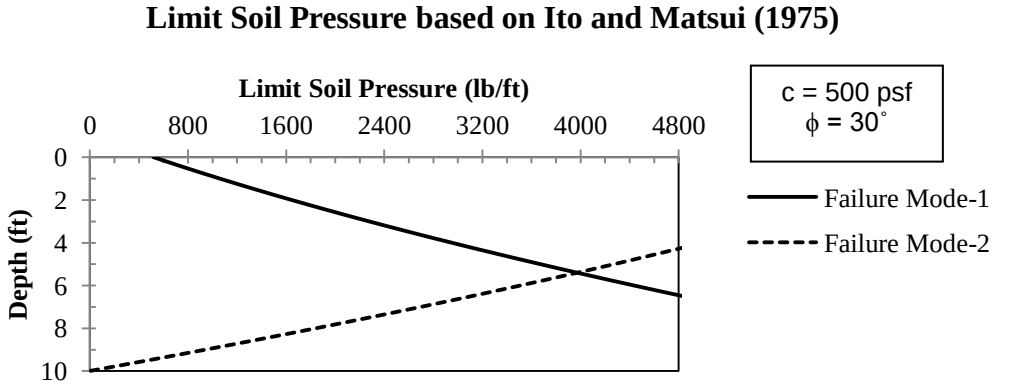


(a)

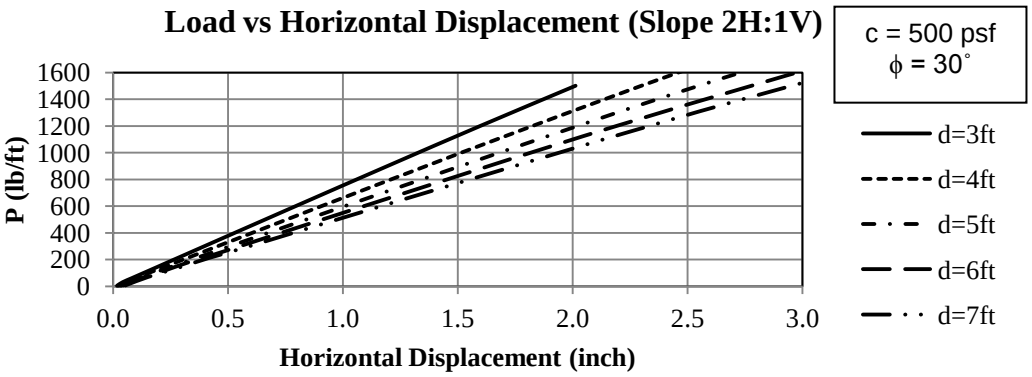


(b)

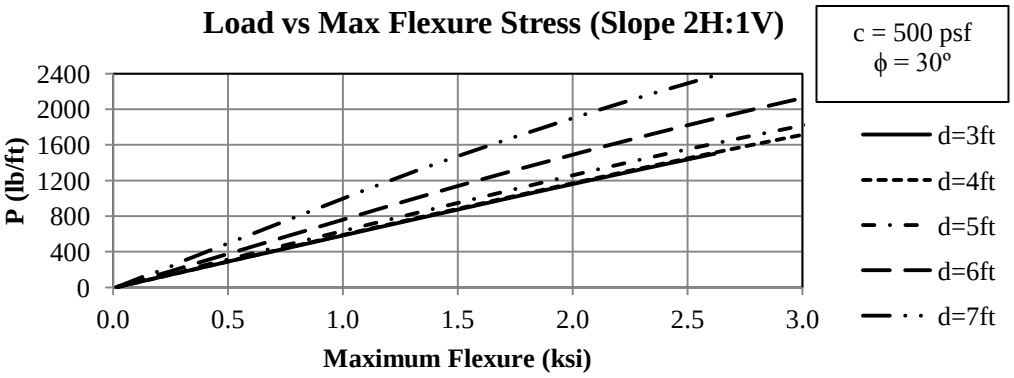


(c)

Figure B54 Design Chart for c = 500 psf and ϕ = 30˚, a. Limit soil curve, b. Load vs Horizontal Displacement for slope 2H:1V, c. Load vs Maximum Flexure for slope 2H:1V

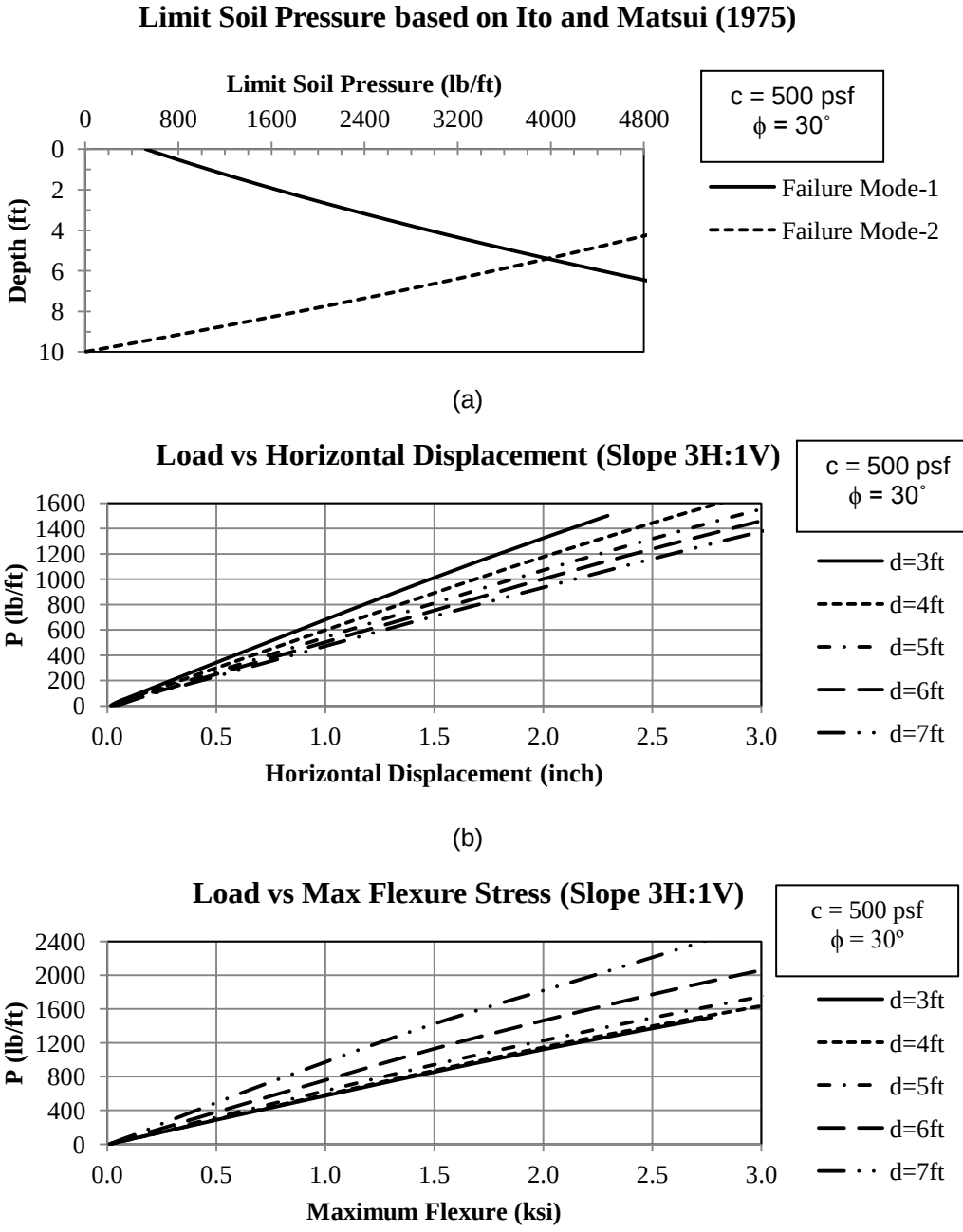


Figure B55 Design Chart for c = 500 psf and ϕ = 30˚, a. Limit soil curve, b. Load vs Horizontal Displacement for slope 3H:1V, c. Load vs Maximum Flexure for slope 3H:1V

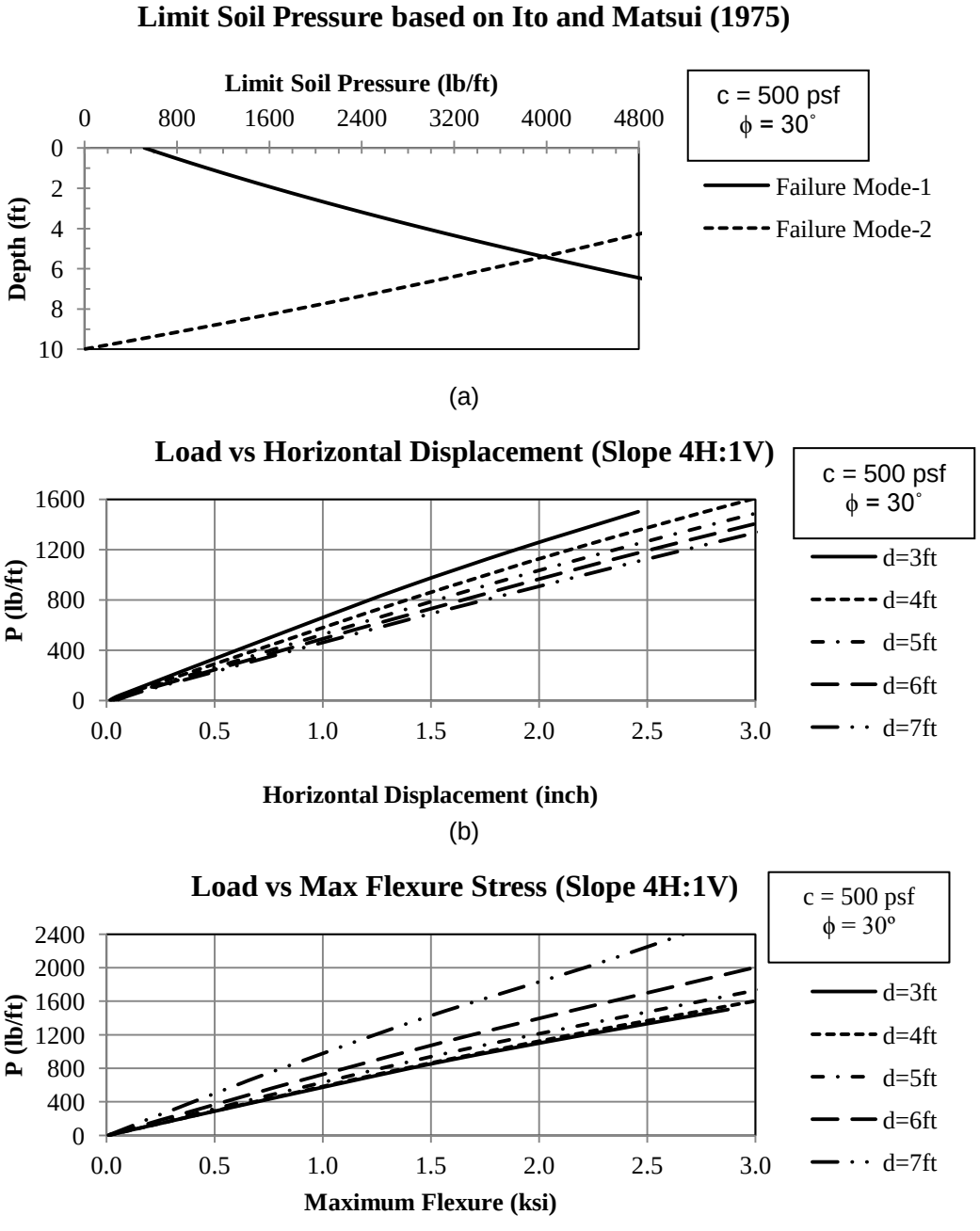


Figure B56 Design Chart for c = 500 psf and ϕ = 30˚, a. Limit soil curve, b. Load vs Horizontal Displacement for slope 4H:1V, c. Load vs Maximum Flexure for slope 4H:1V

# Appendix C

## Sample Calculations

SAMPLE CALCULATION USING ORDINARY METHOD OF SLICE

Problem Definition: The current example presents the hand calculation of the design steps using the US 287 slope geometry and back calculated soil parameter from FEM analysis.

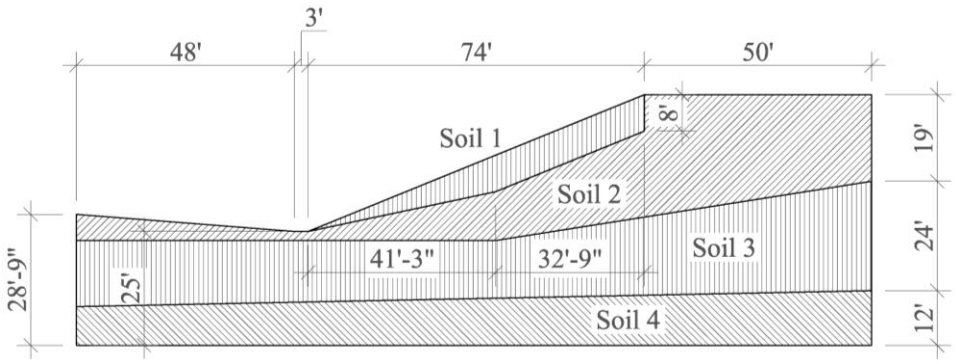


Figure 1 Geometry of the US 287 slope

Table 1 Soil Parameters

| Soil Type | Friction angle φ | Cohesion c | Unit Weight γ |
|---|---|---|---|
| - | ◦ | lb/ft2 | lb/ft3 |
| 1 | 10 | 120 | 125 |
| 2 | 23 | 120 | 125 |
| 3 | 15 | 250 | 130 |
| 4 | 35 | 3000 | 140 |

Step 1: Critical Slope stability analysis using commercially available limit equilibrium method

The geometry with the soil parameters was model in commercially available program GSTABL to determine the critical slip surface and factor of safety. The obtained critical slip surface is presented in Figure 2. In addition, the details of the analysis results are included at the end of this section.

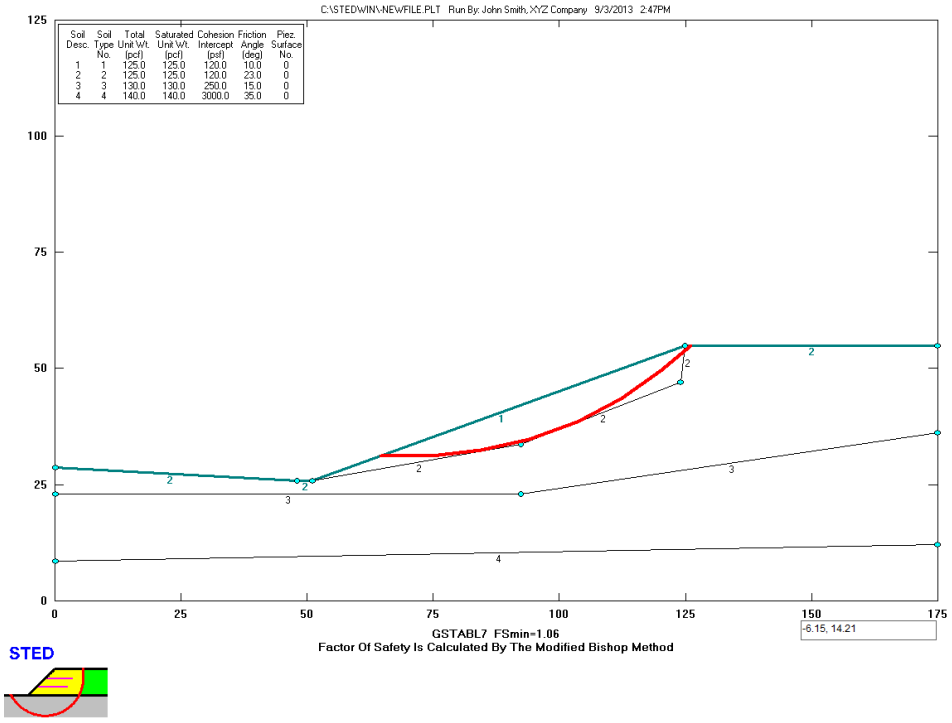


Figure 2 Critical Slip Surface from GSTABL using Modified Bishop method (FS = 1.06)

Step 2: Hand calculation of the unreinforced slope using the ordinary method of slice

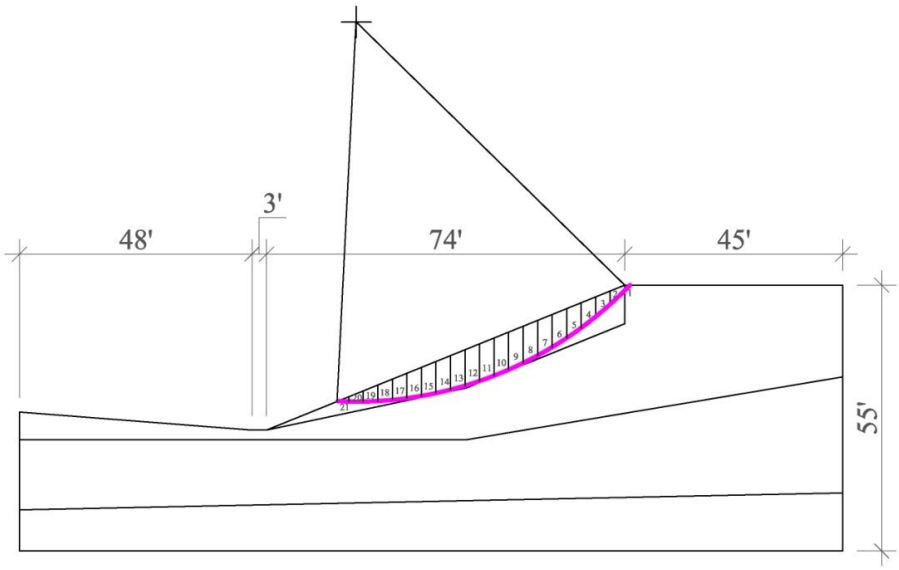


Figure 3 Distribution of slices for hand calculation

Table 2 Detail Calculation of Unreinforced Slope using Ordinary Method of slice

| Slice No | L1 | L2 | β | A | Ɣ | W | α | N | Wsinα | c | φ | cβ+Ntanφ |
|---|---|---|---|---|---|---|---|---|---|---|---|---|
| | ft | ft | ft | ft2 | pcf | lb | deg | lb | lb | psf | deg | lb |
| 1 | 0.00 | 1.08 | 1.08 | 0.59 | 125.00 | 73.31 | 43.00 | 53.61 | 49.99 | 130.00 | 10.00 | 150.24 |
| 2 | 1.08 | 2.75 | 3.00 | 5.75 | 125.00 | 718.69 | 43.00 | 525.61 | 490.14 | 130.00 | 10.00 | 482.68 |
| 3 | 2.75 | 4.08 | 3.00 | 10.25 | 125.00 | 1281.19 | 41.00 | 966.92 | 840.53 | 130.00 | 10.00 | 560.49 |
| 4 | 4.08 | 5.17 | 3.00 | 13.88 | 125.00 | 1734.38 | 38.00 | 1366.71 | 1067.79 | 130.00 | 10.00 | 630.99 |
| 5 | 5.17 | 6.08 | 3.00 | 16.88 | 125.00 | 2109.38 | 35.00 | 1727.90 | 1209.89 | 130.00 | 10.00 | 694.68 |
| 6 | 6.08 | 6.75 | 3.00 | 19.25 | 125.00 | 2406.19 | 32.00 | 2040.56 | 1275.09 | 130.00 | 10.00 | 749.81 |
| 7 | 6.75 | 7.25 | 3.00 | 21.00 | 125.00 | 2625.00 | 30.00 | 2273.32 | 1312.50 | 130.00 | 10.00 | 790.85 |
| 8 | 7.25 | 7.52 | 3.00 | 22.15 | 125.00 | 2768.63 | 27.00 | 2466.86 | 1256.93 | 130.00 | 10.00 | 824.97 |
| 9 | 7.52 | 7.75 | 3.00 | 22.90 | 125.00 | 2862.38 | 25.00 | 2594.19 | 1209.69 | 130.00 | 10.00 | 847.43 |
| 10 | 7.75 | 7.83 | 3.00 | 23.37 | 125.00 | 2921.25 | 22.00 | 2708.54 | 1094.32 | 130.00 | 10.00 | 867.59 |
| 11 | 7.83 | 7.67 | 3.00 | 23.25 | 125.00 | 2906.25 | 20.00 | 2730.98 | 994.00 | 130.00 | 10.00 | 871.55 |
| 12 | 7.67 | 7.42 | 3.00 | 22.63 | 125.00 | 2828.81 | 18.00 | 2690.36 | 874.15 | 130.00 | 10.00 | 864.38 |
| 13 | 7.42 | 7.08 | 3.00 | 21.75 | 125.00 | 2718.75 | 15.00 | 2626.11 | 703.66 | 130.00 | 10.00 | 853.05 |
| 14 | 7.08 | 6.50 | 3.00 | 20.37 | 125.00 | 2546.81 | 13.00 | 2481.54 | 572.91 | 130.00 | 10.00 | 827.56 |
| 15 | 6.50 | 5.92 | 3.00 | 18.63 | 125.00 | 2328.13 | 11.00 | 2285.36 | 444.23 | 130.00 | 10.00 | 792.97 |
| 16 | 5.92 | 5.17 | 3.00 | 16.63 | 125.00 | 2078.19 | 10.00 | 2046.62 | 360.87 | 130.00 | 10.00 | 750.87 |
| 17 | 5.17 | 4.25 | 3.00 | 14.13 | 125.00 | 1765.69 | 7.00 | 1752.53 | 215.18 | 130.00 | 10.00 | 699.02 |
| 18 | 4.25 | 3.33 | 3.00 | 11.37 | 125.00 | 1421.25 | 4.00 | 1417.79 | 99.14 | 130.00 | 10.00 | 639.99 |
| 19 | 3.33 | 2.17 | 3.00 | 8.25 | 125.00 | 1030.69 | 2.00 | 1030.06 | 35.97 | 130.00 | 10.00 | 571.63 |
| 20 | 2.17 | 1.00 | 3.00 | 4.75 | 125.00 | 593.81 | 0.00 | 593.81 | 0.00 | 130.00 | 10.00 | 494.71 |
| 21 | 1.00 | 0.00 | 2.25 | 1.13 | 125.00 | 140.63 | 0.00 | 140.63 | 0.00 | 130.00 | 10.00 | 317.30 |
| Total | | | | | | | | | 14106.99 | | | 14282.75 |

Factor of Safety of Unreinforced Slope (ordinary Method of slice) =

$$FS = \frac{\sum c\beta + N tan\phi}{\sum W Sin\alpha}$$

$$FS = \frac{14282}{14106.99} = \mathbf{1.012}$$

Step 3: Design of Reinforced Slope

Step 3A: Selection of RPP

Based on different commercially available samples, the following RPP was selected for the design.

RPP Properties:

Dimension of RPP: 3.5 inch x 3.5 inch

Ultimate Flexural Strength: 4 ksi

Allowable Flexural Strength: 4*.35 = 1.4 ksi

Step 3B: Hand calculation of the reinforced slope using the ordinary method of slice

To determine the factor of safety of the reinforced slope, it is important to select a trail RPP spacing for the analysis. The current example considered a RPP spacing of 4 ft c/c as presented in Figure 4. The final spacing of RPP should be selected with few iteration based on the target factor of safety.

The current analysis for the reinforced slope was performed considering the specific limit resistance of RPP based on the depth of the slip surface. The limit resistance of RPP was determined based on the limit resistance curve presented in Table 3.

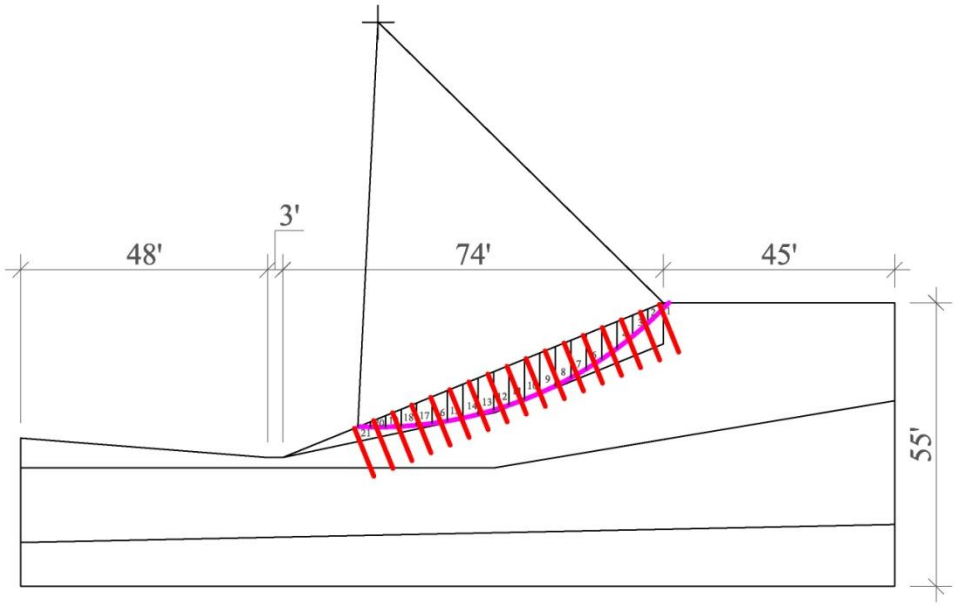


Figure 5 location of RPP respected to different slices

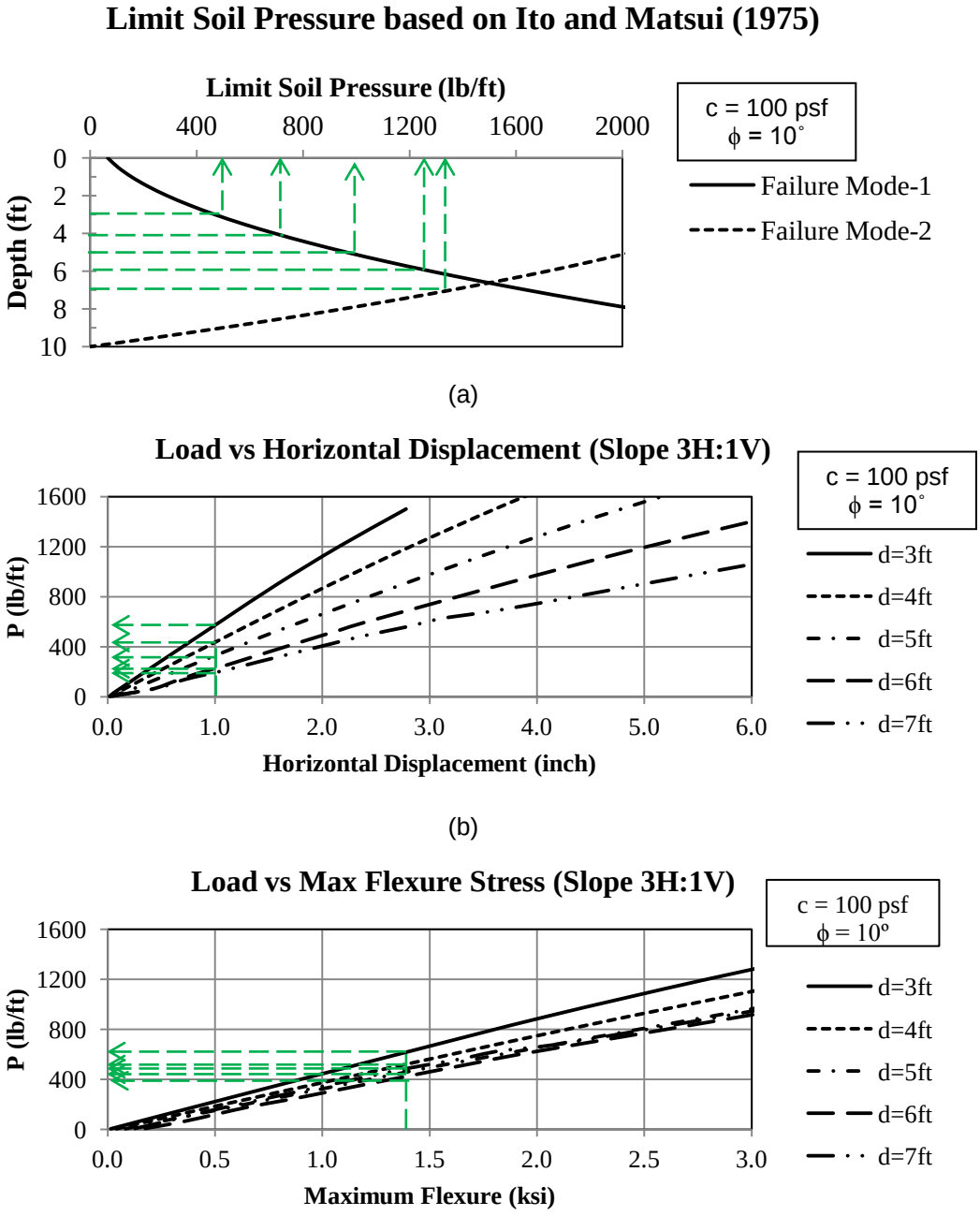


Figure B1 Design Chart for c = 100 psf and ϕ = 10˚, a. Limit soil curve, b. Load vs Horizontal Displacement for slope 3H:1V, c. Load vs Maximum Flexure for slope 3H:1V

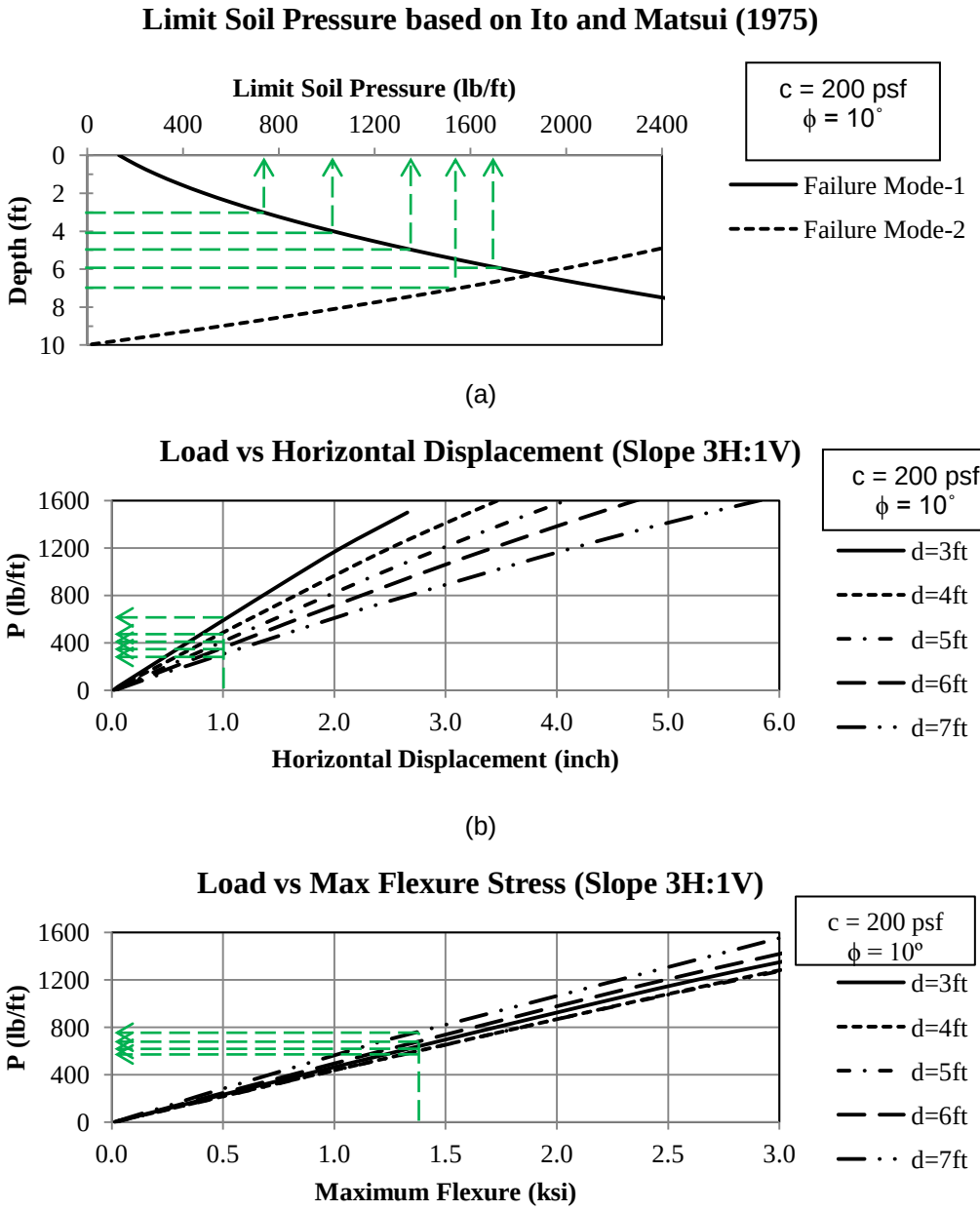


Figure B13 Design Chart for c = 200 psf and ϕ = 10˚, a. Limit soil curve, b. Load vs Horizontal Displacement for slope 3H:1V, c. Load vs Maximum Flexure for slope 3H:1V

Table 3 Detail Calculation of Reinforced Slope using Ordinary Method of slice

| Slice No | α | W | N | Wsinα | c | φ | cβ+Ntanφ | d | P1 (Figure B1) | P2 (Figure B13) | P | cβ+Ntanφ+P |
|---|---|---|---|---|---|---|---|---|---|---|---|---|
| | deg | lb | lb | lb | psf | deg | lb | ft | lb (B1) | lb (B13) | lb (avg) | lb |
| 1 | 43 | 73.3 | 53.6 | 50.0 | 130.0 | 10.0 | 150.2 | 0.0 | 0.0 | 0.0 | 0.0 | 150.2 |
| 2 | 43 | 718.7 | 525.6 | 490.1 | 130.0 | 10.0 | 482.7 | 3.0 | 550.0 | 600.0 | 565.0 | 1047.7 |
| 3 | 41 | 1281.2 | 966.9 | 840.5 | 130.0 | 10.0 | 560.5 | 3.0 | 550.0 | 600.0 | 565.0 | 1125.5 |
| 4 | 38 | 1734.4 | 1366.7 | 1067.8 | 130.0 | 10.0 | 631.0 | 4.0 | 430.0 | 520.0 | 457.0 | 1088.0 |
| 5 | 35 | 2109.4 | 1727.9 | 1209.9 | 130.0 | 10.0 | 694.7 | 5.0 | 350.0 | 410.0 | 368.0 | 1062.7 |
| 6 | 32 | 2406.2 | 2040.6 | 1275.1 | 130.0 | 10.0 | 749.8 | 5.0 | 350.0 | 410.0 | 368.0 | 1117.8 |
| 7 | 30 | 2625.0 | 2273.3 | 1312.5 | 130.0 | 10.0 | 790.8 | 6.0 | 210.0 | 350.0 | 252.0 | 1042.8 |
| 8 | 27 | 2768.6 | 2466.9 | 1256.9 | 130.0 | 10.0 | 825.0 | 7.0 | 200.0 | 300.0 | 230.0 | 1055.0 |
| 9 | 25 | 2862.4 | 2594.2 | 1209.7 | 130.0 | 10.0 | 847.4 | 7.0 | 200.0 | 300.0 | 230.0 | 1077.4 |
| 10 | 22 | 2921.3 | 2708.5 | 1094.3 | 130.0 | 10.0 | 867.6 | 7.0 | 200.0 | 300.0 | 230.0 | 1097.6 |
| 11 | 20 | 2906.3 | 2731.0 | 994.0 | 130.0 | 10.0 | 871.5 | 7.0 | 200.0 | 300.0 | 230.0 | 1101.5 |
| 12 | 18 | 2828.8 | 2690.4 | 874.2 | 130.0 | 10.0 | 864.4 | 7.0 | 200.0 | 300.0 | 230.0 | 1094.4 |
| 13 | 15 | 2718.8 | 2626.1 | 703.7 | 130.0 | 10.0 | 853.1 | 7.0 | 200.0 | 300.0 | 230.0 | 1083.1 |
| 14 | 13 | 2546.8 | 2481.5 | 572.9 | 130.0 | 10.0 | 827.6 | 0.0 | 0.0 | 0.0 | 0.0 | 827.6 |
| 15 | 11 | 2328.1 | 2285.4 | 444.2 | 130.0 | 10.0 | 793.0 | 6.0 | 210.0 | 350.0 | 252.0 | 1045.0 |
| 16 | 10 | 2078.2 | 2046.6 | 360.9 | 130.0 | 10.0 | 750.9 | 5.0 | 350.0 | 410.0 | 368.0 | 1118.9 |
| 17 | 7 | 1765.7 | 1752.5 | 215.2 | 130.0 | 10.0 | 699.0 | 4.0 | 430.0 | 520.0 | 457.0 | 1156.0 |
| 18 | 4 | 1421.3 | 1417.8 | 99.1 | 130.0 | 10.0 | 640.0 | 0.0 | 0.0 | 0.0 | 0.0 | 640.0 |
| 19 | 2 | 1030.7 | 1030.1 | 36.0 | 130.0 | 10.0 | 571.6 | 3.0 | 550.0 | 600.0 | 565.0 | 1136.6 |
| 20 | 0 | 593.8 | 593.8 | 0.0 | 130.0 | 10.0 | 494.7 | 3.0 | 550.0 | 600.0 | 565.0 | 1059.7 |
| 21 | 0 | 140.6 | 140.6 | 0.0 | 130.0 | 10.0 | 317.3 | 0.0 | 0.0 | 0.0 | 0.0 | 317.3 |
| | | | | 14106.99 | | | | | | | | 20444.75 |

Factor of Safety of Reinforced Slope (ordinary Method of slice)

$$FS = \frac{\sum c\beta + Ntan\phi + P}{\sum WSin\alpha}$$

$$FS = \frac{20444.75}{14106.99} = \mathbf{1.45}$$

The similar calculation can be repeated with smaller RPP spacing (<4 ft c/c) to increase the factor of safety.

OUTPUT OF GSTABL TO DETERMINE THE CRITICAL SLIP SURFACE DURING STEP 1

*** GSTABL7 ***

** GSTABL7 by Garry H. Gregory, P.E. **

** Version 1.0, January 1996; Version 1.16, May 2000 **

--Slope Stability Analysis--

Simplified Janbu, Modified Bishop

or Spencer`s Method of Slices

(Based on STABL6-1986, by Purdue University)

Run Date: 9/3/2013

Time of Run: 2:47PM

Run By: John Smith, XYZ Company

Input Data Filename: C:-NEWFILE.

Output Filename: C:-NEWFILE.OUT

Unit System: English

Plotted Output Filename: C:-NEWFILE.PLT

PROBLEM DESCRIPTION

BOUNDARY COORDINATES

4 Top Boundaries

10 Total Boundaries

| Boundary No. | X-Left (ft) | Y-Left (ft) | X-Right (ft) | Y-Right (ft) | Soil Type Below | End |
|---|---|---|---|---|---|---|
| 1 | 0.00 | 28.75 | 48.00 | 25.75 | 2 | |
| 2 | 48.00 | 25.75 | 51.00 | 25.75 | 2 | |
| 3 | 51.00 | 25.75 | 125.00 | 55.00 | 1 | |

| | | | | | |
|---|---|---|---|---|---|
| 4 | 125.00 | 55.00 | 175.00 | 55.00 | 2 |
| 5 | 51.00 | 25.75 | 92.25 | 33.75 | 2 |
| 6 | 92.25 | 33.75 | 124.00 | 47.00 | 2 |
| 7 | 124.00 | 47.00 | 125.00 | 55.00 | 2 |
| 8 | 0.00 | 23.00 | 92.25 | 23.00 | 3 |
| 9 | 92.25 | 23.00 | 175.00 | 36.00 | 3 |
| 10 | 0.00 | 8.50 | 175.00 | 12.00 | 4 |

ISOTROPIC SOIL PARAMETERS

4 Type(s) of Soil

| Soil Type No. | Total Unit Wt. (pcf) | Saturated Unit Wt. (pcf) | Cohesion Intercept (psf) | Friction Angle (deg) | Pore Pressure Param. | Pressure Constant (psf) | Piez. Surface No. |
|---|---|---|---|---|---|---|---|
| 1 | 125.0 | 125.0 | 120.0 | 10.0 | 0.00 | 0.0 | 0 |
| 2 | 125.0 | 125.0 | 120.0 | 23.0 | 0.00 | 0.0 | 0 |
| 3 | 130.0 | 130.0 | 250.0 | 15.0 | 0.00 | 0.0 | 0 |
| 4 | 140.0 | 140.0 | 3000.0 | 35.0 | 0.00 | 0.0 | 0 |

Trial Failure Surface Specified By 8 Coordinate Points

| Point No. | X-Surf (ft) | Y-Surf (ft) |
|---|---|---|
| 1 | 64.49 | 31.08 |
| 2 | 74.49 | 31.09 |
| 3 | 84.41 | 32.36 |
| 4 | 94.09 | 34.88 |
| 5 | 103.37 | 38.60 |
| 6 | 112.11 | 43.46 |

7 120.16 49.39

8 126.04 55.00

Circle Center At X = 69.5 ; Y = 109.4 and Radius, 78.5

* * Factor Of Safety Is Calculated By The Modified Bishop Method * *

Factor Of Safety For The Preceding Specified Surface = 1.064

***Table 1 - Individual Data on the 9 Slices***

| Slice No. | Width (ft) | Weight (lbs) | Water Force Top (lbs) | Water Force Bot (lbs) | Tie Force Norm (lbs) | Tie Force Tan (lbs) | Earthquake Force Hor (lbs) | Earthquake Force Ver (lbs) | Surcharge Load (lbs) |
|---|---|---|---|---|---|---|---|---|---|
| 1 | 10.0 | 2465.6 | 0.0 | 0.0 | 0.0 | 0.0 | 0.0 | 0.0 | 0.0 |
| 2 | 9.9 | 6535.3 | 0.0 | 0.0 | 0.0 | 0.0 | 0.0 | 0.0 | 0.0 |
| 3 | 9.7 | 8771.4 | 0.0 | 0.0 | 0.0 | 0.0 | 0.0 | 0.0 | 0.0 |
| 4 | 9.3 | 9136.5 | 0.0 | 0.0 | 0.0 | 0.0 | 0.0 | 0.0 | 0.0 |
| 5 | 8.7 | 7808.8 | 0.0 | 0.0 | 0.0 | 0.0 | 0.0 | 0.0 | 0.0 |
| 6 | 8.0 | 5102.6 | 0.0 | 0.0 | 0.0 | 0.0 | 0.0 | 0.0 | 0.0 |
| 7 | 4.7 | 1400.3 | 0.0 | 0.0 | 0.0 | 0.0 | 0.0 | 0.0 | 0.0 |
| 8 | 0.1 | 18.2 | 0.0 | 0.0 | 0.0 | 0.0 | 0.0 | 0.0 | 0.0 |
| 9 | 1.0 | 64.5 | 0.0 | 0.0 | 0.0 | 0.0 | 0.0 | 0.0 | 0.0 |

***Table 2 - Base Stress Data on the 9 Slices***

| Slice No. * | Alpha (deg) | X-Coord. Slice Cntr (ft) | Base Leng. (ft) | Available Shear Strength (psf) | Mobilized Shear Stress (psf) |
|---|---|---|---|---|---|
| 1 | 0.04 | 69.49 | 10.00 | 163.45 | 0.19 |
| 2 | 7.30 | 79.45 | 10.00 | 231.26 | 82.98 |

| | | | | | |
|---|---|---|---|---|---|
| 3 | 14.59 | 89.25 | 10.00 | 268.21 | 220.92 |
| 4 | 21.84 | 98.73 | 10.00 | 275.31 | 340.02 |
| 5 | 29.08 | 107.74 | 10.00 | 254.12 | 379.48 |
| 6 | 36.38 | 116.13 | 10.00 | 206.55 | 302.68 |
| 7 | 43.65 | 122.51 | 6.49 | 148.99 | 148.83 |
| 8 | 43.65 | 124.93 | 0.19 | 126.57 | 64.40 |
| 9 | 43.65 | 125.52 | 1.44 | 105.99 | 30.97 |

Sum of the Resisting Forces (including Pier/Pile,

Tieback, and Reinforcing Forces if applicable) = 15137.83 (lbs)

Average Available Shear Strength (including Tieback,

Pier/Pile, and Reinforcing Forces if applicable) = 222.20(psf)

Sum of the Driving Forces = 14286.11 (lbs)

Average Mobilized Shear Stress = 209.70(psf)

Total length of the failure surface = 68.13(ft)

Sample Calculation: Infinite Slope (Approach 2)

Given:

| Slope Type | Slope Height ft | Slope Inclination | Top Soil c psf | Top Soil φ deg | Top Soil ϒ pcf | Foundation Soil c psf | Foundation Soil φ deg | Foundation Soil ϒ pcf |
|---|---|---|---|---|---|---|---|---|
| Slope 1 | 40 | 3H:1V | 250 | 10 | 125 | 400 | 30 | 125 |

d = 7 ft

L = 126.5 ft

β = 18.42°

$\Upsilon'$ = 125 pcf

$\Upsilon_{sat}$ = 125 pcf

Factor of Safety of Unreinforced Slope:

h = d/cosβ = 7/cos18.25 = 7.37 ft

$$FS = \frac{c' + h\,\gamma' cos^2\beta * tan\varphi'}{\gamma_{sat} * h * sin\beta * cos\beta}$$

$$FS = \frac{250 + 7.37 * 125 * cos^2 18.42 * tan10}{125 * 7.37 * sin18.42 * cos18.42}$$

$$FS = 1.45$$

Factor of Safety of Reinforced Slope:

P = 335 lb/ft

S = 3 ft c/c

$$FS = \frac{c'L + hL\,\gamma' cos^2\beta * tan\varphi' + \left(\frac{L}{S} + 1\right) * P}{\gamma_{sat} * hL * sin\beta * cos\beta}$$

$$FS = \frac{250 * 126.5 + 7.37 * 126.5 * 125 * cos^2 18.42 * tan10 + \left(\frac{126.5}{3} + 1\right) * 335}{125 * 7.37 * 126.5 * sin18.42 * cos18.42}$$

$$FS = 1.85$$

References

Abramson, L., Lee, T., Sharma, S., and Boyce, G., (2002). Slope Stability and Stabilization Methods, John Wiley, New York, 712 p.

Berg, R. R., Christopher, B. R., & Samtani, N. C. (2009). Design of Mechanically Stabilized Earth Walls and Reinforced Soil Slopes–Volume II (No. FHWA-NHI-10-025).

Bowders, J. J., Loehr, J. E., Salim, H., & Chen, C. W. (2003). Engineering properties of recycled plastic pins for slope stabilization. *Transportation Research Record: Journal of the Transportation Research Board*, 1849(1), 39-46.

Breslin, V.T., Senturk, U., Berndt, C.C. (1998) “Long-term engineering properties of recycled plastic lumber in pier construction”. *Resources, Conservation and Recycling 23* (1998), 243–258.

Cai, F., and Ugai, K., (2003). “Reinforcing mechanism of anchors in slopes: a numerical comparison of results of LEM and FEM”, *Int. J. Numer. Anal. Meth. Geomech*., 27 (2003), 549-564.

Chen, C. W., Salim, H., Bowders, J., Loehr, E., and Owen, J. (2007). “Creep Behavior of Recycled Plastic Lumber in Slope Stabilization Applications” *J. Mater. Civ. Eng.*, 19(2), 130-138.

Day, R. W., & Axten, G. W. (1989). Surficial stability of compacted clay slopes. *J. of Geotech. Engg.*, 115(4), 577-580.

Day, R. W. (1996). Design and Repair for Surficial Slope Failures. *Practice Periodical on Structural Design and Construction*, 1(3), 83-87.

Elias, V., B. Christopher, and R. Berg, Mechanically Stabilized Earth Walls and Reinforced Soil Slopes Design and Construction Guidelines, Report FHWA-NHI-00-043, Federal Highway Administration, Washington, D.C., 2001.

Evans, D. A. (1972). Slope Stability Report. Slope Stability Committee, Department of Building and Safety, Los Angeles, CA.

Fay, L., Akin, M., & Shi, X. (2012). Cost-Effective and Sustainable Road Slope Stabilization and Erosion Control (Vol. 430). Transportation Research Board, Washington, D.C.

Gopu, V. K. and Seals, R. K., (1999), “Mechanical Properties of Recycled Plastic Lumber and Implications in Structural Design”. *Composites Institute's, International Conference Proceedings*. CRC PressI Llc, 1999. Session 7-c/1 to Session & 7-c/6

Gray, D.H. and Sotir, R. B. (1996). “Biotechnical and Soil Bioengineering Slope Stabilization: A Practical Guide for Erosion Control”, John Wiley & Sons, New York, N.Y.

Hossain, J. (2012). “Geohazard Potential of Rainfall Induced Slope Failure on Expansive Clay”. Ph.D. Dissertation, The University of Texas at Arlington, Arlington, Texas.

Hossain, M.S., Maganti, D., and Hossain, J. (2010). “Assessment of geo-hazard potential and site investigations using Resistivity Imaging.” *Int. J. Environmental Technology and Management*, 13 (2), 116-129.

Inci, G. (2008) "Numerical Modeling of Desiccation Cracking in Compacted Soils. *Proc. IACMAG*. Goa, India.

Ito, T., and T. Matsui (1975), “Methods to estimate lateral force acting on stabilizing piles,” *Soils and Foundations*, Vol. 15, No. 4, 43-59.

Jutkofsky, W. S., Sung, J. T., & Negussey, D. (2000). Stabilization of embankment slope with geofoam. *Transportation Research Record: Journal of the Transportation Research Board*, 1736(1), 94-102.

Kandaris, P.M., “Use of Gabions for Localized Slope Stabilization in Difficult Terrain,” *Proc. 37th U.S. Symposium on Rock Mechanics*, Vail, Colo., June 7–9, 2007.

Kayyal, M. K. and Wright S.G. (1991). "Investigation of Long-Term Strength properties of Paris and Beaumont Clays in Earth Embankments." Research Report 1195-2F, Center for Transportation Research, The University of Texas at Austin, November, 1991.

Krishnaswamy, P. and Francini. R., (2000), “Long Term Durability of Recycled Plastic Lumber in Structural Application”, http://www.environmental-expert.com/Files/0/articles/2183/2183.pdf accessed May 22, 2013

Lampo, R., & Nosker, T. J. (1997). Development and testing of plastic lumber materials for construction applications. US Army Corps of Engineers, Construction Engineering Research Laboratories, USACERL Technical Report 97/95.

Lazarte, C. A., Elias, V., Espinoza, R. D., & Sabatini, P. J. (2003). Geotechnical Engineering Circular No. 7: Soil Nail Walls. Federal Highway Administration, Washington, DC.

Loehr, J. E., Bowders, J., Owen, J., Sommers, L., & Liew, L. (2000). Stabilization of slopes using recycled plastic pins. *Transportation Research Board : Transportation Research Record*, 1-8.

Loehr, J. E., and Bowders, J. J. (2007). “Slope Stabilization using Recycled Plastic Pins – Phase III”, Final Report: RI98-007D, Missouri Department of Transportation, Jefferson City, Missouri.

Loehr, J. E., Fennessey, T. W., & Bowders, J. J. (2007). Stabilization of surficial slides using recycled plastic reinforcement. *Transportation Research Record: Transportation Research Record*, 1989(1), 79-87.

Lynch, J. K., Nosker, T. J., Renfree, R. W., Krishnaswamy, P., & Francini, R. (2001). Weathering effects on mechanical properties of recycled HDPE based plastic lumber. *Proc. ANTEC 2001*, Dallas, Texas, May 6-10.

Malcolm, G. M. (1995), “Recycled Plastic Lumber and shapes design and specifications”, *Proc. Structures congress 13*, Boston, Massachusetts, April 2-5, 1995.

McCormick, W., and Short, R. (2006). “Cost Effective Stabilization of Clay Slopes and Failures using Plate Piles”, Proc., IAEG2006, The Geological Society of London, London, United Kingdom, 1-7.

Mclaren, M. G., and Pensiero, J. P. (1999), “Simplified Design of Recycled Plastic as Structural Materials”. Composites Institute's, International Conference Proceedings. CRC PressI Llc, 1999. Session 7-b/1 to Session & 7-b/8.

Nosker, T., and R. Renfree. (2000). "Recycled Plastic Lumber: From Park Benches to Bridges." *Approved for Proceedings of R’2000 5th World Congress*, Toronto, Canada.

Nosker, T. (1989). Improvements in the Properties of Commingled Waste by the Selective Mixing of Plastics Waste. *Proc*., *SPE Recycling RETEC*, Charlotte, NC.

Nosker, T. (1999). The Development of Polyolefin Based Oriented Glass Fiber Building Materials. *Proc.* SPE ANTEC.

Parra, J. R., Loehr, J. E., Hagemeyer, D. J., & Bowders, J. J. (2003). Field performance of embankments stabilized with recycled plastic reinforcement. *Transportation Research Record: Transportation Research Record*, 1849(1), 31-38.

Pearlman, S.L., B.D. Campbell, and J.L. Withiam, “Slope Stabilization Using In-Situ Earth Reinforcements,” *Proc. Stability and Performance of Slopes and Embankment II (GSP 31)*, 1992, pp. 1333–1348.

Richard Lampo, R., Nosker, T., Barno, D., Busel, J. Mäher, A., Dutta, P., and Odello, R. (1998), “Development and Demonstration of FRP Composite Fender and Sheet Piling Systems” USACERL Technical Report 98/121, pp 20-21.

Rogers, L. E. and Wright, S. G. (1986). "The Effects of Wetting and Drying on the Long-Term Shear Strength Parameters for Compacted Beaumont Clay." Research Report 436-2F, Center for Transportation Research, the University of Texas at Austin, November 1986.

Sabatini, P.J., Elias, V., Schmertmann, G.R., Bonaparte, R. (1997). "Geotechnical Engineering Circular No. 2, Earth Retaining Systems." Publication FHWA-SA-96-038, Federal Highway Administration, Washington, D.C.

Santi, P. M., Elifrits, C. D., & Liljegren, J. A. (2001). Design and installation of horizontal wick drains for landslide stabilization. *Transportation Research Board: Transportation Research Record*, 1757(1), 58-66.

Short, R. Collins, B.D., Bray, J.D, and Sitar, N. (2005). "Testing and Evaluation of Driven Plate Piles in a Full Size Test Slope: A New Method for Stabilizing Shallow Landslides", http://www.sloperepair.com/downloads/trb_document.pdf accessed August 20, 2013.

Short, R. and Collins, B.D., (2006), "Testing and Evaluation of Driven Plate Piles in Full-Size Test Slope: New Method for Stabilizing Shallow Landslides", *TRB 85th Annual Meeting Compendium of Papers CD-ROM*, January 22-26, Washington D.C.

Skempton, A.W. (1977) "Slope Stability of Cuttings in Brown London Clay." *Proc., Ninth Int.Conf. on Soil Mechanics and Foundation Engineering*, Tokyo, Vol. 3, 261-270.

Sommers, L., Loehr, J. E., & Bowders, J. J. (2000). Construction Methods for Slope Stabilization with Recycled Plastic Pins. *Proc. Mid-Continent Transportation Symposium 2000*. Iowa State University, Ames, Iowa, May 15-16, 2000.

Taquinio, F. and Pearlman, S.L. (1999). "Pin Piles for Building Foundations," presented at the 7th Annual Great Lakes Geotechnical and Geoenvironmental Conference, Kent, Ohio, May 10.

Titi, H., & Helwany, S. (2007). Investigation of Vertical Members to Resist Surficial Slope Instabilities (No. WHRP 07-03). Wisconsin Department of Transportation, Madison, WI.

U.S. Department of Agriculture (USDA), (1992). Natural Resources Conservation Service, National Engineering Handbook, Part 650, Engineering Field Handbook, Chapter 18, “Soil Bioengineering for Upland Slope Protection and Erosion Reduction,” USDA, Washington, D.C.,

U.S. Department of the Interior | U.S. Geological Survey, “Texas geologic map data”. http://mrdata.usgs.gov/geology/state/state.php?state=TX, Accessed July 25, 2013

## Biographical Information

Mohammad Sadik Khan graduated with a Bachelor of Science in Civil Engineering from Bangladesh University of Engineering and Technology, Dhaka, Bangladesh in June 2007. After graduation, he started his career as Assistant Engineer in China National Electric Wire & Cable Import/Export Corporation (CCC). On December 2007, he joined Sinamm Engineering Limited, Dhaka, Bangladesh as Assistant Manager. He served as a Project Coordinator in the same company from April 2009 to December 2009. Mohammad started his graduate studies at The University of Texas at Arlington on Spring 2010. As a graduate student, he got the opportunity to work as a graduate research assistant under supervision of Dr. Sahadat Hossain. The author's research interests include slope stability analysis, slope stabilization, numerical modeling, deep foundation, retaining wall, excavation support system, forensic study, geophysical investigation, non destructive testing and bioreactor landfills.